DISSERTATION ZUR ERLANGUNG DES DOKTORGRADES
DER
FAKULTÄT FÜR CHEMIE UND PHARMAZIE
DER
LUDWIG-MAXIMILIANS-UNIVERSITÄT MÜNCHEN

NEW HYBRID GUANIDINE-QUINOLINE COPPER COMPLEXES AND THEIR USE IN ATOM TRANSFER RADICAL POLYMERIZATION

Johannes Sebastian Mannsperger
aus
Heidelberg, Deutschland

2018

Erklärung

Diese Dissertation wurde im Sinne von §7 der Promotionsordnung vom 28. November 2011 von Frau Prof. Dr. Sonja Herres–Pawlis betreut.

Eidesstattliche Versicherung

Diese Dissertation wurde eigenständig und ohne unerlaubte Hilfe erarbeitet.

München, den 01. 04. 2018

. . . .
Johannes Sebastian Mannsperger

Dissertation eingereicht am	04. Januar 2018
1. Gutachterin	Frau Prof. Dr. Sonja Herres–Pawlis
2. Gutachter	Herr Prof. Dr. Hans–Christian Böttcher
Mündliche Prüfung am	07. Februar 2018

Acknowledgment

The preparation of this doctoral thesis has been a journey with many fascinating and productive moments. As with most scientific projects, success can never be achieved by anyone alone. Therefore, certain important persons who have supported my work should be mentioned.

First and foremost, I would like to express my sincerest gratitude towards my adviser Prof. Dr. Sonja Herres-Pawlis for her confidence in and support of my work. Her openness to new ideas and her willingness to grant scientific freedom to her doctoral students encouraged me to look beyond the horizon and find my own ways.

I would like to thank Prof. Dr. Hans-Christian Böttcher for examining my doctoral thesis and Prof. Dr. Peter Klüfers, Prof. Dr. Heinz Langhals, Prof. Dr. Lena Daumann and Prof. Dr. Konstantin Karaghiosoff for being on my defense committee.

Furthermore, I am very grateful to Prof. Dr. Peter Klüfers for hosting me in his laboratories at the Ludwig-Maximilians-Universität München.

The Konrad-Adenauer-Stiftung granted me financial supported with its doctorate scholarship program, which I am very thankful for. The foundation's seminar program opened up new perspectives in very interdisciplinary topics.

Among all the great scientists of the Herres-Pawlis group, Thomas Rösener has to be mentioned in particular. Many advancements of our analytical methods were established by him and both of us profited from a close collaboration and many fruitful discussions. Pascal Schäfer presented himself as a wonderful friend and host during my trips to the RWTH Aachen University, which I am grateful for. I also enjoyed the months sharing a laboratory with Angela Metz and Julia Stanek, which I am thankful for. Furthermore, I would like to thank Dr. Alexander Hoffmann for his commitment during the finalization procedures of our molecular structures, for his corrections of the experimental part of this thesis and for his efforts in maintaining the laboratory equipment.

All members of the Klüfers group are thanked for having me accepted as one of their peers. Sebastian Brück and Helen Funk were wonderful lab mates and I would like to additionally thank Christine Sturm, Helen Funk and Daniel Beck for X-ray diffraction measurements of my crystals.

During the time of my doctorate, I had the opportunity to mentor many talented and motivated students. I would like to thank Jens Rickmeier, Patricia Scheurle, Alexander Pütz, Szabolcs Makai, Gloria Betzenbichler, Fabian Hernichel and Julian Jaser for their work under my supervision.

My work would not have been possible without the permanent staff and the analytical department. I would like to thank Lida Holowatyj-den Toom and Christine Neumann as members of the Klüfers group who supported my daily adventures. Dr. Peter Mayer is greatly acknowledged for his work on the X-ray diffraction measurements. Furthermore, Peter Mayer, Brigitte Breitenstein and Christine Neumann were of great importance to the NMR facility. Dr. Werner Spahl, Sonja Kosak and Carola Draxler are thanked for their work in the mass spectrometry department.

At the very last, I would like to express my gratefulness to all my friends and family who have continuously supported me during the last years. In particular, I owe my parents and my brother gratitude for believing in me and my abilities. Among my friends, Hannes Erdmann, Meike Simon, Heinrich Rudy, Robert Rampmaier and Henrik Eickhoff contributed significantly to my great years in Munich. Tatjana Huber, the joy of my life, has been the greatest support within the last years. Both scientifically and personal her impact on the preparation of this doctoral thesis cannot be overestimated.

Abstract

In this thesis, the synthesis and characterization of a family of seven new guanidine-quinoline hybrid ligands and their six Cu^I and seven Cu^{II} complexes is presented. The catalytic activities of the copper complexes in atom transfer radical polymerization (ATRP) reactions were studied and their electrochemical potentials, ATRP equilibria and reaction rate constants were determined.

The molecular structures of the CuBr complexes showed bischelate tetrahedral coordination of the electron-rich ligands and a trigonal-planar geometry for the electron-poor ligands. Similar, the Cu^{II} halide complexes exhibited distorted bischelate trigonal-bipyramidal coordination for the electron-rich ligands and monochelate distorted square-pyramidal coordination for electron-poor $CuCl_2$ complexes. All catalysts were found to polymerize styrene in high polymerization rates under controlled conditions. The use of copper complexes with electron-rich ligands resulted in faster catalysis and the $[Cu(TMG6Methoxyqu)_2]Br$ complex led to outstandingly fast ATRP reactions, yielding two to five times higher rate constants k_p than other investigated catalysts.

Electrochemical examinations of the $CuBr_2$ complexes revealed that they exhibited increasing negative potentials for complexes with stronger electron-donating substituents. The potentials ranged from $-0.439\,V$ to $-0.545\,V$ (vs. Fc/Fc^+). For the CuBr complexes, an increase of the electrochemical potential was found to lie in between 10 mV and 35 mV and the potentials of the $CuCl_2$ complexes were found to be 40 mV to 60 mV lower than their $CuBr_2$ counterparts. Most of the electrochemical potentials showed strong correlations with the data from polymerization studies.

In correlation with the determined polymerization rates and electrochemical data, the K_{ATRP} values of the CuBr complexes were found to be larger for ligands bearing more electron-donating substituents. Our UV/Vis measurements afforded K_{ATRP} values ranging from 3.6×10^{-8} to 3.6×10^{-7}. After addition of TEMPO to the equilibrium reaction, the k_{act} values were determined to lie between $0.34\,s^{-1}$ and $2.33\,s^{-1}$ and values for k_{deact} were found to range from $5.9 \times 10^6\,s^{-1}$ to $1.3 \times 10^7\,s^{-1}$. The data further indicated, that the electron-rich ligands TMG6dmaqu and TMG6dbaqu form bidentate ATRP catalysts with the highest K_{ATRP} values known in the literature. The values are increased by one order of magnitude compared to 4,4'-dinonyl-2,2'-bipyridine (dNbpy) complexes.[1,2]

Abbreviations

Atom Transfer Radical Polymerization	ATRP
Bond Dissociation Energy	BDE
Controlled Radical Polymerization reactions	CRP
Conventional Radical Polymerization	RP
Conversion	C
Counter Electrode	CE
Cyclic Voltammetry	CV
Dead Chain Fraction	DCF
Equivalent	equiv
Gel Permeation Chromatography	GPC
Inner Sphere Electron Transfer	ISET
Nuclear Magnetic Resonance	NMR
Outer Sphere Electron Transfer	OSET
Persistent Radical Effect	PRE
Polydispersity	PD
Radical Addition-Fragmentation Transfer	RAFT
Reference Electrode	RE
Single Electron Transfer	SET
Single Electron Transfer Living Radical Polymerization	SET-LRP
Stable Free Radical Polymerization	SFRP
Thin Layer Chromatography	TLC
Working Electrode	WE

dimethylethyleneguanidine	DMEG
di-*tert*-butyl dicarbonate	Boc$_2$O
ethyl 2-bromoisobutyrate (methyl 2-bromo-2-methylpropanoate)	EBriB
Lithium bis(trimethylsilyl)amide	LiHMDS
methyl 2-bromoisobutyrate (methyl 2-bromo-2-methylpropanoate)	MBriB
N-(6-methoxyquinolin-8-yl)-1,3-dimethylimidazolidin-2-imine	DMEG6Methoxyqu
tetrabutylammonium hexafluorophosphate	(TBA)PF$_6$
tetrabutylammonium bromide	TBAB
tetrabutylammonium chloride	TBAC
tetrahydrofuran	THF
tetramethylguanidine	TMG
tert-butyl carbamate	Boc
tris(2-(dimethylamino)ethyl)amine	Me$_6$TREN
(1-Bromoethyl)benzene	1-PEBr
(1-Chloroethyl)benzene	1-PECl

1,1,3,3-tetramethyl-2-(6-bromoquinolin-8-yl)guanidine	TMG6Brqu
1,1,3,3-tetramethyl-2-(6-nitroquinolin-8-yl)guanidine	TMG6Nitroqu
1,1,3,3-tetramethyl-2-(pyridin-2-ylmethyl)guanidine	TMGpy
1,1,3,3-tetramethyl-2-(quinolin-8-yl)guanidine	TMGqu
2-(2-(diisopropylamino)ethyl)-1,1,3,3-tetramethylguanidine	TMG^{i}pae
2-(6-(dibutylamino)quinolin-8-yl)-1,1,3,3-tetramethylguanidine	TMG6dbaqu
2-(6-(dimethylamino)quinolin-8-yl)-1,1,3,3-tetramethylguanidine	TMG6dmaqu
2-(6-((2-ethylhexyl)oxy)quinolin-8-yl)-1,1,3,3-tetramethylguanidine	TMG6EHoxyqu
2-(4-methoxyquinolin-8-yl)-1,1,3,3-tetramethylguanidine	TMG4Methoxyqu
2-(6-methoxyquinolin-8-yl)-1,1,3,3-tetramethylguanidine	TMG6Methoxyqu
2,2,6,6-tetramethylpiperidin-1-yl)oxyl	TEMPO
4-dimethylaminopyridine	4-DMAP

Lists of Ligands and Complexes

List of Ligands

Ligand	Substance Number
TMG6Methoxyqu	**4**
DMEG6Methoxyqu	**8**
TMG6EHoxyqu	**10**
TMG6Nitroqu	**16**
TMG6Brqu	**17**
TMG6dmaqu	**20**
TMG6dbaqu	**31**

List of Complexes

Complex	Substance Number
$[Cu(TMG6Methoxyqu)_2]Br$	**C1**
$[Cu(TMG6dmaqu)_2]Br$	**C2**
$[Cu(TMG6Nitroqu)Br]$	**C3**
$[Cu(TMG6Brqu)Br]$	**C4**
$[Cu(TMG6Methoxyqu)_2Br]Br$	**C5**
$[Cu(TMG6dmaqu)_2Br]Br$	**C6**
$[Cu(TMG6Nitroqu)_2Br]Br$	**C7**
$[Cu(TMG6Brqu)_2Br]Br$	**C8**
$[Cu(TMG6Methoxyqu)_2]Cl$	**C9**
$[Cu(TMG6Nitroqu)_2]CuCl_2$	**C10**
$[Cu(TMG6Methoxyqu)_2Cl]Cl$	**C11**
$[Cu(TMG6Brqu)_2Cl]Cl$	**C12**
$[Cu(TMG6Nitroqu)Cl_2]$	**C13**
$[Cu(DMEG6Methoxyqu)_2Br]Br$	**C14**

Contents

1. Introduction

1.1. Radical Polymerization

The free radical polymerization reaction (RP) is one of the most widely used polymerization techniques. Today, around 50% of all commercial polymer products are produced by a RP route.[1,3] Important bulk polymers, such as polyethylene (PE), polystyrene (PS) and poly(vinyl chloride) (PVC) are synthesized in a radical polymerization process. Together with specialty polymers, they are fabricated on a billion ton scale.[4] Important specialty polymers are styrene-acrylonitrile co-polymers (SAN), or vinyl polymers which are mostly poly(vinylidene chloride) or poly(vinyl acetate) (PVAc). Acrylate polymers such as the rigid poly(methyl methacrylate) (PMMA) or softer poly(acrylic acid) esters belong to a group of polymers with a diverse set of properties. Chemically resistant fluoropolymers like polytetrafluoroethylene (PTFE) or polychlorotrifluoroethylene (PCTFE) and elastomers derived from dienes such as 1,3-butadiene, isoprene or chloroprene are products with very unique features.

With different inexpensive and well understood production processes, products obtained by radical polymerization are being used in almost every industry and find countless applications. The materials can be fabricated as bulk polymer or ready to use commodities. They are used in personal care or medical products, as raw materials for the packaging, construction or automotive industries and as chemicals for highly specific applications such as surface treatment or microelectronics.[5]

Radical polymerization methods can be applied to almost all monomers containing reactive C$-$C double bonds. The reactions can be conducted under a large variety of polymerization conditions. Homogeneous polymerization protocols are commonly used in bulk material or in solution. Heterogeneous polymerization processes are employed in emulsions, suspensions or form precipitates during the reaction. Bulk reactions are usually challenging. The processes often exhibit strong exothermic behavior and require high activation energies. Furthermore, an increasing viscosity in course of the reaction progress requires sufficient stirring and limits the heat flow. Preventing runaway reactions, improved temperature control is mandatory. As a result, bulk polymerization methods are mainly used in large mass products such as PE,PS and PMMA. Overcoming high viscosity and poor heat flow conditions, polymerization reactions can be conducted in solution. As a disadvantage, solvent-related side reactions and impurities in the final product must be considered. Alongside others, solvent polymerization protocols are used for vinyl acetate, acrylonitrile and acrylic acid ester co-polymers. Independent of the polymerization protocol, most polymers synthesized from radical polymerization reactions exhibit thermoplastic behavior. As an exception, monomers with more than one C$-$C double bond, such as 1,3-butadiene, isoprene or chloroprene can form crosslinked elastomers without thermopastic properties.[5]

1.1.1. Mechanism of Conventional Radical Polymerization

The radical polymerization reaction mechanism is composed of three major reaction steps: the initiation, the radical chain growth reactions and different termination reactions (Scheme 1.1). Usually, a polymerization reaction is initiated by decomposition of an initiator (Scheme 1.1a). The decomposition reaction can be induced by thermal or photochemical energy transfer to the initiator. After bond homolysis, the initiator radical can add to the C−C double bond of a monomer, creating a new radical chain end (Scheme 1.1b). The continuous addition of monomers to the radical chain is considered as the chain growth or chain propagation reaction. The decomposition kinetics of a conventional radical initiator exhibit an exponential decrease of the initiator concentration. Hence, small amounts of initiator still decompose at high degrees of polymerization, yielding polymer products with polymer chains of different lengths.[6] The polymerization reaction can be described as a formal dissociation of one sp^2 hybridized double bond and a formal formation of two sp^3 hybridized single bonds for each monomer. The reaction is thermodynamically driven by the formation of the two single bonds. During a hypothetical polymerization reaction of ethene, the bond dissociation energy of the double bond is around $28\,\mathrm{kJ\,mol^{-1}}$ lower ($720\,\mathrm{kJ\,mol^{-1}}$, C=C in ethene) than the energy gained by formation of two C−C single bonds (each $374\,\mathrm{kJ\,mol^{-1}}$ in ethane, $748\,\mathrm{kJ\,mol^{-1}}$ in total).[7] This enthalpic gain compensates the entropic losses caused by a decrease of the number of monomer molecules. In conventional radical polymerization reactions, termination reactions generally result from recombination or disproportionation reactions of radicals (Scheme 1.1c). Hereby, two radical chains are terminated and therefore polymerization activity is lost.

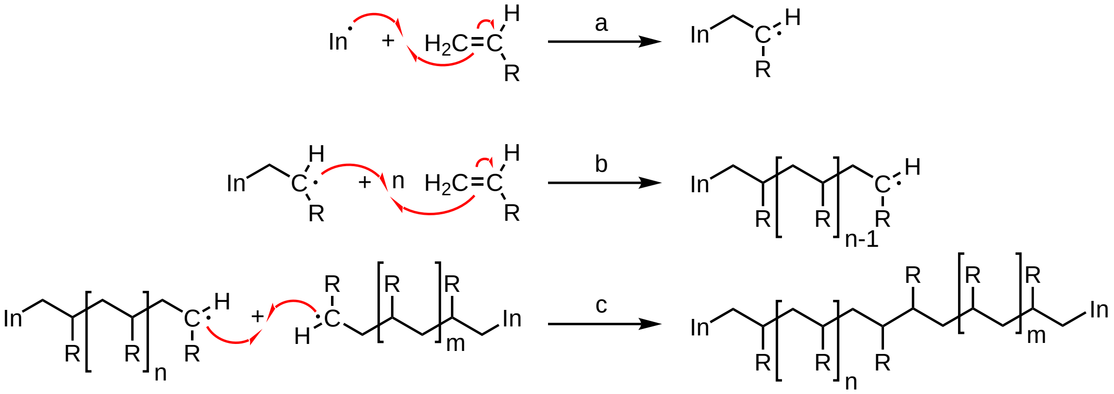

Scheme 1.1: Simplified mechanism of a radical polymerization reaction. **a:** Initiation by conventional initiator $In^{\bullet}$, **b:** chain growth reaction, **c:** recombination of two polymer radicals.

During an early stage of a polymerization reaction, termination reactions result in short polymer chains. In contrast, the recombination of two radicals at a later stage usually results in polymer chains which are strongly elongated compared to the average chain length. Together with late stage initiation, statistically distributed termination reactions increase the polydispersity (PD) and prevent the synthesis of defined polymer structures with precise molecular weights.[1] For a full completion of a polymerization reaction, the propagation reactions need to be at least 1000 times faster than the termination reactions.[1] Otherwise, only short-chained products with inferior properties will be received. The high reactivity of the radicals (lifetime $< 1\,\mathrm{s}$) results in low chemoselectivity. Side reactions, such as back-biting or chain transfer reactions can occur.[8] In summary, the RP limits the control over the molecular structure of polymers.

1.1.2. Controlled Radical Polymerization Methods

Controlled polymerization methods can be employed to produce highly precise polymeric structures. Some of these structures contain block co-polymers in which precise blocks of different monomers are combined in one single polymer molecule. This necessary precision cannot be easily achieved with free RP reactions. Due to termination and late stage initiation, the polymeric blocks suffer from broad molecular weight distribution.

Anionic "living" polymerization methods were long considered to be the only methods capable of producing well defined polymers with a low molecular weight distribution. The absence of termination reactions allowed superior control of the polymerization process.[5] Unfortunately, the reactions require an exceptional high purity of the chemicals and reaction vessels. Furthermore, absolutely dry and oxygen-free conditions are mandatory, dramatically increasing the costs of the obtained products. Finally, many functional groups, such as ester or alcohol groups are not tolerated.[5] Hence, methods that can produce polymers with similar precision from less pure chemicals with a broader variety of functional groups are of great interest.

Generally, radical reactions can be applied to monomers containing a great variety of functional groups and many different conditions have been described in the past. Hereby, protic reaction media such as alcohols or water can be used as well as most aprotic organic solvents.[5] The main challenge for controlled radical polymerization is the suppression of radical termination. The rate of radical termination reactions is proportional to the second order of the radical concentration $[\mathrm{R}^\bullet]$ (equation 1). Therefore, a change in radical concentration affects the recombination rate R_t quadratically. In contrast, the rate of chain propagation is directly proportional to the radical concentration (equation 2). As a consequence, a change in radical concentration results in a quadratic amplification of the termination rate R_t while influencing the polymerization rate R_p linearly. Although termination reactions cannot be eliminated completely, extensive reduction of the radical concentration can result in a decrease of termination reactions to a negligible degree. These reactions can be considered as controlled radical polymerization (CRP) reactions.[9]

$$R_t = \frac{\mathrm{d}[\mathrm{R}^\bullet]}{\mathrm{d}t} \propto -\, k_{term} \cdot [\mathrm{R}^\bullet]^2 \tag{1}$$

$$R_p \propto k_{obs} \cdot \mathrm{d}[\mathrm{R}^\bullet] \tag{2}$$

Over the last 20 years, the development of a variety of CRP methods provided attractive alternatives to living anionic polymerization reactions.[10] The incorporation of a fast dynamic equilibrium between active propagating radical species and their dormant counterparts is a very characteristic feature of most controlled polymerization methods (Scheme 1.2). The equilibrium which is usually shifted to the dormant side decreases the concentration of active radicals, resulting in a reduced termination rate. In modern CRP methods, termination reactions caused by recombination or disproportionation of radicals can be considered as negligible.[11]

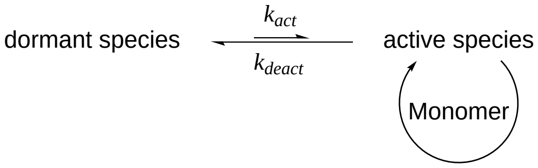

Scheme 1.2: The equilibrium between the active and dormant state of a radical.

During a conventional radical polymerization reaction, a radical lifetime is shorter than one second (Table 1.1). Within this period, an average polymer chain has reached its final chain length and has terminated. Further reactions of this chain only occur as side reactions of other polymer radicals present in the reaction mixture. Under controlled radical polymerization conditions, a radical can be deactivated within one millisecond. The reactivation can take one minute, increasing the lifespan of a polymeric reaction mixture to more than one day.[8,12]

Table 1.1: Transient and persistent radicals.[13,14]

	transient	**persistent**
simple name	reactive	stabilized
average half-life $\tau_{1,2}$	$< 1\,\mathrm{s}$	$> 1\,\mathrm{s}$
remarks	often alkyl or phenyl radicals, react rapidly	stabilized by electron-donating substituents, delocalization or steric hindrance

The dynamic equilibrium of a CRP reaction favors a uniform growth of all polymer chains. Through statistically distributed deactivation and reactivation all polymer chains grow with the same speed and the number of growing polymer chains remains constant. Beside the reduction in polydispersity, the increased chemoselectivity further reduces intermolecular side reactions, such as long chain branching. For further reduction of the polydispersity, all polymer chains need to be initiated simultaneously. For this purpose, the rate of initiation is required to be as high or higher than the rate of polymerization. Under ideal conditions, polymers with a polydispersity close to unity can be synthesized.[1]

Since the concentration of active radicals is held low by reaction of the free radicals with the deactivator, most polymer chains are capped with a specific functional group. This chain end functionality is present for all deactivated and non-terminated chains. Therefore, a reaction mixture can still be active after depletion or removal of monomers. This unique property allows further reactions, such as polymerization reactions with new monomers or other end group substitutions. This feature is sometimes falsely called "living polymerization", although this term applies for ionic polymerization reactions only.[1]

The increased lifespan of a CRP allows the preparation of very defined polymeric structures. Although most monomers used in CRP reactions are already used in radical polymerization reactions, the remaining chain end functionality during a CRP allows further reactions. After depletion or removal of monomers, addition of new monomers allows the reaction to continue. The previously homogeneous polymer chain composed of a hypothetical monomer A can then add to a different kind of monomer B forming A–B block co-polymers. This process can be repeated multiple times leading to A–B–A, A–B–A–B or periodically alternating block co-polymers. Aside from two periodically alternating monomer species, block co-polymers with multiple species such as A–B–C or A–B–C–A are accessible with CRP. In 2011, a A–B–C–D–A–B–C–D–A–B decablock co-polymer with four different types of monomer was reported.[15] In general, almost any combination of monomers is feasible.

Initiators which impose specific structural motifs, such as the four-pointed star motif of pentaerythritol tetrakis(2-bromoisobutyrate) (Figure 1.1) can be used to access polymers with precisely defined macromolecular architectures. In contrast, the use of similarly structured initiators during a conventional radical polymerization is less promising. Side reactions could alter the molecular structure, yielding polymers in which the specific structural motif is undesirably changed. With the correct choice of reaction conditions, a CRP reaction can yield an exceptionally broad range of polymeric architectures, making it an interesting tool for the synthesis of polymers with unusual properties.

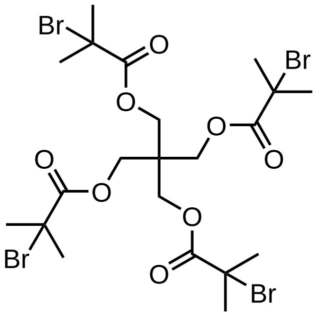

Figure 1.1: Pentaerythritol tetrakis(2-bromoisobutyrate) as tetra-functional ATRP initiator. For the ATRP mechanism see 1.2.

Currently, three major methods of CRP were described in the literature: atom transfer radical polymerization (ATRP), stable free radical polymerization (SFRP) and radical addition-fragmentation transfer (RAFT). While all of them are controlled radical polymerization methods with a radical buffer equilibrium, they differ in the mechanism of radical generation and in the type of species implementing the equilibrium. As seen in Scheme 1.3 and summarized in

Table 1.2 the CRP methods can be distinguished by their mechanistic characteristics.[5]

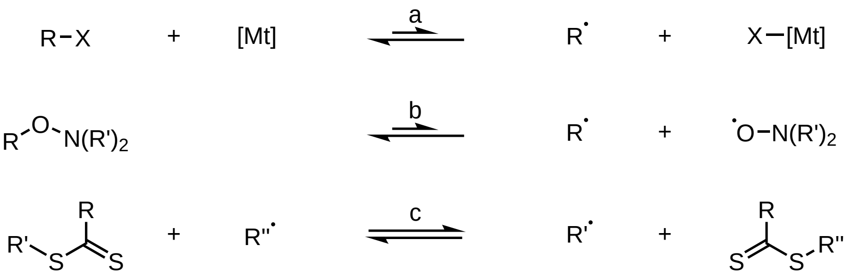

Scheme 1.3: Simplified mechanisms of the equilibria implemented in different CRP methods, **a:** ATRP, **b:** SFRP, **c:** RAFT. More details in Scheme 1.4, Scheme 1.5 and Scheme 1.6

In ATRP, radicals are generally formed by an inner sphere electron transfer (ISET) reaction. During activation, a transition metal catalyst reacts with an alkyl (pseudo-)halide and transfers an electron. As a result, a free radical is formed and the halide coordinates to the catalyst (Scheme 1.6) which is oxidized. In a polymerization reaction, the free radical can react with the present monomers via a radical addition reaction thereby starting the polymerization reaction. In literature, most ATRP reactions use Cu^{I} catalysts as activators (Figure 1.2).[16] The equilibrium is established by the reverse reaction of the Cu^{II} complex with the radical chain regenerating the activator complex and an alkyl halide.[5]

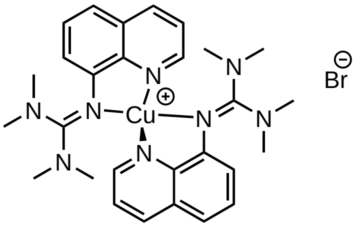

Figure 1.2: Copper bromide complex of di(1,1,3,3-tetramethyl-2-(quinolin-8-yl)guanidine) (TMGqu CuBr), an ATRP catalyst.[16,17]

In SFRP, the activation reaction mainly consists of a thermal decomposition reaction of an SFRP initiator. As a result, both transient alkyl radicals and persistent radicals are formed (Table 1.1). The decomposition products form an equilibrium with the starting material. Analogous to ATRP reactions, the persistent radical is considered as the deactivator. The free radical can undergo radical polymerization reactions. Predominantly, SFRP is conducted with nitroxides as deactivators and is then called nitroxide mediated polymerization, (NMP, Scheme 1.4).[5]

The third CRP method, RAFT, has major mechanistic differences to ATRP and SFRP. The radical initiation is conducted analogous to conventional radical polymerization protocols. However, a radical trapping agent such as cumyl dithiobenzoate (Scheme 1.5) can add to free radicals and form a stable radical. The trapping agent or chain transfer agent forms a labile end group with the growing polymer chain, which can undergo cleavage and release the original or a cumyl radical. In the latter case the chain transfer agent can add to a second growing polymer chain

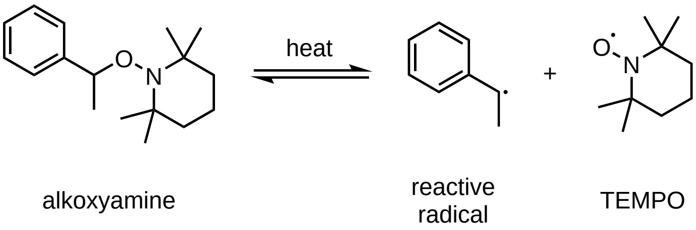

Scheme 1.4: 2,2,6,6-Tetramethyl-1-piperidinoxyl (TEMPO) as a stable free radical in SFRP.[5]

and form another labile intermediate. Upon cleavage, one of the polymer chains can undergo further polymerization reactions. The concentration and choice of chain transfer agents has a crucial influence on the polymerization kinetics. As a major difference to ATRP and SFRP, the chain transfer agent only distributes the probability of propagation evenly between the growing chains and it usually does not retard the polymerization rate.[5]

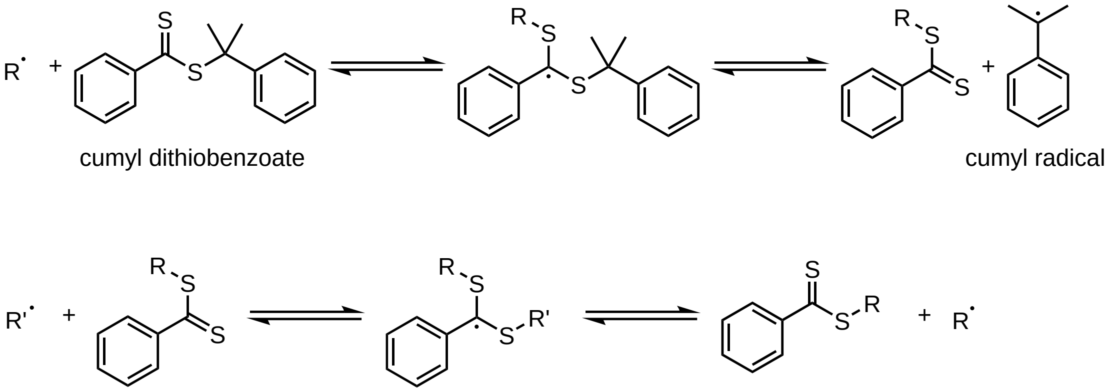

Scheme 1.5: Cumyl dithiobenzoate as chain transfer agent in RAFT-polymerization.[5]

Table 1.2: Major differences between ATRP, SFRP and RAFT.

	Initiation	**Equilibrium**
ATRP	ISET from a metal catalyst to a carbon-halogen bond	Redox equilibrium between the catalyst's lower oxidation state with an alkyl halide and the upper oxidation state with a free radical
SFRP	Initiator thermally decomposes to a transient and a persistent radical	Homolysis equilibrium between a radical chain with a persistent radical deactivator and the recombination product thereof
RAFT	Conventional radical initiator	The propagation probability of the growing polymer chains is distributed evenly by a chain transfer agent

1.2. Atom Transfer Radical Polymerization

Since its simultaneous discovery by the groups of Matyjaszewski[9] and Sawamoto[18] in 1995, ATRP has become the most widely used CRP method.[a] The method appeals with a simple experimental setup and mild reaction conditions. A broad variety of monomers with different functional groups is tolerated. Protocols for the use of monomers from renewable sources, such as rosin acid derivatives or plant oils have been developed.[12] Multi-site initiators or macromonomers can be applied to access unique polymer topologies, such as stars, networks, or brush like polymer grafts (Scheme 1.6).

The range of ATRP applications is quite versatile. ATRP derived polyacrylonitrile-block-poly(*n*-butyl acrylate) has been used for the synthesis of nitrogen-enriched porous carbon materials.[19] Acrylated alkyds, polyesters with fatty acid side chains, that exhibit autooxidative curing have been prepared by ATRP for improved outdoor paints.[20] Many products for surface treatment, such as self-cleaning membranes with photoresponsive side groups[21], different covalently bound polymer coatings[22] of which some exhibit improved antifouling properties[23] or grafted quarternized agarose co-polymers with antimicrobial activity[24] are accessable through ATRP. Cu_7S_4 nanoparticles were coated with specific photothermo-responsive polymers that could be used for chemo- or photothermo-therapy.[25] A highly optimized ATRP procedure utilizing dopamine-based initiators and sodium methacrylate was used to cover living yeast cells with a protective layer of poly(sodium methacrylate) creating living cell-polymer hybrid structures.[26]

In recent years, many procedures have been developed to incorporate renewable carbon sources into polymers. In most ATRP processes using renewable sources, plant oils, lignin, rosin acid and their derivatives have been reacted to acrylate esters before polymerization.[27–31] As a second major branch, polymers have been grafted onto cellulose backbones. Beside crude oil based polymers such as polystyrene[32,33], also fatty acid or furfural-methacrylate esters have been employed.[34] Polymers from naturally abundant monomers that do not need any further modifications prior to polymerization are rarely found in the literature. As a rare exception for plant based monomers, Tulipalin A (α-methylene-γ-butyrolactone), was directly polymerized under standard ATRP conditions.[35] In another remarkable experiment, macroscopic pieces of wood have been used as scaffolds for surface-initiated ATRP of polystyrene or poly(*N*-isopropylacrylamide). Through previous treatment with an initiator, the polymer chains were introduced deep into the pores inside the wood cell walls.[36]

The catalysts used in common ATRP methods are composed of a metal ion center, usually copper$^{I/II}$ or iron$^{II/III}$ which is coordinated by electron-donating ligands.[12,37] The ligands have a great influence on the properties of the metal complex. The choice of electron-rich ligands can lead to an increased electron density at the metal ion center and therefore alter reaction

---

[a] Scifinder search terms "atom transfer radical polymerization", "stable free radical polymerization", "nitroxide-mediated polymerization" and "reversible addition-fragmentation chain transfer". Accessed on October 24, 2017.

parameters dramatically.[38] Accordingly, electron-deficient ligands can reduce the electron density and have reverse effects. In an idealized model, however, the catalyst's activity does not affect the polymer topology. It certainly influences the reaction dynamics, but under negligible termination conditions, the structural parameters of the polymer are not affected.

In ATRP, the polymerization is started by the reaction of the catalyst with an initiator. The initiator bears one or more functional groups that can be activated by the catalyst. During this process, the polymerization reaction is started and the initiator molecule remains bound to that particular end of the growing polymer chain. Hence, the structural parameters of the initiator are still present in the final product. Most commercially available initiators contain carbon halogen bonds in close proximity to radical stabilizing groups. These bonds can be cleaved during activation by the catalyst. An initiator bearing multiple initiation sites can lead to the formation of multiple polymer chains that are all connected. The resulting polymer topology is considered as a star architecture (Scheme 1.6). Initiators which contain double bonds can form polymer networks or cyclic topologies. Initiators carrying functional groups that are inert under the polymerization conditions can be modified after the polymerization reaction. For example, the common acrylate derivative methyl 2-bromo-2-methylpropionate (MBriB Figure 1.3), contains an ester functionality which can undergo saponification or other substitution reactions. Many initiators with different functional groups are commercially available. After a polymerization reaction, the implementation of more sophisticated structures like DNA-strands or proteins is feasible. The diverse functionality of initiators can also be used to attach the initiator to other molecules or macroscopic surfaces before polymerization. A unique ATRP method called surface-initiated-ATRP (SI-ATRP) was optimized for this purpose.[1,22]

The ATRP method represents a tool for the synthesis of very well defined polymer structures with a vast majority of substrates. Under optimized conditions, polymerization reactions with low concentrations of non-toxic catalysts and monomers from renewable sources contribute in making ATRP a sustainable polymerization method.[1,12]

1.2.1. Mechanism, Kinetics, Constants

During an ATRP process, many individual reactions have to be considered. The catalyst's equilibrium is established through an activation and a deactivation reaction. The active radicals can undergo radical addition reactions or can follow different paths of termination reactions (Scheme 1.6). In some processes, disproportionation and comproportionation reactions of the catalysts also seem to be possible.

The equilibrium of copper-mediated ATRP is established by a dormant alkyl halide and a Cu^{I} *activator* complex (A) which are opposed by the active radical species and a Cu^{II} *deactivator* complex (D). The copper complexes used for ATRP, usually consist of a copper center and organic ligands with nitrogen atoms as donating species. Some complexes have additional

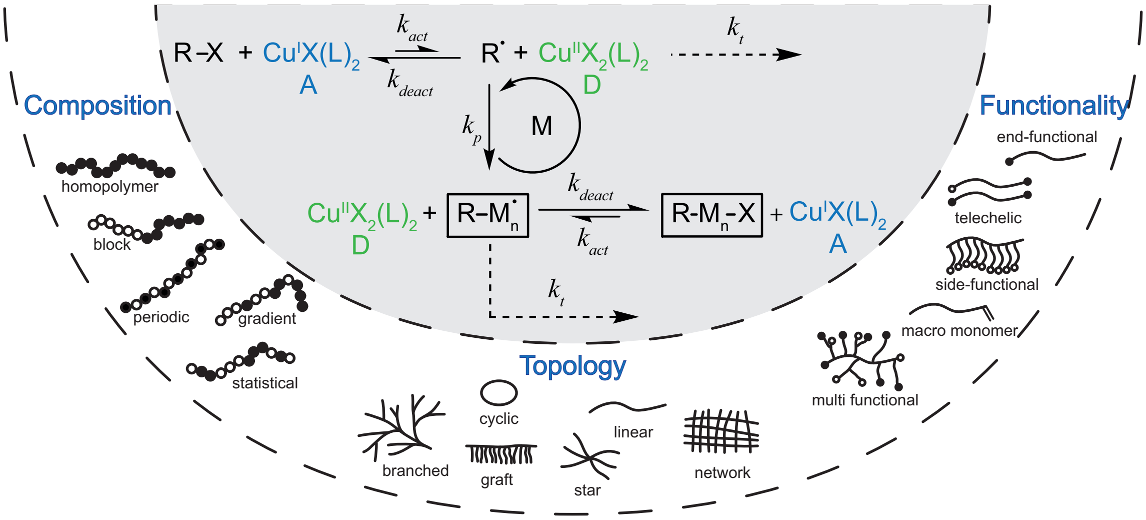

Scheme 1.6: Simplified mechanism of an arbitrary ATRP reaction including the ATRP equilibrium (k_{act}, k_{deact}), radical propagation (k_p) and termination reactions (k_t). A: activator, D: deactivator complex. In an ATRP, the composition, topology and functionality of a polymer can be prepared precisely. Adapted from Matyjaszewski and Tsarevsky.[1]

halide ligands directly coordinating to the metal center. The organic ligands lead to an enhanced solubility of the metal ion and alter its structural parameters, such as its coordination sphere or reduction potential. In the activation reaction, the alkyl halide (R−X) undergoes a SET with the Cu^I complex. During homolysis, the alkyl halide forms a radical ($R^\bullet$) the resulting halide coordinates to the catalyst, which is is oxidized to a Cu^{II} species. The radical can then undergo addition reactions to monomers (M) and participate in chain propagation or react in a reverse reaction with the deactivator complex. The latter reaction regenerates the Cu^I catalyst and an alkyl halide. The (de)activation processes are considered to follow an *inner sphere electron transfer* (ISET) mechanism. Generally, any existing radical can be trapped by the deactivator complex and reach a dormant state.[1,39–41]

The equilibrium of the ATRP process can be described by its law of mass action (equation 3). Its thermodynamic equilibrium constant K_{ATRP} is a material property of the catalytic system under the respective conditions. Furthermore, it can be derived from the equilibrium's forward and reverse reaction rate constants k_{act} and k_{deact}. Mechanistically, the activation and deactivation reactions are composed of four elemental reactions and their reverse reactions, respectively. As seen in the equation set 4, the four elementary reactions divide into the electron transfer reaction (K_{ET}), the halide transfer reaction (K_X), the electron affinity of the halide (K_{EA}) and the bond dissociation reaction (K_{BD}).[5]

$$K_{ATRP} = \frac{k_{act}}{k_{deact}} = \frac{[\mathrm{R}^\bullet][\mathrm{X{-}Mt}^{z+1}\mathrm{L}_m]}{[\mathrm{R{-}X}][\mathrm{Mt}^z\mathrm{L}_m]} \tag{3}$$

$\mathrm{Mt}^z\mathrm{L}_m$: metal complex with oxidation state z and ligand L, $\mathrm{R}^\bullet$: any chain radical, R–X: dormant polymer chain.

$$\begin{aligned} \mathrm{Mt}^z\mathrm{L}_m &\xrightleftharpoons{K_{ET}} \mathrm{Mt}^{z+1}{\mathrm{L}_m}^+ + \mathrm{e}^- \\ \mathrm{X}^- + \mathrm{Mt}^{z+1}{\mathrm{L}_m}^+ &\xrightleftharpoons{K_X} \mathrm{X{-}Mt}^{z+1}\mathrm{L}_m \\ \mathrm{X}^\bullet + \mathrm{e}^- &\xrightleftharpoons{K_{EA}} \mathrm{X}^- \\ \mathrm{R{-}X} &\xrightleftharpoons{K_{BD}} \mathrm{R}^\bullet + \mathrm{X}^\bullet \\ K_{ATRP} &= K_{ET}K_XK_{EA}K_{BD} \end{aligned} \tag{4}$$

In any radical polymerization reaction, the polymerization rate depends on many factors. The experimental conditions, such as temperature, solvents, pressure or choice of monomers are as important as the concentrations of the relevant species. The mathematical rate expression (equation 5) incorporates all of these factors in one term. The rate constant of chain propagation k_p is dependent on all experimental conditions, however, it does not include any concentration dependencies. In controlled radical polymerization reactions, the radical equilibrium concentration can be derived from the mass action law. For an ATRP reaction, this can be expressed as in the last term of equation 5. In this expression the dependencies of the polymerization rate on the growing chain concentration as well as the catalyst's equilibrium concentrations are noticeable.[5]

$$R_p = k_p[\mathrm{M}][\mathrm{R}^\bullet] = k_p[\mathrm{M}]K_{ATRP}\frac{[\mathrm{R{-}X}][\mathrm{Mt}^z\mathrm{L}_m]}{[\mathrm{X{-}Mt}^{z+1}\mathrm{L}_m]} \tag{5}$$

From a different perspective, the rate of polymerization can also be seen as the rate of monomer consumption (equation 6). After comparison with equation 5 and further transformations (equation 7) a linear dependency of the natural logarithm of the monomer concentration and the reaction time can be identified (equation 8). This linear relation is a key feature in the analysis of controlled polymerization reactions. If the consumption of monomers during a polymerization experiment does not follow this kinetic behavior, it is not to be considered as a completely controlled polymerization reaction.

$$R_p = -\frac{d[\mathrm{M}]}{dt} \tag{6}$$

$$\ln\left(\frac{[\mathrm{M}]_0}{[\mathrm{M}]}\right) = k_pK_{ATRP}\frac{[\mathrm{R{-}X}][\mathrm{Mt}^z\mathrm{L}_m]}{[\mathrm{X{-}Mt}^{z+1}\mathrm{L}_m]}t \tag{7}$$

$$\ln\left(\frac{[\mathrm{M}]_0}{[\mathrm{M}]}\right) = k_p[\mathrm{R}^\bullet]t \tag{8}$$

The degree of control of an ATRP reaction can be derived from its kinetic parameters as seen above. However, in the final polymer product a second major property gives insight into the polymerization process. The polydispersity which describes the broadness of the molecular mass distribution is considered as a key parameter of the final product. During the reaction, the evolution of the polydispersity of the polymer depends on a few reaction parameters. As seen in equation 9, the polydispersity PD depends on the degree of polymerization $\mathrm{DP_n}$ and the conversion C (in 100%) as factors of reaction progress. Furthermore, the reaction conditions, such as the choice of monomers, temperature and pressure account for the propagation rate constant k_p. The choice of catalyst and the concentration thereof influence the deactivation rate constant k_{deact} as well as the deactivator concentration $[\mathrm{X{-}Cu^{II}L}_m]$. The original initiator concentration $[\mathrm{R{-}X}]_0$ accounts for the number of growing chains during the reaction.

In a perfectly controlled polymerization reaction, all polymer chains would have the same molecular mass and the polydispersity would reach a value of $\mathrm{PD} = 1$. As depicted in equation 9, fast deactivation as intrinsic property of the catalyst (k_{deact}) or as a result of a large deactivator concentration improves polydispersity. Furthermore, a small polymerization rate constant k_p also decreases the final polymer mass deviations. As a result, one can argue that slower polymerization and improved deactivation distribute the probability of chain propagation more evenly over the bulk of growing chains. Additionally, a decrease in the number of growing chains is helpful. In summary, the key to controlled radical polymerization is a low radical concentration.

$$\mathrm{PD} = \frac{\mathrm{M_w}}{\mathrm{M_n}} = 1 + \frac{1}{\mathrm{DP_n}} + \left(\frac{k_p[\mathrm{R{-}X}]_0}{k_{deact}[\mathrm{X{-}Cu^{II}L}_m]}\right)\left(\frac{2}{C} - 1\right) \tag{9}$$

$\mathrm{M_w}$: mass average molecular mass, $\mathrm{M_n}$: number average molecular mass.[1]

The value of K_{ATRP} only predicts the outcome of a ATRP to a limited degree. As seen in equation 3, the material property does affect the radical concentration, however, the reaction conditions play a vital role. Therefore, the K_{ATRP} value rather directs to the amount of catalyst and initiator that is required to obtain an optimal radical concentration. Also, the properties of the product, such as targeted polydispersity and final chain length, have to be taken into consideration. As a consequence, the choice of catalyst and the concentration thereof need to be carefully selected.

In practice, the value of K_{ATRP} is impacted by the bond dissociation energy of the C−X bond, the heterolytic cleavage energy of the $\mathrm{Cu^{II}{-}X}$ bond (*halidophilicity*, $\mathrm{X^-} + [\mathrm{Cu^{II}L}_m]^{2+} \rightleftharpoons [\mathrm{X{-}Cu^{II}L}_m]^{+}$), all solvation energies of the individual species and by the reduction potential $E_{1/2}$ of the $\mathrm{Cu^I}$ complex (equation 10).[40,41]

$$\ln\left(K_{ATRP}\right) \propto E_{1/2} \tag{10}$$

Under the same conditions, the natural logarithm of K_{ATRP} values of different complexes show linear correlations with their respective $E_{1/2}$ values (equation 10), provided that the halidophilicity of the complexes stay constant. This holds true for most of the neutral nitrogen-based ligands commonly used in ATRP reactions. A similar linear correlation can be found for the K_{ATRP} values of complexes and the ratio of their respective complex stability constants β^{I} and β^{II} (β^{I} for $\mathrm{Cu^{I}} + m\,\mathrm{L} \rightleftharpoons \mathrm{Cu^{I}L}_m$ and β^{II}, respectively) as seen in equation 11.[40,41]

$$K_{ATRP} \propto \frac{\beta^{II}}{\beta^{I}} \tag{11}$$

In the case of stable complexes with an equal metal to ligand ratio, the ratio of stability constants can directly be calculated from the standard reduction potentials of ligated copper complexes and the redox couple without ligand (equation 12)

$$\ln \frac{\beta^{II}}{\beta^{I}} = \frac{F}{RT}\left(E^{\ominus\prime}_{\mathrm{Cu^{II}/Cu^{I}}} - E^{\ominus\prime}_{\mathrm{Cu^{II}L/Cu^{I}L}}\right) \tag{12}$$

Furthermore, the ratio $\beta^{II}/(\beta^{I})^2$ can be obtained from catalyst disproportionation studies in the reaction $2\,\mathrm{Cu^{I}L} \rightleftharpoons \mathrm{Cu^{0}} + \mathrm{Cu^{II}L} + \mathrm{L}$. Omitting the concentration of solid $\mathrm{Cu^{0}}$, the equilibrium constant for disproportionation $K_{disp,\mathrm{CuL}}$ can be expressed as in equation 13. Along with the stability constants of the complexes ($\mathrm{Cu}^{n} + \mathrm{L} \rightleftharpoons \mathrm{Cu}^{n}\mathrm{L}$, n=I or II) as seen in equation 14, the disproportionation constant of ligated copper atoms can be expressed as in equation 15.[40,41]

$$K_{disp,\mathrm{CuL}} = \frac{[\mathrm{Cu^{II}L}][\mathrm{L}]}{[\mathrm{Cu^{I}L}]^2} \tag{13}$$

$$\beta^{n} = \frac{[\mathrm{Cu}^{n}\mathrm{L}]}{[\mathrm{Cu}^{n}][\mathrm{L}]} \tag{14}$$

$$K_{disp,\mathrm{CuL}} = \frac{\beta^{II}[\mathrm{Cu^{II}}]}{(\beta^{I})^2[\mathrm{Cu^{I}}]^2} = \frac{\beta^{II}}{(\beta^{I})^2}K_{disp,\mathrm{Cu}} \tag{15}$$

Finally, values of the individual stability constants can be obtained from rearranging equation 15 to yield the ratio of $\beta^{II}/(\beta^{I})^2$ and comparing the result with the values from equation 12.[40,41]

In practice, the disproportionation equilibrium constant can be measured by UV/Vis spectroscopy of the forward or reverse reaction. The specific target wavelength certainly depends on the catalyst's absorption spectra. However, the UV/Vis relevant d–d excitations of a $\mathrm{Cu^{II}}$ complex usually lie between 800 nm and 1100 nm.[17]

In determination of ATRP kinetics and thermodynamics, irreversible termination reactions can often be neglected. Nevertheless, during longer polymerization reactions irreversibly terminated polymer chains accumulate. An irreversibly terminated chain does not bear any functionality that can undergo further polymerization. Therefore, the relative amount of irreversibly terminated chains [T] is called dead chain fraction (DCF). Chain termination can occur through two major processes: disproportionation (Scheme 1.7) or recombination (Scheme 1.1**c**) reactions. For simplification, the small decrease in the total chain concentration $[\mathsf{R{-}X}]_0$ caused by bimolecular recombination reactions is neglected.[11] The initial concentration of growing chains depends on the targeted degree of polymerization at full conversion $\mathsf{DP}_{\mathsf{n,targ}}$. Therefore, the only two practical options for decreasing the amount of terminated chains lie in the deceleration of the polymerization reaction (increases t) and in finishing the reaction at low conversion rates C, as depicted in equation 16.

$$\begin{aligned}\mathsf{DCF} &\equiv \frac{[\mathsf{T}]}{[\mathsf{R{-}X}]_0}\\ &= \frac{2k_t\mathsf{DP}_{\mathsf{n,targ}}(\ln(1-\mathsf{C}))^2}{[\mathsf{M}]_0{k_p}^2t}\\ &= \frac{2k_t(\ln(1-C))^2}{[\mathsf{R{-}X}]_0{k_p}^2t}\end{aligned} \tag{16}$$

k_t: rate constant of termination reactions, $[\mathsf{M}]_0$: initial concentration of monomers, t: reaction time.

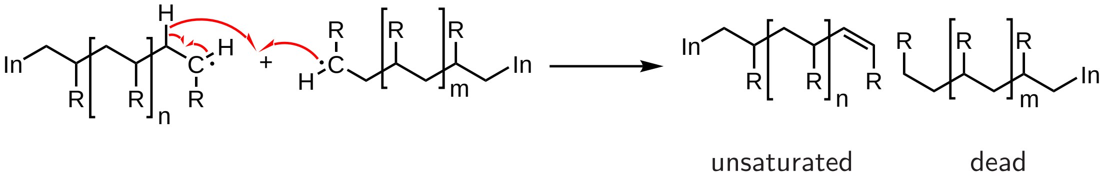

Scheme 1.7: Irreversible termination of active chains by a radical disproportionation reaction.

The electron transfer mechanism during an ATRP process has been under dispute for some time. ATRP reactions with metallic Cu^0 that showed unexpected behavior resulted in the proposal of an outer sphere electron transfer (OSET) mechanism which was called single-electron-transfer living radical polymerization (SET-LRP) by the group of Percec in 2006.[42] As seen in Scheme 1.8, the proposed SET-LRP mechanism for activation involves Cu^0 species that react with alkyl halides and form Cu^{I} complexes. The latter disproportionate to Cu^0 and $\mathsf{Cu}^{\mathsf{II}}$ species. The $\mathsf{Cu}^{\mathsf{II}}$ complexes are then able to deactivate the growing radical chains and therefore impose controlled conditions. In contrast, SARA ATRP is related to the standard ATRP process, however additional Cu^0 metal acts as a supplemental activator and reducing agent (SARA). During SARA ATRP, Cu^0 is able to activate alkyl halides and undergoes further comproportionation reactions with the $\mathsf{Cu}^{\mathsf{II}}$ complex, regenerating the Cu^{I} species. In comparison, SET-LRP relies on rapid disproportionation of the Cu^I species, whereas SARA ATRP assumes slow rates of comproportionation and disproportionation accompanied by much faster activation through Cu^I species.[43]

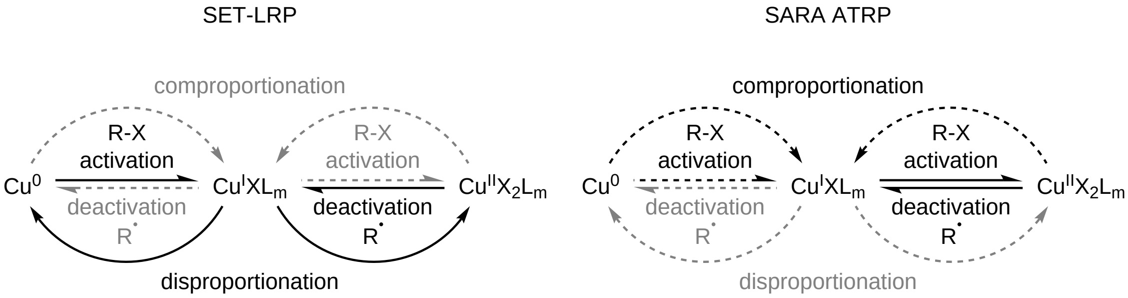

Scheme 1.8: Proposed mechanisms for SET-LRP (left) and SARA ATRP (right).[1]

For clarification of this aspect, numerous studies were conducted, mostly confirming the SARA ATRP mechanism, rendering ISET as the main contributor to alkyl halide activation. The studies included electrochemical experiments,[44–48] respective simulations[46,49] and methods of computational chemistry.[44,50] In additional studies on disproportionation and comproportionation equilibria, in most organic solvents comproportionation was favored over disproportionation. In many cases where disproportionation was favored, the use of ligands reversed this behavior. This even held true in dimethylsulfoxide (DMSO) where disproportionation is otherwise strongly favored.[51,52] With the ligand tris[2-(dimethylamino)ethyl]amine (Me_6TREN) which was also used in the studies of the Percec group mentioned above, mostly comproportionation was observed.[43] However, small amounts of Cu^0 were present, explaining the visually detectable Cu^0 precipitate in some experiments.[43,53] Further studies implied that the activation of an alkyl halide by ISET should be around nine magnitudes faster than by OSET. Comparison of reaction parameters using the activation coefficients of OSET activation evidently exhibits the strong deviation to experimental results.[44,54,55] Finally, ATRP experiments conducted in water, where disproportionation is generally favored, revealed that it only plays a minor role. Due to exceptionally high K_{ATRP} values in water, a low catalyst concentration was used, essentially suppressing bimolecular disproportionation reactions.[56,57]

1.2.2. The Effects of Initiators, Ligands and Solvents on the Value of K_{ATRP}

The value of the ATRP equilibrium constant K_{ATRP} depends on a variety of factors, as mentioned above. Important parameters are for example the bond dissociation energy (BDE) required for the homolysis of the C−X bond of the initiator as well as the bond strength of the Cu−X bond. Moreover, the equilibrium constant depends on the reduction potential of the Cu^I species which is strongly related to the donor capabilities of the ligands. Solvation energies that depend on the choice of solvents and ligand design features also affect K_{ATRP}.[1]

The initiator's impact on K_{ATRP} is derived from two major criteria. First, an increased stabilization of the radical species tremendously increases the value of K_{ATRP}. Second, the choice of halogen that is bound to the initiator plays a vital role. The radical stabilization is influenced by two properties of the initiator: first, the degree of substitution at the specific carbon atom and second, the use of radical stabilizing groups. The installation of a methyl group at the respective carbon atom, for example, increases the K_{ATRP} value by one to two orders of magnitude (Figure 1.3a) due to increased steric repulsion and radical stabilization by hyperconjugation.[58] The appropriate choice of radical stabilizing substituents can change the equilibrium constant by more than five orders of magnitude through delocalization (Figure 1.3b). Substituents with aryl, ester or nitrile groups exhibit a pronounced effect.[58] The selection of the halogen atoms as substituents affects both the BDE of the C−X bond and the Cu−X bond strength. Although the BDE decreases in the order C−Cl $>$ C−Br $>$ C−I, the K_{ATRP} value for iodine substituted initiators is exceptionally low (Figure 1.3c). This can be referred to the weak Cu−I bond, which leads to a reduced stabilization of the Cu^{II} complex.[59] Furthermore, the C−I bond is prone to bond heterolysis, which results in a range of side reactions.[60,61]

Generally, fast and complete initiation of an ATRP reaction is required for an even growth of polymer chains. Hence, the initiation reaction must be as fast or faster as the propagation reaction ($k_{act} > k_p$).[1]

The properties of ligands used for ATRP catalysts have extraordinarily strong effects on the ATRP equilibrium constant (Figure 1.4). Nine orders of magnitude difference of K_{ATRP} values between very slow and very fast ATRP catalysts demonstrate the importance of careful ligand design. In comparison to the influence of initiators or solvents (Figure 1.3 and Figure 1.5), the significance of a proper choice of ligand cannot be stressed enough.

Most of the catalyst properties discussed in the previous section (section 1.2.1) are derived from interactions of the copper ion centers with the ligands. As seen in equation 11, the stability constants of the complexes are of great importance. Therefore, chelating ligands with higher denticity are generally favored. Furthermore, the reduction potential of the $Cu^{II}L_m/Cu^{I}L_m$ couple (equation 10) as well as the affinity of the Cu^{II} complex toward the halide anion (Figure 1.3) need to be considered.[41,59,62] Electron-rich ligands with strong donor abilities increase the electron density at the copper center and thus stabilize Cu^{II} complexes. This leads to a more negative reduction potential and to a shift of the thermodynamic equilibrium toward increased polymerization activity. In summary, complexes with low reduction potentials, stabilized higher oxidation states and strong Cu^{II}−X bonds, result in larger ATRP equilibrium constants. These requirements can be fulfilled by copper complexes with N-donor ligands.[38,63]

In addition to these electronic effects, precisely tuned coordination angles and strain imposed on the metal center can have a large effect on the catalyst activity. Due to a general relation of orbitals and coordination geometry, electronic properties of coordination compounds can also be altered by steric strain. Despite structural similarities between the coordinating nitrogen atoms

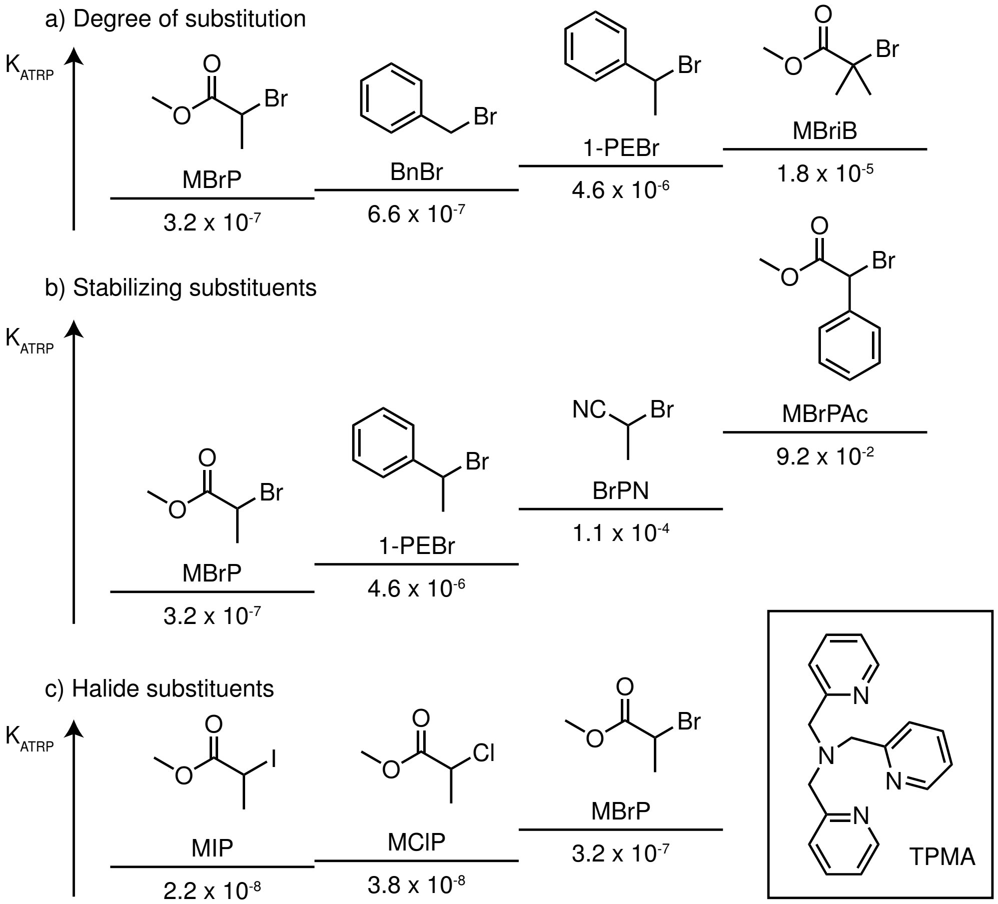

Figure 1.3: K_{ATRP} values for the initiation reaction. Effects of the initiator species, for the reaction with the Cu^{I} complex of tris(2-pyridylmethyl)amine (TPMA) in acetonitrile at 22 °C.[59]

in the ligands N3[2,3,2], HMTETA, Me_6TREN and DMCBCy (Figure 1.4), exceptionally large differences in K_{ATRP} values are revealed upon comparison. For this class of aliphatic amine-type ligands, the linker between the donor atoms accounts for the major part of the coordinative strain. Except for DMCBCy, the series of ligands with different linkers between two adjacent coordinating atoms exhibits considerably increased catalytic activity for ligands with C_2 bridges between the two atoms. In the case of DMCBCy, the specific strain and the coordination angles imposed on the copper center by the tetradentate ligand yield an exceptionally active catalyst without the incorporation of particular strong donor substituents.[64] In conclusion, the sole activity of DMCBCy relies on its very restrictive strain that results in optimal conditions for ATRP.[1] Combining steric and electronic properties, it appears comprehensible that the dimethyl cross-bridged cyclam (DMCBCy) and the electron rich tetradentate ligand tris[2-(3,5-dimethyl-4-methoxy)pyridylmethyl]amine (TPMA*) form the most active ATRP catalysts (Figure 1.4).[63]

The solvation of the catalyst in different solvents has an influence on different factors, such as the redox potential of the activator-deactivator pair, the electron affinity of the transferable halogen atom, and the Cu^{II} halidophilicity. The physical base of solvent effects rests in the com-

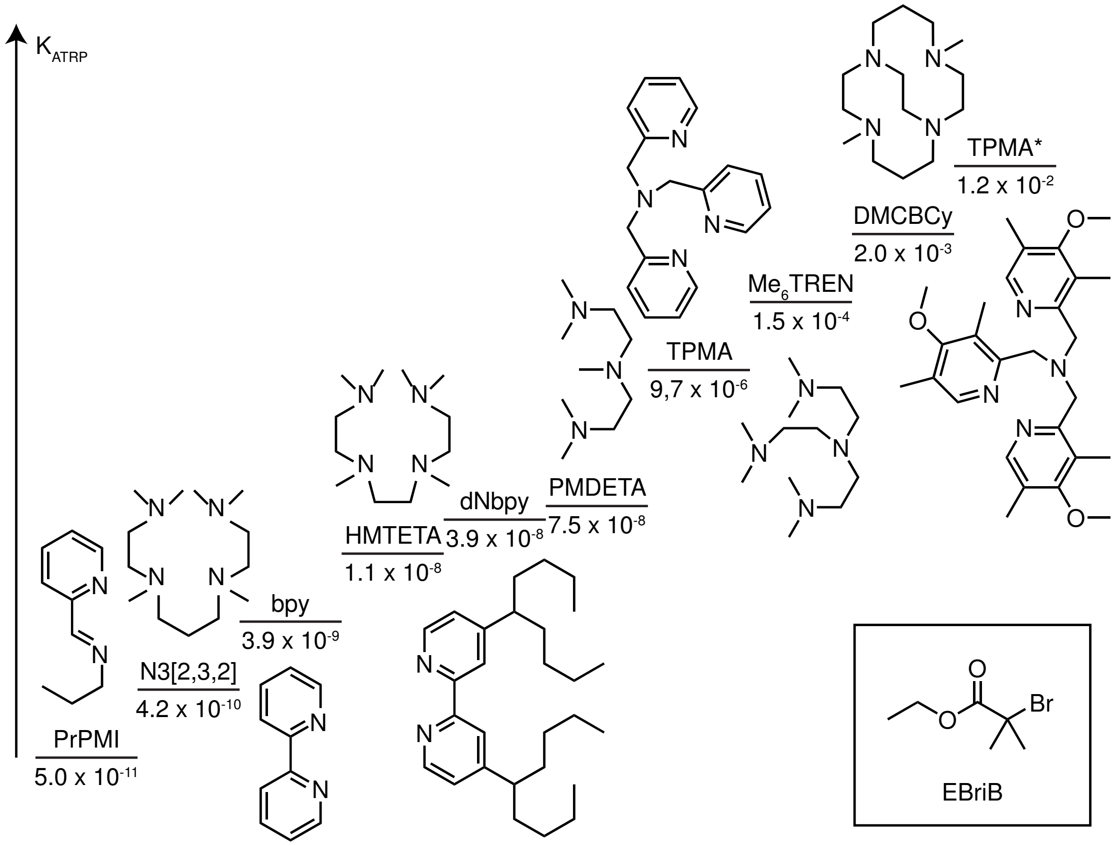

Figure 1.4: K_{ATRP} values of copper complexes with different ligands for the reaction between ethyl 2-bromoisobutyrate (EBriB) and Cu^{I} complexes in acetonitrile at 22 °C.[1,59,63]

plex stability constants which essentially depends on the solvation of all individual components of a catalytic system. As illustrated in Figure 1.5, the K_{ATRP} values rise with increasing dipole moments of the aprotic solvents. For protic solvents, however, dissociation of the deactivator is observed. The loss of a halogen anion results in a decrease of the deactivator concentration. In a 1:1 mixture of water and methanol, for example, the deactivator complex [Cu^{II}(bpy)$_2$Br]$^+$ is dissociated by 79%.[62] Therefore, in protic solvents, such as water or methanol unusually large K_{ATRP} values are being noticed.

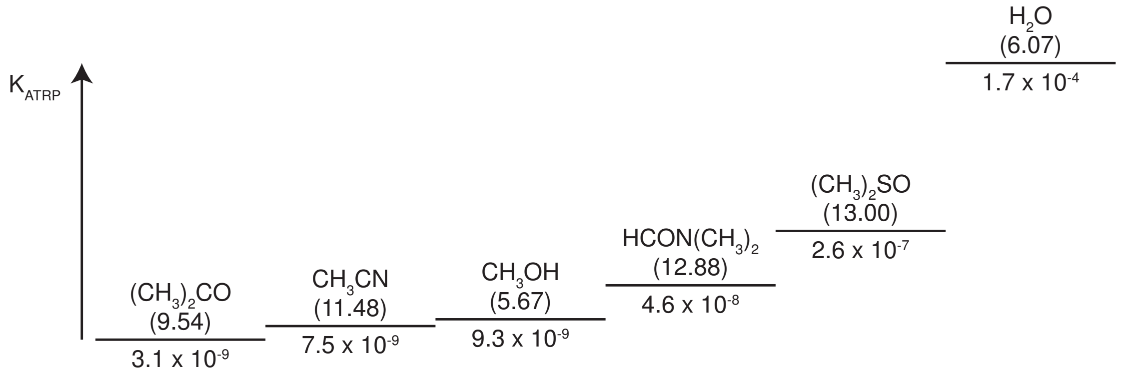

Figure 1.5: Effects of the solvents (dipole moments in 10^{-30} C m)[65] on the K_{ATRP} value for the reaction between ethyl 2-bromoisobutyrate (EBriB) and the Cu^{I} complex with HMTETA (Figure 1.4) at 25 °C.[66]

1.3. Guanidine-Metal Complexes

1.3.1. The Guanidine Moiety

The guanidine moiety is composed of a characteristic CN_3 unit. It can be described by a centering carbon atom connected to three nitrogen atoms. For neutral guanidines, two of the latter are amine-type nitrogen atoms whereas the third is usually considered an imine-type nitrogen atom. This nitrogen analog of carbonic acid can be easily protonated and stabilizes the positive charge through delocalization (Scheme 1.9).[67] Beside proton sponges, which need two or more substituted amino groups in close proximity, guanidines are regarded as the strongest neutral organic bases ($pK_a = 28.5$ (DMSO) for the unsubstituted guanidine).[68–70] Since most guanidine superbases are sterically unhindered, their high basicity translates into a proper nucleophilicity. With five positions applicable for diversification, neutral guanidines are used as *N*-donor ligands in coordination chemistry for a multitude of purposes.

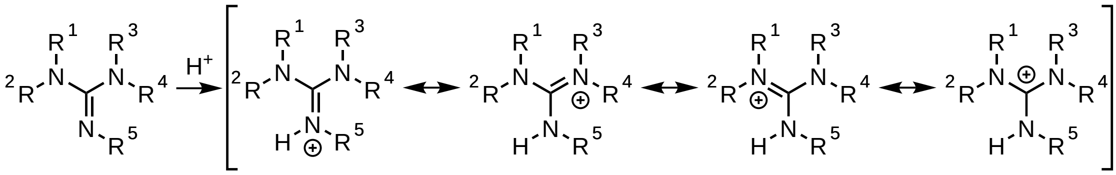

Scheme 1.9: Protonation of an arbitrary guanidine and the delocalization of the positive charge on the guanidinium cation.

Exclusively organic guanidine derivatives have been used in chemical industry in the last decades. During the last century, cyanoguanidine was used for the synthesis of melamine which was further processed to hard, thermosetting melamine resins. More recently, guanidine derivatives were used in symmetric and asymmetric organocatalysis[71] and the use of peralkylated guanidinium salts as environmentally friendly ionic liquids is under investigation.[72]

Generally, guanidines are synthesized from tetra *N*-alkylated chloroformamidinium chlorides which are derived from urea. The two commonly employed chlorination and deoxygenation conditions are the reaction of urea with either phosgene[17,72,73] or oxalyl chloride[74] (Figure 1.6, a). Cyclic aromatic guanidines, such as benzimidazole derivatives can be prepared by cross coupling of the open ring precursor with an intramolecular aromatic bromide in *ortho*-position (Figure 1.6, b).[75]

Under standard conditions, aliphatic guanidines can be regarded as stable molecules. However, similar to hydroquinone, electron-rich aromatic bisguanidine derivatives are prone to oxidation under air atmosphere.[74] Furthermore, hydrolysis of the guanidine moiety can take place under aqueous acidic conditions and at elevated temperatures. For example, the corresponding ureas are obtained by hydrolysis of the guanidines in 3 M sulfuric acid and above 100 °C.[76]

The exceptionally strong electron-donating capabilities originate from the ability to distribute

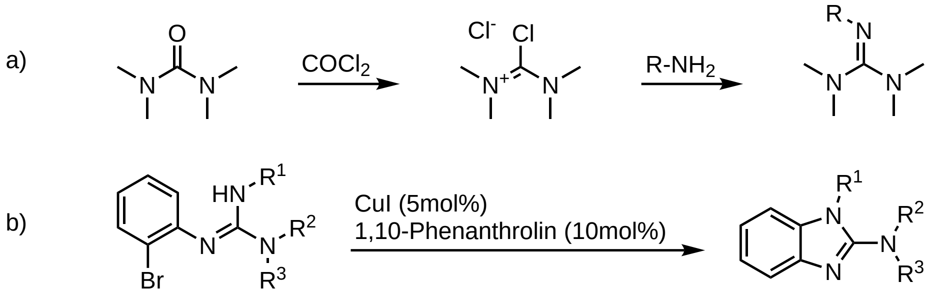

Figure 1.6: Two major synthetic routes to guanidines. a) Synthesis from a urea precursor,[17,72,73] b) cyclization via cross coupling.[75]

the positive charge over all four atoms of the CN_3 unit by delocalization. The delocalization energy gain, which has been compared to the delocalization of benzene, was raised to awareness in the 1970s leading to debates about Y-aromaticity.[77]

1.3.2. Guanidine Coordination Compounds

Historically, the first coordination compounds of tetramethylguanidine (TMG) were reported in 1965 by Longhi and Drago. They described homoleptic complexes of Co^{II}, Cu^{II}, Zn^{II}, Pd^{II}, Ni^{II} and Cr^{III} with TMG as monodentate ligand.[78] By means of infrared spectroscopy they were able to identify a shift of the C=N bond vibration to lower energies. It was interpreted as evidence for the lone coordination of the imine-nitrogen atom of the guanidine moiety. The complexes were reported to show tetrahedral geometry obtained from X-ray powder diffraction experiments. Nowadays, a multitude of complexes consisting of many guanidine derivatives and most transition or main group metals have been reported in the literature.[79] Molecular structures, obtained from single crystal X-ray diffraction experiments confirmed the binding of the imine-nitrogen atom.[80] Although the CN_3 unit acts as σ donor, π donor and as $\pi^\star$ acceptor, examination of the C−N bond lengths reveals that during coordination of the imine-nitrogen atom all nitrogen atoms are electronically engaged.[79] Overall, monodentate guanidines coordinate with their imine-nitrogen atom, whereas derivatives with additional donor moieties tend to interact with metal ions as bi- or polydentate ligands.[81–83] As examples, $[Cu(BL^{iPr})Cl]$[84] and $[Cu(hppH)_2Cl]$[80] are schematically shown in Figure 1.7.

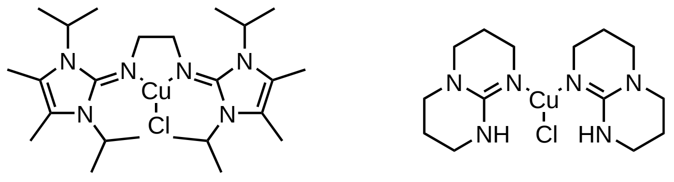

$[Cu(BL^{i\text{-}Pr})Cl]$ $[Cu(hppH)_2Cl]$

Figure 1.7: Cu^I complexes of 1,2-bis(1,3-diisopropyl-4,5-dimethylimidazoline-2-imino)ethane (BL^{iPr}) and 1,3,4,6,7,8-hexahydro-2*H*-pyrimido-[1,2*a*]pyrimidin (hppH)[80,84].

Guanidine complexes have a broad range of properties and applications. Guanidine ligands that show fluorescent behavior in their unbound state can be regulated by coordination to metal ions. Fluorescence of bidentate aromatic derivatives of TMG and dimethylethyleneguanidine (DMEG), which exhibit emission maxima from 450 nm to 530 nm, can be quenched upon coordination to CoCl.[16] Precisely tuned guanidine-type ligands can yield Zn complexes that exhibit high polymerization activity in the ring-opening polymerization of lactide.[85–87] Since zinc and guanidine-moieties are non-toxic and can be found in many biological systems, zinc-guanidine catalysts are regarded as ecologically friendly catalysts for the production of polylactic acid. Bridged TMG bisguanidines, such as $(TMG)_2$tol and other derivatives can be subjected to saturated solutions of oxygen in various solvents at low temperature to yield bis(μ-oxido)Cu_2^{III} species with different half-life.[84,88,89]

1.3.3. Hybrid Guanidine-Quinoline Ligands for ATRP

In an ATRP reaction, well performing catalysts exhibit good complex stability and are composed of ligands with high donor capability, which are otherwise chemically inert under the reaction conditions (see chapter 1.2.2). As mentioned above, guanidine-based ligands fulfill all of the prerequisites. In recent years, the group of Herres–Pawlis used different guanidine-based ligands in copper-mediated ATRP.[17,39,82,90,91]

The rate of the electron transfer reaction, one of the four elementary reaction of an ATRP equilibrium (section 1.2.1, first of equation 4), is strongly dependent on the geometry of the copper complexes. During the rearrangement of normally tetrahedral Cu^I complexes to planar Cu^{II} complexes the reorganization energy has to be overcome, which makes this process much slower.

In 1955, Hammond postulated a strong relation between a transition state geometry and its state of energy.[92] This rather general postulate does find its application in developing highly controlled ATRP catalysts. As stated above, the impediment of the electron transfer is caused by additional rearrangements of the individual complexes. Each geometrical state of the electron transfer reaction is related to an energy state. The transition state is a geometrically intermediate and electronically elevated state between the two oxidation states of the copper center. If the coordination geometry of the two individual copper complexes are shifted toward the intermediate state, their individual energy states rise as well. Independent of possible equilibrium changes, smaller geometrical rearrangements between the two oxidation states result in a smaller energy barrier. A decreased activation energy generally increases the rate of a reaction. Therefore, ATRP catalysts with very similar geometry between their two oxidation states tend to exhibit improved reaction conditions independent of their equilibrium state.

Comparing three similar guanidine-derived ligands for ATRP, the geometric differences can be related to their capability of improved polymerization control. Substituents like (*N*,*N*-

diisopropylamino)ethyl in TMG^{i}pae (Figure 1.8) are very flexible and allow their respective Cu^I and Cu^{II} complexes to reach energetically reduced states with distinguishably different geometries. As a result, the required re-orientation between the two oxidation states leads to an increased activation barrier for a SET resulting in decreased rates of activation and deactivation. During a polymerization reaction this characteristic feature is observable by increased polydispersity values.[82] Implementing more rigid ligands with similar donor abilities improves the chemoselectivity of the reaction due to improved SET kinetics. Substituents such as pyridinyl-methyl in TMGpy show improved molecular mass distribution.[39,82] Further rigidification conducted by the group of Herres–Pawlis yielded complexes with a geometry closer to the intermediate of both oxidation states.[17,93,94] For that purpose, the ethylene bridge of TMG^{i}pae was incorporated into a quinoline system (TMGqu). The quinoline moiety is a reasonably electron rich aromatic system that stabilizes both Cu^I and Cu^{II} complexes in a similar geometry. The strain imposed by ligation results from the planarity of the former ethylene bridge which is part of the aromatic ring system.

During electron self-exchange experiments, TMGqu and DMEGqu complexes exhibited the highest electron-transfer rates of copper complexes with pure *N*-donor ligands ever reported. These results obtained by experiments using the Marcus theory were supported by examination of the reorganization energy though Eyring theory and DFT calculations.[95] It was further highlighted, that TMGqu derivatives exhibited a considerably smaller reorganization energy than DMEGqu complexes and therefore showed an accelerated electron self-exchange.

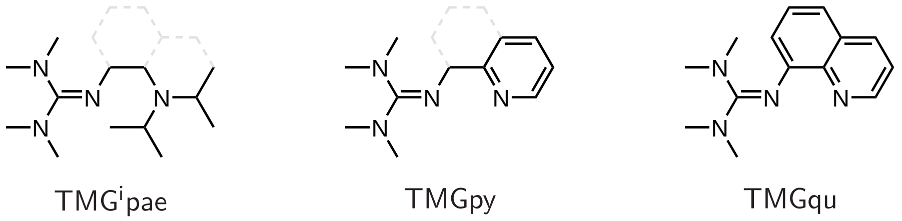

Figure 1.8: The evolution of ligands from 2-(2-(diisopropylamino)ethyl)-1,1,3,3-tetramethylguanidine (TMG^{i}pae) and 1,1,3,3-tetramethyl-2-(pyridin-2-ylmethyl)guanidine (TMGpy) to 1,1,3,3-tetramethyl-2-(quinolin-8-yl)guanidine(TMGqu).[17,39,82,93,94]

2. Project Outline

Guanidine copper complexes have been examined in ATRP catalysis in the Herres-Pawlis work group for some time.[17,39,82,90,91] They were perceived as catalysts that mediate the radical polymerization of styrene with high polymerization rates and good chemoselectivity.

In 2012, the group of Matyjaszewski reported the synthesis and examination of modified bipyridine ligands.[38] In their work, they described the influence of electron-withdrawing and -donating substituents on the polymerization activity of the resulting catalysts. Additionally, the electrochemical potentials were determined by cyclic voltammetry. Upon addition of electron-donating groups, the activity of the bipyridine copper catalysts increased dramatically. Unfortunately, the molecular structures of the catalysts were not determined. Therefore, potential changes in their coordination geometry could not be detected. The determination of the K_{ATRP} equilibrium constants was also not conducted for all of the different derivatives. As a result, possible conclusions regarding the relations of these aspects could not be drawn.

For similar experiments with the 1,1,3,3-tetramethyl-2-(quinolin-8-yl)guanidine (TMGqu) copper catalyst present in our group, ligand derivatives with electron-donating and -withdrawing substituents should be synthesized. Subsequently, the molecular structures of their copper complexes should be determined and possible correlations with the polymerization activity of the catalysts should be found. In addition, analytical methods, such as cyclic voltammetry and UV/Vis spectroscopy, should be used to gain further insights into the mechanistic aspects of the catalytic processes. For further comparison, the ATRP equilibrium constants K_{ATRP} and the rate constants k_{act} and k_{deact} should be determined.

The modifications which were envisioned should only be placed at positions in which steric implications were expected to be negligible. Therefore, the positions C4, C5 and C6 were considered as potential targets (Figure 2.1). Unpublished density functional theory (DFT) calculations in our group indicated that derivatization at the position of carbon atom C6 should result in the highest impact on the electronical properties of the catalysts. Consequently, this position was declared as major target for substitution.

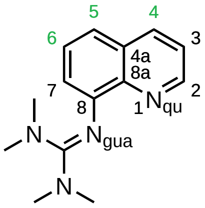

Figure 2.1: Atom numbering in the aromatic system of 1,1,3,3-tetramethyl-2-(quinolin-8-yl)guanidine (TMGqu).

3. Results and Discussion

The goal of this thesis was the investigation of the reactivity of novel copper complexes in ATRP catalysis. Therefore, a library of structurally related guanidine-quinoline hybrid ligands (section 3.1), which are based on the previously described TMGqu ligand (section 1.3.3),[17] was designed and synthesized. The individual ligands were used to complex copper halides followed by crystallization and analysis of the obtained molecular structures (section 3.2). The performance of the individual complexes in polymerization experiments was examined afterwards (section 3.3). For deeper insights into mechanistic aspects, the electronic properties of the copper complexes were examined by electrochemical methods (section 3.4). Furthermore, optical methods were used for the determination of the ATRP activation rate constants k_{act} and the thermodynamic equilibrium constants K_{ATRP} of the different catalysts (section 3.5).

3.1. Ligand Design and Synthesis

The influence of electron-donating or -withdrawing substituents on ATRP catalysis should be examined for a series of related TMGqu ligands. The choice of substitution pattern, on which the ligand library was based on, resulted from unpublished results of our group. Following a series of density functional calculations, it was suggested to prepare TMGqu derived ligands which bear electronically active groups on the carbon atom C6 (Figure 3.1). Furthermore, these modifications were separated into a class of smaller compact substituents with improved crystallization behavior and a class of well soluble alkylated groups. The compact groups were used for analytical structure determination methods, which often required solid crystalline material. In contrast, the solubility of the complexes in many polymerization media was improved when the ligands contain long or branched alkyl substituents impeding aggregation. Therefore, the preparation of a library consisting of both compact ligands expected to form solid complexes (Figure 3.2, upper line) and more soluble ligands with longer branched alkyl chains (lower line) was devised. The first group of ligands was employed in both structure determination and polymerization assays, the latter group was used to determine polymerization kinetics in bulk styrene.

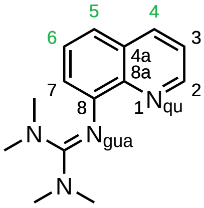

Figure 3.1: TMGqu core structure with atom numbering.

The guanidine-quinoline hybrid ligands can be readily prepared from their corresponding amines. A general procedure for their synthesis was established by the group of Kantlehner in 1983.[73]

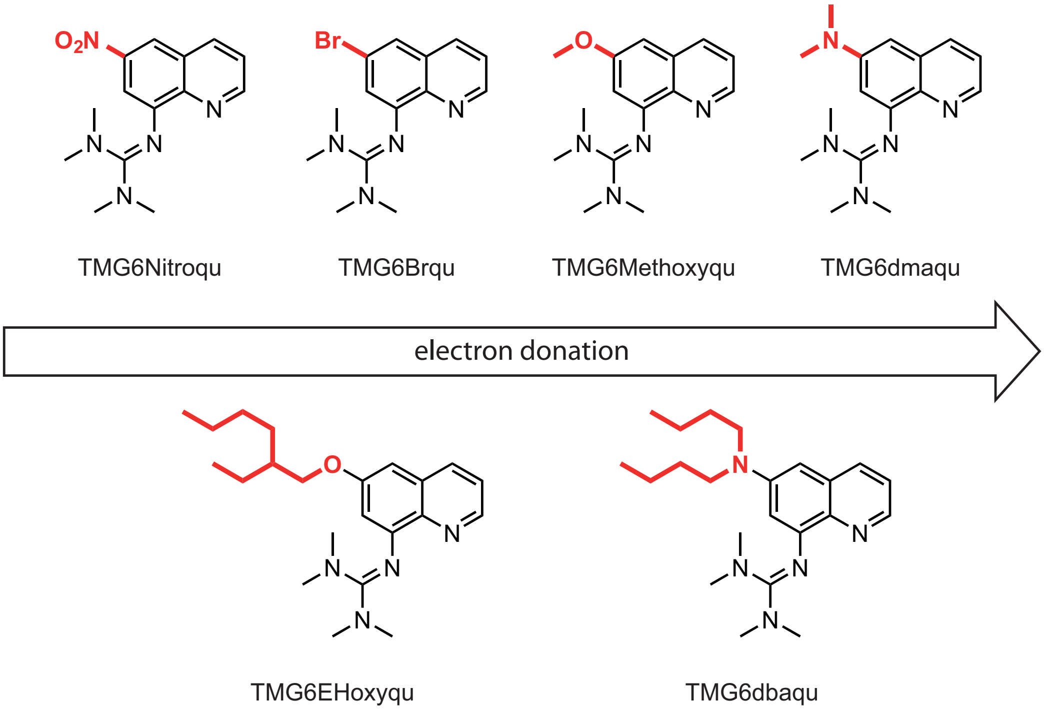

Figure 3.2: TMGqu derived ligands, ordered by their electron-donating abilities. First line: ligands that form solid copper complexes, second line: ligands with increased solubility.

First, variously substituted chloroformamidium chlorides (**2**) were prepared from their urea precursors (**1**) by treatment with phosgene (Scheme 3.1). Subsequent reaction of these guanidine precursors with primary amines finally resulted in the formation of their respective guanidines (**3**). Since only a very limited number of procedures to synthetically access guanidines have been described in the literature, all novel ligands were prepared using these conditions. The final products were purified by distillation or sublimation with a *kugelrohr* distillation apparatus.

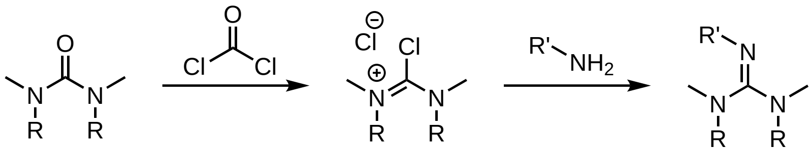

1 **2** **3**

Scheme 3.1: Preparation of substituted guanidines from the respective urea upon treatment with phosgene and an amine.[73]

The ligand 2-(6-methoxyquinolin-8-yl)-1,1,3,3-tetramethylguanidine (TMG6Methoxyqu, **4**) was prepared from 6-methoxy-8-nitroquinoline (**5**), which is commercially available. First, reduction of the nitro group with hydrogen gas and palladium on charcoal as catalyst afforded 8-amino-6-methoxyquinoline (**6**) in excellent yield (Scheme 3.2). The following conversion of amine **6** to tetramethylguanidine (TMG) derivative **4** with tetramethylchloroformamidium chloride (TMG-Cl, **7**, Figure 3.3) was realized by using Kantlehner's procedure (Scheme 3.1).

The structurally related ligand *N*-(6-methoxyquinolin-8-yl)-1,3-dimethylimidazolidin-2-imine (DMEG6Methoxyqu, **8**) was synthesized in a similiar fashion using dimethylethylenechloroformamidium chloride (DMEG-Cl, **9**) for the installation of the guanidine moiety.

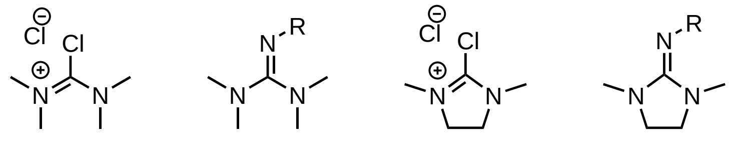

7 TMG **9** DMEG

Figure 3.3: The two different guanidine moieties TMG and DMEG and their corresponding precursors TMG-Cl (**7**) and DMEG-Cl (**9**) used in this work.

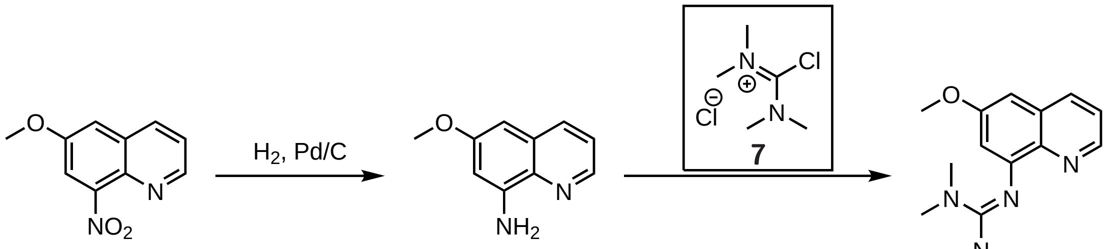

5 **6** **4**

Scheme 3.2: Synthetic route to TMG6Methoxyqu (**4**).

The third ligand of the quinoline ether family, 2-(6-((2-ethylhexyl)oxy)quinolin-8-yl)-1,1,3,3-tetramethylguanidine (TMG6EHoxyqu, **10**) was also synthesized from the same precursor (**5**) as TMG6Methoxyqu (**4**) and DMEG6Methoxyqu (**8**). However, the synthesis of the ligand commenced with a cleavage of the ether group by subjection to hydrobromic acid (Scheme 3.3).[96,97] The generated alcohol **11** was then alkylated with 3-(bromomethyl)heptane (**12**) to give the branched ether 6-((2-ethylhexyl)oxy)-8-nitroquinoline (**13**). The installation of the guanidine moiety was then achieved by using the same procedure as for ligands **4** and **8**.

As counterpart to the electron-rich ligands **4**, **8** and **10**, a TMGqu derivative with an electron-withdrawing nitro group was synthesized. The corresponding 6,8-dinitroquinoline (**14**) was not commercially available and therefore had to be prepared. In first attempts, 8-nitroquinoline was exposed to nitrosulfuric acid in various concentrations and temperatures (Table 3.1). Furthermore, liquid N_2O_4 as such or dissolved in chloroform was also used. However, no synthetic method yielded satisfying or even reproducible results. Therefore, 6,8-dinitroquinoline was prepared according to Skraup's conditions,[98] which was published by Rieche *et al*. for this particular target.[99] In this reaction, 2,4-dinitroaniline was reacted with acrolein, which was prepared *in situ*. For that purpose, a mixture of the aniline derivative, glycerol, arsenic(V)oxide and concentrated sulfuric acid was heated to 140 °C (Scheme 3.4). The generation of acrolein was indicated by foaming of the black solution. The resulting heterocyclic compound was oxidized to 6,8-dinitroquinoline (**14**) by arsenic(V)oxide. After neutralization, the product was isolated

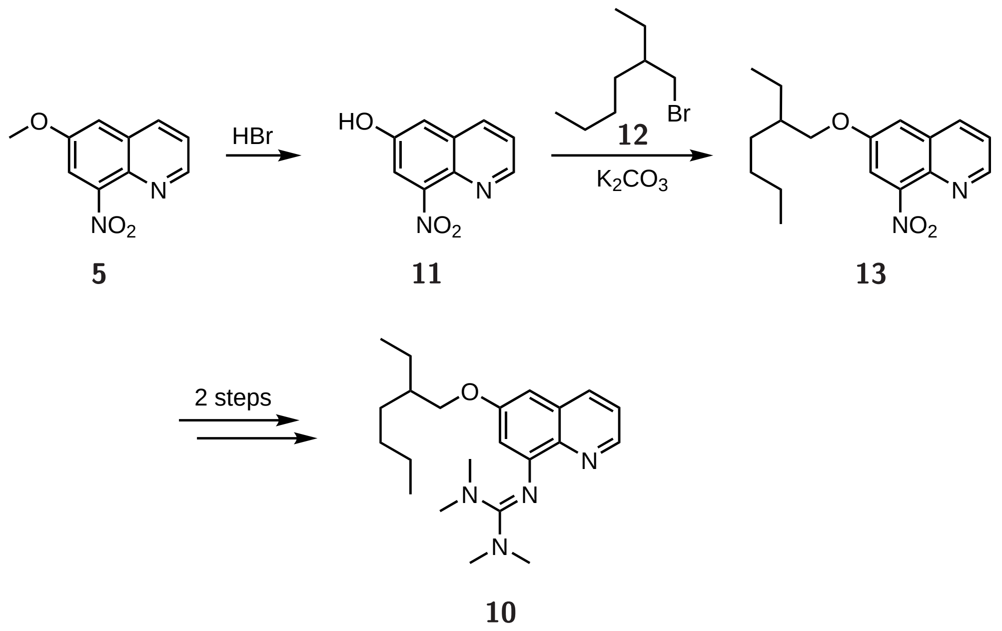

Scheme 3.3: Synthetic route to the intermediate 6-((2-ethylhexyl)oxy)-8-nitroquinoline (**13**) and the target ligand TMG6EHoxyqu (**10**).

by extraction with a Soxhlet apparatus. The drawbacks of this synthetic approach were the need to perform numerous purification steps and the formation of large amounts of side and decomposition products. However, the route provided sufficient quantities of 6,8-dinitroquinoline (**14**) to continue with the synthesis of the ligand. For the following chemoselective reduction of the nitro substituent in C8-position, titanium(III)chloride was used as reducing agent. According to a reaction procedure established by Smalley *et al.*, the dinitroquinoline was dissolved in acetone and then treated with exactly six equivalents of $TiCl_3$.[100] If an excess of reduction agent was used, the second nitro group was reduced immediately, yielding 6,8-diaminoquinoline. For receiving high yields, the concentration of the titanium(III)chloride solution (12% in HCl) needed to be determined accurately. Therefore, the solution was titrated with ferric thiocyanate solution multiple times (section 6.2.4). The resulting 8-amino-6-nitroquinoline (**15**), was further reacted to the tetramethylguanidine ligand TMG6Nitroqu (**16**) as mentioned above in good yields.

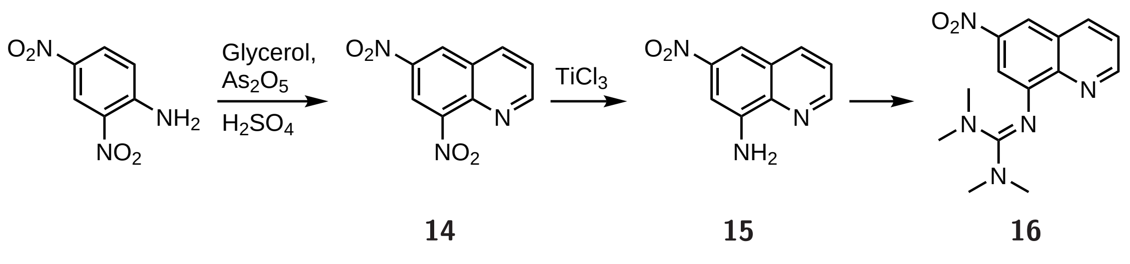

Scheme 3.4: Synthetic approach to a fused ring system from 2,4-dinitroanilin with glycerol, yielding 6,8-dinitroquinoline (**14**). Reduction with $TiCl_3$ yields 8-amino-6-nitroquinoline (**15**), followed by the synthesis of the ligand TMG6Nitroqu (**16**).

Table 3.1: Different nitration approaches of 8-nitroquinoline to afford 6,8-dinitroquinoline. Parts: volume.

	parts HNO_3[a]	**parts H_2SO_4**[a]	**T [°C]**	**reaction time**	**yield**[b]
1	1 (65%)	2 (98%)	100	1.5 hours	40%[c]
2	1 (100%)	1 (98%)	83, (reflux)	6 hours	50%[d]
3	4 (100%)	13 (98%), 9 (fum. 65%)[e]	83, (reflux)	5 hours	25%[d]
4	1 (100%)	—	83, (reflux)	13 hours	no reaction
5	7.2 (100%)	20 (98%), 20 (fum. 65%)[e]	83, (reflux)	5 days	7%
6	liquid NO_2		ambient	10 hours	no reaction
7	liquid NO_2 in dichloromethane		ambient	10 hours	no reaction

[a] (%): concentration of the acids
[b] isolated yield after purification by precipitation and flash column chromatography
[c] not reproducible
[d] not isolated, yield was determined by ^1H NMR spectroscopy
[e] fum.: fuming

For the synthesis of the TMG6Brqu (**17**) ligand, a synthetic route analogous to the TMG6Nitroqu ligand synthesis was pursued. However, the Skraup synthesis for the quinoline core structure produced large amounts of tar, reducing the overall yield and increasing the effort in purification. In the approach by Rieche *et al*., the harsh reaction conditions were required for the acid-mediated generation of acrolein from glycerol. When glycerol was replaced by stabilized acrolein, milder reaction conditions were applicable. Furthermore, aqueous acids were able to substitute the concentrated sulfuric acid and arsenic(V)oxide could be replaced with tetrachloro-1,4-benzoquinone (Chloranil) as oxidizing agent. As a result, the preparation of the quinoline fused ring system was conducted at 110 °C in *n*-butanol and aqueous hydrochloric acid (Scheme 3.5). For purification, the resulting 6-bromo-8-nitroquinoline (**18**) was precipitated as its $ZnCl_2$ complex and could be isolated in good yields.[101] Subsequent reduction of the nitro group to the corresponding amine was first conducted using hydrogen gas and a palladium catalyst. Unfortunately, these reactions resulted in the formation of complex mixtures containing several unidentified products. Additionally, reduction of the bromide could easily occur under these reaction conditions. Therefore, the previously established mild reduction procedure using $TiCl_3$ was also employed in this approach, affording 8-amino-6-bromoquinoline (**19**) in good yields.[100]

The synthesis of the ligand TMG6dmaqu (**20**) was found to be very challenging due to the reactivity of intermediates. Therefore, several synthetic routes were investigated (Scheme 3.6). The key intermediate N^6,N^6-dimethylquinoline-6,8-diamine (**21**) was planned to be prepared from three building blocks (**14**, **18** and N^1,N^1-dimethyl-1,4-phenylenediamine). The first synthetic approach (Scheme 3.6a) was based on the previous synthesis of TMG6Nitroqu. The quinoline **14** was chemoselectively reduced to the amine **15** with $TiCl_3$, as mentioned above. Protection of the amine **15** with acetyl chloride then afforded *N*-(6-nitroquinolin-8-yl)acetamide (**22**). This stable compound was treated with hydrogen gas and a palladium catalyst in methanol at room

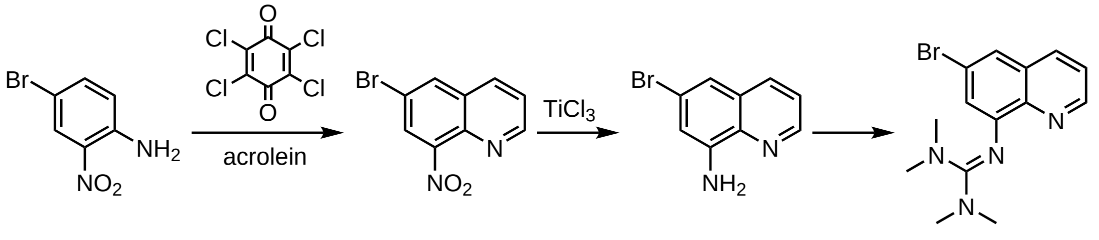

18 **19** **17**

Scheme 3.5: Improved synthesis of substituted quinolines, employing acrolein as building block and Chloranil as oxidazing agent.

temperature. However, reduction did not occur and the addition of one equivalent of concentrated hydrochloric acid did not produce any significant improvements. In conclusion, the synthesis of *N*-(6-aminoquinolin-8-yl)acetamide (**23**) could not be achieved and consequently, the final alkylation to yield *N*-(6-(dimethylamino)quinolin-8-yl)acetamide (**24**) could not be performed.

In a second approach (Scheme 3.6b), the building block **18** was directly treated with a solution of dimethylamine in THF under Buchwald–Hartwig cross-coupling conditions. The reaction was conducted at 65 °C in a threaded sealed pressure flask (Ace Glass Inc.). Unfortunately, the available seals (FETFE®) did not tolerate the reaction conditions for a prolonged time. Therefore, the yield of this reaction could not be improved to more than 25%. Small amounts of *N*,*N*-dimethyl-8-nitroquinolin-6-amine (**25**) received after reduction with sodium thionite were used as analytical samples and reference material.

In the third approach, the cross-coupling conditions were optimized (Scheme 3.6c). In order to increase the substrate reactivity, nitroquinoline **18** was reduced with $TiCl_3$ to amine **19**. The amine was then protected using di-*tert*-butyl dicarbonate (Boc_2O). The protection procedure required the use of a tenfold excess of Boc_2O and 4-dimethylaminopyridine (4-DMAP). Although the low atom efficiency resulted in a tedious workup procedure, the reaction yield was almost quantitatively in small scale. Unfortunately, performance of the reaction on larger scale resulted in a considerable decrease in yield, but provided ample material to continue with the synthesis. The double Boc-protected di(*tert*-butyl)(6-bromoquinolin-8-yl)bicarbamat (**26**), was coupled to dimethylamine in a Buchwald–Hartwig amination reaction.[102] During the reaction or workup one of the two Boc protection groups was cleaved. As a result, *tert*-butyl (6-(dimethylamino)quinolin-8-yl)carbamate (**27**) was isolated in mediocre yields. Final cleavage of the remaining Boc protection group with trifluoroacetic acid (TFA) in dichloromethane, afforded the free base **21** in quantitative yields.

Since the first synthetic approach did not lead to the desired product and both of the other routes exhibited limitations in scalability, a fourth synthetic route was devised. During previous pathways, existing quinoline species were modified to produce the desired target compound

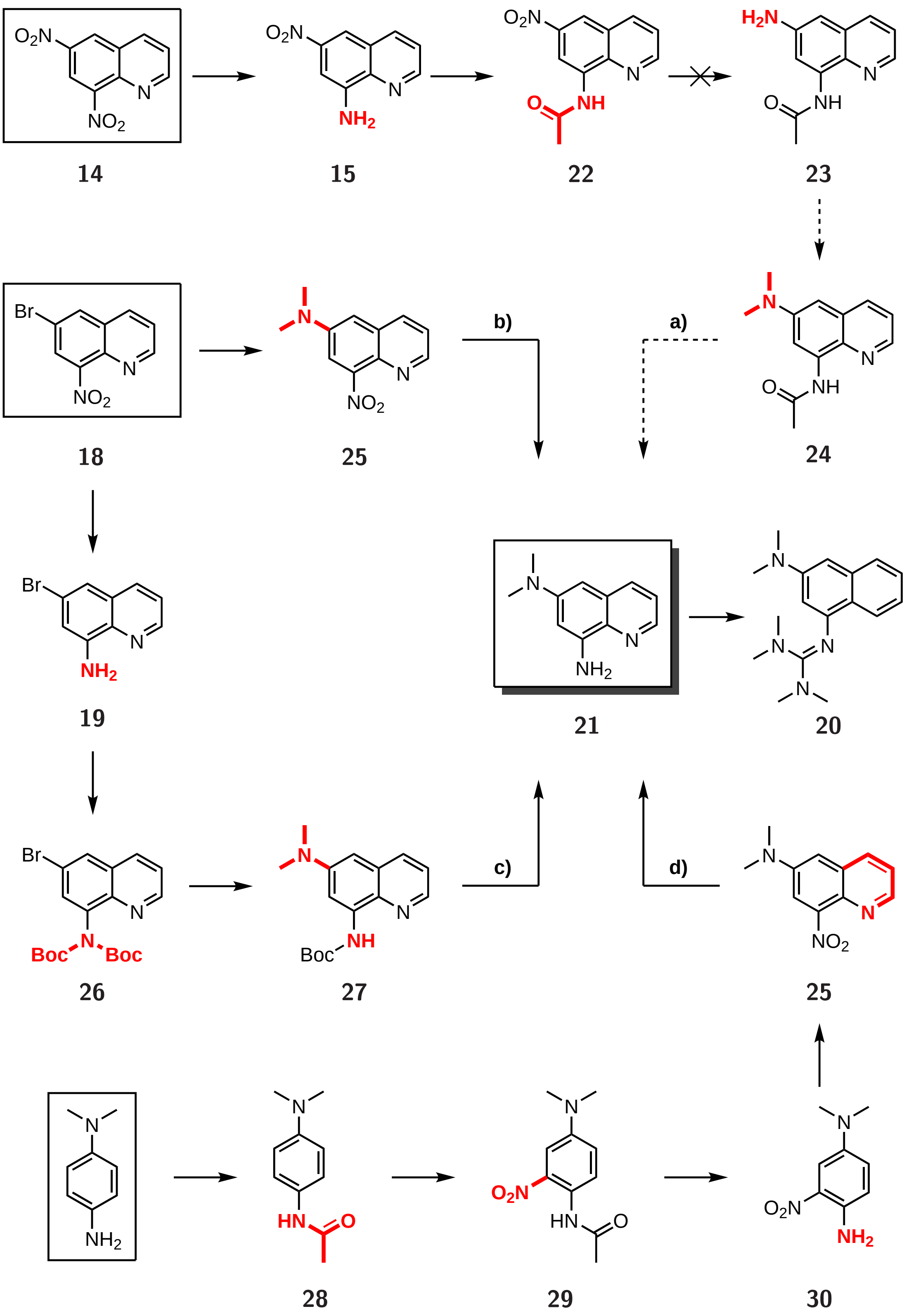

Scheme 3.6: Four synthetic approaches to the key intermediate N^6,N^6-dimethylquinoline-6,8-diamine (**21**) followed by synthesis of the ligand TMG6dmaqu (**20**).

21. In contrast, the fourth synthetic approach (Scheme 3.6d) aimed at the synthesis of an aniline derivative with a dimethylamino substituent already in place. This intermediate was then treated with acrolein to receive the final quinoline target.[101] During the first reaction step, N^1,N^1-dimethyl-1,4-phenylenediamine was protected with acetyl chloride under basic conditions to form *N*-(4-(dimethylamino)phenyl)acetamide (**28**). The acetamide was then treated with nitrosulfuric acid at 0 °C to give *N*-(4-(dimethylamino)-2-nitrophenyl)acetamide (**29**). After deprotection, N^1,N^1-dimethyl-1,4-diamino-3-nitrobenzene (**30**) was subjected to the optimized Skraup conditions using acrolein and Chloranil. Unfortunately, the presence of the dimethylamino group had a considerably strong influence on the reaction outcome. The formation of large amounts of unidentified decomposition products was observed. Furthermore, no acidic workup could be performed due to the basic amino group, which resulted in inefficient product isolation. Therefore, *N*,*N*-dimethyl-8-nitroquinolin-6-amine (**25**) could only be isolated in 25% yield. The target molecule **21** was then prepared by reduction of the parent compound with sodium dithionite in aqueous ethanol (50%). The combined amount of product received from all synthetic approaches yielded sufficient material for further experiments. Due to tedious workup routines and low to moderate yields on larger reaction scales, reproduction of these synthetic routes is not recommended.

Thus, we suggest the investigation of a modified procedure Scheme 3.6a for the synthesis of target molecule **21**, which was not further pursued due to time constraints. First, the preparation of building block **14** should be conducted with the optimized reaction conditions as mentioned above. Later, the reduction of compound **22** should be performed with sodium dithionite analog to the reduction procedure in Scheme 3.6d. The resulting product is expected to be prone to oxidation. The following alkylation, however, should be feasible and numerous procedures can be found in the literature.[103–107] The deprotection of **24** should give **21** in reasonable yields.

The ligand TMG6dbaqu (**31**) was synthesized by a Buchwald–Hartwig amination, starting with aryl bromide **18** (Scheme 3.7). Unlike the previously described cross-coupling reactions with dimethylamine, the amination with dibutylamine was successful. The higher boiling point of dibutylamine (bp. 161 °C) allowed the cross-coupling reaction to be conducted at higher temperatures. In contrast, dimethylamine, which is gaseous at room temperature (bp. 7 °C), had to be used as stock solution in tetrahydrofuran (THF). However, the seals of the reaction vessel (threaded round bottom flasks with FETFE®seals, Ace Glass Inc.) were not capable to endure the solvent THF or volatile amines at elevated temperatures for a prolonged period of time. We therefore used toluene as solvent. Prolonged reaction times and increased reaction temperatures lead to an improved yield of quinoline **32**. The quinoline **32** was then reduced to the diaminoquinoline **33** by treatment with sodium dithionite. The product was prone to oxidation and was immediately used for the synthesis of TMG6dbaqu.

In addition to variations of the quinoline moiety, the guanidine moiety was also varied.

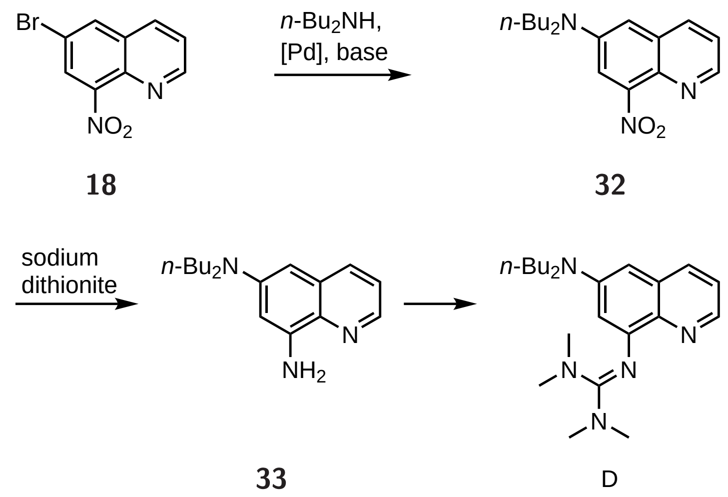

Scheme 3.7: Synthesis of the diaminoquinoline **33** by Buchwald–Hartwig cross-coupling reaction, followed by reduction with sodium dithionite.

In the synthesis of the ligand *N*-(6-methoxyquinolin-8-yl)-1,3-dimethylimidazolidin-2-imine (DMEG6Methoxyqu **8**) the tetramethylguanidine unit was replaced by the dimethylethyleneguanidine (DMEG) substituent (Scheme 3.8). The preparation was conducted analog to the TMG synthesis, starting with the reduction of nitroquinoline **5**, followed by condensation of the resulting amine **6** with DMEG-Cl (**9**) to afford the ligand. The solid product was sublimed twice, yielding pure yellow crystals.

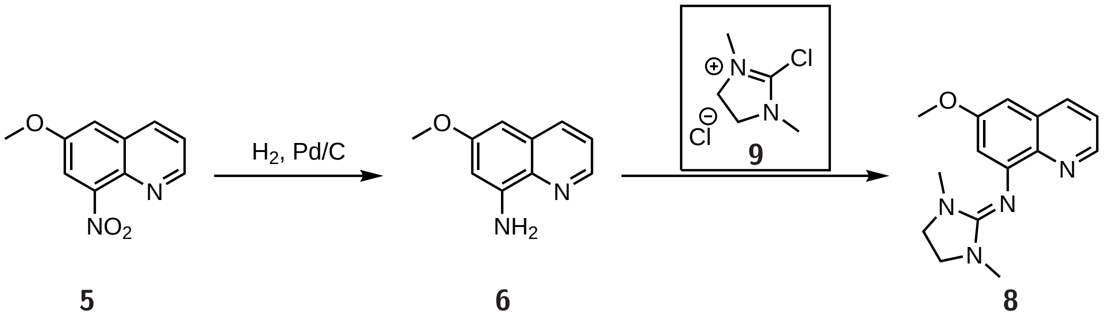

Scheme 3.8: Synthetic route to DMEG6Methoxyqu (**8**).

First estimation of the donating abilities of the TMGqu derivatives were obtained from comparison of the corresponding ^{13}C NMR shifts. Whereas the chemical shifts of some carbon atoms did not vary significantly (C3, Figure 3.4) others exhibited shifts that could be related to the electron-donation of the substituents at position C6 (Figure 3.4 left). It was observed that upon substitution with stronger donors, the carbon atoms C2, C4 and C8a experienced a decline of their chemical shifts. A decline in chemical shift is usually associated with stronger magnetic shielding due to an increased electron density at the respective atom. As a conclusion, the carbon atoms C2 C4 and C8a are considered to experience an increased electron density. In contrast, the carbon atom C4a exhibits a decline of electron density upon substitution. Altogether, the carbon atoms mentioned above are separated from the hetero atom of the substituent with at least three carbon-carbon bonds. Therefore, the electronic influence is considered to be distributed through the aromatic π system of the quinoline. In contrast, the carbon atom C6 is at the center of substitution. The variation of its chemical shifts differs exceptionally from other carbon atoms (Figure 3.4 right). Strongest down field shifts can be obtained in the TMG6Methoxyqu and TMG6EHoxyqu ligands, followed by the TMG6Nitroqu, TMG6dmaqu and TMG6dbaqu ligands. The TMGqu and TMG6Brqu ligands exhibit smaller down field shifts.

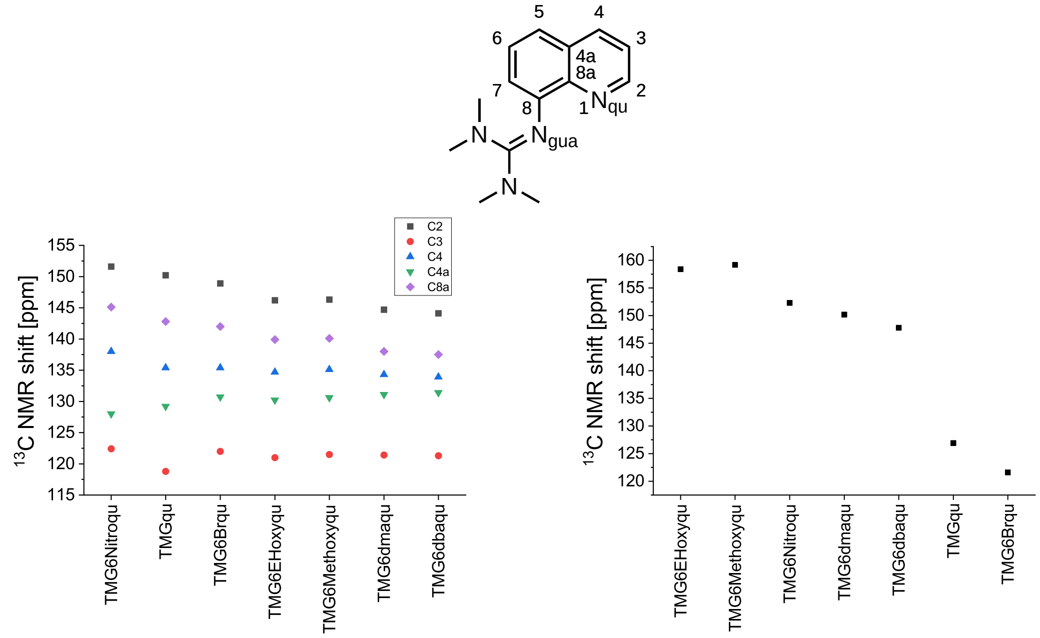

Figure 3.4: ^{13}C NMR shifts for different carbon atoms at the pyridine ring (left) and at the C6-position of the substituted ring of different TMGqu derivatives.

Upon comparison to chemical shifts of the carbon atoms C2, C4 and C8a, two major differences were found for C6. The change of the chemical shifts could be attributed to three different groups of substituents. The largest chemical shifts close to 160 ppm were found for ether derivatives, followed by nitrogen based ligands at approximately 150 ppm. Non-substituted or less electronically active groups afforded chemical shifts of 120 ppm to 125 ppm. As a second distinction, the overall differences between the chemical shifts were exceptionally large. It was concluded, that the mechanisms of electron density distribution at carbon atom C6 differed significantly from distribution to other positions. The sequence in which the ligands exhibited their chemical shifts indicated that the hetero atom that is bound to the carbon atom is of high importance. In terms of NMR spectroscopy, the hetero atoms mainly differ in their electronegativity. A high electronegativity of an atom results in a reduced partial charge of the neighboring atoms which is distributed through the σ bonds. In conclusion, both the sequence and the exceptionally large differences of the chemical shifts were attributed to the electron withdrawal of the electronegative hetero atoms. As a result, substitution at carbon atom C6 resulted in a reduced electron density at this position. In contrast, increased electron density was observed in the pyridine ring of the TMGqu derivatives, being distributed through the aromatic π system.

During the course of this work, ligand derivatives with modifications at different positions became of interest. Therefore, the ligand family of C6-substituted TMGqu ligands was pursued to be accompanied by a family of C4-substituted TMGqu derivatives. The different electron-donation pathways of the same substituents within the two ligand families should be analyzed. Potential structural variations of the copper complexes and deviations in their catalytic activity should be pointed out. The possible synthetic approaches deviated strongly between these families of C6- and C4-substituted TMGqu ligands.

Procedures that should give access to C4-substituted quinoline derivatives were published by Ochiai in 1953.[108] In his approaches he oxidized quinoline with hydrogen peroxide to yield quinoline 1-oxide (**34**), which was subsequently nitrated to yield 4-nitroquinoline 1-oxide (**35**, Scheme 3.9). Thereby, it was further found that the oxide **34** exhibited considerably increased reactivity at the C4-position.

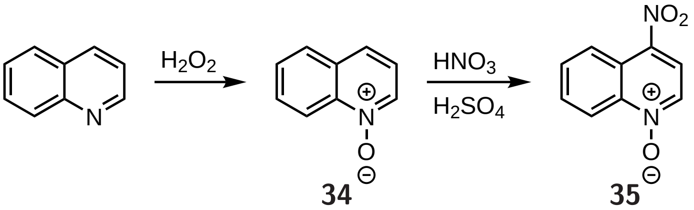

Scheme 3.9: Synthetic approach to C4-substituted quinolines developed by Ochiai.[108]

In the syntheses of C4-family members, the two quinoline oxides (**34** and **35**) were considered as key intermediates. Since quinoline-8-amine derivatives were required for preparation of their respective guanidine ligands, oxidation approaches with nitrogen containing functional groups at the C8-position were examined (Scheme 3.10). At first, 8-nitroquinoline was treated with hydrogen peroxide (30%) although the electron-withdrawing character of the nitro group resulted in reduced reactivity. Additionally, the use of 3-chloroperbenzoic acid (*m*-CPBA) resulted in no product formation. In both cases, the starting material could be recovered. To improve the reactivity of the substrate, the acetyl-protected *N*-(quinolin-8-yl)acetamide was used for further investigations. Although treatment with hydrogen peroxide did not lead to any reaction, oxidation with *m*-CPBA in refluxing chloroform afforded the desired product, 8-acetamidoquinoline 1-oxide, in good yield. Nitration of the quinoline oxide was then found to be challenging and no product formation was observed. If nitration would be feasible, the resulting product could be reduced twofold to the respective quinoline amine (Scheme 3.10a).[108] Alkylation and deprotection should then yield N^4,N^4-dimethylquinoline-4,8-diamine as ligand precursor. The nitrated product could also be subjected to an *ipso* substitution with alcoholates, leading to a 4-alkoxyquinoline 1-oxide derivative (Scheme 3.10b).[108] In an alternative reaction sequence, 8-bromoquinoline should be used as starting material, since its electronic effect on the nitration is rather small as compared to the nitro group. In this approach, the oxidized quinoline should be nitrated and reduced akin to the literature procedure (Scheme 3.11).

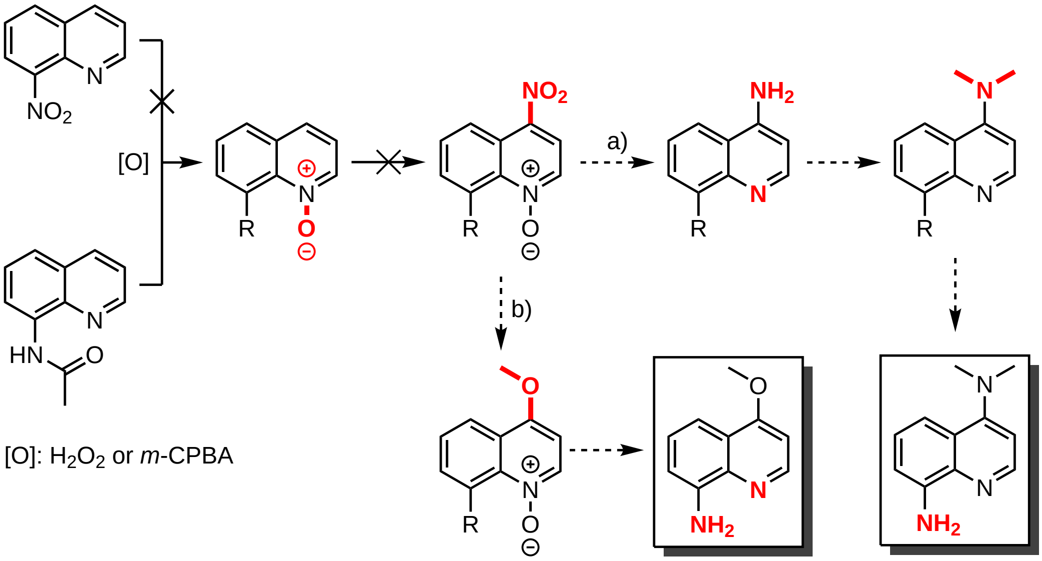

Scheme 3.10: Synthetic routes to C4-modified quinolines. Nitrogen containing groups are present at C8-position throughout all synthetic steps.

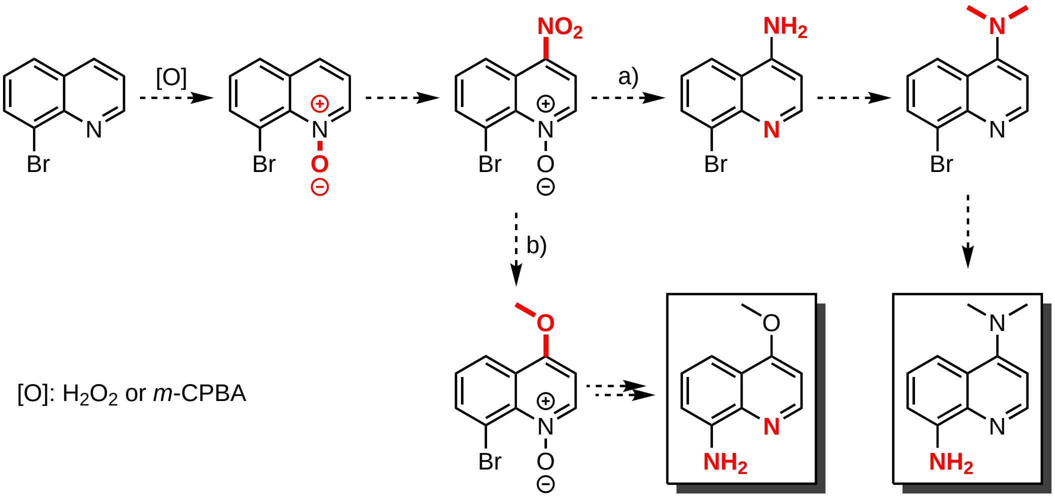

Scheme 3.11: A planned approach to C4-substituted quinolines starting from 8-bromoquinoline. The bromide should be converted to an amine in the last reaction step.

A reaction leading to 4-hydroxyquinoline has been reported in 1887.[109] After many improvements, the general reaction is nowadays called the Gould–Jakob reaction.[109–113] In course of the development of a synthetic route to 2-(6-methoxyquinolin-8-yl)-1,1,3,3-tetramethylguanidine (TMG4Methoxyqu, **36**) this reaction has been studied on numerous examples and conditions (Scheme 3.12). In a first attempt, 2-nitroaniline was reacted with diethyl ethoxymethylenemalonate to a condensation product, which was cyclized to give quinoline **37**. After saponification of the resulting carboxylic ester, the free acid (**38**) should be decarboxylated. Under several conditions, only starting material was isolated. This result can be attributed to the electron-withdrawing influence of the nitro substituent which is known to result in impeded decarboxylation reactivity.[114] Therefore, the carboxylic acid was converted into its silver salt and subjected to similar decarboxylation conditions. Unfortunately, product formation was not observed.

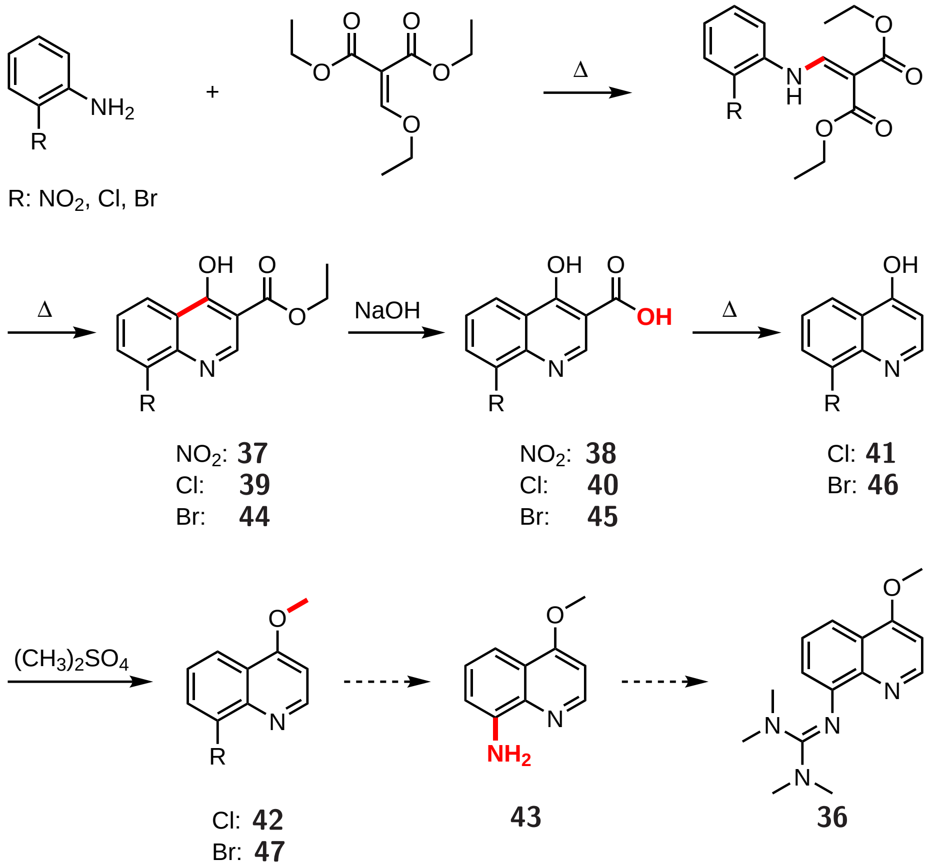

Scheme 3.12: A series of Gould–Jakobs reactions towards the ligand TMG4Methoxyqu **36**.

Therefore, 2-nitroaniline was replaced by 2-chloroaniline. Again, the condensation was conducted without solvent at 110 °C, until formation of ethanol ceased. The reaction setup was further improved by addition of a Claisen distillation head and Liebig condenser, facilitating the removal of ethanol. After the first step, diphenyl ether was added as solvent and the reaction was heated to 220 °C to 250 °C with an infrared bath. After the removal of a second equivalent of ethanol, the reaction mixture was allowed to cool to room temperature. Upon cooling, the product precipitated. After filtration, quinoline **39** was saponified, leading to 8-chloro-4-hydroxyquinoline-3-carboxylic acid (**40**). Decarboxylation of the free acid yielded 8-chloro-4-hydroxyquinoline (**41**) quantitatively. In conclusion, the replacement of the electron-withdrawing nitro group by a halide dramatically increased the reactivity of the substrate in the decarboxylation reaction. During the reaction the product **41** resublimed in colorless needles at the cooling finger, rendering additional purification steps unnecessary. The obtained hydroxyquinoline **41** was then subjected to base-mediated methylation with iodomethane. However, the major product was found to be 8-chloro-1-methylquinolin-4(1*H*)-one (not shown). In contrast, alkylation with dimethyl sulfate led to the desired product 8-chloro-4-methoxyquinoline (**42**) in good yields.

For the formation of the ligand precursor 4-methoxyquinolin-8-amine (**43**), the chloroquinoline **42** was attempted to react with amine equivalents under a broad range of conditions.[115–118] Initial Buchwald–Hartwig cross-coupling reactions of **42** were conducted with lithium bis(trimethylsilyl)amide (LiHMDS), benzophenone imine and triphenylsilylamine as ammonia equivalents. Further experiments using a variety of ligands and palladium-catalysts were conducted. For example, CyJohnPhos, XPhos, *t*-BuXPhos, *t*-BuBrettPhos or BrettPhos were used as ligands together with either their precatalyst complexes or other palladium catalysts (Figure 3.5). Unfortunately, under all reaction conditions no product formation was observed. A palladium-mediated cross-coupling reaction of **42** and ammonia in 1,4-dioxane with the exceptionally expensive Josiphos ligand[119] gave the desired product **43** for the first time in 60% yield. The reaction underwent full conversion but the formation of the twofold aminated product was also observed. Performing the reaction at a larger scale resulted in an increased amount of side product formation. Therefore, the reaction was considered as unreliable. Changing the solvent to a solution of *N*-methyl-2-pyrrolidone (NMP) in concentrated aqueous ammonia and using Cu_2O as catalyst led to the desired product **42** in low yield (25%). However, the removal of NMP during purification proved to be challenging. Further modifications of the reaction conditions did not lead to improved yields. The difficulties associated with the amination of chloroquinoline **42** can presumably be attributed to the low reactivity of aryl chloride in palladium-catalyzed cross-coupling reactions. We therefore decided to use the corresponding bromo-quinoline instead.

The synthesis of 8-bromo-4-methoxyquinoline (**47**) was performed according to the synthesis of **42**. 2-Bromoanilin was reacted with diethyl ethoxymethylenemalonate to yield ester **44**, which was hydrolyzed to its free acid **45**. After decarboxylation, 8-bromo-4-hydroyquinoline (**46**) was alkylated with dimethyl sulfate to yield methyl ether **47**. In an amination reaction of the bromoquinoline with aqueous ammonia the ligand precursor **43** should be accessible in good yields. This reaction was not yet conducted due to time constraints.

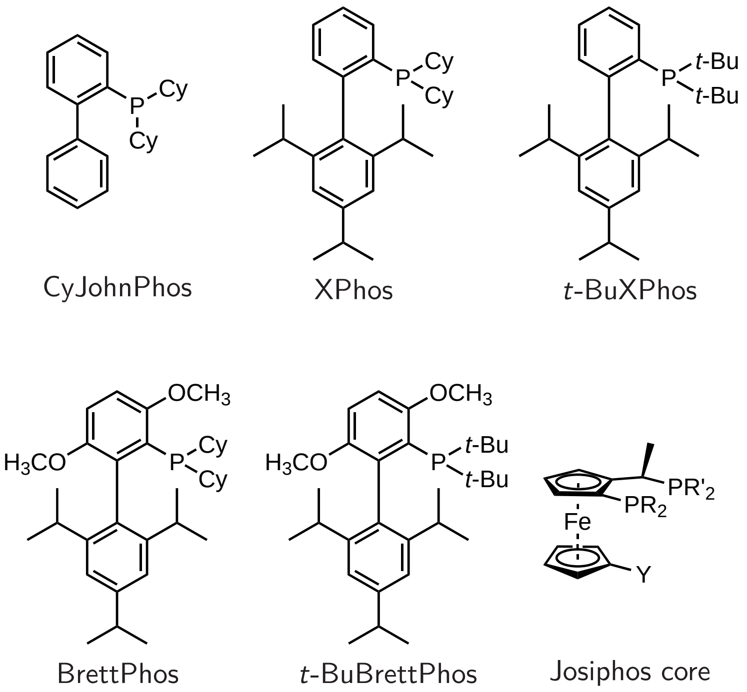

CyJohnPhos XPhos *t*-BuXPhos

BrettPhos *t*-BuBrettPhos Josiphos core

Figure 3.5: Ligands used during screening for cross-coupling reaction conditions in the synthesis of 4-methoxyquinoline-8-amine (**43**).

3.2. Copper Complex Syntheses and Molecular Structures

The bidentate quinoline-guanidine hybrid ligands form stable copper complexes with copper centers, that can be applied in ATRP catalysis.[17] For examination of mechanistic aspects that can be related to different structural parameters, complexes of our modified TMGqu derivatives were synthesized and crystallized. The single crystals were then examined by X-ray diffraction. Besides elucidation of the molecular composition, the determination of bond lengths, bond angles and the general conformation of the copper catalysts were of interest. Furthermore, the τ_4 and τ_5 parameters were determined during analysis.[120,121] These parameters quantify certain distortions that can be present in fourfold or fivefold geometries. For tetra-coordinated complexes, the τ_4 parameter reaches a value of $\tau_4 = 0$ for square-planar geometry, whereas undistorted tetrahedral complexes give a parameter of $\tau_4 = 1$ (equation 17). Fivefold coordinated metal centers can be analogously specified by the τ_5 parameter (equation 18). It reaches $\tau_5 = 0$ for square-pyramidal conformation and $\tau_5 = 1$ for trigonal-bipyramidal complexes.

$$\tau_4 = \frac{360° - \alpha - \beta}{141°} \tag{17}$$

$$\tau_5 = \frac{\alpha - \beta}{60°} \tag{18}$$

In guanidine chemistry, the structural parameter ρ is introduced to quantify the elongation of the guanidine C=N double bond upon coordination. It is defined as the ratio of the imine bond length (a) and the mean amine bond lengths (b, c, equation 19). A non-coordinated tetramethylguanidine exhibits values of around $\rho = 0.93$, whereas protonated and completely delocalized species can lead to a value of $\rho = 1.00$.[69]

$$\rho = \frac{2a}{b+c} \tag{19}$$

The angles between the guanidine plane (derived from $\mathrm{N_{gua}}$ and two $\mathrm{N_{amine}}$ atoms) and the neighboring planes incorporating the carbon atoms (each a $\mathrm{C_{gua}}$ and two $\mathrm{CH_3}$ atoms) are called guanidine twist.[122] These twists can be observed in molecular structures obtained from X-ray diffraction and result from interactions between the adjacent $\mathrm{N{-}CH_3}$ groups. Smaller twist allow an increased overlap of the conjugated orbitals, leading to a greater delocalization and stabilization of the guanidine π system.

The solid complexes were synthesized by combining ligand and copper salt solutions followed by crystallization through vapor diffusion. Hence, two equivalents of the ligand and one equivalent of the copper halide were dissolved in acetonitrile. The copper halide solution was then added to the ligand solution and the complex formation was observed by a red shift of the absorption spectra. In practice, coordination was perceived as darkening of the yellowish ligand solutions. The complex solutions were then filled into test tubes (10 mL), which were placed inside Schlenk tubes (50 mL). Crystallization was induced by vapor diffusion of anti-solvents (5 mL to 8 mL), such as diethyl ether or toluene, which were added to the outer chamber of the Schlenk tube.[123] All procedures were conducted in a nitrogen filled glove box and all solvents were distilled and degassed prior to use. The sealed crystallization assays of $\mathrm{Cu^I}$ complexes were stored within the glove box, whereas the sealed $\mathrm{Cu^{II}}$ assays were removed and stored outside the glove box due to space limitations.

3.2.1. Copper(I) bromide Complexes

The molecular structures of the CuBr complexes obtained from single crystal X-ray diffraction can be separated into two classes. The ligands TMGqu, TMG6Methoxyqu and TMG6dmaqu form homoleptic bischelate cationic complexes with non-coordinating bromide counterions ($\mathrm{[Cu(TMGqu)_2]Br}$ Figure 3.6,[17] $\mathrm{[Cu(TMG6Methoxyqu)_2]Br}$ (**C1**) Figure 3.7 and $\mathrm{[Cu(TMG6dmaqu)_2]Br}$ (**C2**) Figure 3.8). In contrast, the electron-deficient TMG6Nitroqu ligand and the TMG6Brqu ligand form neutral monochelate complexes with coordinating bromide ligands ([Cu(TMG6Nitroqu)Br (**C3**) Figure 3.9 and [Cu(TMG6Brqu)Br] (**C4**) Figure 3.10).

Upon investigation of the bond lengths of the bischelate complexes, certain variations were identified (Table 3.2). The molecular packing within the crystal lattice resulted in small distortions. For estimation of the complex geometry in solution, it was assumed that for equivalent bonds, the individual bond lengths should oscillate around an average value. Therefore, average bond length values for equivalent bonds were calculated. Although the bond length of the $\mathrm{N_{gua}-Cu}$ bond within each complex differ considerably, their average values are surprisingly constant ($\mathrm{N_{gua}-Cu}$ TMGqu 2.121 Å, TMG6Methoxyqu 2.124 Å and TMG6dmaqu 2.122 Å). In contrast, the average $\mathrm{N_{qu}-Cu}$ bonds show a clear trend to elongation when ligands with electron-donating substituents are used ($\mathrm{N_{qu}-Cu}$ TMGqu: 1.980 Å, TMG6Methoxyqu 1.990 Å and TMG6dmaqu 2.021 Å). As a result of the elongated $\mathrm{N_{qu}-Cu}$ bonds, the average bite angle of the ligands decreases slightly (TMGqu: 82.1°, TMG6Methoxyqu: 81.2° and TMG6dmaqu: 81.0°). All three complexes exhibit a strongly distorted tetrahedral coordination with angles from 64° to 69° between the chelate planes and values of $\tau_4 \approx 0.6$. The bonds of the guanidine moieties are of similar lengths, affording ρ parameters around $\rho \approx 0.98$. The amine ($-\mathrm{N(CH_3)_2}$) groups of the guanidines are twisted out of the planes by average twist angles of 29° to 31°. These parameters are within the expected range[17] and unlike the variations of the N–Cu bonds, no trends of these parameters could be related to differences in electron-donation of the substituents at position C6.

Table 3.2: Key parameters of the bischelate CuBr complexes $\mathrm{[Cu(TMGqu)_2]Br}$[17], $\mathrm{[Cu(TMG6Methoxyqu)_2]Br}$ (**C1**) and $\mathrm{[Cu(TMG6dmaqu)_2]Br}$ (**C2**).

bond lengths [Å]	$\mathrm{[Cu(TMGqu)_2]Br}$	**C1**	**C2**
$\mathrm{N_{gua}-Cu}$	2.1175(15)	2.131(3)	2.141(2)
$\mathrm{N_{qu}-Cu}$	1.9861(15)	1.979(4)	1.999(2)
$\mathrm{N'_{gua}-Cu}$	2.1240(15)	2.116(3)	2.1036(19)
$\mathrm{N'_{qu}-Cu}$	1.9738(15)	2.000(4)	2.043(2)
average $\mathrm{N_{gua}-Cu}$	2.121	2.124	2.122
average $\mathrm{N_{qu}-Cu}$	1.980	1.990	2.021
angles [°]			
$\mathrm{N_{gua}-Cu-N_{qu}}$	81.71(6)	80.82(14)	81.20(8)
$\mathrm{N'_{gua}-Cu-N'_{qu}}$	82.53(6)	81.52(14)	80.92(8)
chelate planes	65.6	69.4	64.4
τ_4	0.58	0.62	0.59
guanidine moiety			
average ρ	0.98	0.97	0.98
twist angle	31.3	29.6	29.2

The [Cu(TMG6Nitroqu)Br] complex (**C3**) was crystallized from an assay containing two equivalents of the ligand. The [Cu(TMG6Brqu)Br] complex (**C4**) however, was obtained from a solution with an excess of CuBr after evaporation of the solvent. It was concluded that the stabilization of the $\mathrm{Cu^I}$ metal center by the TMG6Nitroqu ligand was not sufficient to replace the bromide anion affording a cationic complex. Due to the use of an excess of CuBr, a similar conclusion cannot be drawn for the TMG6Brqu copper complex. Nevertheless, these compounds prove the existence of monochelate complexes of this ligand family. Similar to the bischelate copper catalysts, the monochelate complexes do not exhibit significant changes

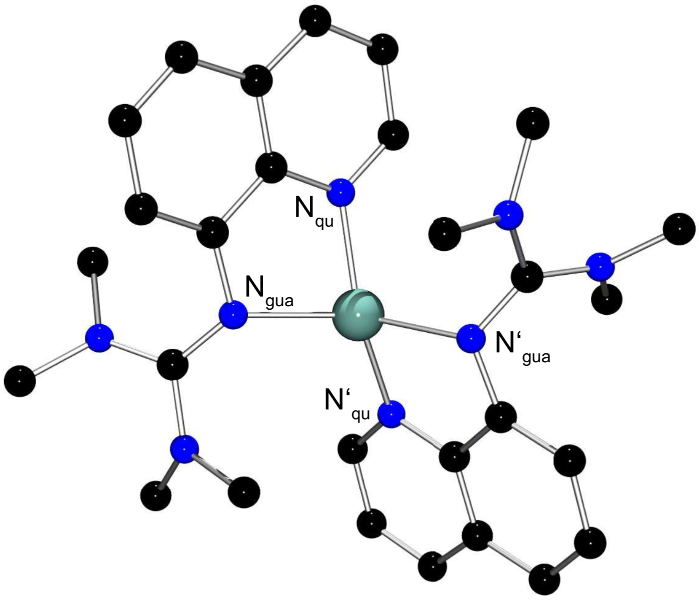

Figure 3.6: Molecular structure of $[Cu(TMGqu)_2]^+$ in crystals of $[Cu(TMGqu)_2]Br$. Hydrogen atoms and non-coordinating bromide anions were omitted for clarity.[17]

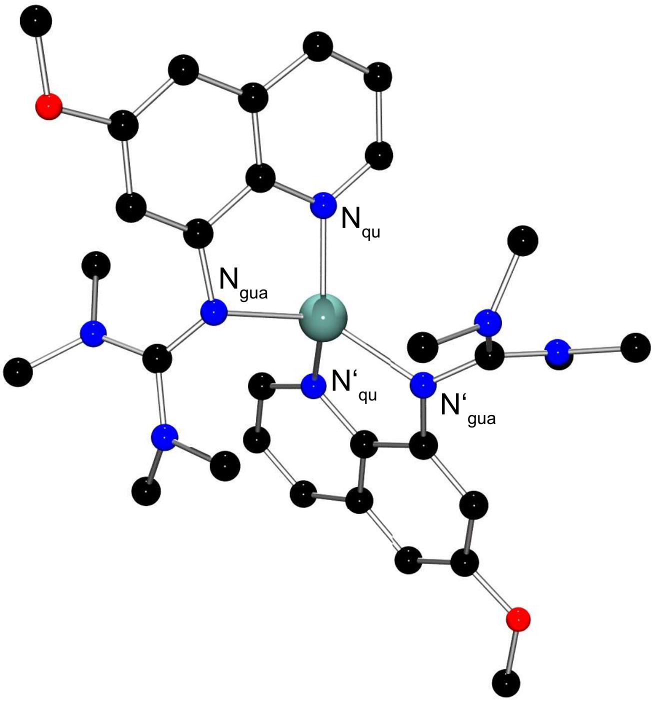

Figure 3.7: Molecular structure of $[Cu(TMG6Methoxyqu)_2]^+$ in crystals of $[Cu(TMG6Methoxyqu)_2]Br$ (**C1**). Hydrogen atoms and non-coordinating bromide anions were omitted for clarity.

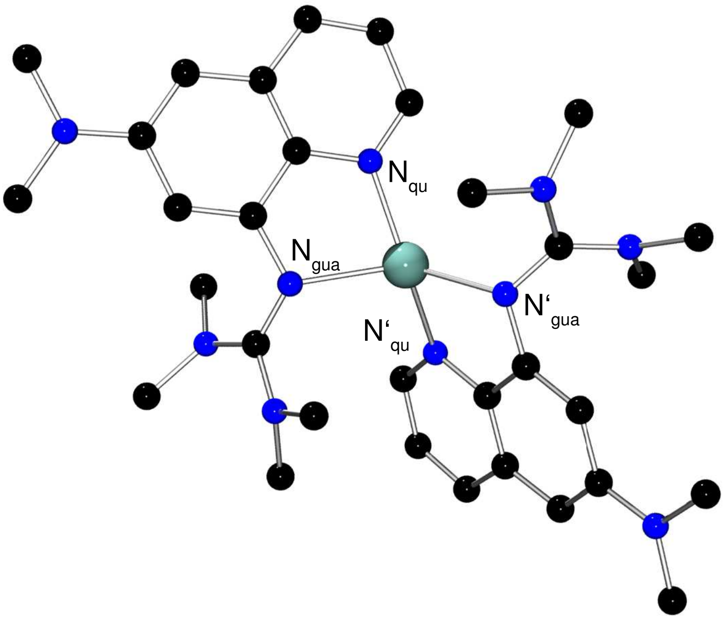

Figure 3.8: Molecular structure of $[Cu(TMG6dmaqu)_2]^+$ in crystals of $[Cu(TMG6dmaqu)_2]Br$ (**C2**). Hydrogen atoms and non-coordinating bromide anions were omitted for clarity.

of the average $N_{gua}-Cu$ bond (Table 3.3). In analogy with these observations, the average $N_{qu}-Cu$ bond is elongated for the less electron-deficient TMG6Brqu complex. In contrast to the bischelate complexes, additional bromide ligands are bound to these copper metal centers. Beside a longer Cu−Br bond for the TMG6Brqu complex, the resulting trigonal-planar geometry is similar. The guanidine moieties exhibit the same bond lengths for their C=N and C−N bonds, affording delocalization parameters of around $\rho \approx 1.00$. The amine groups are twisted out of the guanidine plane by 28°. In comparison to the bischelate complexes, the guanidine moiety experiences smaller distortion and more uniform bond lengths.

Table 3.3: Key parameters of monochelate CuBr complexes [Cu(TMG6Nitroqu)Br] (**C3**) and [Cu(TMG6Brqu)Br] (**C4**).

bond lengths [Å]	**C3**	**C4**
$N_{gua}-Cu$	2.076(2)	2.067(3)
$N_{qu}-Cu$	2.005(2)	2.029(3)
Cu−Br	2.2493(4)	2.2733(6)
angles [°]		
$N_{gua}-Cu-N_{qu}$	82.14(8)	82.25(12)
$N_{gua}-Cu-Br$	129.77(6)	133.29 (8)
$N_{qu}-Cu-Br$	147.96 (6)	143.37 (9)
guanidine moiety		
average ρ	0.99	1.00
twist angle	27.9	28.5

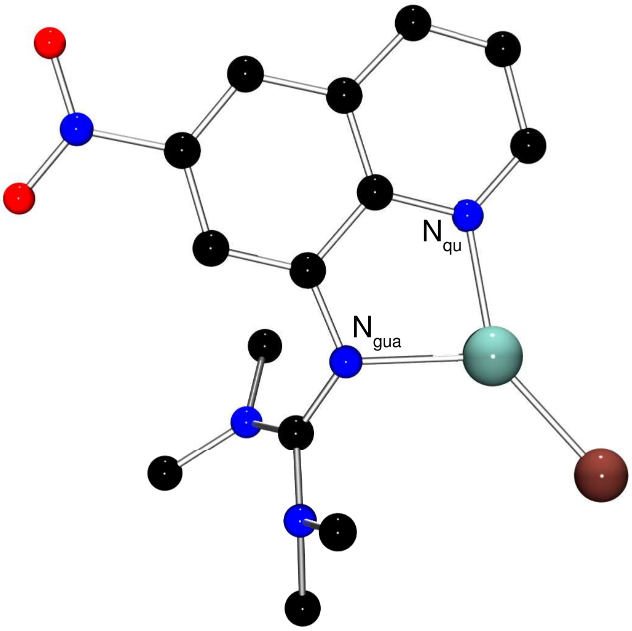

Figure 3.9: Molecular structure of the monochelate complex [Cu(TMG6Nitroqu)Br] (**C3**), exhibiting trigonal-planar geometry. Hydrogen atoms were omitted for clarity.

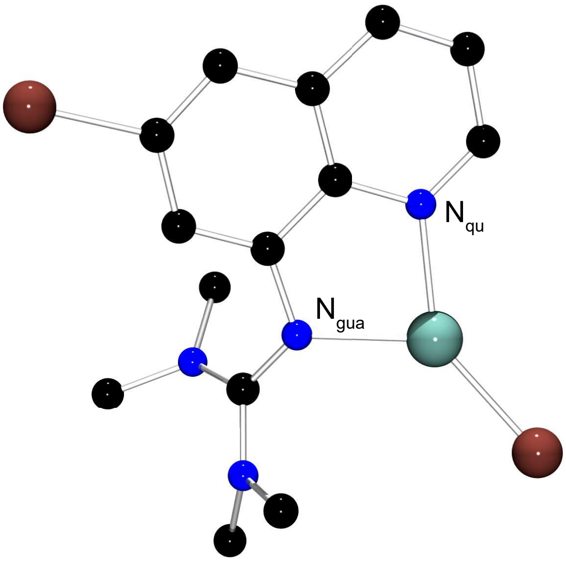

Figure 3.10: Molecular structure of the monochelate complex [Cu(TMG6Brqu)Br] (**C4**), exhibiting trigonal-planar geometry. Hydrogen atoms were omitted for clarity.

3.2.2. Copper(II) bromide Complexes

All $CuBr_2$ complexes of the TMGqu ligand derivatives exhibit bischelate coordination with an additional coordinating bromide ligand ($[Cu(TMGqu)_2Br]Br$[17] Figure 3.11, $[Cu(TMG6Methoxyqu)_2Br]Br$ (**C5**) Figure 3.12, $[Cu(TMG6dmaqu)_2Br]Br \cdot 2\,C_2H_3N$ (**C6**) Figure 3.13, $[Cu(TMG6Nitroqu)_2Br]Br \cdot C_2H_3N$ (**C7**) Figure 3.14 and $[Cu(TMG6Brqu)_2Br]Br \cdot 2\,C_2H_3N \cdot 0.5\,C_7H_8$ (**C8**) Figure 3.15). Comparing the average N−Cu bonds of the ligands, only small deviations are found (Table 3.4). While no significant difference in the average $N_{qu}-Cu$ bond length of the complexes can be observed, the average $N_{gua}-Cu$ bond is slightly elongated for the more electron-rich ligand TMG6Methoxyqu (**C5**) and the shortest for the most electron-rich complex **C6** with the TMG6dmaqu ligand. However, the obtained bond length differences are rather small, exhibiting statistic significance only between the shortest and longest average bonds. Furthermore, the electron-deficient ligand TMG6Nitroqu affords the complex **C7** with the second longest $N_{gua}-Cu$ bonds. Hence, a relation of the bond lengths similar to the CuBr complexes is not observed. However, major variations are found for the Cu−Br bonds. The TMGqu complex[17] possesses the longest copper halide bond (2.648 Å), followed by the much shorter Cu−Br bond of the TMG6dmaqu complex (**C6**, 2.5963 Å). The TMG6Nitroqu $CuBr_2$ complex **C7** exhibited the shortest Cu−Br bond (2.518 Å), whereas the values of the TMG6Methoxyqu (**C5**, 2.546 Å) and TMG6Brqu (**C8**, 2.575 Å) complexes are found to lie in between. The C=N and C−N bonds of each guanidine unit are of similar lengths, leading to ρ values around $\rho \approx 1.00$. The average guanidine twists are almost constant for all the complexes with twist angles of 27° to 28°. Due to the severely elongated bond in the TMGqu complex, structure-property relations could not be deduced for the $CuBr_2$ complexes.

Crystallization assays of the DMEG6Methoxyqu ligand with $CuBr_2$ did not lead to well-defined structures. A partial charge close to the C5 position of the ligands indicated that bromination of small amounts of the ligands could have occurred. This bromination presumably resulted from a reaction of the quinoline core with an excess of $CuBr_2$.[124] Furthermore, assays which were left to develop for elongated periods of time appeared to contain larger amounts of the respective products. These findings were in accordance to the synthetic experiences, rendering exceptionally electron-rich ligands susceptible to oxidation. As a result, future crystallization assays should be conducted under conditions that improve faster crystal growth, although the risk of inferior data quality might be increased. Furthermore, assays at lower temperatures without subjection to UV light (storage in a fridge or freezer) could reduce oxidative side reactions. Most importantly, the use of an excess of $CuBr_2$ should be avoided.

Table 3.4: Structural parameters of the $CuBr_2$ complexes $[Cu(TMGqu)_2Br]Br \cdot CH_3CN$[17], $[Cu(TMG6Methoxyqu)_2Br]Br$ (**C5**), $[Cu(TMG6dmaqu)_2Br]Br \cdot 2\,C_2H_3N$ (**C6**), $[Cu(TMG6Nitroqu)_2Br]Br \cdot C_2H_3N$ (**C7**) and $[Cu(TMG6Brqu)_2Br]Br \cdot 2\,C_2H_3N \cdot 0.5\,C_7H_8$ (**C8**).

bond length [Å]	$[Cu(TMGqu)_2Br]Br$	**C5**	**C6**	**C7**	**C8**
$N_{gua}-Cu$	2.047(6)	2.1223(38)	2.069(7)	2.0722(43)	2.048(3)
$N_{qu}-Cu$	1.979(6)	1.9656(38)	1.969(6)	1.9730(41)	1.976(3)
$N'_{gua}-Cu$	2.061(6)	2.0551(35)	2.036(7)	2.0644(42)	2.077(3)
$N'_{qu}-Cu$	1.984(6)	1.9830(39)	1.979(6)	1.9709(40)	1.980(3)
$Cu-Br$	2.6478(11)	2.5461(7)	2.5963(12)	2.5180(8)	2.5745(6)
avg. $N_{gua}-Cu$	2.054	2.084	2.053	2.068	2.063
avg. $N_{qu}-Cu$	1.982	1.974	1.974	1.972	1.978
angles [°]					
$N_{gua}-Cu-N_{qu}$	81.7(2)	80.65(15)	81.5(3)	81.37(17)	81.62(11)
$N'_{gua}-Cu-N'_{qu}$	81.8(2)	81.67(15)	82.0(3)	81.33(17)	81.44(11)
τ_5	0.72	0.73	0.74	0.92	0.79
guanidine moiety					
average ρ	1.01	1.00	1.00	1.01	1.01
average twist	26.8	27.3	28.2	27.2	28.4

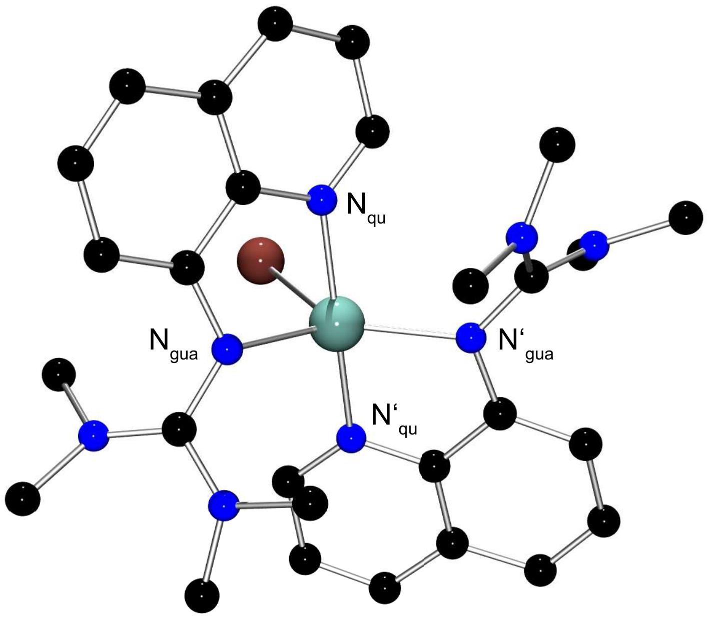

Figure 3.11: Molecular structure of $[Cu(TMGqu)_2Br]^+$ in crystals of $[Cu(TMGqu)_2Br]Br \cdot CH_3CN$.[17] Hydrogen atoms, acetonitrile solvent molecules and non-coordinating bromide anions were omitted for clarity.

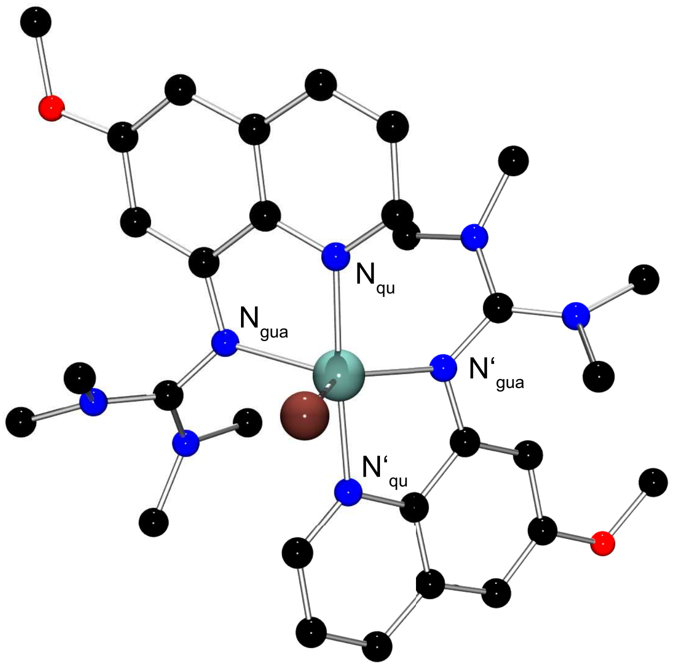

Figure 3.12: Molecular structure of $[Cu(TMG6Methoxyqu)_2Br]^+$ in crystals of $[Cu(TMG6Methoxyqu)_2Br]Br$ (**C5**). Hydrogen atoms and non-coordinating bromide anions were omitted for clarity.

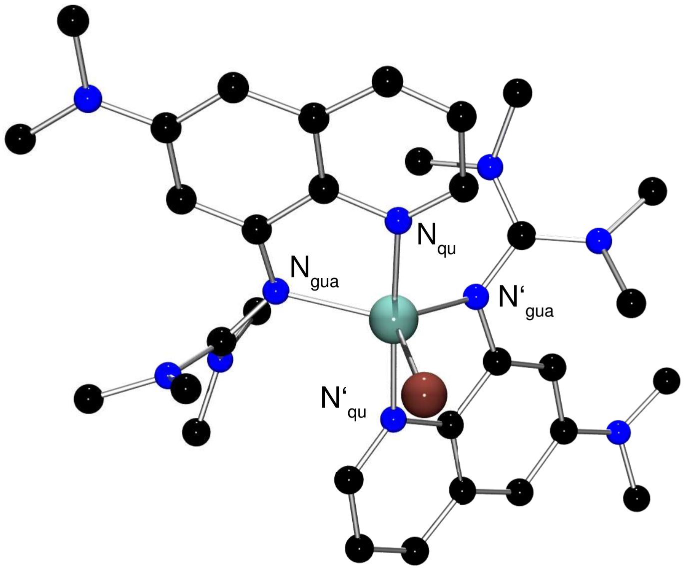

Figure 3.13: Molecular structure of $[Cu(TMG6dmaqu)_2Br]^+$ in crystals of $[Cu(TMG6dmaqu)_2Br]Br \cdot 2\,CH_3CN$ (**C6**). Hydrogen atoms, acetonitrile solvent molecules and non-coordinating bromide anions were omitted for clarity.

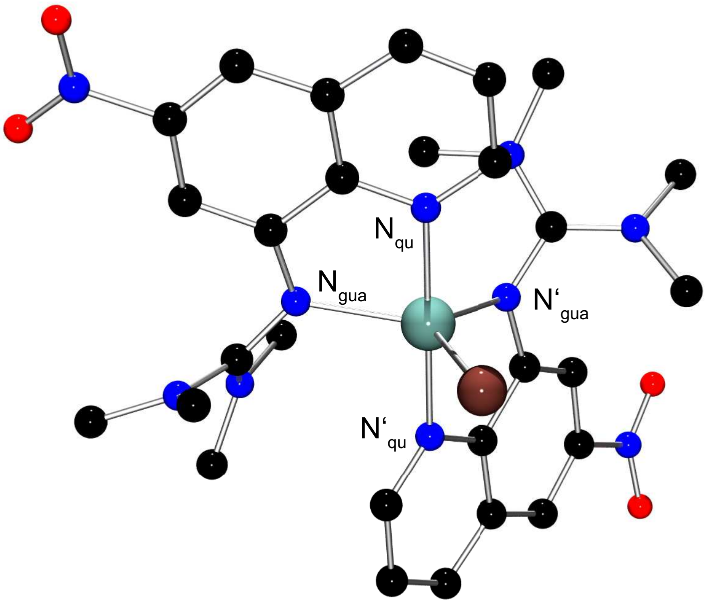

Figure 3.14: Molecular structure of $[Cu(TMG6Nitroqu)_2Br]^+$ in crystals of $[Cu(TMG6Nitroqu)_2Br]Br \cdot CH_3CN$ (**C7**). Hydrogen atoms, acetonitrile solvent molecules and non-coordinating bromide anions were omitted for clarity.

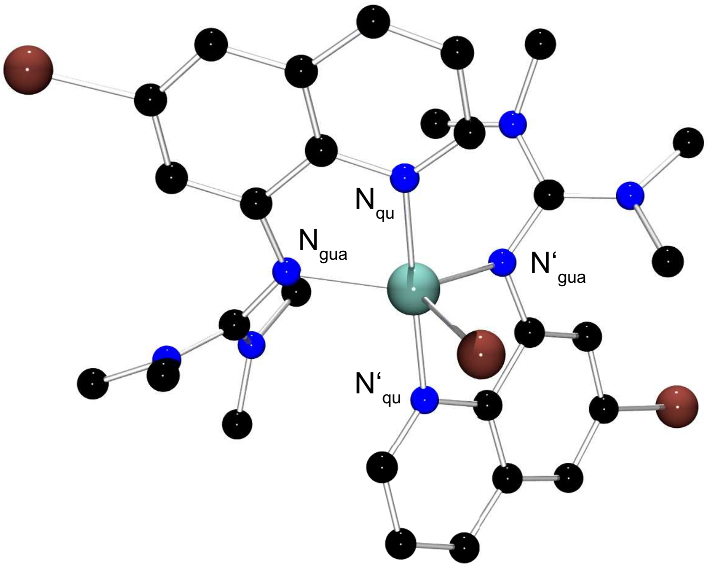

Figure 3.15: Molecular structure of $[Cu(TMG6Brqu)_2Br]^+$ in crystals of $[Cu(TMG6Brqu)_2Br]Br \cdot CH_3CN \cdot 2\,C_7H_8$ (**C8**). Hydrogen atoms, acetonitrile and toluene solvent molecules and non-coordinating anions were omitted for clarity.

3.2.3. Copper(I) chloride Complexes

In ATRP reactions, copper halide complexes with electron-donating ligands can be employed as catalysts. Due to their increased reactivity, CuBr compounds are usually applied. For achieving a better understanding of the coordination sphere of these complexes, CuCl analogs were synthesized, followed by crystallization and single crystal X-ray diffraction analysis. It was expected that the ligands would coordinate to the Cu^I metal centers, forming cationic complexes that should by closely related to their bromide counterparts. The ligands TMGqu,[17] TMG6Methoxyqu and TMG6Nitroqu were investigated and were found to form bischelate cationic complexes with non-coordinating counter anions (for $[Cu(TMGqu)_2]Cl$ and $[Cu(TMG6Methoxyqu)_2][CuCl_2]$ (**C9**), see bromide figures above (Figure 3.6 and Figure 3.7), for $[Cu(TMG6Nitroqu)_2][CuCl_2]$ (**C10**) see Figure 3.16). Although Cu−Cl bonds are generally stronger than Cu−Br bonds, the TMG6Nitroqu ligand does not show monochelate coordination and is able to replace the chloride anion at the copper center of **C10**. Furthermore, the comparison of the different bond lengths does not reveal trends that can be related to the molecular structures of the CuBr complexes (Table 3.5). The longest average $N_{gua}-Cu$ bond is found in the TMGqu complex (2.118 Å). The substituted derivatives display considerably shorter bonds almost with the same length (**C9** 2.086 Å and **C10** 2.074 Å). The variations of the average $N_{qu}-Cu$ bonds are much smaller, showing significant differences only for the longest and the shortest bonds (TMGqu 1.978 Å, **C10** 1.987 Å and **C9** 1.997 Å). After all, the ligands average bite angles are the same for all of the three complexes (TMGqu: 82.1°, **C9** 82.2° and **C10** 82.3°). Similar to the bischelate CuBr complexes (3.2.1), the ρ parameters lie around $\rho \approx 0.98$ with twist angles between 29° and 31° and the angles between the chelate planes range from 66° to 69°. Upon comparison of the those values, the angles between the chelate planes of the TMG6Methoxyqu Cu^I complexes are increased by around 3° compared to the other derivatives.

Table 3.5: Key parameters of the CuCl complexes $[Cu(TMGqu)_2]Cl$[17], $[Cu(TMG6Methoxyqu)_2][CuCl_2]$ (**C9**) and $[Cu(TMG6Nitroqu)_2][CuCl_2]$ (**C10**).

bond lengths [Å]	$[Cu(TMGqu)_2]Cl$	**C9**	**C10**
$N_{gua}-Cu$	2.120(3)	2.093(2)	2.0792(19)
$N_{qu}-Cu$	1.974(3)	1.985(3)	1.9775(20)
$N'_{gua}-Cu$	2.115(3)	2.078(3)	2.0691(19)
$N'_{qu}-Cu$	1.981(3)	2.009(3)	1.9974(21)
average $N_{gua}-Cu$	2.118	2.086	2.074
average $N_{qu}-Cu$	1.978	1.997	1.987
angles [°]			
$N_{gua}-Cu-N_{qu}$	81.8(1)	82.48(10)	82.09(8)
$N'_{gua}-Cu-N'_{qu}$	82.4(1)	81.82(10)	82.49(8)
chelate planes	65.9	68.8	65.5
τ_4	0.56	0.62	0.58
guanidine moiety			
average ρ	0.97	0.98	0.98
average twist	31.2	30.1	29.2

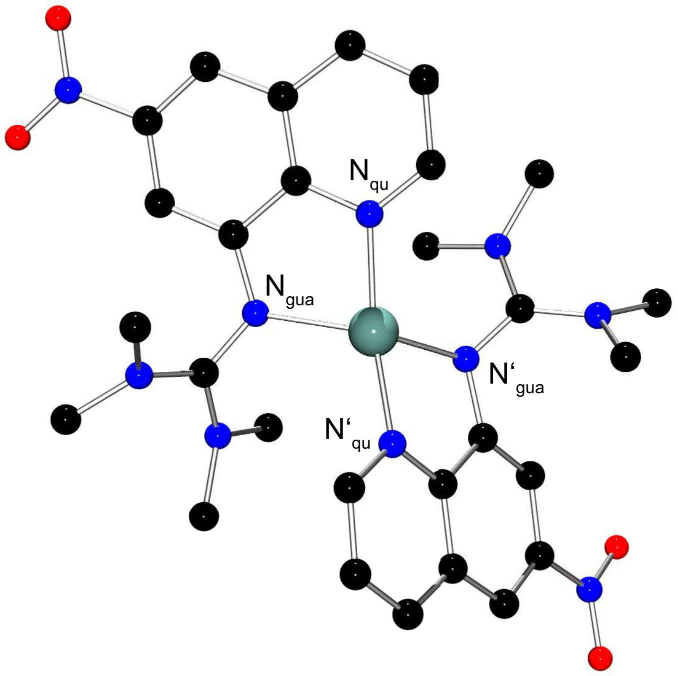

Figure 3.16: Molecular structure of $[Cu(TMG6Nitroqu)_2]^+$ in crystals of $[Cu(TMG6Nitroqu)_2][CuCl_2]$ (**C10**), with distorted tetrahedral geometry. Hydrogen atoms and non-coordinating $CuCl_2^-$ anions were omitted for clarity.

3.2.4. Copper(II) chloride Complexes

Reactions of the ligands TMGqu, TMG6Methoxyqu and TMG6Brqu with $CuCl_2$ afforded bischelate cationic complexes with coordinating chloride ligand ($[Cu(TMGqu)_2Cl]Cl$ Figure 3.17, $[Cu(TMG6Methoxyqu)_2Cl][CuCl_2]$ (**C11**) Figure 3.18 and $[Cu(TMG6Brqu)_2Cl]Cl \cdot 2\,C_2H_3N \cdot 0.5\,C_7H_8$ (**C12**) Figure 3.19). TMG6Nitroqu, however, yielded a monochelate neutral complex with two coordinating chloride ligands ($[Cu(TMG6Nitroqu)Cl_2] \cdot C_{6.92}H_{7.91}$ (**C13**) Figure 3.20). The $CuCl_2$ complexes of the less electron-rich ligands TMGqu and TMG6Brqu (**C12**) exhibit similar coordination geometries (Table 3.6) with statistically indifferent average $N_{gua}-Cu$ and $N_{qu}-Cu$ bond lengths (average $N_{gua}-Cu$ in TMGqu 2.081 Å and **C12** 2.075 Å, average $N_{qu}-Cu$ in TMGqu 1.982 Å and **C12** 1.977 Å). The electron-rich ligand TMG6Methoxyqu afforded the complex **C11** with an elongated average $N_{gua}-Cu$ bond length (2.118 Å). The average $N_{qu}-Cu$ bond length, however, does not change (1.982 Å). The Cu−Cl bond length of complex **C11** is the shortest of the three ligands (2.362 Å), whereas the TMG6Brqu ligand yielded the complex with the longest Cu−Cl bond (**C12** 2.401 Å). The average bite angle is insignificantly smaller for the TMG6Methoxyqu complex **C11** (80.7°) due to the elongated bond. In comparison to the $CuBr_2$ complexes, both the value of ρ and the guanidine twist are very similar. The elongated C=N bonds result in ρ values slightly above one, the twist angles lie between 27° and 28°.

Table 3.6: Key parameters of the $CuCl_2$ complexes $[Cu(TMGqu)_2Cl]Cl \cdot H_2O$[17], $[Cu(TMG6Methoxyqu)_2Cl]Cl$ (**C11**), $[Cu(TMG6Brqu)_2Cl]Cl \cdot 2\,C_2H_3N \cdot 0.5\,C_7H_8$ (**C12**) and $[Cu(TMG6Nitroqu)Cl_2] \cdot C_{6.92}H_{7.91}$ (**C13**)

bond lengths [Å]	$[Cu(TMGqu)_2Cl]Cl$	**C11**	**C12**	**C13**
$N_{gua}-Cu$	2.133(2)	2.065(2)	2.0952(18)	1.9686(25)
$N_{qu}-Cu$	1.979(2)	1.9820(19)	1.9771(18)	2.0030(26)
$N'_{gua}-Cu$	2.029(2)	2.170(2)	2.0546(18)	
$N'_{qu}-Cu$	1.985(2)	1.9813(19)	1.9770(18)	
Cu−Cl	2.375(1)	2.3618(7)	2.4007(6)	2.2227(9)
Cu−Cl'				2.2352(9)
average $N_{gua}-Cu$	2.081	2.118	2.075	1.969
average $N_{qu}-Cu$	1.982	1.982	1.977	2.003
angles [°]				
$N_{gua}-Cu-N_{qu}$	80.9(1)	81.32(8)	81.10(7)	81.68(10)
$N'_{gua}-Cu-N'_{qu}$	81.7(1)	79.98(8)	81.55(7)	
τ_4				0.41
τ_5	0.62	0.63	0.85	
guanidine moiety				
average ρ	1.01	1.00	1.01	1.02
average twist	26.6	28.2	28.4	27.0

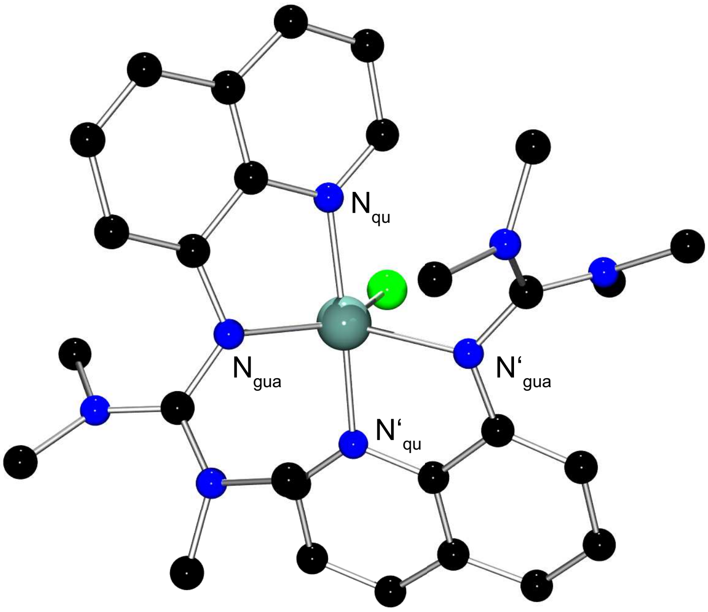

Figure 3.17: Molecular structure of $[Cu(TMGqu)_2Cl]^+$ in crystals of $[Cu(TMGqu)_2Cl]Cl \cdot H_2O$.[17] Hydrogen atoms, crystal water and non-coordinating chloride anions were omitted for clarity.

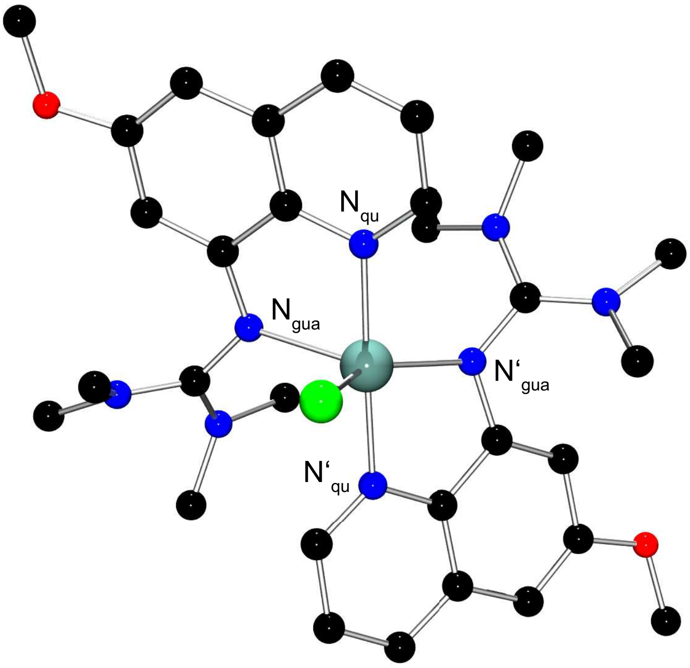

Figure 3.18: Molecular structure of $[Cu(TMG6Methoxyqu)_2Cl]^+$ in crystals of $[Cu(TMG6Methoxyqu)_2Cl]Cl$ (**C11**). Hydrogen atoms and non-coordinating chloride anions were omitted for clarity.

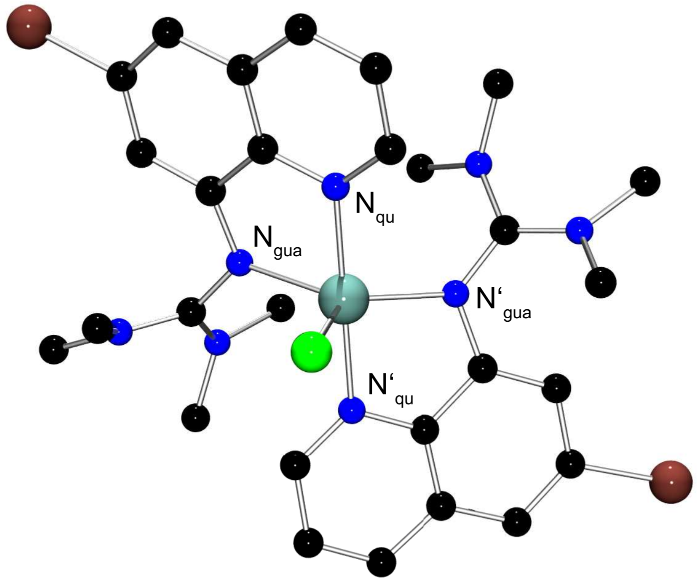

Figure 3.19: Molecular structure of $[Cu(TMG6Brqu)_2Cl]^+$ in crystals of $[Cu(TMG6Brqu)_2Cl]Cl \cdot 2\,C_2H_3N \cdot 0.5\,C_7H_8$ (**C12**). Hydrogen atoms, acetonitrile and toluene solvent molecules and non-coordinating chloride anions were omitted for clarity.

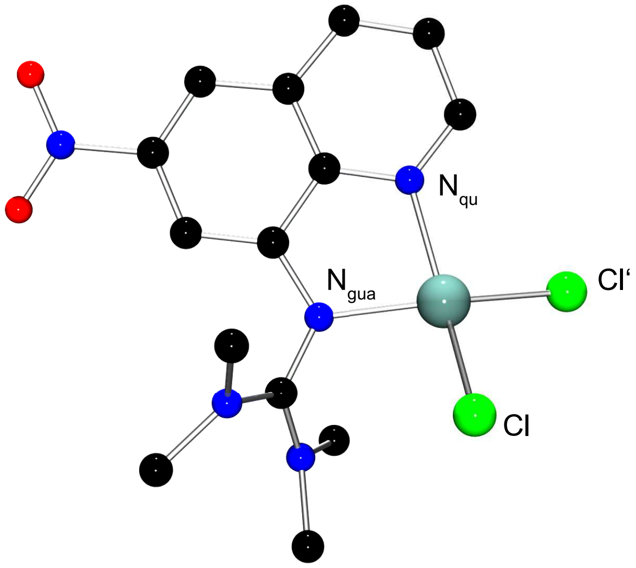

Figure 3.20: Molecular structure of monochelate $[Cu(TMG6Nitroqu)Cl_2]$ in crystals of $[Cu(TMG6Nitroqu)Cl_2] \cdot C_{6.92}H_{7.91}$ (**C13**). Hydrogen atoms, toluene molecules and non-coordinating anions were omitted for clarity.

3.2.5. Complex Summary

Copper halide complexes of our new TMGqu derived ligands have been synthesized and examined. The packing of the complexes within the crystal lattice seemed to have a major impact on the molecular geometry. All complexes showed non-symmetrical bonding of the ligands, resulting in different bond lengths of equivalent ligands. It was assumed that the molecular structure in solution would not exhibit such alternations. For evaluation of potential structural implications on the polymerization activity, the bond length values of the corresponding N−Cu bonds were averaged.

The molecular structures of the ATRP active CuBr catalysts exhibit tetrahedral coordination with two bidentate TMGqu derived ligands. Whereas the average $N_{gua}-Cu$ bonds do not show significant differences between the various complexes, the $N_{qu}-Cu$ bonds are elongated for the more electron-rich ligands. The electron-poor trigonal-planar CuBr complexes exhibit a similar elongation for the $N_{qu}-Cu$ bonds. As a consequence, it might be debated if the $N_{qu}-Cu$ bond could act as the major electron-donation path from the ligands to the copper centers.

The distortion of the tetrahedral coordination of the catalysts affords τ_4 values close to the transition towards the square-planar geometry ($\tau_4 \approx 0.6$). Similar coordination geometries are received for the CuCl complexes. However, the trend of the bond elongation observed in the previous complexes is not perceived in the chloride counterparts. The $[Cu(TMG6Methoxyqu)_2]^+$ cations exhibits the largest angle between the chelate planes of all Cu^I complexes.

Upon comparison of all crystal structures a tendency to form monochelate complexes is found for the TMG6Brqu and TMG6Nitroqu ligands. In dependence of the crystallization conditions coordination halide anion were not always replaced by TMGqu derivatives. During application, potential ligand dissociation reactions could therefore alter polymerization kinetics.

The Cu^{II} complexes do not exhibit structural trends similar to the CuBr complexes. The observed parameters of these compounds do not allow elucidations of aspects concerning the ligand influence on the properties of the complexes. However, the guanidine moieties of Cu^{II} complexes exhibit increased ρ parameters and decreased twist angles. Both aspects indicate an increased delocalization and stabilization of the π system.[122]

After all, a trend of bond elongation upon stronger electron-donation was perceived for CuBr complexes. In contrast, this trend was not found in the corresponding CuCl complexes. The strong influence of the counter anion and the crystal lattice seemed to impede the correlation of structural parameters and electron-donation of the ligand substituents. It was concluded that solid state structures of hybrid guanidine-quinoline copper complexes do not necessarily relate to other properties found in solution studies.

3.3. Polymerization

3.3.1. Polymerization setup and procedure

The synthesis of the copper catalysts and the subsequent identification of structural properties provided knowledge about the specific complexes. However, determination of catalytic activity required the application of the catalysts in polymerization reactions. The ATRP experiments mainly served analytical purposes and were therefore optimized thereto. As a result, the polymerization procedures provided excellent insights into the catalytic process. For application in industrial processes, reaction parameters should be adapted. With respect to analytical methods, styrene was used as monomer of choice. It offers very prominent signals during NMR spectroscopy for both the monomer and the polymer. Due to calibration with polystyrene standards, examination of the polymer samples with a gel permeation chromatography (GPC) reliably gave reproducible results.

The ATRP experiments were conducted in a Schlenk tube (10 mL) which was sealed with glass stoppers and high vacuum silicon grease. During preparation, the thoroughly cleaned Schlenk tubes were oven-dried at 150 °C before being introduced into a nitrogen-filled glove box. In the glove box, the catalyst complex or its single components were added, the joints were greased and the tubes were sealed. Following the removal of the reaction tubes from the glove box, they were connected to a Schlenk line. After sufficient purging, the tubes were filled with inert gas and a polymerization solution with distilled and degassed styrene and benzonitrile was introduced through an inert gas countercurrent.

In early polymerization experiments, the Schlenk tubes were heated in an oil bath. During analysis of the polymerization results, strong deviations in reaction rates for the same catalyst were observed. It was suggested that the large temperature gradient of the oil bath could have resulted in different reaction temperatures. On the surface, an oil bath can have a significantly lower temperature than at the bottom close to the heating plate. Reaction vessels which were placed in the oil bath could have been subjected to different temperatures, depending on their immersion depth. After replacing the oil bath with an aluminum heating block, the deviations diminished. In this improved setup, the Schlenk tubes were subjected to a constant gradient with an equal insertion depth, removing temperature dependent variations between individual samples.

During the first polymerization attempts, reactions were performed with the CuBr catalyst [Cu(TMG6Methoxyqu)$_2$]Br in styrene as solvent and monomer. After several runs, the obtained kinetic data indicated a loss of polymerization control at higher conversion. It was concluded, that the increasing viscosity of the polymerization mixture lead to reduced stirring. Additionally, an induction period of the polymerization reaction was observed. Although the solid activator complex was introduced, polymerization was impeded at first. It was concluded that a slow dissolution of the solids resulted in a decreased catalyst concentration in the beginning of the polymerization reaction. As a consequence, the polymerization mixture was diluted with solvents. After tests with several solvent combinations, styrene was diluted with benzonitrile. This optimization yielded slightly lower polymerization rates with significant improvements of the kinetic profile of the reaction.[17]

The first catalyst subjected to an ATRP reaction with optimized polymerization conditions was [Cu(TMG6Methoxyqu)$_2$]Br. The complex was prepared beforehand by reacting CuBr with two equivalents of the ligand in acetonitrile at room temperature. The catalyst was crystallized by vapor diffusion of diethyl ether into the solution. When introducing the crystalline solid into the reaction without the benzonitrile additive, delayed dissolution was observed, as mentioned above. With addition of benzonitrile, the solubility was greatly improved. In contrast, some of the catalysts were designed to be applied in bulk styrene without the addition of solubilizing benzonitrile. As a natural consequence of their design, these ligands formed complexes that could not be crystallized or precipitated. Therefore, the formation of the active catalyst was required to take place in the polymerization mixture. If the reaction was subjected to a preheating period prior to initiation, the *in situ* approach delivered the same results as a polymerization with crystalline catalyst. A preheating of ten minutes was regarded as sufficient for solvation and catalyst formation. As a result, all following polymerization reactions were conducted with addition of the catalyst in its single components. After preheating, the reaction mixture was initiated and the timer was started. The degassed 1-PEBr initiator was injected by syringe and it was taken care that no initiator droplets remained on the walls of the reaction tube above the solution. In doing so, it was ensured that the initiation took place immediately.

Samples of the polymerization reactions were taken after initiation and then every ten to fifteen minutes. The samples (approximately 0.2 mL) were collected with thoroughly purged Pasteur pipettes and filled in NMR tubes. The pipettes were rinsed with deuterated chloroform (0.6 mL $CDCl_3$) into the NMR tubes, minimizing systematic errors. In only very few occurances, improper purging of the pipettes resulted in contamination of the polymerization reaction with oxygen. As a result, the catalyst was oxidized and the reaction ceased (Figure 3.30). This phenomenon was well observable during analysis of the NMR data. As a consequence, all reaction assays that did not show this kind of retardation or termination were considered as successful. Generally, this method of sample taking was observed to be reliable.

Following the NMR experiments, the samples were removed from the NMR tubes and transferred into centrifuge tubes (10 mL). There, they were precipitated with ethanol (approximately 5 mL) at room temperature. Samples with short polymer chains that did not form precipitates were disposed. Afterwards, the polymer samples were subjected to centrifugation for approximately 20 min. The liquid phases were decanted and the samples were dissolved in dichloromethane. After precipitation with ethanol, the samples were placed in a centrifuge for a second time. Subsequently, the liquid phases were decanted and the polymer samples were dried in an oven at 50 °C over night. Finally, 5 mg of each white polymer powder were dissolved in THF (1 mL) and analyzed in a GPC unit.

3.3.2. Analysis of the polymerization reactions

The data obtained from the NMR spectra was analyzed to gain insight into the kinetic evolution of the polymerization reactions. For each sample, the monomer conversion was calculated from the integrals of the respective signals in the ^{1}H NMR spectra (Figure 3.21). The two methylene proton signals of the remaining styrene starting material (Ha) and the three proton signals of the resulting polymer (H1 and H2) were averaged (equations 20 and 21).

$$I_M = \frac{I_{a_1} + I_{a_2}}{2} \tag{20}$$

$$I_P = \frac{\frac{1}{2}I_1 + I_2}{2} \tag{21}$$

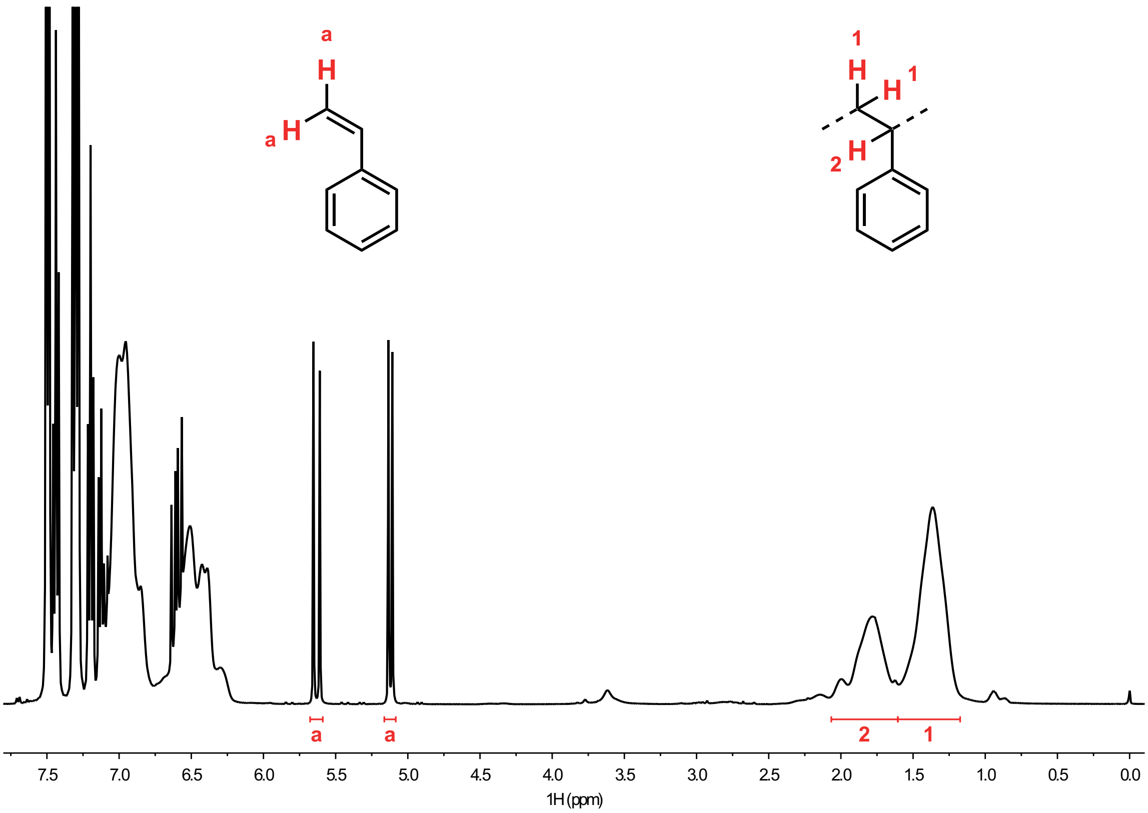

Figure 3.21: ^{1}H NMR Spectrum of a polymerization sample. Conversion can be determined from the integrals of the styrene (Ha) and polymer (H1, H2) proton signals.

The conversion C can be expressed as the ratio of reacted monomer [M]$_0$−[M] and the initial monomer concentration [M]$_0$ (22). Furthermore, the initial monomer concentration [M]$_0$ can be expressed as the remaining monomer concentration [M] and the concentration of monomers that are being incorporated into polymer chains [P] (23). Replacing $[\mathrm{M}]_0$ with [M] and [P], the conversion can be assessed from both the remaining and incorporated monomer concentrations. The ratio of these concentrations is directly proportional to the integral of their corresponding proton NMR signals. As a consequence, the reaction conversion can be determined from the sample spectra (24).

$$C = \frac{[\mathrm{M}]_0 - [\mathrm{M}]}{[\mathrm{M}]_0} \tag{22}$$

$$[\mathrm{M}]_0 = [\mathrm{M}] + [\mathrm{P}] \tag{23}$$

$$C = \frac{[\mathrm{P}]}{[\mathrm{M}] + [\mathrm{P}]} = \frac{I_P}{I_M + I_P} \tag{24}$$

After rearrangement of equation 22 and comparison with equation 8 (section 1.2.1), equation 25 is obtained. It describes how the apparent polymerization reaction rate constant k_{app} for the corresponding reaction conditions can be analytically related to the experimental data.

$$\ln\left(\frac{1}{1-C}\right) = k_{app}[\mathrm{R}^\bullet]t \tag{25}$$

As mentioned above (section 1.2.1), the relation expressed in equation 25 is an eminent characteristic of a controlled radical polymerization reaction. Plotting $\ln\left(\frac{1}{1-C}\right)$ against the reaction time t of an ATRP reaction should give k_{app} as the slope of the resulting linear regression. The polymerization rate constant k_p can then be calculated by division of k_{app} with the catalyst concentration $[\mathrm{C}]_0$ (equation 26).

$$k_p = \frac{k_{app}}{[\mathrm{C}]_0} \tag{26}$$

Following the kinetic analysis, the purified polymers were placed in a GPC unit. The resulting data showed the molecular mass distribution of each sample. Commonly in CRP, the molecular masses of all polymer chains in a reaction increase homogeneously. As a result, the theoretical molecular mass $\mathrm{M}_{\mathrm{theo}}$ is linearly dependent on the reaction conversion and can be calculated from the targeted molecular mass $\mathrm{M}_{\mathrm{targ}}$ and the conversion C (equation 27). The polymer's targeted molecular mass can be calculated from the initial concentrations of the initiator ($[\mathrm{I}]_0$) and the molar mass of the styrene monomer ($\mathrm{M}_{\mathrm{sty}}$).

$$\mathrm{M}_{\mathrm{theo}} = \mathrm{M}_{\mathrm{targ}} \cdot C = \frac{[\mathrm{M}]_0}{[\mathrm{I}]_0} \cdot \mathrm{M}_{\mathrm{sty}} \cdot C \tag{27}$$

The ligand TMG6Methoxyqu was applied in ATRP reactions as a bischelate CuBr complex. Due to its well crystallizing nature, the polymerization reactions were conducted in styrene benzonitrile mixtures. A degree of polymerization of 100 styrene units was targeted for all polymerization reactions. Therefore, a molar ratio of styrene to initiator of 100 was used with a catalyst concentration of 1 mol% (short: 100:1:1, sty:i:c). The catalyst [Cu(TMG$_6$Methoxyqu)$_2$]Br exhibited fast polymerization reactions with a high degree of control (Figure 3.22). The polymerization rate constant k_p, which was averaged from six polymerization reactions, was determined as $k_p = 3.4 \times 10^{-3}\,\mathrm{L\,mol^{-1}\,s^{-1}}$ for this reaction condition. The average polydispersity was low (PD $= 1.11$) and the obtained molecular masses were close to the theoretical values.

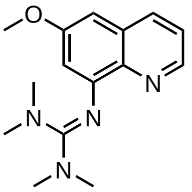

TMG6Methoxyqu

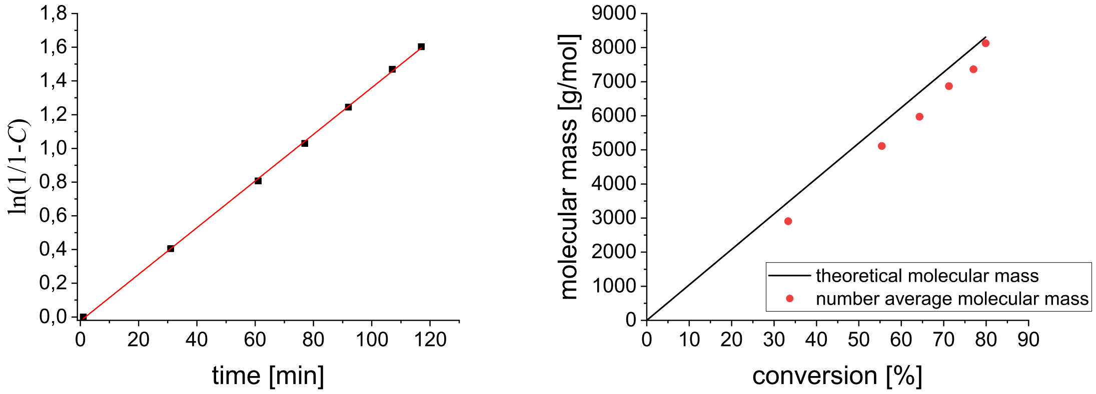

Figure 3.22: Plots of the polymerization reaction of styrene in benzonitrile with the catalyst [Cu(TMG6Methoxyqu)$_2$]Br (100:1:1). Left: kinetic analysis of the reaction conversion (black) and linear regression (red), right: molecular masses of the obtained polymer samples. C: conversion.

In bulk styrene, ATRP catalysts derived from the ligand TMG6Methoxyqu exhibited a reduced solubility. The data from these experiments showed long induction periods and slow initiation of the polymerization reactions (not shown). Consequently, the ligand TMG6EHoxyqu with improved solubility in bulk styrene was developed. The catalyst complexes were prepared *in situ* and the polymerization conditions were not altered otherwise. The previously used styrene benzonitrile solution was polymerized (Figure 3.23) and compared to kinetics of bulk styrene polymerization (Figure 3.24). With molar ratios of 100:1:1 (sty:i:c) all reactions were conducted at 110 °C, as above. The kinetic results were quite similar for both assays. During the bulk polymerization an average polymerization rate constant of $k_p = 7.5 \times 10^{-4}\,\mathrm{L\,mol^{-1}\,s^{-1}}$ was observed. A similar rate constant of $k_p = 7.2 \times 10^{-4}\,\mathrm{L\,mol^{-1}\,s^{-1}}$ was obtained from solution polymerization in benzonitrile. The addition of a solvent seemed to slightly slow down the reaction. However, the error margins of both polymerization assays overlapped, rating the difference as statistically insignificant. Comparing TMG6EHoxyqu to catalysts with less soluble ligands, the polymerization reaction kinetics in bulk monomer was drastically improved. With this ligand the molecular masses of the polymer samples were well within the order of accuracy for both bulk and solvent polymerization conditions.

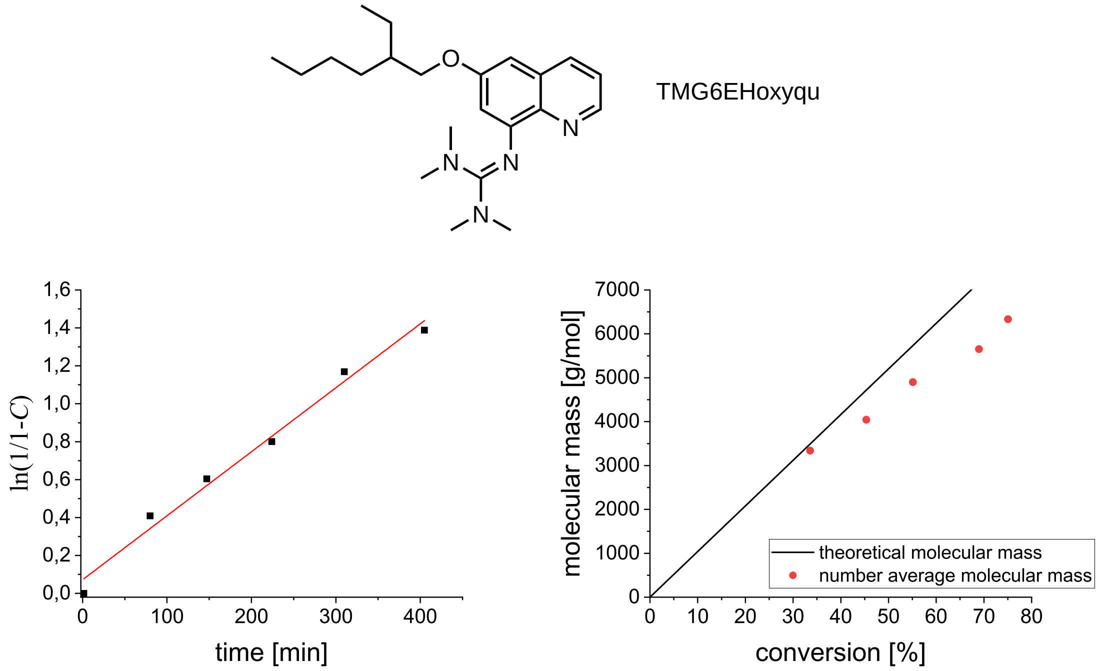

Figure 3.23: Plots of a styrene polymerization in benzonitrile with a TMG6EHoxyqu CuBr catalyst (100:1:1). Left: kinetic analysis of the reaction conversion (black) and linear regression (red), right: molecular masses of the obtained polymer samples. C: conversion.

The ligand TMG6Brqu was only applied in polymerization of styrene in benzonitrile solution. It was expected that the bromide substituent did not increase catalyst solubility considerably, rendering polymerization in bulk styrene not promising. The reactions were performed using our previously described standard procedure (section 6.4). In ATRP reactions, the CuBr complex of the ligand reacted notably slower than other substituted catalysts. The progress of the conversion exhibited a high degree of control (Figure 3.25), contrasting the retarded increase of the molecular masses, which showed a non-ideal growth. At higher conversions, the molecular mass of the polymer was reduced and the slope was lower than expected. The contrast to the ideally rising conversion might indicate inhomogeneous reaction conditions or other influences that are to be discussed. The use of the TMG6Brqu-derived CuBr catalyst resulted in a polymerization rate constant of $k_p = 6.7 \times 10^{-4}\,\mathrm{L\,mol^{-1}\,s^{-1}}$ after four polymerization assays. The average polydispersity reached a low PD $= 1.06$, although the propagation of the molecular masses followed non ideal-growth.

Taking the previously discussed polymerization reactions into account, the influence of the different substituents at the quinoline moiety on the polymerization rate was confirmed. Further investigating this feature, the stronger donating ligand TMG6dmaqu containing a dimethyl-

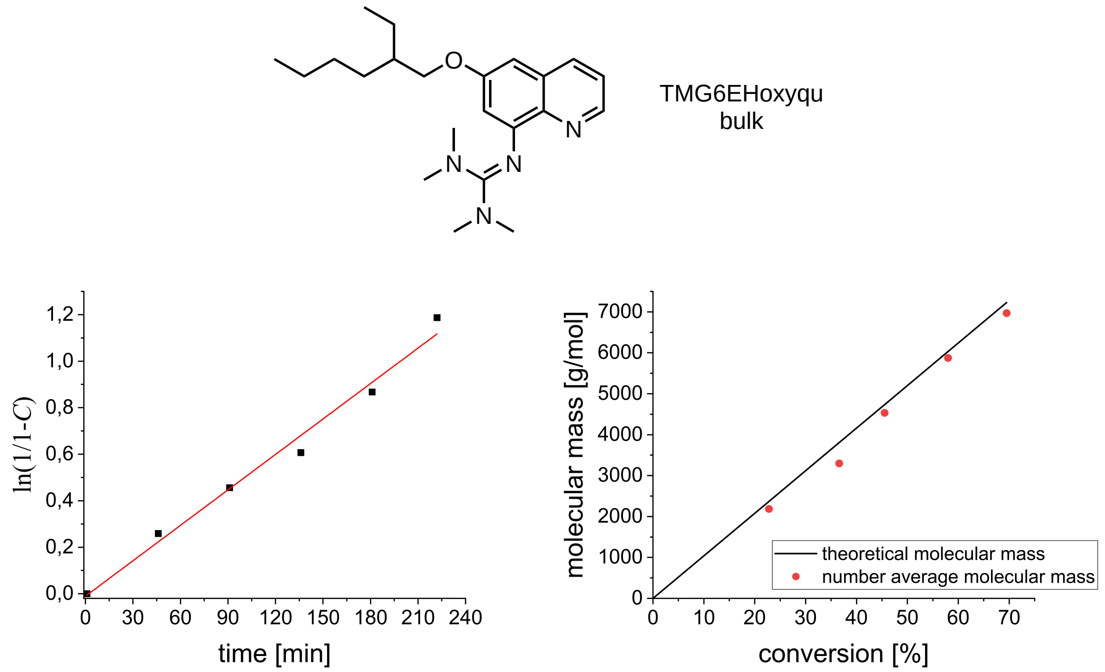

Figure 3.24: Plots of a bulk styrene polymerization with a TMG6EHoxyqu CuBr catalyst (100:1:1). Left: kinetic analysis of the reaction conversion (black) and linear regression (red), right: molecular masses of the obtained polymer samples. C: conversion.

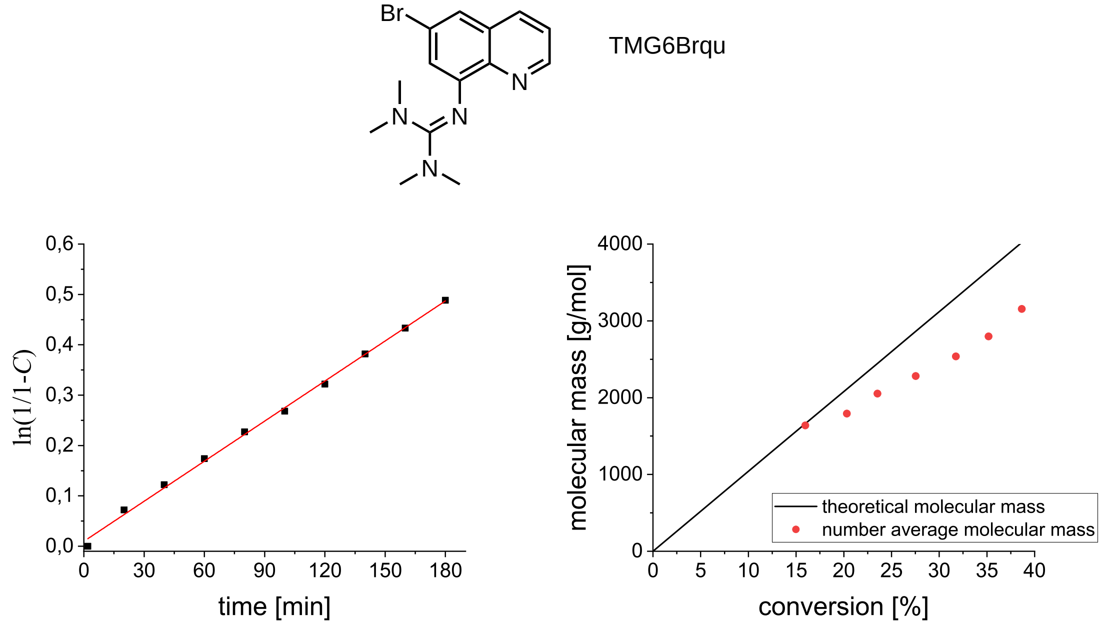

Figure 3.25: Styrene solvent polymerization with the catalyst $[Cu(TMG6Brqu)_2]Br$ in benzonitrile (100:1:1). Left: kinetic analysis of the reaction conversion (black) and linear regression (red), right: molecular masses of the obtained polymer samples. C: conversion.

amine group in C6 was examined. The amine substituent was expected to further shift the equilibrium to the active side, thus yielding faster reactions. The catalyst derived from the TMG6dmaqu ligand was used in the standard polymerization protocol with a ratio of (100:1:1). Major termination was observed and the kinetic parameters deviated strongly from ideal behavior, indication the presence of higher radical concentrations. Analyzing the first test run, evidence was found that the catalyst was too fast for these reaction conditions. Reducing the catalyst loading by half (100:1:0.5), improved the kinetic profile (Figure 3.26). Although the molecular mass evolution exhibited longer polymer chains at low conversion, the theoretical growth was approximated at higher conversion. The kinetic reaction profile showed a well controlled reaction with a high polymerization rate constant $k_p = 1.3 \times 10^{-3}\,\mathrm{L\,mol^{-1}\,s^{-1}}$.

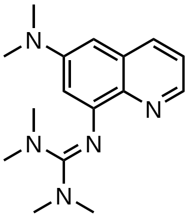

TMG6dmaqu

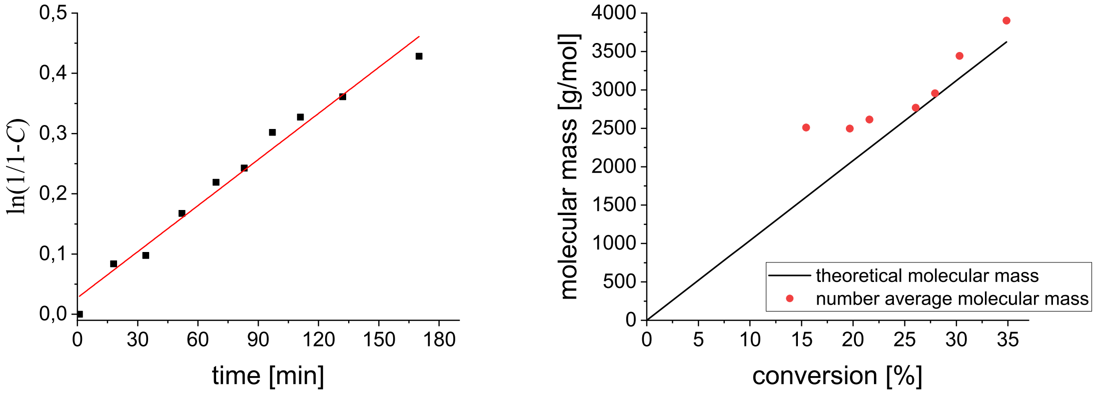

Figure 3.26: Solvent polymerization of styrene in benzonitrile with the TMG6dmaqu CuBr catalyst (100:1:0.5). Left: kinetic analysis of the reaction conversion (black) and linear regression (red), right: molecular masses of the obtained polymer samples. C: conversion.

Improving the solvation of amine-substituted catalysts, TMG6dbaqu was introduced. As expected, CuBr complexes of the ligand did not form solid crystals. The catalyst was similarly well reactive as TMG6dmaqu, leading to a catalyst loading of 0.6 mol% (100:1:0.6). The polymerization reaction showed ideal behavior of its kinetic parameters, although the molecular mass evolution showed a strong deviation from theory (Figure 3.27). The average reaction rate constant $k_p = 1.1 \times 10^{-3}\,\mathrm{L\,mol^{-1}\,s^{-1}}$ was close to the [Cu(TMG6dmaqu)$_2$]Br catalyst.

All TMGqu derived catalysts were able to polymerize styrene under controlled conditions. It was found, that electron-rich ligands afforded faster catalysts then less electron-rich ligands. The ligand TMG6Methoxyqu was found to afford particularly fast ATRP catalysts. In comparison to other catalysts, [Cu(TMG6Methoxyqu)$_2$]Br yielded two to five times higher polymerization rate constants k_p (Table 3.7). In general, k_p is independent of the catalyst concentration

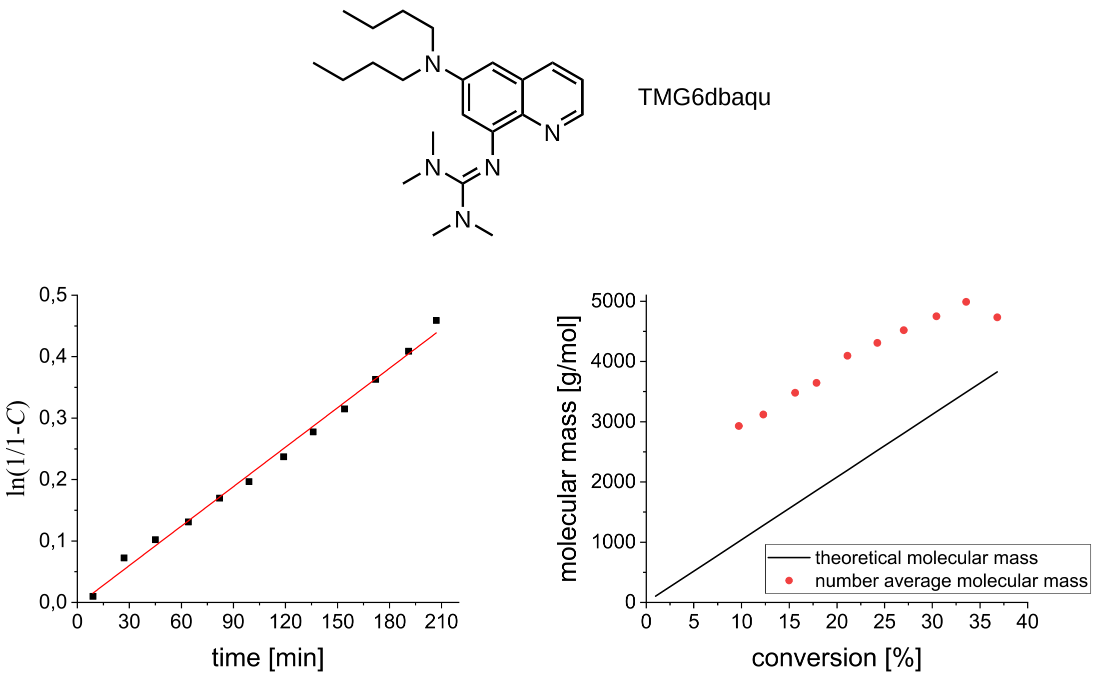

Figure 3.27: Solvent polymerization of styrene in benzonitrile with the TMG6dbaqu CuBr catalyst (100:1:0.6). Left: kinetic analysis of the reaction conversion (black) and linear regression (red), right: molecular masses of the obtained polymer samples. C: conversion.

(equation 26) and faster catalysts should afford higher values thereof. However, exceptionally fast catalysts could result in particularly high radical concentrations, leading to termination and an increased concentration of $\mathrm{Cu^{II}}$. The increased concentration of the oxidized state would then result in a shift of the equilibrium to the dormant side. As a consequence, the catalyst would exhibit kinetic parameters very similar to a severely slower catalyst. The ligands TMG6dmaqu and TMG6dbaqu were expected to afford catalysts with faster polymerization kinetics than TMG6Methoxyqu. Their slower catalytic properties could therefore result from early termination reactions which could be a consequence of an increased K_{ATRP} value.

Table 3.7: Summary of k_{app} and k_p values for the different CuBr ATRP catalysts in styrene polymerization reactions. Unless noted otherwise, reactions were conducted in benzonitrile at a temperature of 110 °C and initiated with 1-PEBr.

Ligand	k_{app} [s^{-1}]	[C]$_0$ [mol L^{-1}]	k_p [L mol^{-1} s^{-1}]
TMG6Methoxyqu	2.1×10^{-4}	6.2×10^{-2}	3.4×10^{-3}
TMG6dmaqu	4.1×10^{-5}	3.1×10^{-2}	1.3×10^{-3}
TMG6dbaqu	3.9×10^{-5}	3.7×10^{-2}	1.1×10^{-3}
TMG6EHoxyqu (bulk)	6.6×10^{-5}	8.8×10^{-2}	7.5×10^{-4}
TMG6EHoxyqu	4.5×10^{-5}	6.2×10^{-2}	7.2×10^{-4}
TMG6Brqu	4.2×10^{-5}	6.2×10^{-2}	6.7×10^{-4}

The well soluble ligand TMG6EHoxyqu was expected to polymerize with a similar rate constant as TMG6Methoxyqu. Although the longer branched alkyl chain was only expected to increase the catalyst solubility, TMG6EHoxyqu was perceived much slower than its short chained counter part. Since solubility is considered as the main difference between the two, the TMG6Methoxyqu ligand might result in decreased solubility of its Cu^{II} complex. The decreased solubility could have led to a constant removal of the deactivator, leading to higher radical concentrations. Usually, this would result in higher rates of termination, therefore it might be concluded that TMG6Methoxyqu could be close to a certain sweet-spot, balancing many individual processes.

As depicted in the polymerization reaction with the ATRP catalyst [Cu(TMG6dbaqu)$_2$]Br (Figure 3.27) non-ideal progression of the molecular masses was received in many individual reactions with all of the examined ligands. The deviation of the molecular masses alone suggested that some polymerization reactions suffered from slow initiation (Figure 3.28). In general, a reaction suffering from slow initiation would result in an upward curve of the $ln\left(\frac{1}{1-C}\right)$ vs. time plot (Figure 3.29).[5] In opposition, all polymerization reaction kinetics with increased molecular masses exhibited a linear correlation of the kinetic plot. Therefore, slow initiation should not be the cause of the increased molecular masses. Generally, the radical concentration is proportional to k_{app}. If any curve of a kinetic plot should be above the linear regression, the reaction would be faster potentially leading to decreased control and increased molecular masses. However, small deviations above and below the linear regression can be observed in all of our polymerization reactions, whereas notably increased molecular masses are only found in a few of these reactions. Originally, the increased molecular masses were attributed to solubility issues of the catalyst or at least of its Cu^{II} species. In contrast, this anomaly was also observed during polymerization reactions with the ligands TMG6EHoxyqu and TMG6dbaqu which exhibit improved solubility. Furthermore, it was found in both the solvent and bulk polymerization. A solubility issue would further result in non-linear kinetics, similar to the "slow initiation"-effect (Figure 3.28).

Styrene self-polymerization was considered as a cause of the increased molecular masses. Polymerization attempts with a TMG6Nitroqu CuBr catalyst, however, did not yield any polymer product within two days. The exceptionally inactive catalyst or some Cu^{II} impurities thereof appeared to rather act as a styrene stabilizer instead. It was assumed that self-polymerization would initiate after potential Cu^{II} deactivator impurities would have been converted to their Cu^{I} activator equivalents. Instead, absence of polymer product indicated that a self-polymerization mechanism did not contribute significantly to the unexpected results. Closely examining GPC traces of samples with increased molecular masses no further abnormalities were found. A second peak of polymer chains with a different molecular mass indicating uncontrolled behavior was not observed. Furthermore, for all polymerization reactions the polydispersity was usually below 1.15, confirming controlled behavior. In additional control experiments with other catalysts, Cheng *et al*. received self-polymerization reaction rates, which were found to be few orders of magnitude smaller than the polymerization rates of our controlled experiments, rendering this mechanism of little importance to our experiments.[125]

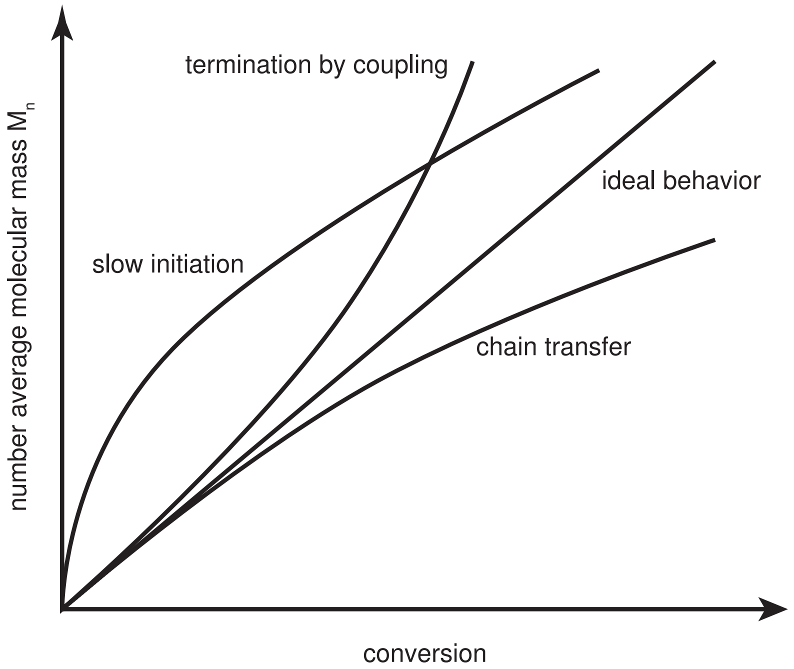

Figure 3.28: Molecular mass evolution of a controlled polymerization reaction with typical deviations and their cause.[5]

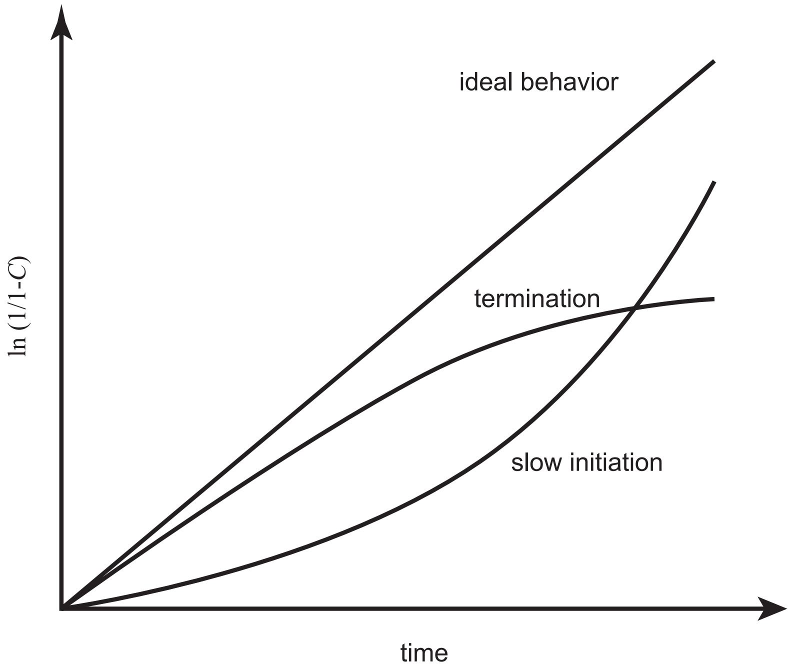

Figure 3.29: Change in $ln\left(\frac{1}{1-C}\right)$ over time. Idealized behavior as well as typical deviations.[5]

Further investigating the cause of increased molecular masses, a potentially disadvantageous workup procedure of the polymer samples was taken into account. The precipitation and decantation of the polymer solutions could have resulted in the loss of short chain polymers. However, this systematic aberration would affect all polymer samples. In contrast, many samples did not exhibit such a deviation from the ideal composition (Figure 3.22). After all, the various deviations found within the data obtained from all polymerization experiments could not be derived from systematic errors or imprecision.

During data analysis, it became evident that it is inevitable to improve analytical methods for polymer samples at lower conversions. Analyzing samples with a GPC unit requires the removal of the monomer, benzonitrile, the NMR solvent and the catalyst. Otherwise, the unit and its separation columns could be damaged. In the precipitation process, short polymer chains might not precipitate from the solvents and could potentially be lost during decantation. In consequence, the molecular mass distribution of polymer samples with low reaction conversions cannot be examined. To circumvent this issue, other workup procedures or analytical methods should be considered. Liquid contents like solvents or monomers could be removed by evaporation at atmospheric or reduced pressure. The obtained samples could be analyzed with a mass spectrometer. Some ionization methods, such as Matrix-Assisted Laser-Desorption-Ionization (MALDI) are designed to ionize larger molecules, such as bio-molecules or polymers. However, due to the use of a matrix material, which can be detected by the mass spectrometer itself, smaller molecules cannot be analyzed with this method. As a result, measurements with polymer samples of very low reaction conversions could be impeded. In addition, for GPC analysis of the evaporated samples, the removal of the catalyst would be required. Therefore, dialysis of the polymer with a protic solvent such as methanol or diluted hydrochloric acid could afford the samples in higher purity. The feasibility of a dialysis assay would depend on the solubility of the short polymer chains in the respective solvents and the permeability of the dialysis material to the short chain polymers and the solvents. As a third option, a standard organic workup should be feasible. Thereby, the organic phase containing the polymer could be washed with aqueous diluted acidic solutions, such as diluted hydrochloric acid. This could help to remove the catalyst from the organic phase and would in turn allow the direct subjection of the dried and solvent free polymer sample to GPC separation. In general, any new workup procedure should be carefully evaluated and compared to the existing method for benchmarking.

Some polymerization reactions showed interesting features that resulted in a better understanding of certain processes. During one polymerization reaction, contamination with oxygen resulted in a strong retardation of the reaction progress (Figure 3.30). In this particular series, the contamination shows a distinguished reduction of the polymerization rate after the third sample. It was concluded that during removal of an aliquot sample, the pipette must have been contaminated with non-inert atmosphere. The resulting retardation of the reaction progress was used as a reference for this particular error. Upon comparing other kinetic deviations to the reference, oxidation was not rated as part of the observed deviations from the theoretical model.

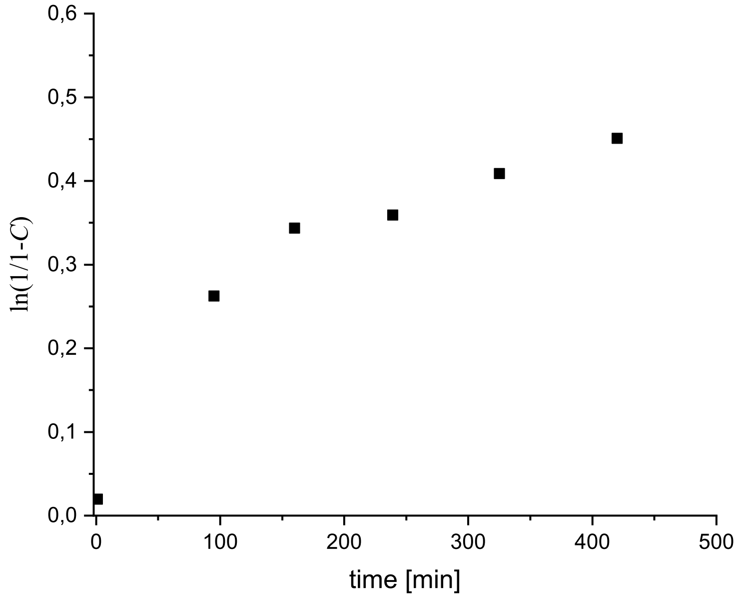

Figure 3.30: Plot of a ATRP polymerization with a TMG6EHoxy catalyst. Due to oxygen contamination, the reaction was retarded after the third sampling.

As mentioned above, analysis of low conversion polymerization samples was found to be challenging. Besides the determination of the molecular mass distributions, the signal-to-noise ratio of some samples impeded reliable assessment of the reaction conversion. Before a series of polymerization experiments was conducted, preliminary tests should give a rough orientation in order to choose reaction parameters appropriately. In one of the polymerization experiments, many samples were taken within a short period of time (Figure 3.31). Hence, a number of samples was also taken at low conversion. Analysis of the NMR data revealed that the statistical error at a conversion below 5% was exceptionally large. In this particular case, it became very apparent due to a sudden increase of conversion after the fourth sample. In contrast, the other samples of the same series indicated a well controlled reaction. Hence, this kind of error was regarded as an issue that must be considered and assessed during reaction planning and analysis.

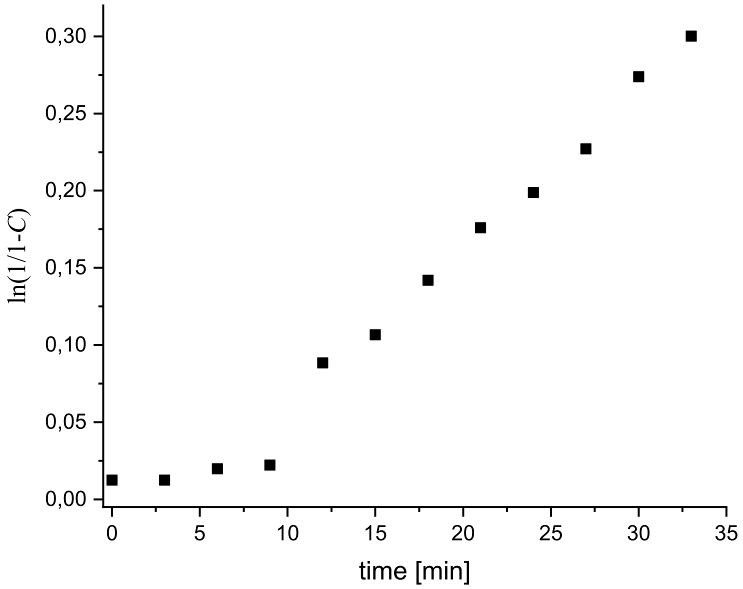

Figure 3.31: This plot of a bulk styrene polymerization with TMG6EHoxyqu exhibits that analysis of samples at low conversion is statistically prone to errors.

3.4. Electrochemical Studies

In atom transfer radical polymerization reactions, the activity of the copper catalysts is determined by their influence on the ATRP equilibrium. It is composed of a dormant alkyl halide with a $\mathrm{Cu^I}$ activator complex and an active alkyl radical with the $\mathrm{Cu^{II}}$ deactivator (Scheme 3.13). The value of the equilibrium constant K_{ATRP} is affected by all participating reactants. Besides radical stabilization, carbon–halide bond strengths and other aspects (1.2.2), the redox potential of the copper catalyst has to be considered. The thermodynamic potential ΔE that is determined by the $\mathrm{Cu^I/Cu^{II}}$ electrochemical couple is an essential parameter for these reactions. The potential can be directly related to the thermodynamic equilibrium constant K_{ATRP} (equations 28, 29 and 30, z: number of transferred electrons, F: Faraday constant, R: universal gas constant, T: temperature). In general, an electrochemical couple with a more negative potential has a stronger thermodynamic driving force towards oxidation than a couple with a more positive electron potential. Regarding the ATRP equilibrium, catalysts with a more negative electron potential usually exhibit an improved activity compared to structurally related species with a more positive potential.[59]

$$\Delta G = -zF\Delta E \tag{28}$$

$$\Delta G = -RTln(K) \tag{29}$$

$$\Delta E \propto ln(K_{ATRP}) \tag{30}$$

$$[\mathrm{Cu^{I}}] \quad + \quad \mathrm{R{-}X} \quad \overset{K_{ATRP}}{\rightleftharpoons} \quad \mathrm{R^{\bullet}} \quad + \quad \mathrm{X{-}[Cu^{II}]}$$

Scheme 3.13: ATRP equilibrium composed of the $\mathrm{Cu^{I}/Cu^{II}}$ couple with alkyl halide and alkyl radical.

The reduction potentials depicted in this work were obtained from cyclic voltammetry (CV) experiments. During CV experiments, an analyte solution is subjected to an alternating triangular electrical potential. The potential causes oxidation or reduction reactions at the surfaces of the electrodes in the analyte solution. When exceptionally high electrical currents are being detected, these electrochemical potentials are called peak potentials. For each oxidation or reduction reaction, an individual peak potential should be observable. In a reversible redox reaction, an oxidation and a reduction process can therefore be identified. The midpoint of these two peak potentials is called redox potential.

Usually, CV experiments are conducted in an electrochemical cell with a three-electrode-setup.[17] At the working electrode, the electrochemical reaction takes place. Here, the redox-active components of the analyte solution are reduced and oxidized. In our experiments, platinum disc electrodes with polished surfaces were used. Establishing a closed electrical circuit, a counter electrode is added to the setup. The counter electrodes used during the experiments were either platinum wire electrodes or glassy-carbon-tip electrodes. The third electrode of the setup is called a reference electrode. It is used as reference point, which allows different measurements to be compared to each other. Usually, reference electrodes are secondary electrodes, representing an individual half cell. In our case, the secondary electrode was composed of a Ag/AgCl half cell. Additionally, an internal standard was used. For this type of reference, a substance that exhibits a redox potential which is invariant to the experimental conditions is usually applied. In our case, a ferrocene standard was introduced into the electrochemical cell after each measurement. Therefore, variations of the experimental conditions can be excluded. The results of all electrochemical reactions were referred to the ferrocene redox potentials which were determined after each experiment. As a consequence, in most CV experiments the secondary reference electrode could be replaced by a polished silver wire, reducing experimental efforts.

The CV analysis of our catalyst samples was conducted in acetonitrile. Acetonitrile was chosen as solvent, because it can be used in a large range of electrochemical potentials without solvent-induced side reactions. Furthermore, our copper catalysts are well soluble therein and the UV/Vis experiments for the determination of K_{ATRP} and k_{act} were also conducted in acetonitrile. Unlike water, most organic solvents display a poor electric conductivity. For example, the increased electrical resistance (R) of pure acetonitrile would result in both a large voltage drop and in low electric currents (I) within the cell. Minimizing this IR-drop, certain electrolytes can be added to the solution. Usually, organic ionic compounds, such as alkylated ammonium salts are well performing soluble electrolytes. For most purposes, tetrabutylammonium bromide (TBAB) or tetrabutylammonium chloride (TBAC) can be used. However, if the presence of halide anions poses potential implications, TBAB or TBAC are not suitable. Halide anions can act as ligands for many complexes. Since our ATRP catalysts are coordinated by halides, addition thereof could alter the experimental results. As a consequence, the halide-free organic electrolyte tetrabutylammonium hexafluorophosphate ((TBA)PF_6) was used in a 0.1 M concentration.

Analytical CV is able to detect very small amounts of redox active impurities. Consequently, only chemicals of high purity and electrochemical grade should be used. Prior to CV experiments, HPLC grade acetonitrile was dried and distilled from calcium hydride followed by degassing using the freeze-pump-thaw procedure. This solvent was used for all CV experiments. All procedures with CuBr or $CuCl_2$ complexes were conducted in a nitrogen-flushed glove box. Later, preliminary experiments suggested that our Cu^{II} complexes were sufficiently stable to conduct CV experiments under ambient atmosphere. Therefore, all $CuBr_2$ complexes were analyzed under non-inert conditions, nevertheless, freshly distilled and degassed solvents were used. All samples were analyzed in CV experiments at four different sweep rates ($200\,mV\,s^{-1}$, $100\,mV\,s^{-1}$, $50\,mV\,s^{-1}$ and $20\,mV\,s^{-1}$) to ensure full reversibility. After addition of the internal standard, the reference experiments were conducted at sweep rates of $200\,mV\,s^{-1}$.

Cyclic voltammetry experiments were conducted with the corresponding $CuBr_2$ complexes of all our ligands. At first, the solid deactivator complex $[Cu(TMG6Methoxyqu)_2Br]Br$ was dissolved in the electrolyte solution in the electrochemical cell and was subjected to an alternating voltage. The obtained data was plotted and the peak potentials were determined. The experiment was repeated for the complex after its *in situ* preparation from single components. Upon comparison of both results, no significant deviations were observed. In consequence, most complexes were generated *in situ* before each measurement. CV experiments of all examined $CuBr_2$ complexes showed fully reversible oxidation and reduction reactions. No peak shifts at different sweep rates were detected and the peak currents of both oxidation and reduction reactions were of similar heights (Figure 3.32 and others in appendix B).

Comparing $CuBr_2$ complexes of the modified ligand library with complexes of their parent core structures TMGqu and DMEGqu,[17] the effect of substitution could be observed (Table 3.8 and Figure 3.33). Ligands containing functional groups that are known to exhibit electron-withdrawing properties, such as nitro substituents, yielded copper complexes with considerably increased redox potential ($[Cu(TMG6Nitroqu)_2Br]Br \cdot C_2H_3N$ (**C7**): $-0.439\,V$). In contrast, ligands with electron-donating features ($[Cu(TMG6dmaqu)_2Br]Br \cdot 2\,C_2H_3N$ (**C6**): $-0.545\,V$) reduced the potential of their parent compounds (Figure 3.2). In accordance with data ob-

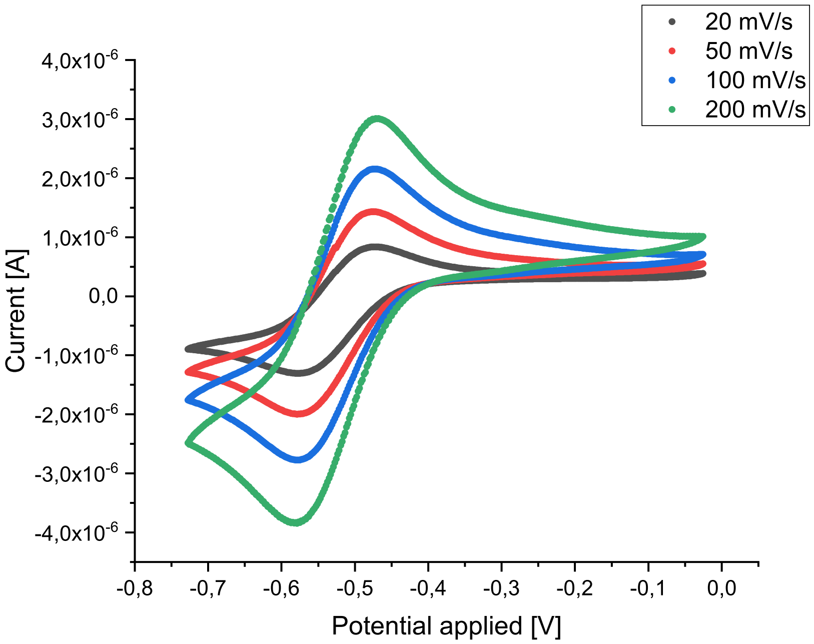

Figure 3.32: Cyclic voltammogram of the complex [Cu(TMG6Methoxyqu)$_2$Br]Br in acetonitrile with (TBA)PF$_6$ (0.1 M) at 22 °C.

tained from polymerization experiments, electron-donating ligands improved the catalytic activity. However, certain deviations could be found. The observed redox potentials of both ether-ligand complexes suggested that TMG6EHoxyqu should afford faster ATRP catalysis ([Cu(TMG6Methoxyqu)$_2$Br]Br (**C5**): -0.522 V, [Cu(TMG6EHoxyqu)$_2$Br]Br: -0.533 V). Furthermore, the polymerization experiments of both complexes were conducted under the same conditions. Although the CuBr$_2$ complexes of the ligand TMG6EHoxyqu exhibited a lower reduction potential than the TMG6Methoxyqu complex, the rate constant k_p was distinguishably lower (section 3.3). If TMG6EHoxyqu actually formed catalysts with increased activity, the high catalyst loading of 1 mol% could have resulted in a high initial radical concentration leading

Table 3.8: Redox potentials of CuBr$_2$ complexes obtained from cyclic voltammetry experiments. Data is referenced to an internal ferrocene standard.

Complex	Redox Potential [V]
[Cu(TMG6Nitroqu)$_2$Br]Br	-0.439
[Cu(TMGqu)$_2$Br]Br[17]	-0.475
[Cu(TMG6Brqu)$_2$Br]Br	-0.480
[Cu(DMEGqu)$_2$Br]Br[17]	-0.502
[Cu(DMEG6Methoxyqu)$_2$Br]Br	-0.521
[Cu(TMG6Methoxyqu)$_2$Br]Br	-0.522
[Cu(TMG6EHoxyqu)$_2$Br]Br	-0.533
[Cu(TMG6dbaqu)$_2$Br]Br	-0.538
[Cu(TMG6dmaqu)$_2$Br]Br	-0.545

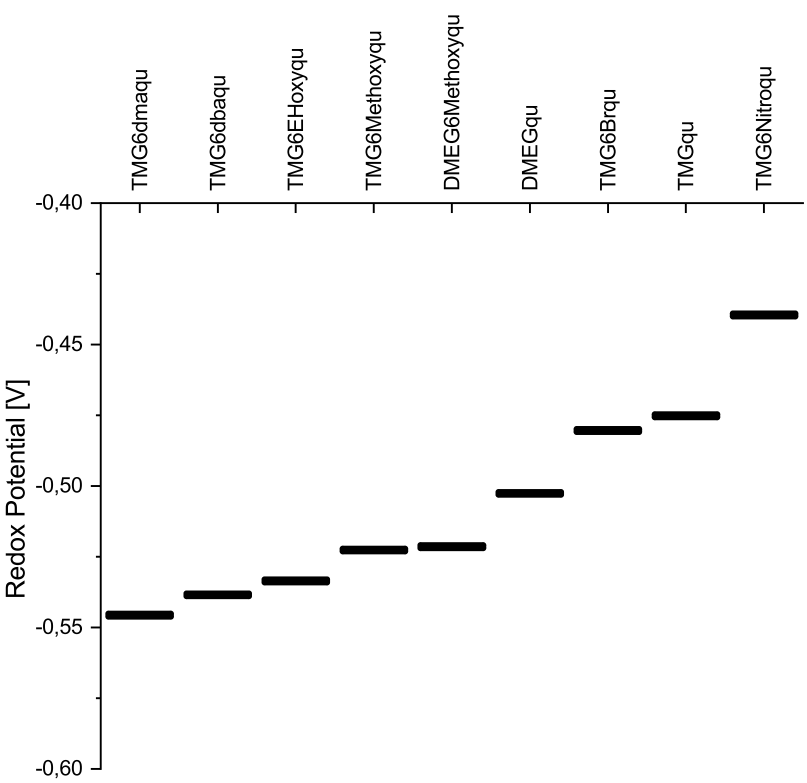

Figure 3.33: Cyclic voltammetry data of $CuBr_2$ complexes. Both crystalline and *in situ* formed complexes were composed of two equivalent of the ligand and one equivalent of $CuBr_2$. Experiments were conducted in acetonitrile, $(TBA)PF_6$ (0.1 M) at 22 °C.

to increased termination at the beginning of the polymerization reactions. As a result, small amounts of terminated polymer and excess of Cu^{II} deactivation could have been produced. The increased deactivator concentration could have led to an equilibrium shift, affording lower radical concentrations and slower polymerization reactions. For examination of this behavior, polymerization reactions at decreased catalyst concentrations should be conducted.

The redox potentials of the previous $CuBr_2$ complexes were in accordance with most of the polymerization reactions. The complexes exhibited a similar coordination geometry with two bidentate hybrid guanidine-quinoline moieties, a bromide ligand and a non-coordinating bromide counter anion (section 3.2). In cyclic voltammetry experiments, complexes are reduced or oxidized by electron transfer. Ligand dissociation reactions would lead to non-reversible redox behavior. Due to the reversibility of our CV experiments, potential ligand dissociation could be neglected. Hence, it was concluded that upon reduction of our $CuBr_2$ complexes during the CV reduction half cycle, penta-coordinated Cu^I complexes should have been generated. In contrast, the respective tetra-coordinated crystalline Cu^I activators, did not contain a coordinating bromide ligand. For comparison thereof, selected Cu^I complexes were analyzed in CV experiments. For example, the solid crystalline complex [Cu(TMG6Nitroqu)Br] exhibited threefold coordination with one organic and one bromide ligand, yielding a trigonal-planar Cu^{I} complex. Although a second ligand was added during crystallization assays, it was not bound to the copper center. Consequently, the redox potential of the complex (−0.417 V, Figure 3.34, Table 3.9) differed strongly from the respective Cu^{II} complex [Cu(TMG6Nitroqu)$_2$Br]Br · C_2H_3N (**C7**, −0.439 V). In contrast, the activator complex of the DMEG6Methoxyqu ligand exhibited the expected fourfold coordination, resulting in a redox potential increase of 14 mV in comparison to its fivefold coordinated deactivator complex (CV: Figure 3.35). This potential difference might be attributed to the additional stabilizing bromide anion coordinated to the Cu^{II} complex.

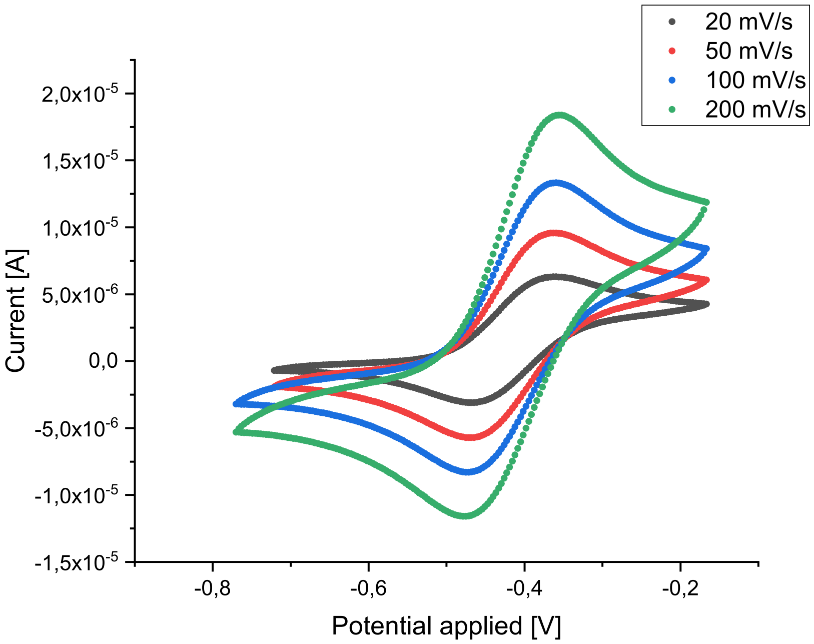

Figure 3.34: Cyclic voltammogram of the monochelate complex [Cu(TMG6Nitroqu)Br] in acetonitrile with (TBA)PF_6 (0.1 M) at 22 °C.

In polymerization experiments, a reduced catalytic activity of TMG6EHoxyqu complexes was observed. After comparison to TMG6Methoxyqu, it was assumed, that the lower activity might result from the sterically demanding side chain, affording complexes with threefold coordination similar to [Cu(TMG6Nitroqu)Br]. Due to the inability of the complex to form solid crystalline material, which could be analyzed by single crystal X-ray diffraction, the composition of the complex needed to be determined in solution. Therefore, CV experiments with CuBr and varying equivalents of ligand were conducted (Figure 3.36, Table 3.9). It was found that two distinguishable redox potentials could be obtained for different ligand concentrations. A redox potential of −0.259 V in respect to ferrocene was determined when only one equivalent or less of ligand was present. Upon addition of further ligand, the current flow at this applied voltage diminished. As a result, a second redox potential appeared at −0.498 V. It was concluded that two equivalents of ligand coordinate to the copper center, if sufficient amounts of the ligand is present. In accordance to most other TMGqu derivatives, the active catalyst should therefore

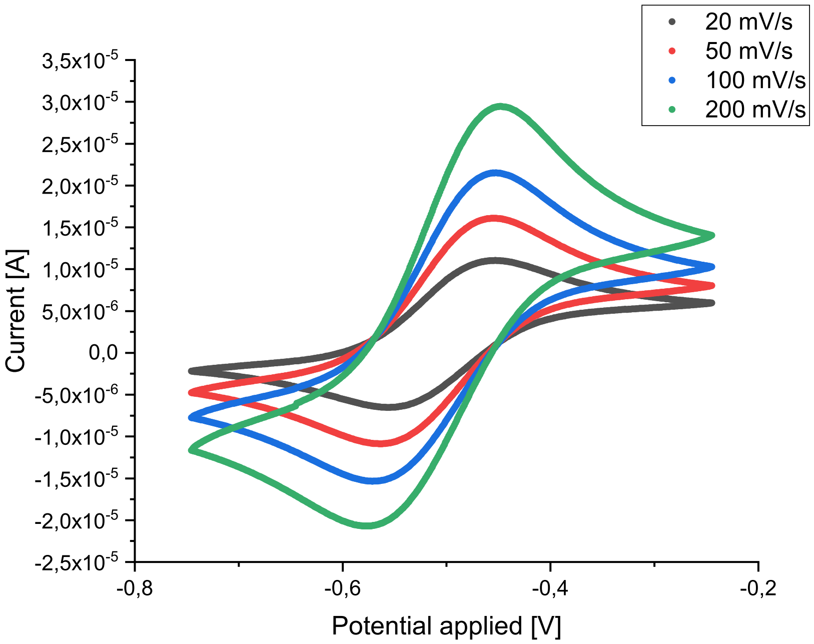

Figure 3.35: Cyclic voltammogram of two equivalents of DMEG6Methoxyqu and one equivalent of CuBr in acetonitrile with (TBA)PF_6 (0.1 M) at 22 °C.

be $[Cu(TMG6EHoxyqu)_2]Br$.

Table 3.9: Redox potentials of CuBr complexes obtained from cyclic voltammetry experiments. Data is referenced to an internal ferrocene standard. *Formal composition, molecular structure not determined.

Complex/Composition	Redox Potential [V]
$[Cu(TMG_6EHoxyqu)Br]$*	-0.259
[Cu(TMG6Nitroqu)Br]	-0.417
$[Cu(TMGqu)_2]Br$	-0.465
$[Cu(DMEGqu)_2]Br$	-0.470
$[Cu(TMG6EHoxyqu)_2]Br$*	-0.498
$[Cu(DMEG6Methoxyqu)_2]Br$*	-0.507

The composition of the CuBr complex of TMG6EHoxyqu was determined by CV experiments. Additionally, the reduced catalytic activity was further investigated. Comparing differences in redox potentials in various activator-deactivator couples, the potential difference between the CuBr and $CuBr_2$ complexes of TMG6EHoxyqu was found to be larger than in other Cu^I/Cu^{II} electrochemical couples (TMGqu: 10 mV, DMEG6Methoxyqu: 14 mV). In contrast to the negative redox potential of the $CuBr_2$ complex, the activator potential was increased by 35 mV (Table 3.10, Figure 3.38). Therefore, the redox potential of the CuBr complex of TMG6EHoxyqu exhibited a reduction potential exceptionally larger than the respective complexes of other ligands. This unexpected high potential seems to be in accordance with the recorded lower polymerization rate constants. In conclusion, it remains unclear if the redox

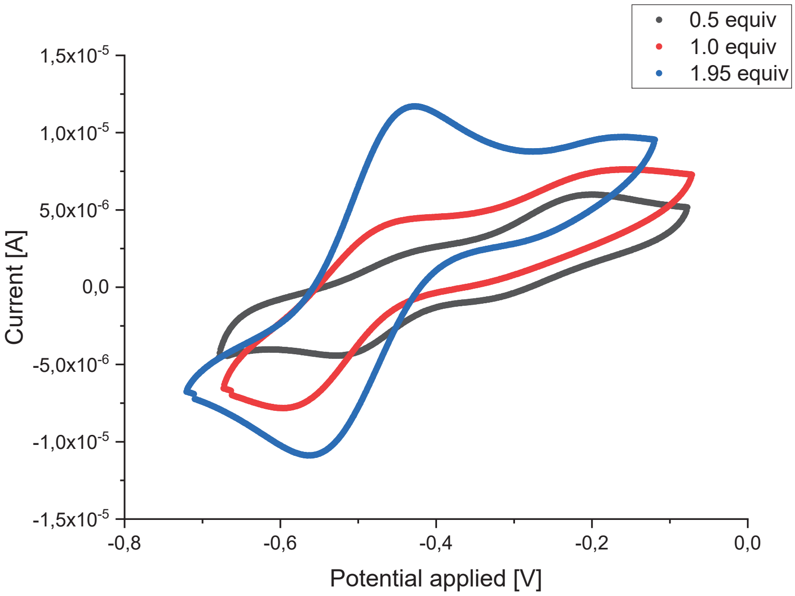

Figure 3.36: Cyclic voltammogram of the ligand TMG6EHoxyqu with CuBr at three different ratios (0.5 equiv, 1.0 equiv and 1.95 equiv). Two different reversible redox potentials can be found at −0.259 V and −0.498 V in respect to ferrocene. Experiments were conducted with a voltage sweep of $200\,\mathrm{mV\,s^{-1}}$ in acetonitrile with $(TBA)PF_6$ (0.1 M) at 22 °C.

potential of the CuBr or $CuBr_2$ complexes should be used to estimate catalyst activities in general.

Table 3.10: Redox potential differences of bischelate CuBr and $CuBr_2$ complexes obtained from cyclic voltammetry experiments. Data is referenced to an internal ferrocene standard.

Ligand (2 equiv each)	Redox Potential Difference [mV]
TMGqu	10
DMEG6Methoxyqu	14
TMG6EHoxyqu	35

ATRP catalysis is usually conducted with CuBr complexes. This relates to the increased bond dissociation energy of C−Cl bonds in contrast to C−Br bonds. However, the redox potential of $CuCl_2$ complexes is usually more negative than the corresponding $CuBr_2$ complexes. For comparison, different redox potentials of TMGqu derived $CuCl_2$ complexes were determined (Table 3.11). Unlike the complex $[Cu(TMG6Brqu)_2Cl]Cl$, which exhibited fully reversible oxidation and reduction half potentials (Figure 3.39), some complexes of our ligands only exhibited irreversible electrochemical reactions. In the CV experiments of crystalline $[Cu(TMG6Nitroqu)Cl_2]$ for example, only one of the half potentials was observed without appearance of the electrochemical reverse reaction. Furthermore, broadening of the peak potential difference was observed for other complexes, such as the *in situ* generated complex $[Cu(DMEG6Methoxyqu)_2Cl]Cl$. Therefore, it was concluded that many products of the elec-

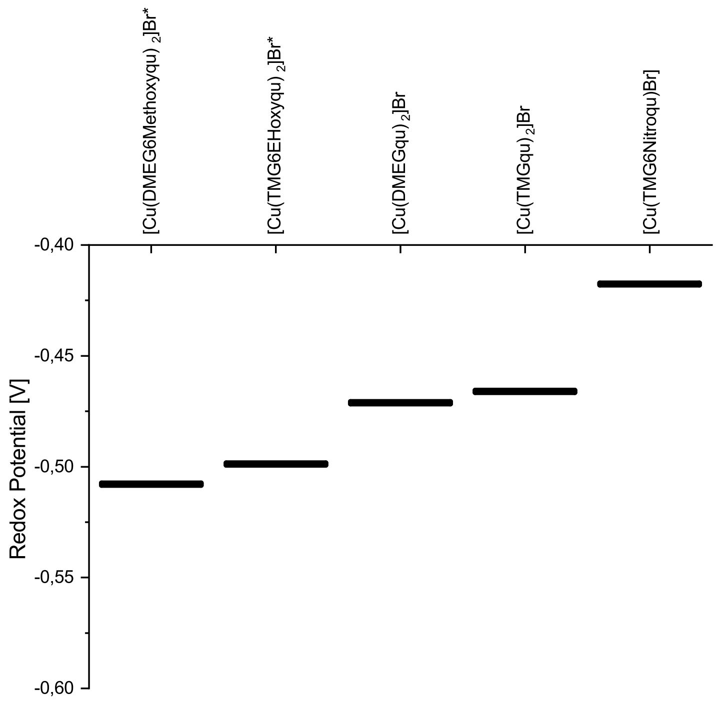

Figure 3.37: Cyclic voltammetry data of CuBr complexes. Experiments were conducted in acetonitrile, (TBA)PF_6 (0.1 M) at 22 °C. *Formal composition, molecular structure not determined.

trochemical reactions were unstable, leading to irreversible side reactions. In the samples that did experience reversible electrochemical reactions, the $CuCl_2$ complexes exhibited 40 mV to 60 mV lower electric potentials than their $CuBr_2$ counterparts (Table 3.11 and Figure 3.40).

Table 3.11: Redox potentials of $CuCl_2$ complexes obtained from cyclic voltammetry experiments. Data is referenced to an internal ferrocene standard. *Formal composition, molecular structure not determined.

Ligand	Redox Potential [V]
[Cu(TMGqu)$_2$Cl]Cl	-0.515
[Cu(TMG6Brqu)$_2$Cl]Cl	-0.540
[Cu(TMG6EHoxyqu)$_2$Cl]Cl*	-0.584

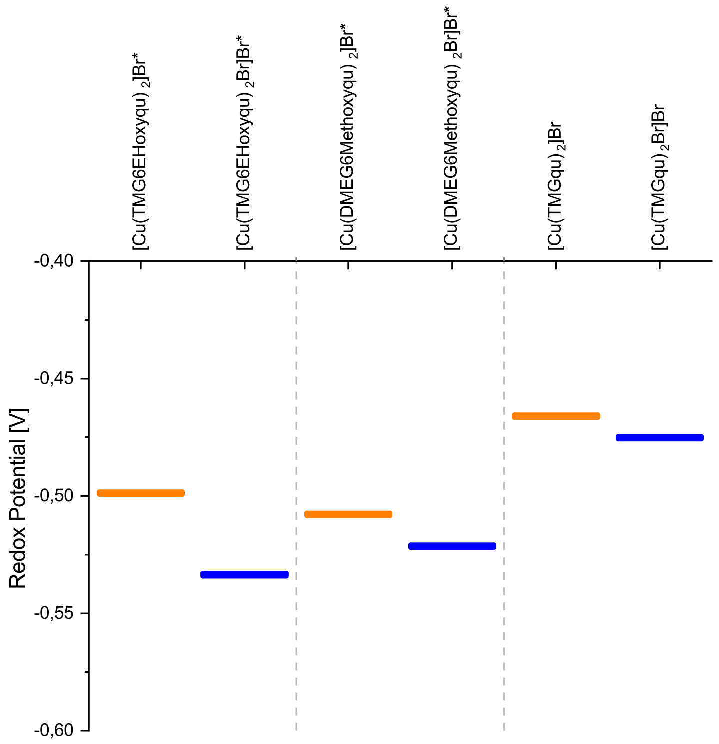

Figure 3.38: Redox potentials of $CuBr_2$ and CuBr complexes. Experiments were conducted in acetonitrile, $(TBA)PF_6$ (0.1 M) at 22 °C. *Formal composition, molecular structure not determined.

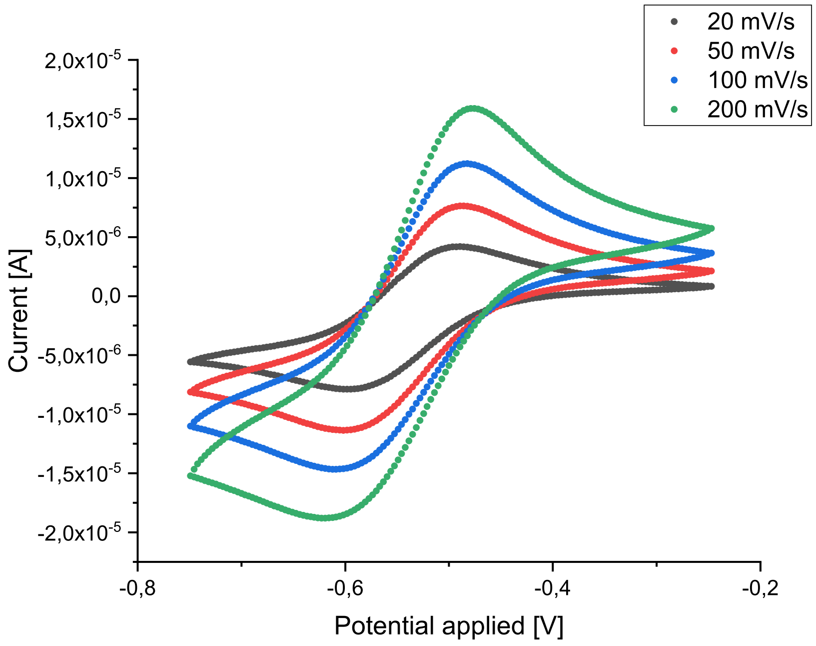

Figure 3.39: Cyclic voltammogram of the complex $[Cu(TMG6Brqu)_2Cl]Cl$ in acetonitrile with $(TBA)PF_6$ (0.1 M) at 22 °C.

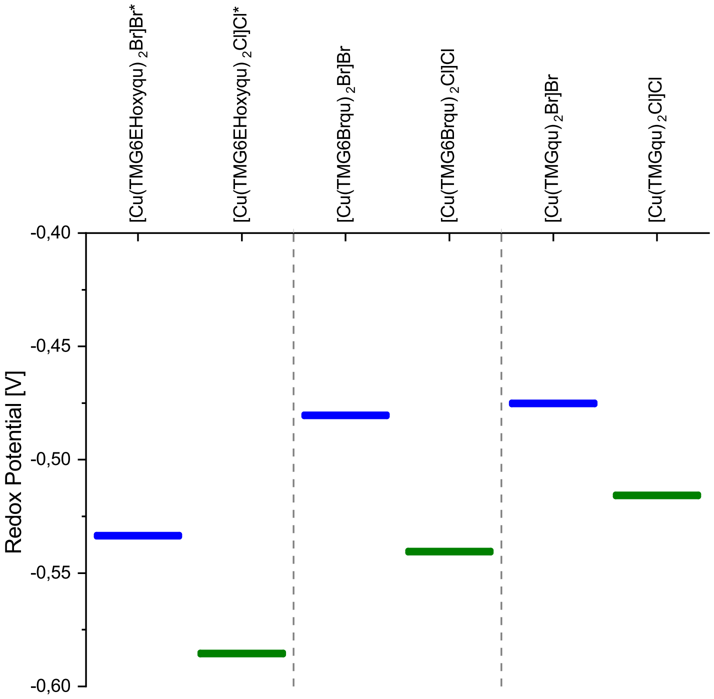

Figure 3.40: Redox potentials of $CuBr_2$ and $CuCl_2$ complexes. Experiments were conducted in acetonitrile and $(TBA)PF_6$ (0.1 M) at 22 °C. *Formal composition, molecular structure not determined.

3.5. ATRP equilibrium and reaction rate constants K_{ATRP}, k_{act} and k_{deact}

The redox equilibrium of an ATRP reaction can be described by its equilibrium constant K_{ATRP}. This constant gives information about the activity of the catalyst and the reagents involved in the polymerization process. Furthermore, the activation and deactivation rate constants k_{act} and k_{deact} reveal how fast an equilibrium can react to restraints. High values of K_{ATRP} indicate that the ATRP equilibrium is shifted to the active side, leading to faster polymerization reactions. However, high values for the deactivation rate constants k_{deact} lead to an increase of the polymerization control. Therefore, successful ATRP catalysts possess high values of both activation and deactivation rate constants resulting in fast and controlled polymerization reactions.

The equilibrium constant K_{ATRP} can be determined by two different approaches. First, the equilibrium constant can be derived from the rate of polymerization. By using this method, the decline of non-reacted monomer can be related to the radical concentration R (equation 31) if the polymerization rate constant k_p is known. As a consequence, the value of K_{ATRP} can be determined from equation 32. For obtaining the K_{ATRP} values with this method, a series of polymerization reactions is required to be conducted for determination of k_p. As a result, the K_{ATRP} values will depend on the choice of monomers and polymerization conditions. Additionally, an excess of the $\mathrm{Cu^{II}{-}X}$ species and constant concentrations of all other species are required ($[\mathrm{I}]_0$: initial initiator concentration, $[\mathrm{C}]_0$ initial catalyst concentration).[126]

$$\mathrm{R} = \frac{1}{k_p} \frac{\mathrm{d} \ln [\mathrm{M}]}{\mathrm{d}t} \tag{31}$$

$$\mathrm{R} = \left(\frac{K_{ATRP} [\mathrm{I}]_0 [\mathrm{C}]_0}{6 k_t} \right)^{\frac{1}{3}} t^{-\frac{1}{3}} \tag{32}$$

In the second method, an ATRP equilibrium is established without an excess of the $\mathrm{Cu^{II}{-}X}$ species (Scheme 3.14). In contrast to the previous method, the equilibrium reaction is conducted in a solvent without monomer. Furthermore, the reduced $\mathrm{Cu^{II}}$ concentration results in radical termination. As a consequence, the concentration of the $\mathrm{Cu^{II}}$ deactivator increases over time. The deactivator concentration can be determined by UV/Vis spectroscopy. The general mechanism of the deactivator increase is called persistent radical effect (PRE). The obtained values for K_{ATRP} are therefore referenced to the radical termination and are independent of the polymerization conditions improving comparison between different catalysts.

$$\mathrm{CuX(L)_2} \;+\; \mathrm{R{-}X} \;\underset{}{\overset{K_{ATRP}}{\rightleftharpoons}}\; \mathrm{CuX_2(L)_2} \;+\; \mathrm{R}^{\bullet} \;\xrightarrow{k_t}$$

Scheme 3.14: Equilibrium reaction during K_{ATRP} determination.

Since the radical concentration at constant reaction conditions depends on the initial reagent concentrations ($[\mathsf{I}]_0$ and $[\mathsf{C}]_0$) and K_{ATRP}, the reaction rate of the Cu$^{\mathsf{II}}$ increase ($\mathsf{Y} = [\mathsf{X}{-}\mathsf{Cu}^{\mathsf{II}}]$) can be related to the equilibrium constant (equation 33, developed by the groups of Fischer *et al*. and Fukuda *et al*.).[8,127,128] For diffusion controlled experiments, the rate constant for radical termination reactions k_t can be found in the literature ($k_t = 2.5 \times 10^9 \, \frac{\mathsf{L}}{\mathsf{mol\,s}}$).[126] After rearrangement, K_{ATRP} can be obtained from equation 34. For analysis of the experimental data, a plot of Y against $t^{\frac{1}{3}}$ should result in a linear correlation. The value of the slope ($\mathsf{Y}/t^{\frac{1}{3}}$), can be inserted to equation 34 for determination of the corresponding K_{ATRP} value.

$$\mathsf{Y} = (6k_t K_{ATRP}^2 [\mathsf{I}]_0^2 [\mathsf{C}]_0^2)^{\frac{1}{3}} t^{\frac{1}{3}} \tag{33}$$

$$K_{ATRP} = \frac{1}{\sqrt{6k_t}[\mathsf{I}]_0[\mathsf{C}]_0} \left(\frac{Y}{t^{\frac{1}{3}}}\right)^{3/2} \tag{34}$$

In 2006, restrictions of the above equations were found by the Matyjaszewski group.[126] It was stated, that the relations found by the groups of Fischer and Fukuda were only true for slower catalysts. As a result, the Fischer–Fukuda equations were used as a starting point to develop analytical methods, which were more accurate for fast ATRP catalysts. As expressed in equation 35, the concentration Y obtained from the Fischer–Fukuda equation was used as a variable in the Matyjaszewski method. Plotting $F(\mathsf{Y})$ against time t results in a linear correlation, from whose slope ($\frac{\Delta F(\mathsf{Y})}{\Delta t}$) K_{ATRP} can be determined (36). As a sole restriction, the equations only apply for diffusion-controlled experiments, due to determination of the termination rate constant k_t under these conditions. Detailed derivation of the equations can be found in the literature.[126]

$$\begin{aligned} F(\mathsf{Y}) = \left(\frac{[\mathsf{I}]_0[\mathsf{C}]_0}{[\mathsf{C}]_0 - [\mathsf{I}]_0}\right)^2 & \left(\frac{1}{[\mathsf{C}]_0^2([\mathsf{I}]_0 - \mathsf{Y})} + \frac{2}{[\mathsf{I}]_0[\mathsf{C}]_0([\mathsf{C}]_0 - [\mathsf{I}]_0)}\right. \\ & \left. \ln\left(\frac{[\mathsf{I}]_0 - \mathsf{Y}}{[\mathsf{C}]_0 - \mathsf{Y}}\right) + \frac{1}{[\mathsf{I}]_0^2([\mathsf{C}]_0 - \mathsf{Y})}\right) \end{aligned} \tag{35}$$

$$K_{ATRP} = \sqrt{\frac{\Delta F(\mathsf{Y})}{2k_t \Delta t}} \tag{36}$$

The concentration of Cu$^{\mathsf{II}}$ species could be easily determined, because of their optical absorption in the red and near infrared bands. This absorption is related to d-d orbital transitions. Since these transitions are not possible for Cu$^{\mathsf{I}}$ species, the Cu$^{\mathsf{II}}$ complexes can be examined well in the presence of Cu$^{\mathsf{I}}$ redox partners. Therefore, the methods of Fischer–Fukuda and Matyjaszewski were used for determination of the K_{ATRP} values of our complexes.

The UV/Vis measurements were conducted in 10 mm screw cap cuvettes with silicone septum. Before measurements, the cuvettes were filled with distilled and degassed acetonitrile and sealed with their septum in a glove box. Then, a Hamilton® gastight syringe was filled with the complex stock solution prepared in the glove box and the septum of the cuvette was penetrated. However, the stock solution was not injected and the needle of the syringe was not allowed to come in contact with the solvent before recording background and stray light correction spectra. After addition of the complex solution, the UV/Vis measurements were started and the EBriB initiator stock solution was added. The evolution of the Cu^{II} band at $\lambda = 940$ nm was recorded and later used for plotting and analysis.

Similar to K_{ATRP}, k_{act} was determined by UV/Vis spectroscopy, but the chemical composition of the experiment was adapted. For determination of the activation rate constant, the deactivation reaction of the ATRP equilibrium had to be suppressed. Therefore, the radicals formed during activation were reacted with the radical trapping agent TEMPO, preventing the reverse reaction (Scheme 3.15). To allow full conversion of the radicals, a tenfold equivalent of TEMPO was added. For improved analysis of the kinetic data, reaction conditions were chosen in such a manner that the activation reaction followed pseudo first-order behavior. Therefore, a tenfold excess of EBriB initiator was added. Prior to staring the measurements, the cuvette was filled with solvent, sealed and punctured as before. However, TEMPO and EBriB were added before background and stray light correction. Then, the spectra recording was started and the complex solution was added. Again, the evolution of the Cu^{II} band was recorded at $\lambda = 940$ nm.

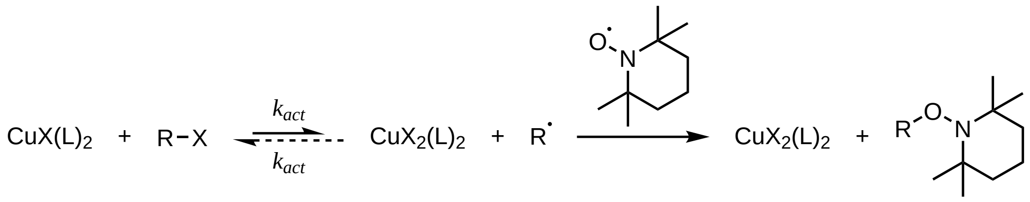

Scheme 3.15: Suppressed deactivation reaction of the ATRP equilibrium during k_{act} determination.

Since the reaction conditions led to full conversion of the activator complex, only Cu^{II} species were present after the reaction. Therefore, the final absorption was used to determine the extinction coefficients of the deactivator complex. In contrast to assessing the extinction coefficient with solutions obtained from crystalline complexes, potential deviations induced by complex dissociation reactions could be eliminated. The obtained coefficients were therefore regarded as average extinction coefficients of all possible Cu^{II} species. Alterations in the compositions of the K_{ATRP} and k_{act} reaction solutions could therefore be avoided. Each of the obtained data was fitted with a regression curve obeying equation 37. The total absorbance of the Cu^{II} complexes $(A_0 + N)$ was used to calculate the extinction coefficient ε_λ at the respective wavelength $(\varepsilon_\lambda = (A_0 + N)/[\mathrm{C}]_0)$. As depicted in equation 38, k_{act} was obtained through division of the k_{obs} value with the initiator concentration $[\mathrm{I}]_0$.

$$A_0\left(1-e^{-k_{obs}t}\right)+N \tag{37}$$

$$k_{act}=\frac{k_{obs}}{[\mathrm{I}]_0} \tag{38}$$

The k_{act} values of a series of CuBr complexes were determined by regression of the experimental data. The quality of the experimental data was good, affording the desired constants with low statistical error. In contrast to most of the catalysts (Figure 3.41 and Figure 3.42), slight deviations could be observed for the fastest complexes (Figure 3.43). However, statistic error remained low. The k_{act} constants showed an increasing trend for the TMGqu derivatives upon addition of electron-donating groups. The slowest catalyst derived from the ligand TMG6Brqu afforded an activation rate constant of $k_{act} = 0.34\,\mathrm{s}^{-1}$ increasing to $k_{act} = 2.33\,\mathrm{s}^{-1}$ for the TMG6dmaqu complex (Table 3.12). In comparison to the TMG6Methoxyqu complex ($k_{act} = 1.11\,\mathrm{s}^{-1}$), the DMEG6Methoxyqu derived catalyst exhibited a slightly increased activation rate constant of $k_{act} = 1.36\,\mathrm{s}^{-1}$. The alkylated derivatives with improved solubility displayed k_{act} values close to their related compounds (TMG6EHoxyqu $k_{act} = 1.25\,\mathrm{s}^{-1}$ and TMG6dbaqu $k_{act} = 1.88\,\mathrm{s}^{-1}$).

The final absorbance of each experiment was used to calculate the respective extinction coefficients. Except for the DMEG6Methoxyqu complex, which exhibited an coefficient of $\varepsilon_\lambda = 410\,\mathrm{L\,mol^{-1}\,cm^{-1}}$ analysis of all $\mathrm{Cu^{II}}$ species gave coefficients of $\varepsilon_\lambda = 470\,\mathrm{L\,mol^{-1}\,cm^{-1}}$ to $540\,\mathrm{L\,mol^{-1}\,cm^{-1}}$ at the relevant wavelength of $\lambda = 940\,\mathrm{nm}$.

These numbers were used to calculate the respective concentrations Y, which were required during determination of the K_{ATRP} values. Therefore, the experimental data was plotted as mentioned above to yield two diagrams for each experiment. First, the concentration of the $\mathrm{Cu^{II}}$ species Y was plotted against $t^{\frac{1}{3}}$ (Figure 3.44, Figure 3.45 and Figure 3.46), affording K_{ATRP} from the Fischer–Fukuda analysis method (equation 34). As expected, more electron-rich ligands, such as TMG6dmaqu and TMG6dbaqu, yielded higher equilibrium constants (2.5×10^{-7} and 2.3×10^{-7}) than the less electron-rich ligands, such as TMG6Brqu (3.4×10^{-8}, Table 3.12). Upon closer inspection of the plots, it was found that the linear regression of the graphs exhibited stronger deviations from the actual values for more electron-rich complexes (Figure 3.46). It was concluded that these types of catalysts might reside at the upper limit at which the Fischer–Fukuda method delivers reliable results. Therefore, the previously obtained values for Y were used to calculate $F(\mathrm{Y})$ (equation 35), which was then plotted again time t (Figure 3.47, Figure 3.48 and Figure 3.49). In comparison to the first method, strongly reduced statistical errors were obtained through the linear fit. The K_{ATRP} values were again increasing in order of the electron-donating groups with TMG6Brqu at the lower end (3.6×10^{-8}) and TMG6dmaqu at the upper end increased by one order of magnitude (3.6×10^{-7}). After determination of K_{ATRP} with this method, the obtained data was evaluated (Table 3.12). In general, it was found that the Fischer–Fukuda method afforded smaller

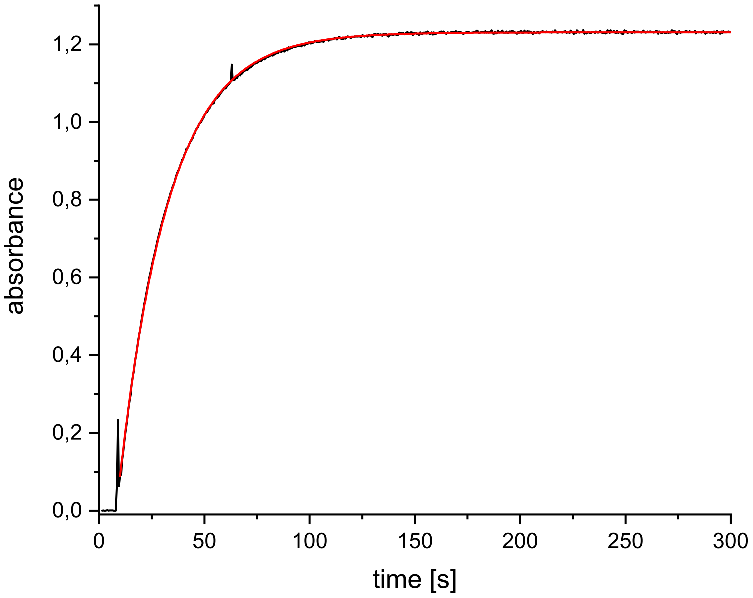

Figure 3.41: Absorbance of the evolving $CuBr_2$ complex at a wavelength of 940 nm during k_{act} determination of the $[Cu(DMEG6Methoxyqu)_2]Br$ catalyst. Black: absorbance, red: regression curve (equation 37).

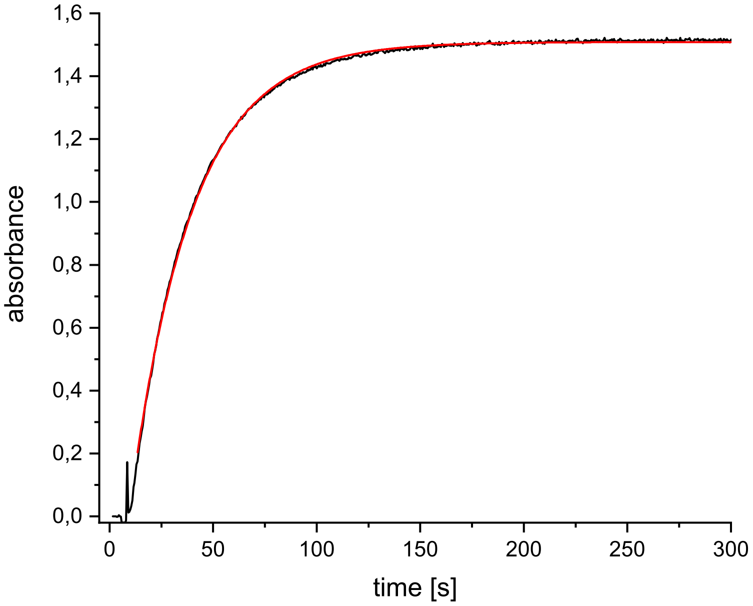

Figure 3.42: Absorbance of the evolving $CuBr_2$ complex at a wavelength of 940 nm during k_{act} determination of the $[Cu(TMG_6Methoxyqu)_2]Br$ catalyst. Black: absorbance, red: regression curve (equation 37).

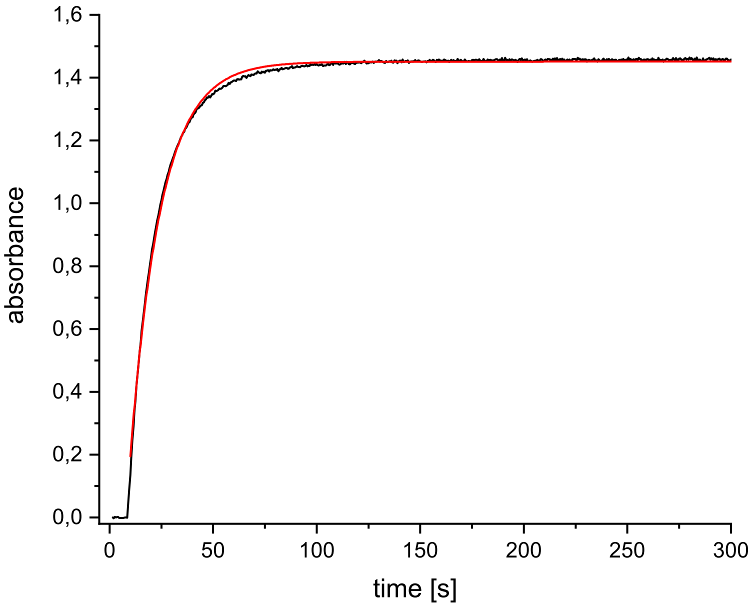

Figure 3.43: Absorbance of the evolving $CuBr_2$ complex at a wavelength of 940 nm during k_{act} determination of the $[Cu(TMG_6dmaqu)_2]Br$ catalyst. Black: absorbance, red: regression curve (equation 37).

values for the equilibrium constant. Furthermore, the deviation between the two methods increased for faster catalysts. For the TMG6Brqu catalyst, for example, Fischer–Fukuda yielded a K_{ATRP} value about 6% smaller than the Matyjaszewski method. This number further increased for the more electron-rich and more active complexes, reaching a deviation of 30% for the TMG6dmaqu ligand.

Upon comparison with other ATRP catalysts found in the literature, our ligands form the fastest catalysts, derived from bidentate ligands. Whereas tetradentate ligands such as tris(2-pyridylmethyl)amine (TPMA) or tris((4-methoxy-3,5-dimethylpyridin-2-yl)methyl)amine (TPMA*) form complexes with very high K_{ATRP} values (TPMA $K_{ATRP} = 9.7 \times 10^{-6}$, TPMA* $K_{ATRP} = 1.2 \times 10^{-2}$), other bidentate ligands form much slower catalysts. The ligand 2,2'-bipyridine (bpy) for example yields catalysts with values of $K_{ATRP} = 3.9 \times 10^{-9}$ and 4,4'-dinonyl-2,2'-bipyridine (dNbpy) affords catalysts with $K_{ATRP} = 3.0 \times 10^{-8}$. In contrast, our electron-rich TMGqu derivative TMG6dmaqu formed complexes with a one order magnitude increased K_{ATRP} value.[1,2]

Finally, the deactivation rate constant k_{deact} could be calculated for each catalyst. Therefore, the K_{ATRP} values of the Matyjaszewski method were used. It was found that the deactivation rate constant slightly declined for the more electron-rich catalysts. The TMG6Brqu complex exhibited a constant of $k_{deact} = 9.4 \times 10^6\,s^{-1}$, whereas TMG6dmaqu resulted in a value of $k_{deact} = 6.5 \times 10^6\,s^{-1}$. As an exception, the DMEG6Methoxyqu derived catalyst yielded the highest value of $k_{deact} = 1.3 \times 10^7\,\mathrm{s}^{-1}$.

In conclusion, the examination of the ATRP kinetics of our catalysts resulted in the determination of reproducible equilibrium and reaction rate constants. All experiments were conducted four times increasing the confidence in their results. The obtained values lied within reason and showed expected trends.

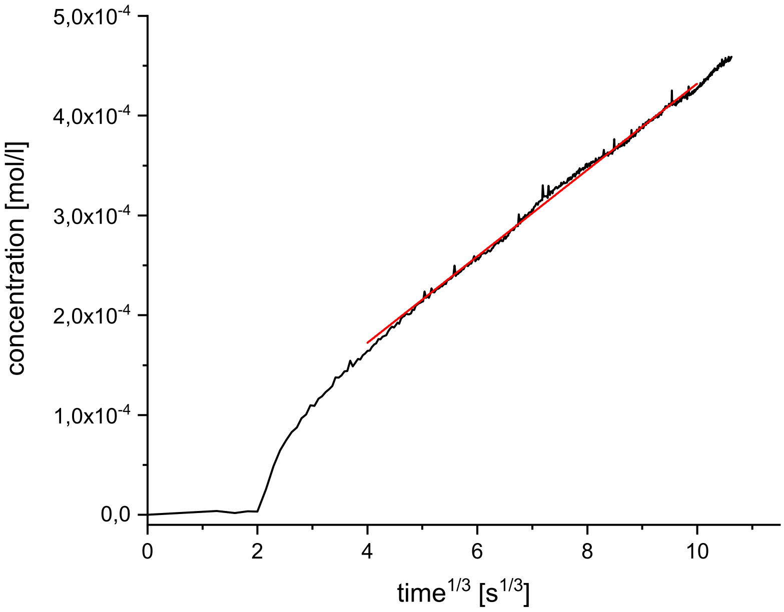

Figure 3.44: Fischer–Fukuda plot of the K_{ATRP} determination of the [Cu(DMEG6Methoxyqu)$_2$]Br catalyst. Black: concentration of the evolving CuBr$_2$ complex, red: linear regression.

Table 3.12: K_{ATRP} and k_{act} values for our series of ligands. K_{ATRP} values were obtained from the respective Matyjaszewski and Fischer–Fukuda plots.

	K_{ATRP}		k_{act} $\left[\frac{1}{s}\right]$	k_{deact} $\left[\frac{1}{s}\right]$
Ligand	**Matyjaszewski**	**Fischer–Fukuda**		
TMG6Brqu	3.6×10^{-8}	3.4×10^{-8}	0.34	9.4×10^{6}
DMEG6Methoxyqu	1.1×10^{-7}	9.4×10^{-8}	1.36	1.3×10^{7}
TMG6Methoxyqu	1.5×10^{-7}	1.3×10^{-7}	1.11	7.4×10^{6}
TMG6EHoxyqu	1.5×10^{-7}	1.2×10^{-7}	1.25	8.3×10^{6}
TMG6dbaqu	3.2×10^{-7}	2.3×10^{-7}	1.88	5.9×10^{6}
TMG6dmaqu	3.6×10^{-7}	2.5×10^{-7}	2.33	6.5×10^{6}

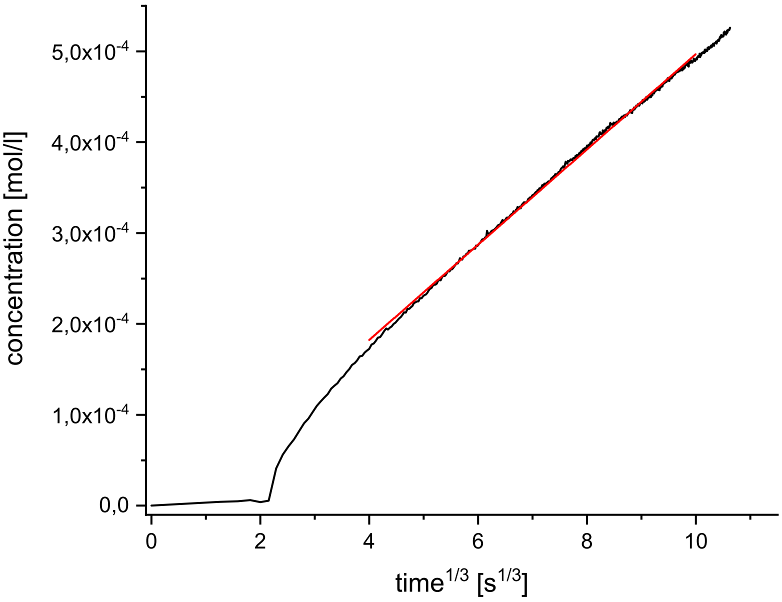

Figure 3.45: Fischer–Fukuda plot of the K_{ATRP} determination of the [Cu(TMG$_6$Methoxyqu)$_2$]Br catalyst. Black: concentration of the evolving CuBr$_2$ complex, red: linear regression.

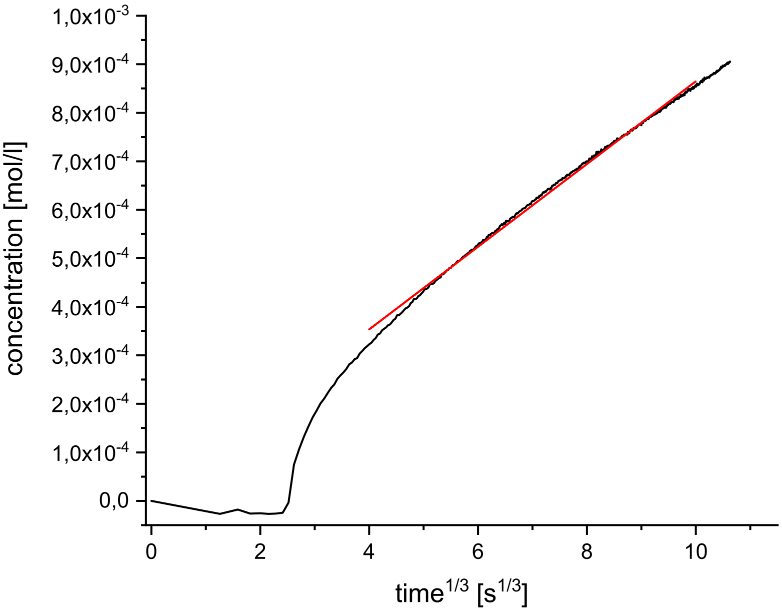

Figure 3.46: Fischer–Fukuda plot of the K_{ATRP} determination of the [Cu(TMG$_6$dmaqu)$_2$]Br catalyst. Black: concentration of the evolving CuBr$_2$ complex, red: linear regression.

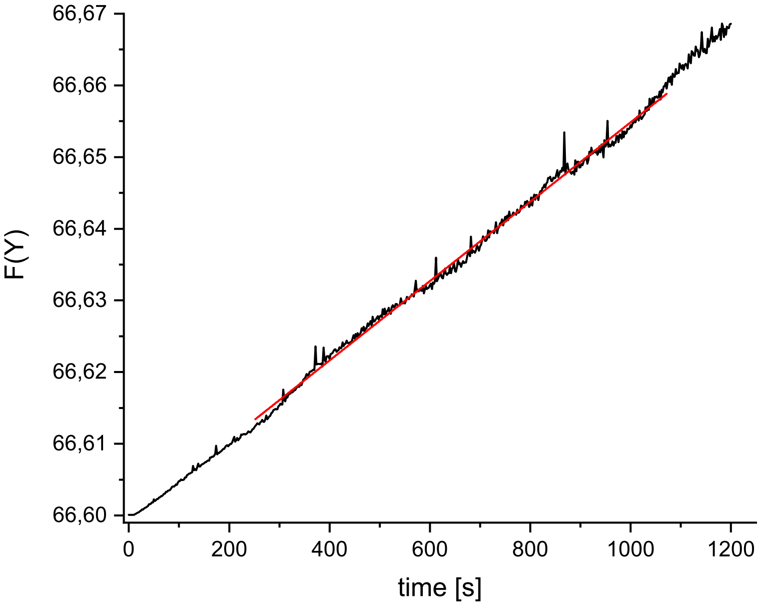

Figure 3.47: Matyjaszewski plot of the K_{ATRP} determination of the [Cu(DMEG6Methoxyqu)$_2$]Br catalyst. Black: F(Y), red: regression curve.

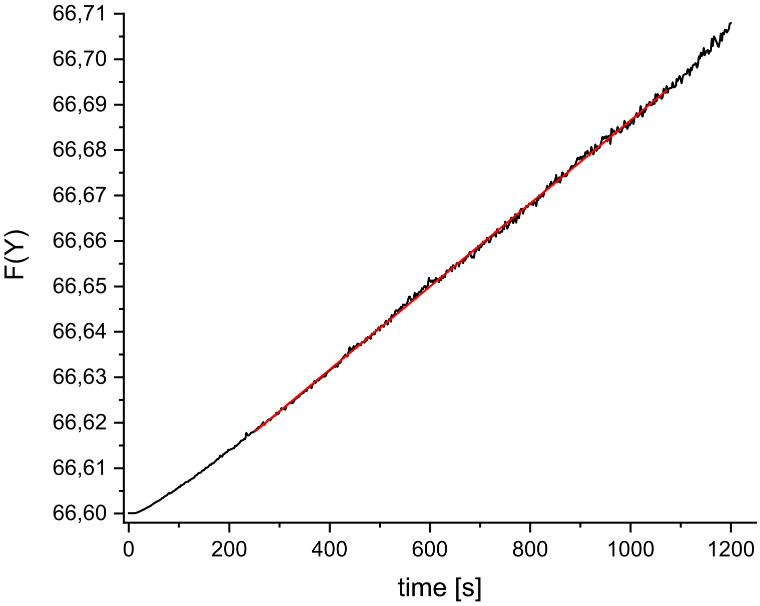

Figure 3.48: Matyjaszewski plot of the K_{ATRP} determination of the [Cu(TMG$_6$Methoxyqu)$_2$]Br catalyst. Black: F(Y), red: regression curve.

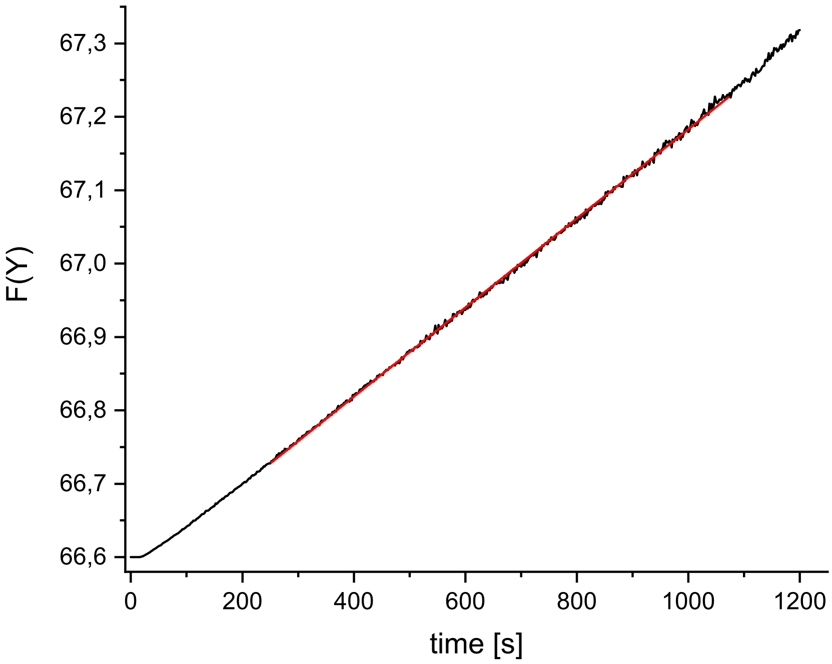

Figure 3.49: Matyjaszewski plot of the K_{ATRP} determination of the [Cu(TMG$_6$dmaqu)$_2$]Br catalyst. Black: F(Y), red: regression curve.

4. Summary

In this thesis, the synthesis and characterization of a new family of guanidine-quinoline hybrid ligands and their Cu^I and Cu^{II} complexes was presented. The copper complexes were analyzed for their molecular structures, catalytic activities in ATRP reactions, electrochemical potential and ATRP equilibrium and rate constants.

The ligand family was based on the 1,1,3,3-tetramethyl-2-(quinolin-8-yl)guanidine (TMGqu) core structure with modifications at position C6. Therefore, extensive optimization studies resulted in the development of reliable synthetic routes to our products. Ligands with electron-withdrawing substituents, such as TMG6Nitroqu (**16**) or TMG6Brqu (**17**), were synthesized, as well as ligands with electron-donating groups, such as TMG6Methoxy (**4**), TMG6EHoxyqu (**10**), TMG6dmaqu (**20**) and TMG6dbaqu (**31**, Figure 4.1). Furthermore, the ligand DMEG6Methoxyqu (**8**) of the DMEGqu family was prepared and different approaches towards TMG4Methoxyqu were examined. Initial investigations of the ligands by ^{13}C NMR spectroscopy revealed insights into the electron distribution within the aromatic ring system, leading to increased electron densities at the pyridine moiety. The syntheses of C4 modified TMGqu derivatives were advanced, leading to building blocks which should yield the desired compounds, such as TMG4Methoxyqu, within two steps.

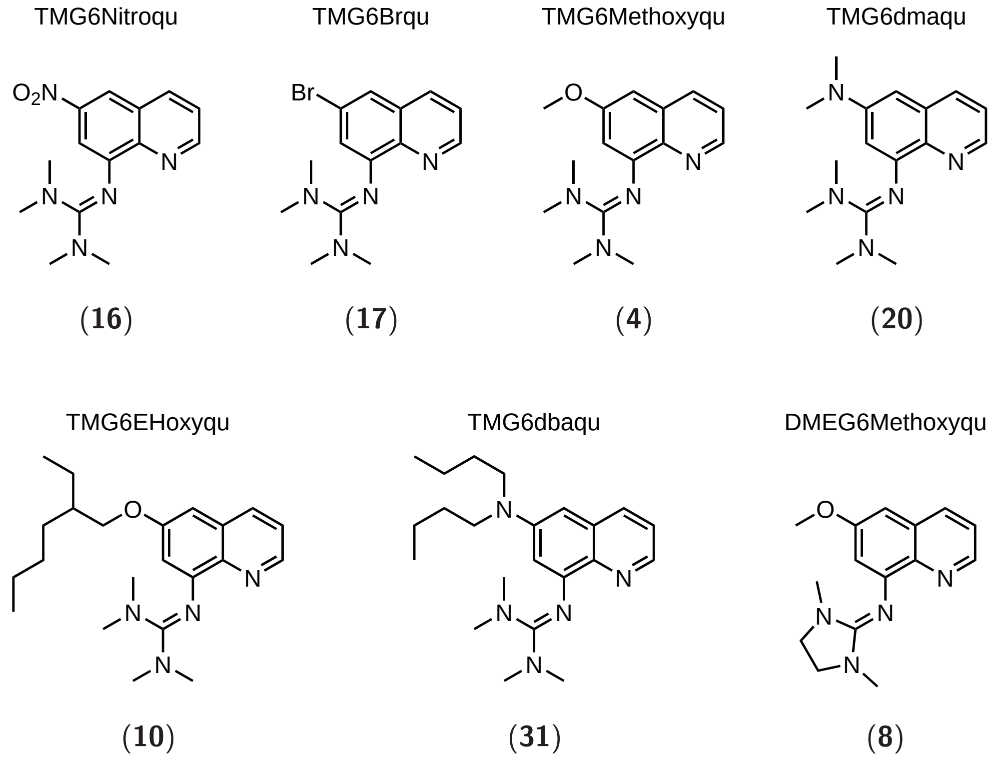

Figure 4.1: Synthesized guanidine-quinoline hybrid ligands.

The synthesized ligands were then used for complexation of different copper halides. All of the resulting bischelate complexes showed unsymmetrical coordination of their guanidine-quinoline hybrid ligands. The packing within the crystal lattice was concluded to have a major impact on the molecular geometry. It was assumed that the molecular structure in solution would not exhibit such alternations. For the evaluation of potential structural implications on the polymerization activity, the average bond lengths of the corresponding N−Cu bonds were used.

The molecular structures of the CuBr complexes showed tetrahedral coordination of the electron-rich ligands with non-coordinating bromide anions. The electron-poor ligands TMG6Nitroqu and TMG6Brqu afforded a trigonal-planar geometry including one bidentate ligand and the bromide anion. For both bischelate and monochelate complexes, the average $N_{gua}-Cu$ bonds did not differ significantly for the same geometries. In contrast, the $N_{qu}-Cu$ bonds were elongated for the more electron-rich ligands. In coherence with the NMR data, it might be debated if the $N_{qu}-Cu$ bond could act as the major electron-donation pathway from the ligands to the copper centers. Similar coordination was found for the CuCl complexes, however, the trend of elongation was not perceived. Furthermore, it was found that the $[Cu(TMG6Methoxyqu)_2]^+$ cations exhibited the largest angles between the chelate planes of all Cu^I complexes.

In contrast to the Cu^I complexes, trends of bond elongation were not found for the Cu^{II} species. However, the guanidine moieties of Cu^{II} complexes exhibited increased ρ parameters and decreased twist angles. Both aspects were considered as indication of an increased delocalization and stabilization of the guanidine π system.

The synthesized ligands of our TMGqu family were used in polymerization experiments to determine the catalytic activity of their copper complexes. Therefore, the ligands and CuBr were added to a solution of the monomer styrene in benzonitrile. The reactions were started by addition of an initiator and the samples were analyzed by NMR spectrometry and by GPC. All TMGqu-derived CuBr catalysts were found to polymerize styrene in high polymerization rates under controlled conditions. As expected, the use of copper complexes with electron-rich ligands resulted in faster catalysis. The $[Cu(TMG6Methoxyqu)_2]Br$ complex afforded outstandingly fast ATRP reactions, yielding two to five times higher rate constants k_p than other catalysts. In contrast, the two ligands TMG6dbaqu and TMG6dmaqu were expected to exhibit higher polymerization activity than TMG6Methoxyqu. However, their lower catalytic activity was related to potential termination reactions, which could have resulted in an increase of the Cu^{II} deactivator concentration, leading to slower polymerization kinetics.

The electrochemical potentials of the copper complexes of our ligand family were examined with cyclic voltammetry. It was found that all $CuBr_2$ complexes followed the expected behavior, affording more negative potentials for the complexes with stronger electron-donating substituents at position C6. The received potentials covered a range of 0.1 V from −0.439 V to −0.545 V (in respect to the ferrocene couple). Besides the exceptionally fast TMG6Methoxyqu catalyst, the sequence of increasing catalytic activity was in accordance with the decreasing

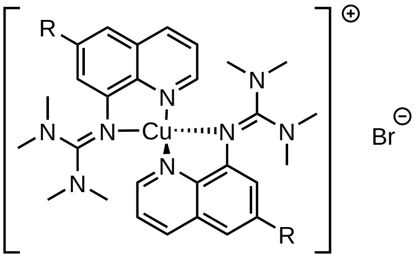

R: OCH_3 [Cu(TMG6Methoxyqu)$_2$]Br, (**C1**)
$N(CH_3)_2$ [Cu(TMG6dmaqu)$_2$]Br, (**C2**)

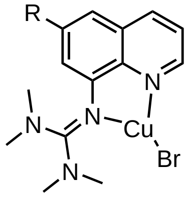

R: NO_2 [Cu(TMG6Nitroqu)Br], (**C3**)
Br [Cu(TMG6Brqu)Br], (**C4**)

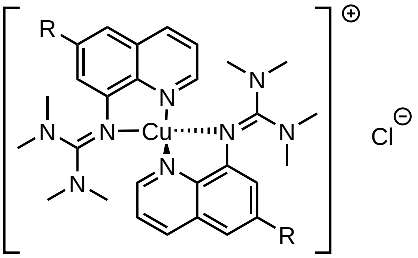

R: OCH_3 [Cu(TMG6Methoxyqu)$_2$]Br, (**C9**)
NO_2 [Cu(TMG6Nitroqu)$_2$]Br, (**C10**)

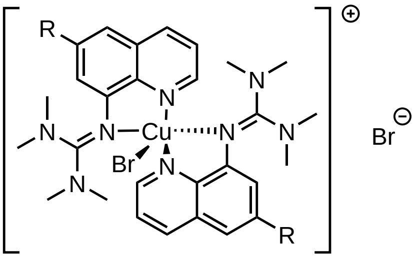

R: OCH_3 [Cu(TMG6Methoxyqu)$_2$Br]Br, (**C5**)
$N(CH_3)_2$ [Cu(TMG6dmaqu)$_2$Br]Br, (**C6**)
NO_2 [Cu(TMG6Nitroqu)$_2$Br]Br, (**C7**)
Br [Cu(TMG6Brqu)$_2$Br]Br, (**C8**)

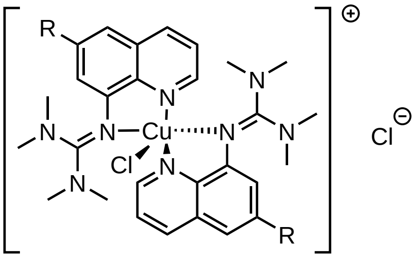

R: OCH_3 [Cu(TMG6Methoxyqu)$_2$Cl]Cl, (**C11**)
Br [Cu(TMG6Brqu)$_2$Cl]Cl, (**C12**)

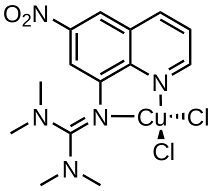

[Cu(TMG6Nitroqu)Cl$_2$], (**C13**)

Figure 4.2: Overview of the synthesized copper complexes.

electrochemical potential of the $CuBr_2$ complexes. However, the [Cu(TMG6Methoxyqu)$_2$Br]Br complex did not display a particularly low potential as suggested by its high polymerization activity.

In contrast, the electrochemical potential of the CuBr complexes showed certain deviations. The lack of an additional stabilizing bromide ligand was expected to result in tetra-coordinated Cu^{II} complexes during the oxidation half-cycle. The experimental data confirmed an increase of the electrochemical potential, although this increase was not found to be equal for all species. The [Cu(TMG6EHoxyqu)$_2$]Br complex exhibited an increase of 35 mV from the $CuBr_2$ couple, whereas the potential of the [Cu(TMGqu)$_2$]Br complex was increased by only 10 mV. Upon comparison, the increased electrochemical potential of the TMG6EHoxyqu CuBr catalyst could not be related to the polymerization reaction rate constant k_p. Excepting the TMG6Methoxyqu catalyst, all $CuBr_2$ electrochemical potentials were in accordance with the corresponding polymerization rate constant.

The electrochemical potentials of the $CuCl_2$ complexes were found to be 40 mV to 60 mV lower than their $CuBr_2$ counterparts. While all bromide complexes exhibited reversible electrochemical behavior, many $CuCl_2$ complexes showed pseudo-reversible behavior by increasing their peak potential differences upon faster voltage sweeps. Furthermore, the monochelate [Cu(TMG6Nitroqu)Cl_2] complex displayed only one half-cycle, which might be followed by a different chemical reaction impeding the reverse-reaction.

For determination of the K_{ATRP}, k_{act} and k_{deact} constants, CuBr complexes of our ligand family were subjected to two different equilibrium reactions with ATRP initiators. The increasing concentration of the resulting Cu^{II} species was then determined by UV/Vis spectroscopy. In the first equilibrium reaction which aimed at affording the K_{ATRP} values, the experimental setup relied on the literature known radical termination rate constant k_t. Due to high catalyst concentrations, the termination was not prevented leading to a constant increase of the Cu^{II} deactivator (persistent radical effect). The rate in which the Cu^{II} concentration changed could be related to the equilibrium constant. In the second experimental setup, the radical trapping agent TEMPO was added to suppress the deactivation reaction. Thereby, the activation rate constant k_{act} could be determined. The deactivation rate constant k_{deact} was then calculated from the ATRP equilibrium equation.

The experimental data showed great reproducibility and accurate results. All CuBr complexes exhibited K_{ATRP} values which increased with more electron-donating substituents. The lowest values were found for the TMG6Brqu complex increasing for the complexes of TMG6Methoxyqu and TMG6EHoxyqu leading to the highest K_{ATRP} values for the complexes with TMG6dbaqu and TMG6dmaqu. The increase of the K_{ATRP} values was accompanied by an increase of the corresponding k_{act} constants and a decrease of the deactivation rate constant k_{deact}. The ligand TMG6dmaqu formed the fastest known ATRP catalyst system derived from bidentate ligands.[1,2] In accordance with the cyclic voltammetry experiments, the TMG6Methoxyqu copper complexes did not exhibit unusual behavior, which could be related to the increased catalytic activity.

The different analytical methods which were used to characterize the ligands of our C6 modified TMGqu library exhibited coherent results for almost all our catalysts. The $N_{qu}-Cu$ bonds of the CuBr catalysts were elongated, the electrochemical potentials were reduced and the K_{ATRP} and k_{act} values were increased for the more electron-rich ligands. However, the ligand TMG6Methoxyqu yielded copper catalysts that resulted in exceptionally high polymerization rate constants. Consequently, the equilibrium constant of the TMG6Methoxyqu catalyst has the optimal value for our polymerization conditions, balancing high polymerization rates and radical termination.

5. Outlook

Different analytical methods implied that the ligands TMG6dmaqu and TMG6dbaqu should afford catalysts which are faster than the TMG6Methoxyqu derivatives. Therefore, the unusually high polymerization activity of the latter should be further examined. By reducing the catalyst concentration in polymerization assays, potential termination reactions could be suppressed. The kinetic profiles that could be obtained from these reaction conditions should give information whether the amino derived catalysts suffer from termination reactions or the TMG6Methoxyqu catalyst is a remarkable outlier. In a different polymerization assay, small amounts of $CuBr_2$ complexes could be added to the reaction mixture, suppressing termination reactions at higher catalyst concentrations.

Additionally, the analytical methods to determine the molecular masses of oligomers which could be present in low conversion polymer samples should be optimized. Therefore, the molecular mass evolution could be tracked even for the early samples helping in the elucidation of molecular mass deviations. The initiator concentration of the polymerization assays could be reduced, leading to longer polymer chains. This could improve the sample workup at smaller conversions. Finally, the polymerization reactions could be examined by UV/Vis spectroscopy, visualizing the equilibrium evolution during the course of the reaction. After some optimization, this method should be able to detect increased termination rates at the beginning of a polymerization reaction.

The ligands which were analyzed in this work were all part of a library of TMGqu derivatives with modifications at position C6. However, the path of donation still remains unclear. Therefore, the synthesis of TMGqu derivatives with modifications at other positions (C4, C5) could clarify this aspect. Since the route towards TMG4Methoxyqu is optimized until the second-last step, the finalization of the ligand should be feasible by the methods which were tested in earlier approaches. Therefore, the 8-bromo-4-methoxyquinoline could be subjected to amination conditions with aqueous ammonia and Cu^I catalysts, such as Cu_2O or Cu^I halides. These reactions could either be conducted at high temperatures and high pressure in stainless steel reactors with PTFE seals or at lower temperatures with additional organic solvents.[129] For targeting TMG4dmaqu or similar amino derivatives, the quinoline 1-oxide approaches could be optimized and complemented by C−H activation for insertion of an amine moiety at C8.[130] A review concerning different approaches towards substituted quinolines was published by Marco-Contelles *et al*. in 2009 and covers a wide range of possible reactions.[131]

Considering previous studies, the synthesis of a new TMGqu ligand derivative is envisioned. The ligand 1,1,3,3-tetramethyl-2-(4,5,6-trimethoxyquinolin-8-yl)guanidine (TMG456Methoxyqu, Scheme 5.1) incorporates three electron-donating methyl ether substituents at the position C4, C5 and C6. The planned synthetic route is based on the reactions conducted in this work. At first, the commercially available 3-bromoveratrole should be nitrated using nitric acid in sulfuric acid. As an alternative, nitric acid (100%) could be used in glacial acetic acid under refluxing conditions. The resulting product 3-bromo-4-nitroveratrole is also commercially available and could be used instead. The following reduction of the nitro group with sodium dithionite should then deliver 4-amino-3-bromoveratrole. The formation of the quinoline carboxylic acid could be realized in a three step one-pot procedure using diethyl ethoxymethylenemalonate as described earlier. After decarboxylation, the resulting 8-bromo-4-hydroxy-5,6-dimethoxyquinoline could be alkylated analogously to the 4-hydroxyquinoline derivatives described in this work. The crucial and most challenging step of this synthetic approach is the amination of the 8-bromoquinoline derivative. The finalization of the TMGqu derived ligands should then be realized by the reactions developed by Kantlehner *et al*.[73]

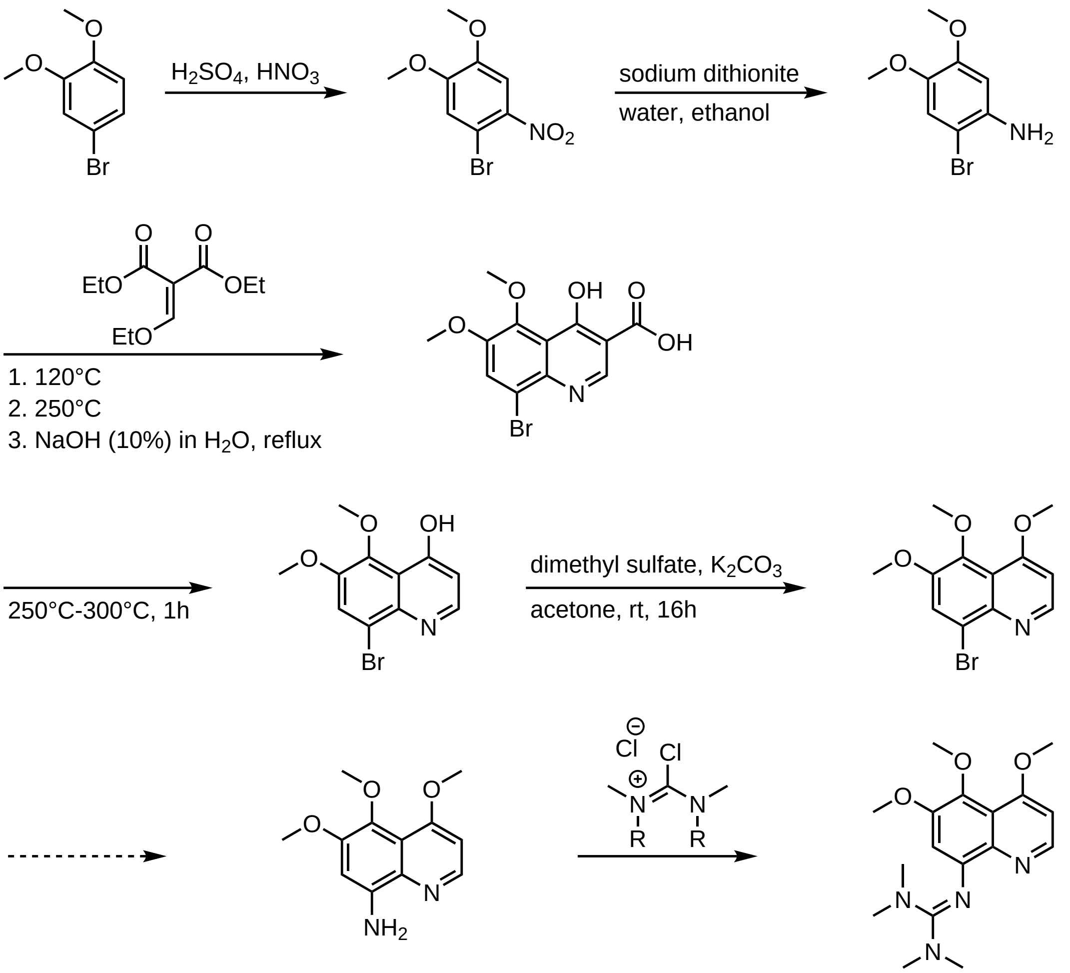

Scheme 5.1: Synthetic route towards 1,1,3,3-tetramethyl-2-(4,5,6-trimethoxyquinolin-8-yl)guanidine (TMG456Methoxyqu).

6. Experimental

6.1. General Experimental Details

Unless stated otherwise, all reactions were performed in oven-dried glassware. All reagents whose origins were not mentioned were purchased from commercial sources, such as Sigma-Aldrich Chemie GmbH (Taufkirchen, Germany), Acros Organics N.V. (Geel, Belgium), TCI Europe N.V. (Zwyndrecht, Belgium), ABCR GmbH & Co. KG (Karlsruhe, Germany) and Carbolution Chemicals GmbH (St. Ingbert, Germany) and used without further purification (Table 6.1). Chloroformamidium chlorides, such as *N*,*N*,*N'*,*N'*-tetramethylchloroformamidinium chloride (TMG−Cl, **7**) and *N*,*N'*-dimethyl-*N*,*N'*-ethylenechloroformamidinium chloride (DMEG−Cl, **9**) were synthesized in our group as described by Kantlehner *et al.*[73] Dry solvents were received from distillation. Tetrahydrofuran and diethyl ether were distilled from benzophenone and sodium, acetonitrile was distilled from calcium hydride.[132] The $TiCl_3$ solution, which was used for reduction reactions was titrated (section 6.2.4), 2,2,6,6-tetramethylpiperidinyloxyl was sublimed and the initiators 1-PEBr and 1-PECl were distilled before use. Benzonitrile which was used in polymerization reactions was distilled over calcium hydride and styrene was destabilized by flash column chromatography over aluminum oxide. For all synthetic procedures, degassing was conducted by ultrasonic treatment at ambient temperature for 10 min. Solvents used during polymerization reactions, cyclic voltammetry or analytical UV/Vis spectroscopy, were degassed by at least four pump-freeze-thaw cycles. Syntheses of copper complexes were held in a dry and oxygen-free glove box. Ferrocene, which was used for electrochemical measurements was sublimed before use. The reactions were magnetically stirred and if possible monitored by analytical thin-layer chromatography (TLC) using E. Merck 0.25 mm silica gel 60 F254 precoated aluminum plates. The TLC plates were visualized by exposure to ultraviolet light (UV, 254 nm) or common analytical stains. Flash column chromatography was performed as described by Still *et al.*[133] employing silica gel (60 Å, 35 µm to 75 µm, Merck) and a forced flow of the eluent. The yields refer to chromatographic and spectroscopic (^{1}H, ^{13}C NMR) pure material unless otherwise noted.

6.1.1. Instrumentation

Proton nuclear magnetic resonance (^{1}H NMR) spectra were recorded on JEOL ECX 400, JEOL ECX 270 and Bruker Avance III HD 400 spectrometers. Proton chemical shifts are expressed in parts per million (δ scale) and are calibrated using residual non-deuterated solvent as an internal reference ($CDCl_3$: δ 7.26, CD_2Cl_2: δ 5.32, CD_3CN: δ 1.94, DMSO-d_6: δ 2.50).[134] Data for ^{1}H NMR spectra are reported as follows: chemical shift (δ ppm) (multiplicity, coupling constant (Hz), integration). Multiplicities are reported as follows: s = singlet, d = doublet, t = triplet, q = quartet, m = multiplet or combinations thereof. **Carbon nuclear magnetic**

Table 6.1: Commercial sources of key chemicals.

Chemical	Commercial Source
6-methoxy-8-nitroquinoline	TCI Europe
8-nitroquinoline	TCI Europe
copper(II) chloride	Sigma-Aldrich
copper(II) bromide	ABCR
nitric acid (100%)	Sigma-Aldrich
titanium(III) chloride solution (12 %wt.)	Sigma-Aldrich
acrolein (90%, with hydroquinone as stabilizer)	Sigma-Aldrich
dimethylamine in THF (2 M)	Sigma-Aldrich
lithium bis(trimethylsilyl)amide in THF/ethylbenzene (1 M)	Acros
ammonia in 1,4-dioxane (0.5 M)	Acros
tetrabutylammonium hexafluorophosphate (for electrochemical analysis, ≥99.0%)	Sigma-Aldrich

resonance (^{13}C NMR) spectra were recorded on JEOL ECX 400 and Bruker Avance III HD 400 spectrometers. Carbon chemical shifts are expressed in parts per million (δ scale) and are referenced to the carbon resonances of the solvent ($CDCl_3$: δ 77.0, CD_2Cl_2: δ 53.84, CD_3CN: δ 1.32, DMSO-d_6: δ 39.52).[134] All NMR-Experiments were conducted at ambient temperature. **Infrared (IR) spectroscopy** was conducted on a Jasco FT/IR-460plus and a FT/IR-4600 both with diamond-ATR probe heads. IR data was recorded with a resolution of 2 cm^{-1} and was reported in wave number (cm^{-1}). **Mass spectroscopy (MS)** experiments were performed on a JEOL JMS-700 instrument with electron ionization (EI, 250 °C, 70 eV) and evaporation on a platinum filament (20 °C to 1600 °C, 120 °C min^{-1}). For the fast atom bombardment method, a Thermo Finnigan MAT 95 instrument was used with ionization by 8 kV fast Xenon atoms. The **single crystal diffraction** data for **C1** to **C13** is presented in appendix C. The data for **C1**, **C3** to **C13** were collected on a Bruker D8 Venture with APEX2 CCD detector and the data for **C2** on an Oxford KM4 XCalibur2 with graphite monochromated Mo-Ka radiation (λ =0.710 73 Å) at 100 K (**C1**, **C3** to **C13**) or at 153 K (**C2**). Data reduction and absorption correction was performed with the programs SAINT and SADABS (**C1**, **C3** to **C13**)[135] or with the programs CRYSALIS (Oxford, 2008) and CRYSALIS RED (Oxford, 2008) (**C2**). The structure was solved by direct and conventional Fourier methods and all non-hydrogen atoms were refined anisotropically with full-matrix least-squares based on F^2 (XPREP,[136] SHELXS[137] and ShelXle[138]). Hydrogen atoms were derived from difference Fourier maps and placed at idealized positions, riding on their parent C atoms, with isotropic displacement parameters Uiso(H) = 1.2Ueq(C) and 1.5Ueq(C methyl). All methyl groups were allowed to rotate but not to tip. Synthesized polymers were purified with a Hettich 2000 centrifuge. The average molecular masses and the mass distributions of the obtained polystyrene samples were determined by **gel permeation chromatography** (GPC) in THF as mobile phase at a flow rate of 1 mL min^{-1}. The utilised GPCmax VE-2001 from Viscotek was a combination of an HPLC pump, two Malvern Viscotek T columns (porous styrene divinylbenzene copolymer) with a maximum pore size of

500 Å and 5000 Å, a refractive index detector (VE-3580) and a viscometer (Viscotek 270 Dual Detector). Universal calibration was applied to evaluate the chromatographic results. **UV/Vis spectroscopy** was conducted with a Avantes AvaSpec-ULS2048 CCD-Spectrometer which was connected by FC-UV200-2 (diameter: 200 µm, length: 2 m) optical fibers to the cuvette holder and to the Avantes AvaLight-DH-S-BAL lightsource. For K_{ATRP} and k_{act} measurements, Hellma QS-Screwcap-Cuvettes with an optical path length of 10.00 mm and two stacked silicon septa were used. Readings of the spectrometer were conducted with Avasoft 8.6.1.0. **Cyclic voltammetry** experiments were performed at room temperature with a Metrohm Autolab Potentiostat PGSTAT 101 using a three electrode arrangement with a Pt working electrode (1 mm diameter), an Ag/AgCl reference electrode (in saturated LiCl in ethanol) and a Pt wire counter electrode in acetonitrile with tetrabutylammonium hexafluorophosphate (0.1 M) with a sample concentration of 0.1 mM. Ferrocene was added as an internal standard after the measurements of the sample and all potentials are referenced relative to the Fc/Fc$^+$ couple. Cyclic voltammograms were measured with sweep rates of 200 mV s^{-1}, 100 mV s^{-1}, 50 mV s^{-1}and 20 mV s^{-1}. Synthesized ligands were purified by *kugelrohr* distillation or sublimation with a Büchi B-585 apparatus. All optical analysis were prepared in a either a MBraun Labstar or a MBraun Labmaster glove box. Both oxygen and water levels were held below 0.1 ppm. For long term storage or crystallization assays a glove box with nitrogen inert gas was used. When liquids needed to be transferred under inert conditions, Hamilton Gastight 1000 Series and Gastight 1700 Series syringes of Hamilton Bonaduz AG, Switzerland were used with different sizes, needle lengths and needle diameters.

6.2. Preparation of catalyst precursors

6.2.1. Preparation of Ligand precursors

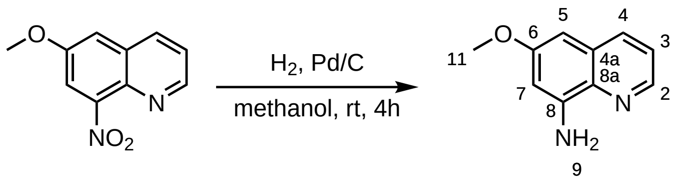

5 **6**

6-Methoxy-8-aminoquinoline (6). To a 250 ml Schlenk flask with degassed methanol (100 ml) 6-Methoxy-8-nitroquinoline (**5**) (2.04 g, 10 mmol, 1.0 equiv) and palladium on carbon (10 %wt) (100 mg, 0.1 mmol, 0.010 equiv) were added. Then, the flask was purged with hydrogen gas and left stirring under hydrogen atmosphere at ambient pressure and room temperature for 4 hours until all starting material was consumed. The reaction mixture was filtrated and the solvent was removed *in vacuo*. The obtained yellow oil was used without further purification. Yield: 99%.

M($C_{10}H_{10}N_2O$) = 174.20 g mol^{-1}. **^{1}H NMR** (400 MHz, $CDCl_3$) δ 8.59 (dd, J = 4.2, 1.7 Hz, 1H, H2), 7.92 (dd, J = 8.3, 1.7 Hz, 1H, H4), 7.29 (dd, J = 8.3, 4.2 Hz, 1H, H3), 6.58 (d, J = 2.6 Hz, 1H, H7), 6.46 (d, J = 2.6 Hz, 1H, H5), 5.02 (s, 2H, H9), 3.86 (s, 3H, H11). **^{13}C NMR** (101 MHz, $CDCl_3$) δ 158.9 (C6), 145.2 (C8), 145.1 (C2), 135.5 (C4), 134.8 (C8a), 129.9 (C4a), 121.9 (C3), 101.6 (C7), 94.6 (C5), 55.3 (C10). **IR** (Diamond-ATR, neat) $\tilde{\nu}_{max}$: 3464 (br), 3363 (br), 3001 (vw), 2958 (vw), 2937 (vw), 2833 (vw), 2112 (vw), 1618 (s), 1589 (s), 1502 (vs), 1466 (m), 1452 (m), 1427 (m), 1381 (vs), 1340 (m), 1275 (w), 1223 (m), 1196 (m), 1157 (vs), 1084 (m), 1041 (m), 1020 (m), 957 (m), 899 (m), 822 (s), 789 (s), 754 (m) cm^{-1}. **Anal. Calcd** for $C_{10}H_{10}N_2O$: C, 68.95; H, 5.79; N, 16.08%, found: C, 68.68; H, 5.68; N, 15.97%. **MS** (EI) m/z (relative intensity): 174 (100%) [$C_{10}H_{10}N_2O^+$], 145 (37%) [$C_9H_9N_2{}^+$], 144 (21%) [$C_9H_8N_2{}^+$], 131 (19%) [$C_8H_5NO^+$], 117 (7%) [$C_7H_5N_2{}^+$]. **HR-MS** (EI): calcd for [$C_{10}H_{10}N_2O$] 174.0793, found: 174.0789.

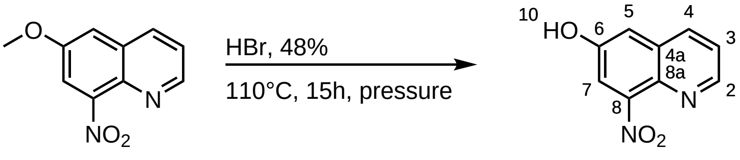

5 **11**

6-Hydroxy-8-nitroquinoline (**11**) was synthesized as described by Mewshaw *et al*. and Smil *et al*.[96,97] The methyl ether (**5**, 2.9 g, 14.2 mmol, 1 eq) was suspended in hydrobromic acid (48%, 16 mL, 24 g, 15 eq) and heated to 100 °C in a sealed pressure flask for 15 hours. Above a temperature of 90 °C, the quinoline was dissolved. After the reaction was completed an orange solid precipitated upon cooling to room temperature. The solid was filtered and washed with water (3×20 mL) before it was suspended in water (10 mL). Then a sodium hydroxide solution (15%, 35 mL) was added to dissolve the crude product. Afterward, the red solution was acidified with hydrochloric acid (37%, ca. 10 mL) to pH=6. The yellow precipitate was filtered, washed with water (3×30 mL) and dried under reduced pressure. For improved drying, some ethanol was added. The product (**11**, 2.0 g, 74%) was used without further purification.

M($C_9H_6N_2O_3$) = 190.16 g mol^{-1}. **TLC** (1% methanol in dichloromethane): R_f = 0.12 (UV) **TLC** (50% ethyl acetate in iso-hexane): R_f = 0.37 (UV) **^{1}H NMR** (400 MHz, DMSO-d_6) δ 10.78 (s, 1H, H10), 8.78 (dd, J = 4.2, 1.6 Hz, 1H, H2), 8.35 (dd, J = 8.5, 1.6 Hz, 1H, H4), 7.79 (d, J = 2.6 Hz, 1H, H7), 7.58 (dd, J = 8.4, 4.2 Hz, 1H, H3), 7.45 (d, J = 2.6 Hz, 1H, H5). **^{13}C NMR** (101 MHz, DMSO-d_6) δ 154.3 (C6), 149.3 (C2), 148.6 (C8), 134.7 (C4), 133.5 (C8a), 129.8 (C4a), 123.1 (C3), 115.4 (C7), 112.3 (C5). **IR** (Diamond-ATR, neat) $\tilde{\nu}_{max}$: 3331 (w), 3061 (w), 3034 (w), 2952 (vw), 2861 (vw), 2808 (vw), 2761 (vw), 2719 (vw), 2663 (w), 2604 (w), 2570 (w), 1633 (w), 1606 (m), 1586 (m), 1546 (m), 1492 (m), 1467 (w), 1414 (m), 1339 (m), 1289 (m), 1269 (w), 1246 (vs), 1213 (m), 1170 (w), 1141 (w), 1053 (w), 1015 (w), 982 (w), 903 (m), 881 (s), 808 (m), 797 (m), 766 (s), 726 (vw) cm^{-1}. **MS** (EI) m/z (relative intensity): 191 [$C_9H_7N_2O_3{}^+$] (50%), 190 (100%) [$C_9H_6N_2O_3{}^+$], 160 (13%)

[$C_9H_6NO_2^+$], 132 (65%) [$C_8H_6NO^+$], 116 (39%), 89 (35%), 63 (17%). **HR-MS** (EI): calcd for [$C_9H_6N_2O_3$] 190.0379, found: 190.0379.

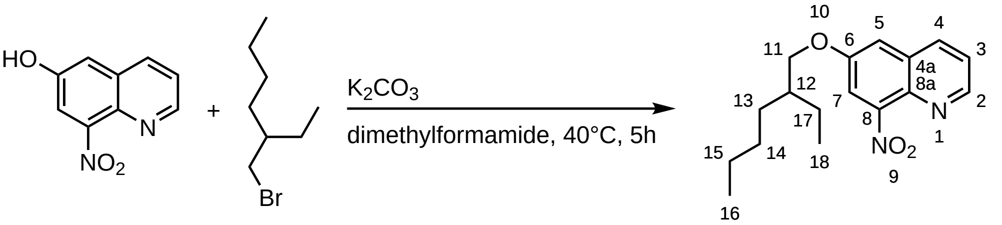

11 **12** **13**

6-((Ethylhexyl)oxy)-8-nitroquinoline (**13**) was synthesized analog to Mewshaw *et al*. and Smil *et al*.[96,97] In a 25 mL Schlenk flask with dimethylformamide (10 mL) 6-hydroxy-8-nitroquinoline (**11**, 380 mg, 2 mmol, 1 eq), 2-ethyl-hexylbromide (**12**, 772 mg, 4 mmol, 0.71 mL, 2 eq) and potassium carbonate (830 mg, 6 mmol, 3 eq) were dissolved under inert atmosphere and heated to 40 °C for 5 h. After all staring material was used up (TLC) the reaction mixture was poured into water (60 mL) and extracted with ethyl acetate (4×50 mL). After removal of the solvents the brown oil was purified by flash column chromatography (silica, ethyl acetate (10%) in iso-hexanes for the first fraction, then 17% ethyl acetate in iso-hexanes). The product was obtained as yellow oil (470 mg, 78%) which solidified by cooling.

M($C_{17}H_{22}N_2O_3$) = 302.37 g mol^{-1}. **TLC** (10% ethyl acetate in iso-hexanes): $R_f = 0.22$ (UV) **^{1}H NMR** (400 MHz, $CDCl_3$) δ 8.70 (dd, J = 4.2, 1.6 Hz, 1H, H2), 8.00 (dd, J = 8.4, 1.7 Hz, 1H, H4), 7.56 (d, J = 2.7 Hz, 1H, H7), 7.32 (dd, J = 8.4, 4.2 Hz, 1H, H3), 7.18 (d, J = 2.7 Hz, 1H, H5), 3.89 (dd, J = 5.7, 1.2 Hz, 2H, H11), 1.69 (hept, J = 6.1 Hz, 1H, H12), 1.49 – 1.31 (m, 4H, H13, H17), 1.24 (m, 4H, H14, H15), 0.86 (t, J = 7.5 Hz, 3H, H18), 0.84 – 0.79 (m, 3H, H16). **^{13}C NMR** (101 MHz, $CDCl_3$) δ 155.6 (C6), 149.5 (C2), 148.5 (C8), 135.0 (C8a), 134.8 (C4), 129.9 (C4a), 122.7 (C3), 116.6 (C7), 109.8 (C5), 71.4 (C11), 39.1 (C12), 30.3 (C13), 28.9 (C14), 23.6 (C17), 22.8 (C15), 13.9 (C16), 10.9 (C18). **IR** (Diamond-ATR, neat) $\tilde{\nu}_{max}$: 3051 (vw), 2958 (w), 2927 (w), 2873 (w), 2860 (w), 1729 (vw), 1630 (m), 1596 (w), 1572 (vw), 1532 (vs), 1493 (m), 1460 (m), 1439 (m), 1372 (m), 1353 (m), 1336 (m), 1243 (s), 1209 (vw), 1163 (m), 1129 (m), 1043 (m), 1027 (m), 948 (v), 892 (m), 853 (m), 785 (m), 765 (m), 731 (w), 667 (vw), 656 (w) cm^{-1}. **Anal. Calcd** for $C_{17}H_{22}N_2O_3$: C, 67.53; H, 7.33; N, 9.26%, found: C, 67.46; H, 7.46; N, 9.07%. **MS** (EI) m/z (relative intensity): 302 (27%) [$C_{17}H_{22}N_2O_3^+$], 191 (82%) [$C_9H_7N_2O_3^+$], 190 (70%) [$C_9H_6N_2O_3^+$], 132 (44%), 127 (24%) [$C_9H_5N^+$], 116 (22%) [$C_7H_{16}O^+$], 115 (38%) [$C_7H_{15}O^+$], 71 (60%) [$C_5H_{11}^+$], 57 (100%) [$C_4H_9^+$], 55 (43%) [$C_4H_7^+$], 43 (99%) [$C_3H_7^+$], 41 (91%) [$C_3H_5^+$], 29 (59%) [$C_2H_5^+$]. **HR-MS** (EI): calcd for [$C_{17}H_{22}N_2O_3$] 302.1631, found: 302.1630.

6-((Ethylhexyl)oxy)-8-aminoquinoline (48). To a 250 mL Schlenk flask with degassed methanol (100 mL) 6-((Ethylhexyl)oxy)-8-nitroquinoline (**48**) (3.02 g, 10 mmol, 1.0 equiv) and palladium on carbon (10 %wt) (100 mg, 0.1 mmol, 0.010 equiv) were added. Then, the flask

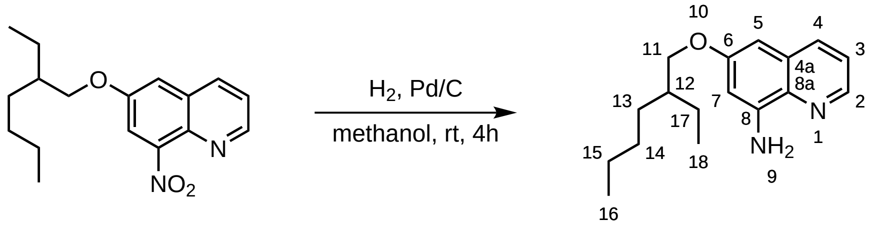

13 **48**

was purged with hydrogen and left stirring under hydrogen atmosphere at ambient pressure and room temperature for 4 h until all starting material was consumed. Then, the solvent was removed *in vacuo* and the obtained oil was purified by flash column chromatography (silica, 1% methanol in dichloromethane) to give a dark green oil (2.4 g, 90%).

M($C_{17}H_{24}N_2O$) = 272.39 g mol^{-1}. **^{1}H NMR** (400 MHz, $CDCl_3$) δ 8.58 (dd, J = 4.2, 1.7 Hz, 1H, H2), 7.93 (dd, J = 8.3, 1.7 Hz, 1H, H4), 7.30 (dd, J = 8.3, 4.2 Hz, 1H, H3), 6.60 (d, J = 2.5 Hz, 1H, H7), 6.48 (d, J = 2.5 Hz, 1H, H5), 4.96 (s, 2H, H9), 3.92 (dd, J = 5.8, 1.3 Hz, 2H, H11), 1.76 (h, J = 6.1 Hz, 1H, H12), 1.63 – 1.37 (m, 4H, H13, H17), 1.38 – 1.29 (m, 4H, H14, H15), 0.95 (t, J = 7.5 Hz, 3H, H18), 0.95 – 0.87 (m, 3H, H16). **^{13}C NMR** (101 MHz, $CDCl_3$) δ 158.8 (C6), 145.1 (C8), 145.0 (C2), 135.4 (C8a), 134.8 (C4), 130.1 (C4a), 121.9 (C3), 102.3 (C7), 95.5 (C5), 70.6 (C11), 39.5 (C12), 30.8 (C13), 29.3 (C14), 24.1 (C15), 23.2 (C17), 14.3 (C16), 11.3 (C18). **IR** (Diamond-ATR, neat) $\tilde{\nu}_{max}$: 3477 (vw), 3375 (vw), 3045 (vw), 2957 (m), 2926 (m), 2871 (w), 2858 (w), 2112 (vw), 1862 (vw), 1619 (s), 1589 (m), 1502 (s), 1459 (m), 1442 (m), 1383 (s), 1337 (w), 1274 (w), 1240 (w), 1222 (w), 1170 (vs), 1125 (w), 1087 (w), 1040 (w), 1014 (m), 904 (w), 818 (m), 789 (s), 727 (w), 674 (w) cm^{-1}. **MS** (EI) *m/z* (relative intensity): 272 (9%) [$C_{17}H_{24}N_2O^+$], 161 (11%) [$C_8{}^{13}CH_8N_2O^+$], 160 (100%) [$C_9H_8N_2O^+$], 131 (5%) [$C_8H_7N_2{}^+$]. **HR-MS** (EI): calcd for [$C_{17}H_{24}N_2O^+$] 272.1883, found: 272.1878.

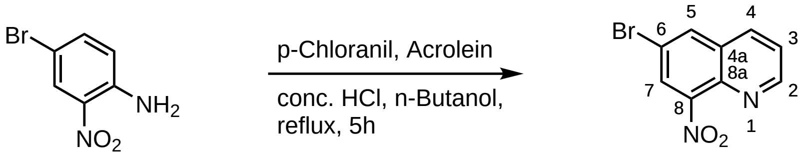

18

6-Bromo-8-nitroquinoline (18) was synthesized analog to Wielgosz-Collin *et al.*[101] In a round bottom flask (250 mL) 4-bromo-2-nitroaniline (10.9 g, 50 mmol, 1.0 equiv), p-chloranil (12.3 g, 50 mmol, 1.0 equiv), n-butanol (25 mL) and concentrated hydrochloric acid (12.5 mL) were heated to reflux. Then a solution of acrolein (90%, 5.6 mL, 1.5 equiv) in n-butanol (12.5 mL) was added over 2.5 h to the refluxing solution. After refluxing for 3 h, a solution of zinc chloride (6.8 g, 50 mmol, 1.0 equiv) in tetrahydrofuran (100 mL) was added and refluxed for 30 min. The mixture was then cooled to room temperature and stored in a fridge (4 °C) over night.

The solid was then filtered and washed with tetrahydrofuran. Afterwards, the solids were collected suspended in water (100 mL) and basified with aqueous sodium hydroxide solution (1M, 70 mL) and concentrated aqueous ammonia (150 mL). Then the mixture was extracted with dichloromethane (3×150 mL). The combined organic layers were dried over sodium sulfate and treated with decolorizing carbon. After filtration, the solvents were removed *in vacuo*. The crude product was subjected to a flash column chromatography (silica, dichloromethane) and yielded a pale yellow solid (10.6 g, 84%).

M($C_9H_5N_2O_2Br$) = 253.06 g mol^{-1}. **^{1}H NMR** (400 MHz, $CDCl_3$) δ 9.07 (dd, J = 4.2, 1.7 Hz, 1H, H2), 8.20 (d, J = 2.0 Hz, 1H, H5), 8.19 (dd, J = 8.2, 1.8 Hz, 1H, H4), 8.12 (d, J = 2.1 Hz, 1H, H7), 7.58 (dd, J = 8.4, 4.2 Hz, 1H, H3). **^{13}C NMR** (101 MHz, $CDCl_3$) δ 153.0 (C2), 148.7 (C8), 138.4 (C8a), 135.3 (C4), 133.9 (C5), 130.2 (C4a), 127.2 (C7), 123.8 (C3), 118.4 (C6). **IR** (Diamond-ATR, neat) $\tilde{\nu}_{\text{max}}$: 3065 (vw), 1763 (vw), 1614 (w), 1589 (w), 1532 (s), 1487 (m), 1387 (m), 1370 (m), 1345 (m), 1322 (m), 1217 (w), 1200 (m), 1095 (w), 1080 (w), 1033 (m), 994 (w), 889 (m), 873 (s), 848 (m), 800 (m), 790 (vs), 734 (m), 713 (w), 674 (s) cm^{-1}. **MS** (EI) *m/z* (relative intensity): 255 (7%) [$C_8{}^{13}CH_5N_2O_2{}^{81}Br^+$], 254 (67%) [$C_9H_5N_2O_2{}^{81}Br^+$], 253 (7%) [$C_8{}^{13}CH_5N_2O_2{}^{79}Br^+$], 252 (67%) [$C_9H_5N_2O_2{}^{79}Br^+$], 224 (17%), 222 (18%), 208 (28%) [$C_9H_5N{}^{81}Br^+$], 206 (27%) [$C_9H_5N{}^{79}Br^+$], 196 (60%), 194 (62%), 127 (100%), 115 (29%), 99 (12%), 74 (15%). **HR-MS** (EI): calcd for [$C_8{}^{13}CH_5N_2O_2{}^{81}Br^+$] 254.9543, found: 254.9524. **HR-MS** (EI): calcd for [$C_9H_5N_2O_2{}^{81}Br^+$] 253.9509, found: 253.9503. **HR-MS** (EI): calcd for [$C_8{}^{13}CH_5N_2O_2{}^{79}Br^+$] 252.9563, found: 252.9557. **HR-MS** (EI): calcd for [$C_9H_5N_2O_2{}^{79}Br^+$] 251.9530, found: 251.9526.

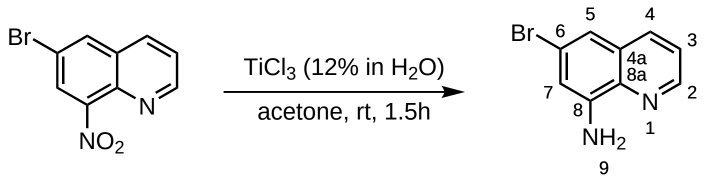

18 **19**

8-Bromo-6-aminoquinoline (19) was prepared analog to Schofield *et al.*[100]. To a Schlenk flask (250 mL) with degassed acetone (100 mL) and 6-bromo-8-nitroquinoline (**18**) (2.67 mg, 1.1 mmol, 1.0 equiv) an aqueous solution of titanium(III)chloride (16.3 %wt.) (6.00 mL, 6.3 mmol, 6.0 equiv) was added dropwise under continuous stirring at room temperature. After decolorization of the purple solution, the reaction mixture was further stirred for 30 min. Then the orange solution was diluted with water (150 mL) before it was neutralized with aqueous sodium hydroxide solution (0.5 M). The colorless suspension was then extracted with dichloromethane (3×200 mL). The organic phase was dried over sodium sulfate before the solvent was removed *in vacuo*. After purification by flash column chromatography (silica, dichloromethane), a yellow solid was received (232 mg, 98%). Note: The aqueous solution of titanium(III) chloride has to be titrated before use (6.2.4).

M($C_9H_7N_2Br$) = 223.07 g mol^{-1}. **TLC** (dichloromethane): R_f = 0.37 (UV, Ninhydrin)

^{1}H NMR (400 MHz, $CDCl_3$) δ 8.73 (dd, J = 4.2, 1.7 Hz, 1H, H2), 7.95 (ddd, J = 8.3, 1.7, 0.4 Hz, 1H, H4), 7.37 (dd, J = 8.3, 4.2 Hz, 1H, H3), 7.28 (d, J = 2.0 Hz, 1H, H5), 7.00 (d, J = 2.0 Hz, 1H, H7), 5.07 (s, 2H, NH). **^{13}C NMR** (101 MHz, $CDCl_3$) δ 147.7 (C2), 145.3 (C8), 137.2 (C8a), 135.1 (C4), 129.9 (C4a), 122.4 (C3), 121.5 (C6), 117.8 (C5), 112.9 (C7). **IR** (Diamond-ATR, neat) $\tilde{\nu}_{\text{max}}$: 3465 (w), 3349 (w), 3042 (vw), 2923 (w), 2850 (vw), 1606 (m), 1587 (m), 1527 (w), 1496 (vs), 1453 (w), 1373 (s), 1325 (m), 1239 (w), 1128 (w), 1031 (w), 977 (vw), 942 (vw), 905 (w), 831 (s), 793 (s), 732 (w) cm^{-1}. **MS** (EI) m/z (relative intensity): 225 (10%) [$C_8{}^{13}CH_7N_2{}^{81}Br^+$], 224 (100%) [$C_9H_7N_2{}^{81}Br^+$], 223 (9%) [$C_8{}^{13}CH_7N_2{}^{79}Br^+$], 222 (99%) [$C_9H_7N_2{}^{79}Br^+$], 142 (13%), 116 (23%), 89 (11%), 71 (9%), 43 (21%). **HR-MS** (EI): calcd for [$C_8{}^{13}CH_7N_2{}^{81}Br^+$] 224.9799, found: 224.9789 **HR-MS** (EI): calcd for [$C_9H_7N_2{}^{81}Br^+$] 223.9766, found: 223.9763 **HR-MS** (EI): calcd for [$C_8{}^{13}CH_7N_2{}^{79}Br^+$] 222.9820, found: 222.9803 **HR-MS** (EI): calcd for [$C_9H_7N_2{}^{79}Br^+$] 221.9787, found: 221.9773

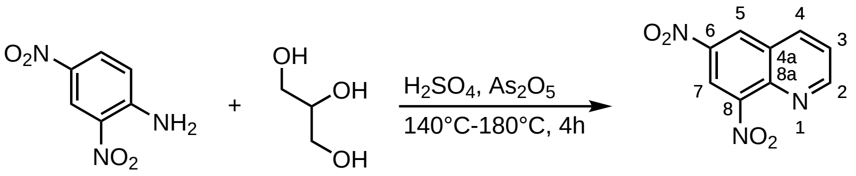

14

6,8-Dinitroquinoline (14) was synthesized analog to Rieche *et al.*[99] To a 100 mL two-neck round bottom flask with reflux condenser 2,4-dinitroaniline (5.49 g, 30 mmol, 1.0 equiv), arsenic pentoxide trihydrate (6.07 g, 26.4 mmol, 1.75 equiv), glycerol (3.97 g, 3.15 mL, 43.1 mmol, 1.4 equiv) and concentrated sulfuric acid (8 mL) were added and heated. At a temperature of 140 °C, the reaction mixture liquified and turned black. The reaction started to foam violently at 180 °C and the oil bath was removed. After the formation of foam subsided the reaction was heated to 170 °C for 2 h. Then the reaction mixture was poured on ice and neutralized with concentrated ammonia. The precipitates were collected by filtration, dried in an oven and then extracted with chloroform in an Soxhlett apparatus at 85 °C for 30 h. The crude product was subjected to a flash column chromatography (silica, 5% methanol in dichloromethane) and yielded a pale yellow solid (2.76 g, 42%).

M($C_9H_5N_3O_4$) = 219.16 g mol^{-1}. **TLC** (33% ethyl acetate in iso-hexane): R_f = 0.29 (UV). **TLC** (5% methanol in dichloromethane): R_f = 0.44 (UV). **^{1}H NMR** (400 MHz, $CDCl_3$) δ 9.25 (dd, J = 4.2, 1.7 Hz, 1H, H2), 9.01 (d, J = 2.4 Hz, 1H, H5), 8.80 (d, J = 2.4 Hz, 1H, H7), 8.51 (ddd, J = 8.5, 1.7, 0.4 Hz, 1H, H4), 7.77 (dd, J = 8.4, 4.3 Hz, 1H, H3). **^{13}C NMR** (101 MHz, $CDCl_3$) δ 155.9 (C2), 148.8 (C6), 144.0 (C8), 141.6 (C8a), 138.2 (C4), 128.4 (C4a), 127.7 (C5), 124.7 (C3), 117.7 (C7). **IR** (Diamond-ATR, neat) $\tilde{\nu}_{\text{max}}$: 3093 (vw), 3073 (vw), 1600 (w), 1576 (vw), 1525 (s), 1494 (m), 1417 (w), 1384 (w), 1344 (m), 1314 (m), 1213 (w), 1138 (w), 1092 (w), 1039 (w), 920 (m), 897 (m), 885 (m), 806 (m), 787 (vs), 751 (m), 727 (m), 682 (m), 637 (m), 625 (w), 606 (m) cm^{-1}. **MS** (EI) m/z (relative intensity): 219 (100%) [$C_9H_5N_3O_4{}^+$], 189 (11%) [$C_9H_{11}N_3O_2{}^+$], 131 (14%), 127 (59%)

[$C_9H_5N^+$], 126 (20%), 115 (58%) [$C_9H_7{}^+$], 114 (14%) [$C_9H_6{}^+$], 101 (37%) [$C_8H_5{}^+$], 100 (38%), 88 (20%) [$C_7H_4{}^+$], 76 (27%) [$C_6H_4{}^+$], 74 (29%), 63 (18%), 50 (25%), 30 (37%) [NO^+]. **HR-MS** (EI): calcd for [$C_9H_5N_3O_4{}^+$] 219.0280, found: 219.0280. **Anal. Calcd** for $C_9H_5N_3O_4$: C, 49.33; H, 2.30; N, 19.17%, found: C, 49.45; H, 2.31; N, 18.95%.

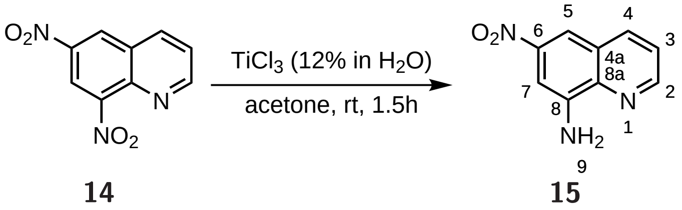

8-Amino-6-nitroquinoline (15) was prepared as described by Schofield *et al.*[100]. To a Schlenk flask (250 mL) with degassed acetone (100 mL) and 6,8-dinitroquinoline (**14**) (2.20 g, 10 mmol, 1.0 equiv) an aqueous solution of titanium(III)chloride (12 %wt.) (77.1 mL, 60 mmol, 6.0 equiv) was slowly added dropwise under continuously stirring at room temperature. After decolorization of the purple solution, the reaction mixture was further stirred for 30 min before it was basified with sodium hydroxide and concentrated *in vacuo*. Then, the yellow suspension was dissolved in degassed water and extracted with dichloromethane (4×100 mL). The organic phase was dried over sodium sulfate before the solvent was removed *in vacuo*. After purification by flash column chromatography (silica, methanol in dichloromethane), a yellow solid was received (1.35 g, 71%).

M($C_9H_7N_3O_2$) = 189.17 g mol^{-1}. **TLC** (33% ethyl acetate in iso-hexane): $R_f = 0.43$ (UV). **TLC** (5% methanol in dichloromethane): $R_f = 0.13$ (UV). **^{1}H NMR** (400 MHz, $CDCl_3$) δ 8.90 (dd, $J = 4.2$, 1.7 Hz, 1H, H2), 8.23 (dd, $J = 8.3$, 1.7 Hz, 1H, H4), 8.06 (d, $J = 2.4$ Hz, 1H, H5), 7.61 (d, $J = 2.4$ Hz, 1H, H7), 7.52 (dd, $J = 8.3$, 4.2 Hz, 1H, H3), 5.35 (s, 2H, H9). **^{13}C NMR** (101 MHz, $CDCl_3$) δ 150.6 (C2), 146.8 (C6), 145.6 (C8a), 140.2 (C8), 138.1 (C4), 127.6 (C4a), 123.2 (C3), 111.8 (C5), 102.1 (C7). **IR** (Diamond-ATR, neat) $\tilde{\nu}_{\text{max}}$: 3461 (w), 3358 (m), 3096 (vw), 3063 (vw), 2923 (vw), 2851 (vw), 1623 (m), 1593 (m), 1539 (vw), 1519 (m), 1489 (s), 1419 (w), 1410 (w), 1387 (m), 1340 (s), 1327 (s), 1271 (m), 1239 (m), 1124 (w), 1090 (m), 1050 (m), 1038 (m), 950 (w), 894 (m), 861 (s) , 838 (w), 794 (vs), 742 (s), 735 (s), 668 (m), 655 (w) cm^{-1}. **MS** (EI) *m/z* (relative intensity): 189 (100%) [$C_9H_7N_3O_2{}^+$], 159 (10%) [$C_9H_9N_3{}^+$], 143 (87%) [$C_9H_7N_2{}^+$], 131 (13%) [$C_9H_9N^+$], 116 (30%) [$C_9H_8{}^+$], 89 (18%) [$C_7H_5{}^+$], 63 (7%) [$C_5H_3{}^+$], 39 (3%). **HR-MS** (EI): calcd for [$C_9H_7N_3O_2{}^+$] 189.0538, found: 189.0536.

N-(6-nitroquinolin-8-yl)acetamide (22). 8-Amino-6-nitroquinoline (**15**) (1.32 g, 7.0 mmol, 1.0 equiv) was added to a round-bottom flask (250 mL) with dichloromethane (70 mL) and triethylamine (4.85 mL, 35 mmol, 5.0 equiv) under inert atmosphere. Then acetyl chloride (2.49 mL, 35 mmol, 5.0 equiv) was slowly added to the reaction solution and was left stirring for 5 h at room temperature. After completion, the reaction mixture was diluted with dichloromethane (150 mL) and basified with aqueous sodium hydroxide solution (10%). Then

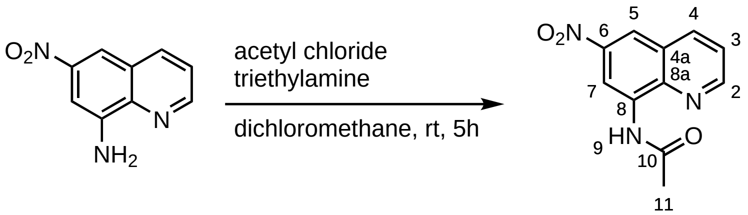

15 **22**

the two phases were separated and the organic phase was washed with sat. aqueous sodium bicarbonate solution (2×100 mL) and with diluted brine (8%, 2×100 mL) before it was dried over sodium sulfate. After removal of the solvents *in vacuo*, the crude product was purified by flash column chromatography (silica, 1% methanol in dichloromethane) and a yellow solid was received (1.52 g, 94%).

M($C_{11}H_9N_3O_3$) = 231.21 g mol^{-1}. **TLC** (1% methanol in dichloromethane): $R_f = 0.24$ (UV). **^{1}H NMR** (400 MHz, $CDCl_3$) δ 9.81 (br, 1H, H9), 9.52 (d, J = 2.5 Hz, 1H, H7), 8.97 (dd, J = 4.3, 1.7 Hz, 1H, H2), 8.46 (d, J = 2.5 Hz, 1H, H5), 8.36 (dd, J = 8.3, 1.7 Hz, 1H, H4), 7.64 (dd, J = 8.3, 4.3 Hz, 1H, H3), 2.39 (s, 3H, H11). **^{13}C NMR** (101 MHz, $CDCl_3$) δ 169.0 (C10), 151.4 (C2), 146.5 (C6), 140.1 (C8a), 138.6 (C4), 136.1 (C8), 126.7 (C4a), 123.5 (C3), 117.6 (C5), 109.8 (C7), 25.2 (C11). **IR** (Diamond-ATR, neat) $\tilde{\nu}_{max}$: 3331 (w), 3132 (vw), 3084 (vw), 1769 (w), 1731 (w), 1683 (s), 1621 (w), 1577 (w), 1515 (vs), 1426 (m), 1412 (m), 1396 (m), 1369 (m), 1345 (vs), 1323 (vs), 1255 (m), 1241 (m), 1192 (m), 1155 (m), 1139 (m), 1105 (w), 1080 (m), 1035 (m), 1011 (m), 955 (w), 882 (s), 806 (w), 798 (s), 782 (vs), 741 (m), 668 (m) cm^{-1}. **MS** (EI) *m/z* (relative intensity): 232 (4%) [$C_{10}{}^{13}CH_9N_3O_3{}^+$], 231 (27%) [$C_{11}H_9N_3O_3{}^+$], 216 (10%) [$C_{10}H_6N_3O_3{}^+$], 190 (10%) [$C_8{}^{13}CH_7N_3O_2{}^+$], 189 (100%) [$C_9H_7N_3O_2{}^+$], 143 (60%) [$C_6H_9NO_3{}^+$], 142 (16%), 131 (13%), 116 (11%), 115 (10%). **HR-MS** (EI): calcd for [$C_{11}H_9N_3O_3{}^+$] 231.0639, found: 231.0637.

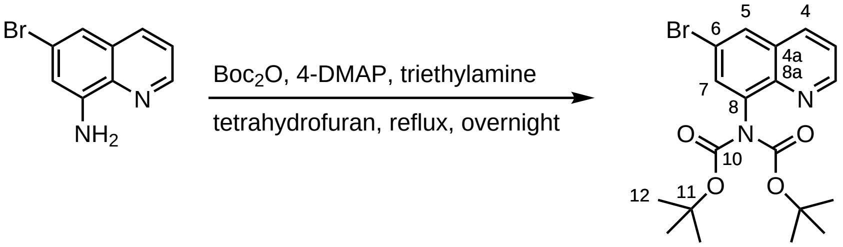

19 **26**

Di(tert-butyl)(6-bromoquinolin-8-yl)bicarbamat (26). In a round-bottom flask (50 mL), 8-amino-6-bromoquinoline (**19**) (223 mg, 1.0 mmol, 1.0 equiv), 4-(dimethylamino)pyridine (4-DMAP, 1220 mg, 10 mmol, 10 equiv), triethylamine (1.39 mL, 10 mmol, 10 equiv) and di-tert-butyl dicarbonate (2180 mg, 10 mmol, 10 equiv)) were dissolved in tetrahydrofuran (10 mL). The reaction was refluxed over night and the evolution of carbon dioxide ceased after 4 h. After cooling to room temperature, the solvent was removed *in vacuo*, before the mixture was extracted with dichloromethane and washed with hydrochloric acid (1%). After drying over sodium sulfate, the solvent was removed and the crude product was purified by flash column chromatography (silica, methanol gradient in dichloromethane) and yielded a yellow solid (45%).

When working with di-tert-butyl dicarbonate, appropriate safety measures are advised and an excess of the reagent needs to be removed prior to the reaction workup.[139]

M($C_{19}H_{23}BrN_2O_4$) = 423.31 g mol^{-1}. **^{1}H NMR** (400 MHz, CD_2Cl_2) δ 8.93 (dd, J = 4.2, 1.7 Hz, 1H, H2), 8.12 (dd, J = 8.3, 1.7 Hz, 1H, H4), 8.00 (d, J = 2.2 Hz, 1H, H5), 7.68 (d, J = 2.2 Hz, 1H, H7), 7.46 (dd, J = 8.3, 4.2 Hz, 1H, H3), 1.33 (s, 18H, H12). **^{13}C NMR** (101 MHz, CD_2Cl_2) δ 152.0 (C10), 151.2 (C2), 143.5 (C8a), 139.0 (C8), 135.6 (C4), 132.4 (C7), 130.2 (C5), 130.1 (C4a), 123.0 (C3), 119.3 (C6), 83.1 (C11), 28.1 (CH_3). **IR** (Diamond-ATR, neat) $\tilde{\nu}_{\max}$: 2979 (w), 2933 (w), 1793 (m), 1752 (m), 1711 (m), 1590 (w), 1523 (w), 1490 (m), 1456 (w), 1393 (m), 1367 (s), 1310 (m), 1272 (s), 1247 (s), 1148 (vs), 1114 (vs), 1097 (vs), 1034 (w), 1004 (w), 974 (w), 954 (w), 926 (vw), 845 (m), 813 (m), 773 (m), 712 (m), 676 (w), 665 (w) cm^{-1}. **MS** (EI) *m/z* (relative intensity): 324 (8%) [$C_{15}H_{17}NO_2{}^{81}Br^+$], 322 (8%) [$C_{15}H_{17}NO_2{}^{79}Br^+$], 268 (14%) [$C_{11}H_9NO_2{}^{81}Br^+$], 266 (14%) [$C_{11}H_9NO^{79}Br^+$], 251 (16%) [$C_{11}H_8NO^{81}Br^+$], 250 (16%) [$C_{11}H_7NO^{81}Br^+$], 249 (16%) [$C_{11}H_8NO^{79}Br^+$], 248 (14%) [$C_{11}H_7NO^{79}Br^+$], 224 (97%) [$C_{10}H_9N^{81}Br^+$], 222 (100%) [$C_{10}H_9N^{79}Br^+$], 142 (10%) [$C_6H_8NO_2{}^+$], 114 (3%) [$C_5H_8NO_2{}^+$], 57 (28%) [$C_4H_9{}^+$]. **HR-MS** (EI): calcd for [$C_{19}H_{23}N_2O_4{}^{79}Br^+$] 422.0836, found: 422.0834. **HR-MS** (EI): calcd for [$C_{18}{}^{13}CH_{23}N_2O_4{}^{79}Br^+$] 423.0869, found: 423.0872. **HR-MS** (EI): calcd for [$C_{19}H_{23}N_2O_4{}^{81}Br^+$] 424.0815, found: 424.0820.

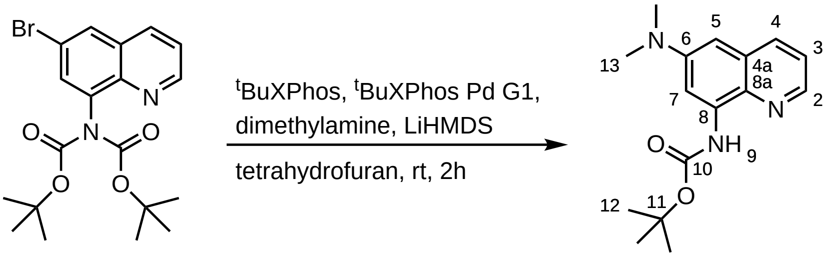

26 **27**

Tert-butyl (6-(dimethylamino)quinolin-8-yl)carbamate (27) was synthesized as described by the group of Buchwald.[102] In a round-bottom flask (10 mL) with silicone septum, the halide (**26**) (847 mg, 2.0 mmol, 1.0 equiv), the palladium precatalyst ^{t}BuXPhos Pd G1 (34 mg, 0.05 mmol, 0.025 equiv) and the ligand ^{t}BuXPhos (21 mg, 0.05 mmol, 0.025 equiv) were placed under inert atmosphere. Afterward, solutions of LiHMDS in tetrahydrofuran (1 M, 3.0 mL 3.0 mmol, 1.5 equiv) and dimethylamine in tetrahydrofuran (2 M, 1.5 mL 3.0 mmol, 1.5 equiv) were added. The reaction was stirred at room temperature for 2 h, before it was extracted with dichloromethane and washed with saturated aqueous ammonium chloride solution. After drying over sodium sulfate, the solvents were removed *in vacuo*, and the crude product was purified by flash column chromatography (silica, dichloromethane). A red solid was yielded (284 mg, 50%).

M($C_{16}H_{21}N_3O_2$) = 287.36 g mol^{-1}. **TLC** (dichloromethane): $R_f = 0.43$ (UV).
^{1}H NMR (400 MHz, CD_2Cl_2) δ 8.92 (s, 1H, NH), 8.45 (dd, J = 4.2, 1.6 Hz, 1H, H2), 8.15 (d, J = 2.7 Hz, 1H, H7), 7.91 (ddd, J = 8.3, 1.6, 0.4 Hz, 1H, H4), 7.28 (dd, J = 8.3, 4.2 Hz, 1H, H3), 6.45 (d, J = 2.7 Hz, 1H, H5), 3.08 (s, 6H, H13), 1.57 (s, 9H, H12). **^{13}C NMR** (101 MHz, CD_2Cl_2) δ 153.3 (C10), 149.8 (C6), 144.2 (C2), 136.1 (C8), 134.5 (C4), 133.4 (C8a), 130.3 (C4a), 122.5 (C3), 104.9 (C7), 98.3 (C5), 80.7 (C11), 41.0 (C13), 28.7 (C12). **IR** (Diamond-ATR, neat) $\tilde{\nu}_{\mathrm{max}}$: 3368 (w), 3053 (vw), 2976 (w), 2927 (w), 2805 (vw), 1718 (m), 1624 (m), 1588 (w), 1577 (w), 1524 (s), 1494 (m), 1464 (m), 1429 (m), 1365 (m), 1296 (m), 1248 (m), 1227 (m), 1149 (vs), 1118 (m), 1062 (w), 1039 (m), 1005 (m), 997 (m), 929 (w), 866 (m), 820 (m), 785 (m), 739 (w), 668 (m), 659 (w) cm^{-1}. **MS** (EI) *m/z* (relative intensity): 287 (35%) [$C_{16}H_{21}N_3O_2^+$], 214 (8%) [$C_{12}H_{12}N_3O^+$], 187 (100%) [$C_{11}H_{13}N_3^+$], 172 (18%) [$C_{11}H_{12}N_2^+$], 144 (11%) [$C_9H_8N_2^+$]. **HR-MS** (EI): calcd for [$C_{16}H_{21}N_3O_2^+$] 287.1629, found: 287.1628. **HR-MS** (EI): calcd for [$C_{15}{}^{13}CH_{21}N_3O_2^+$] 228.1663, found: 228.1663.

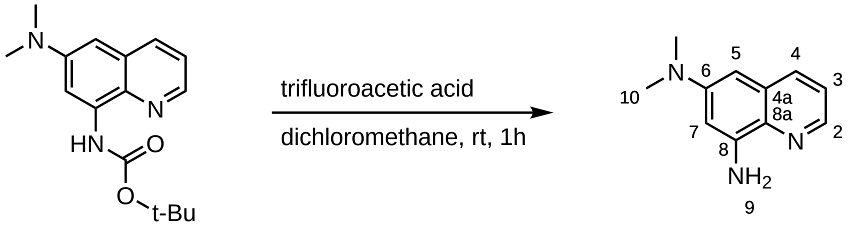

27 **21**

N^6,N^6-dimethylquinoline-6,8-diamine (21). The starting material **27** (287 mg, 1.0 mmol, 1.0 equiv) was added to a round bottom flask (25 mL) with dichloromethane (5 mL) and stirred at room temperature. Then trifluoroacetic acid (5 mL) was slowly added to the solution. Thereby, the yellow solution turned red and then orange. After one hour, the solution was diluted with water (5 mL) and dichloromethane (5 mL) and basified (pH 8) with aqueous sodium hydroxide (10%) under cooling. After separation, the organic phase was washed with half concentrated aqueous bicarbonate solution and the aqueous phase was extracted with dichloromethane. The combined organic phases were dried over sodium sulfate before the solvents were removed *in vacuo*. The yellow solid was received in quantitative yield and was used without any further purification.

M($C_{11}H_{13}N_3$) = 187.25 g mol^{-1}. **^{1}H NMR** (400 MHz, CD_2Cl_2) δ 8.42 (dd, J = 4.1, 1.6 Hz, 1H, H2), 7.85 (ddd, J = 8.3, 1.6, 0.4 Hz, 1H, H4), 7.23 (dd, J = 8.3, 4.1 Hz, 1H, H3), 6.59 (d, J = 2.6 Hz, 1H, H7), 6.25 (d, J = 2.6 Hz, 1H, H5), 4.84 (s, 2H, NH), 3.01 (s, 6H, H10). **^{13}C NMR** (101 MHz, CD_2Cl_2) δ 150.3 (C6), 145.0 (C8), 143.8 (C2), 134.4 (C4), 133.9 (C8a), 131.0 (C4a), 122.2 (C3), 100.1 (C7), 95.6 (C5), 41.0 (C10). **IR** (Diamond-

ATR, neat) $\tilde{\nu}_{max}$: 3469 (vw), 3357 (vw), 2959 (w), 2924 (w), 2903 (w), 2849 (w), 2801 (w), 1773 (vw), 1618 (s), 1585 (m), 1508 (s), 1432 (m), 1381 (m), 1303 (w), 1259 (m), 1218 (w), 1156 (m), 1119 (m), 1059 (vs), 986 (m), 911 (m), 868 (m), 801 (vs), 786 (vs), 752 (m), 724 (w), 694 (m) cm^{-1}. **MS** (EI) *m/z* (relative intensity): 187 (100%) [$C_{11}H_{13}N_3^+$], 172 (29%) [$C_{10}H_{10}N_3^+$], 158 (11%) [$C_9H_8N_3^+$], 144 (34%) [$C_9H_8N_2^+$], 117 (7%) [$C_7H_5N_2^+$], 93 (6%), 73 (3%). **HR-MS** (EI): calcd for [$C_{11}H_{13}N_3^+$] 187.1104, found: 187.1100.

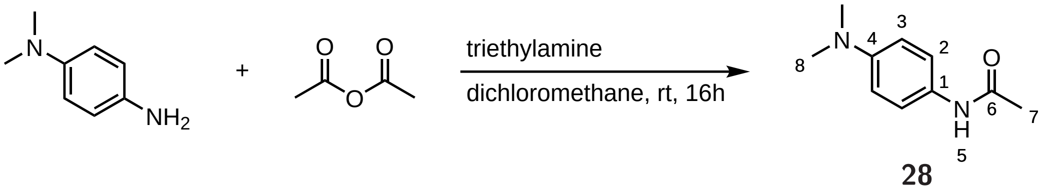

28

4-Acetamido-N^1,N^1-dimethylanilin (28). In a round bottom flask (1 L) with a room temperature water bath N^1,N^1-dimethyl-1,4-phenylenediamine (20.4 g, 150 mmol, 1.0 equiv) was dissolved in dichloromethane (500 mL) and acetic anhydride (17.0 mL, 180 mmol, 1.2 equiv) was added to the reaction mixture. Then, triethylamine (29.3 mL, 210 mmol, 1.4 equiv) was slowly dropped to the solution, which was held at room temperature. The reaction was left stirring for 16 h, before it was washed with water (4×300 mL). After the organic phase was dried over sodium sulfate, the solvents were removed *in vacuo*. The purple solid (22.7 g, 85% yield) was used without further purification.

M($C_{10}H_{14}N_2O$) = 178.24 g mol^{-1}. **^{1}H NMR** (400 MHz, CD_2Cl_2) δ 7.74 (br, 1H, H5), 7.31 (d, J = 8.1 Hz, 2H, H2), 6.67 (d, J = 9.0 Hz, 2H, H3), 2.90 (s, 6H, H8), 2.07 (s, 3H, H7). **^{13}C NMR** (101 MHz, CD_2Cl_2) δ 168.8 (C6), 148.6 (C4), 128.6 (C1), 122.5 (C2), 113.3 (C3), 41.2 (C8), 24.4 (C7). **IR** (Diamond-ATR, neat) $\tilde{\nu}_{max}$: 3307 (w), 3260 (w), 3228 (w), 3109 (w), 3048 (w), 2889 (w), 2801 (w), 1639 (s), 1617 (m), 1601 (m), 1517 (vs), 1442 (m), 1422 (m), 1410 (m), 1356 (m), 1320 (s), 1272 (m), 1225 (m), 1186 (m), 1169 (m), 1129 (w), 1065 (w), 1040 (w), 1016 (w), 1005 (w), 970 (w), 945 (m), 812 (vs), 753 (m), 707 (m), 668 (w), 660 (vw) cm^{-1}. **MS** (EI) *m/z* (relative intensity): 178 (100%) [$C_{10}H_{14}N_2O^+$], 136 (46%) [$C_8H_{12}N_2^+$], 135 (98%) [$C_8H_9NO^+$], 121 (16%) [$C_8H_{11}N^+$], 119 (7%). **HR-MS** (EI): calcd for [$C_{10}H_{14}N_2O^+$] 178.1101, found: 178.1099.

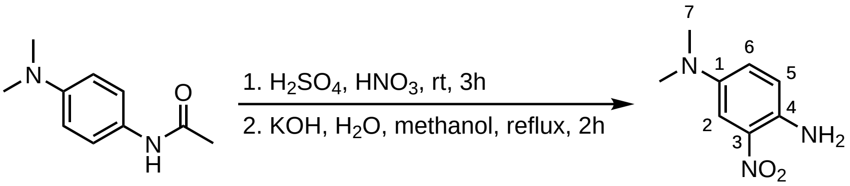

28 **30**

N^1,N^1-dimethyl-1,4-diamino-3-nitrobenzene (30). In a round bottom flask (100 mL) with stir bar, **28** (12.1 g, 67.7 mmol, 1.0 equiv) was dissolved in sulfuric acid (33.9 mL). After complete dissolution, the solution was cooled to 0 °C. In a separate round bottom flask (50 mL), sulfuric acid (10.8 mL) was cooled to 0 °C, before nitric acid (3.67 mL, 88.0 mmol, 1.3 equiv) was slowly added. During addition the temperature was kept below 10 °C. Afterwards, the nitrating acid was transferred into an addition funnel, before it was slowly added to the reaction mixture. During addition the temperature was kept below 10 °C. The reactions mixture was left stirring at 0 °C for 2 h, before it was warmed to room temperature. After one hour, the reaction mixture was purred into an Erlenmeyer flask (500 mL) filled with ice. The red solution was neutralized with concentrated aqueous sodium hydroxide solution and extracted with dichloromethane (3×400 mL). The solvent of the combined organic phases was removed *in vacuo*, before the solids were dissolved in a round bottom flask (250 mL) with stirbar and methanol (95 mL). A solution of aqueous potassium hydroxide (33.0 g in 23.6 mL water) was added and the reaction mixture was refluxed for 1 h. After concentrating under reduced pressure, the reaction mixture was diluted with water (200 mL) and extracted with dichloromethane (3×400 mL). After drying over sodium sulfate, the organic solvents were removed *in vacuo* and the crude product was purified by flash column chromatography (silica, dichloromethane). A dark red solid (9.2 g, 75% yield) was received.

M($C_8H_{11}N_3O_2$) = 181.20 g mol^{-1}. **TLC** (dichloromethane): $R_f = 0.22$ (red color, UV, ninhydrin) **^{1}H NMR** (400 MHz, $CDCl_3$) δ 7.37 (d, J = 2.9 Hz, 1H, H2), 7.05 (ddd, J = 9.1, 3.0, 0.8 Hz, 1H, H6), 6.75 (dd, J = 9.1, 0.4 Hz, 1H, H5), 5.73 (s, 2H, NH), 2.87 (s, 6H, H7). **^{13}C NMR** (101 MHz, $CDCl_3$) δ 143.1 (C1), 137.8 (C4), 132.6 (C3), 125.2 (C6), 119.9 (C5), 107.5 (C2), 41.6 (C7). **IR** (Diamond-ATR, neat) $\tilde{\nu}_{max}$: 3464 (m), 3334 (m), 3161 (w), 2874 (w), 2798 (w), 1898 (vw), 1637 (w), 1587 (m), 1558 (m), 1519 (vs), 1454 (m), 1438 (m), 1419 (s), 1401 (s), 1375 (m), 1335 (vs), 1247 (s), 1220 (vs), 1185 (s), 1160 (vs), 1093 (m), 1055 (m), 974 (m), 892 (m), 816 (s), 755 (s), 745 (m), 669 (m) cm^{-1}. **MS** (EI) m/z (relative intensity): 182 (9%) [$C_7{}^{13}CH_{11}N_3O_2{}^+$], 181 (100%) [$C_8H_{11}N_3O_2{}^+$], 147 (6%) [$C_8H_9N_3{}^+$], 135 (50%) [$C_8H_{11}N_2{}^+$], 119 (18%) [$C_8H_9N^+$], 105 (9%) [$C_7H_7N^+$], 42 (8%). **HR-MS** (EI): calcd for [$C_8H_{11}N_3O_2{}^+$] 181.0850, found: 181.0848.

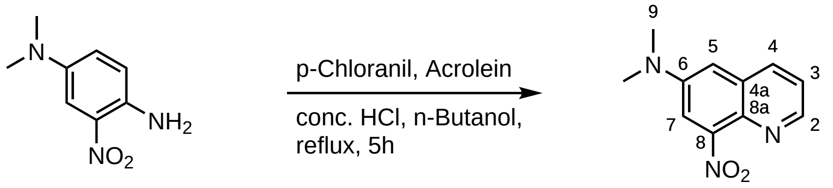

30 **25**

6-Dimethylamino-8-nitroquinoline (25) was synthesized analog to Wielgosz-Collin *et al.*[101] In a round bottom flask (100 mL) N^1,N^1-dimethyl-1,4-diamino-3-nitrobenzene (**30**) (3.62 g, 20 mmol, 1.0 equiv), p-chloranil (4.92 g, 20 mmol, 1.0 equiv), n-butanol (10 mL) and concentrated hydrochloric acid (5 mL) were heated to reflux. Then a solution of acrolein (90%, 2.23 mL, 1.5 equiv) in n-butanol (5 mL) was added over 2.5 h to the refluxing solution. After refluxing for 3 h the reaction was diluted with water (50 mL) and neutralized with aqueous concentrated sodium hydroxide solution. After extraction with dichloromethane (1 L) and washing with brine (700 mL), the organic phase was dried over sodium sulfate and the solvents were remove *in vacuo*. The crude product was purified by flash column chromatography (silica, dichloromethane) and yielded a yellow solid (1.1 g, 25%) containing minor impurities.

M($C_{11}H_{11}N_3O_2$) = 217.23 g mol^{-1}. **TLC** (dichloromethane): R_f = 0.15 (UV or CAM at rt: pink) **^{1}H NMR** (400 MHz, CD_2Cl_2) δ 8.67 (dd, *J* = 4.1, 1.6 Hz, 1H, H2), 8.02 (ddd, *J* = 8.4, 1.6, 0.5 Hz, 1H, H4), 7.59 (d, *J* = 2.8 Hz, 1H, H7), 7.37 (dd, *J* = 8.5, 4.1 Hz, 1H, H3), 6.95 (d, *J* = 2.9 Hz, 1H, H5), 3.10 (s, 6H, H9). **^{13}C NMR** (101 MHz, CD_2Cl_2) δ 149.4 (C8), 148.4 (C2), 147.5 (C6), 134.5 (C4), 133.4 (C8a), 131.1 (C4a), 123.4 (C3), 113.1 (C7), 108.5 (C5), 40.9 (C9). **IR** (Diamond-ATR, neat) $\tilde{\nu}_{max}$: 3084 (vw), 3053 (vw), 2990 (vw), 2918 (w), 2858 (w), 2817 (w), 2117 (vw), 1958 (vw), 1914 (vw), 1870 (vw), 1626 (m), 1591 (m), 1562 (m), 1521 (s), 1507 (s), 1456 (m), 1434 (m), 1418 (m), 1381 (m), 1352 (vs), 1309 (m), 1246 (m), 1205 (m), 1159 (m), 1125 (m), 1072 (m), 1038 (m), 991 (m), 937 (w), 897 (m), 875 (w), 867 (m), 836 (vs), 797 (m), 779 (vs), 755 (s), 710 (m) cm^{-1}. **MS** (EI) *m/z* (relative intensity): 218 (15%) [$C_{10}{}^{13}CH_{11}N_3O_2{}^+$], 217 (100%) [$C_{11}H_{11}N_3O_2{}^+$], 202 (19%) [$C_{10}H_8N_3O_2{}^+$], 171 (12%) [$C_{11}H_{11}N_2{}^+$], 170 (18%) [$C_{11}H_{10}N_2{}^+$], 156 (29%) [$C_{10}H_8N_2{}^+$], 130 (26%) [$C_9H_8N^+$], 116 (14%) [$C_8H_6N^+$], 77 (6%). **HR-MS** (EI): calcd for [$C_{11}H_{11}N_3O_2{}^+$] 217.0846, found: 217.0841.

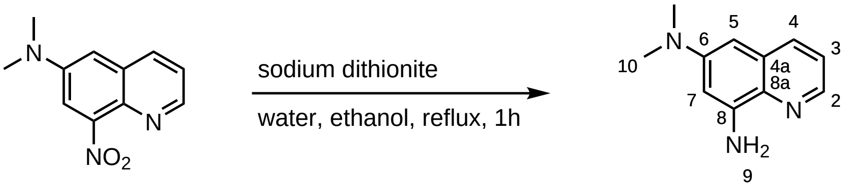

25 **21**

N^6,N^6-dimethylquinoline-6,8-diamine (21). In a round-bottom flask (250 mL) the nitroquinoline (**25**) (1.3 g, 6.0 mmol, 1.0 equiv) was dissolved in ethanol (75 mL). Then sodium dithionite (4.2 g, 24 mmol, 4.0 equiv) was dissolved in water (75 mL) and added to the reaction mixture. The solution was refluxed for one hour, before it was cooled to room temperature. After basifying with aqueous sodium hydroxide solution (1 M), the solution was extracted with dichloromethane and the organic phase was dried over sodium sulfate. After removal of the solvents *in vacuo*, a yellow solid was received in a quantitative yield and was used without further purification. This product is prone to oxidation. Therefore, the workup should be conducted without interruptions. The product should be stored under inert atmosphere at 4 °C or below.

M($C_{11}H_{13}N_3$) = 187.25 g mol^{-1}. **TLC** (3% methanol in dichloromethane): R_f = 0.28 (yellow color, UV, Ninhydrin or CAM) **^{1}H NMR** (400 MHz, CD_2Cl_2) δ 8.42 (dd, *J* = 4.1, 1.6 Hz, 1H, H2), 7.85 (ddd, *J* = 8.3, 1.6, 0.4 Hz, 1H, H4), 7.23 (dd, *J* = 8.3, 4.1 Hz, 1H, H3), 6.59 (d, *J* = 2.6 Hz, 1H, H7), 6.25 (d, *J* = 2.6 Hz, 1H, H5), 4.84 (br, 2H, NH), 3.01 (s, 6H, H10). **^{13}C NMR** (101 MHz, CD_2Cl_2) δ 150.3 (C6), 145.0 (C8), 143.8 (C2), 134.4 (C4), 133.9 (C8a), 131.0 (C4a), 122.2 (C3), 100.1 (C7), 95.6 (C5), 41.0 (C10). **IR** (Diamond-ATR, neat) $\tilde{\nu}_{max}$: 3469 (vw), 3357 (vw), 2959 (w), 2924 (w), 2903 (w), 2849 (w), 2801 (w), 1773 (vw), 1618 (s), 1585 (m), 1508 (s), 1432 (m), 1381 (m), 1303 (w), 1259 (m), 1218 (w), 1156 (m), 1119 (m), 1059 (vs), 986 (m), 911 (m), 868 (m), 801 (vs), 786 (vs), 752 (m), 724 (w), 694 (m) cm^{-1}. **MS** (EI) *m/z* (relative intensity): 187 (100%) [$C_{11}H_{13}N_3^+$], 172 (29%) [$C_{10}H_{10}N_3^+$], 158 (11%) [$C_9H_8N_3^+$], 144 (34%) [$C_9H_8N_2^+$], 117 (7%) [$C_7H_5N_2^+$], 93 (6%), 73 (3%). **HR-MS** (EI): calcd for [$C_{11}H_{13}N_3^+$] 187.1104, found: 187.1100.

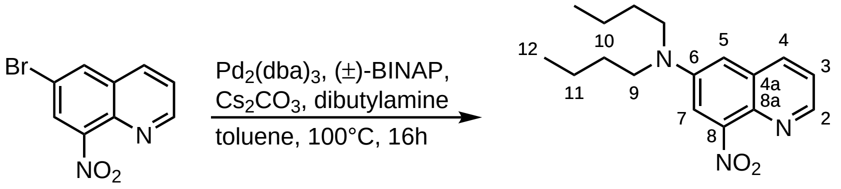

18 **32**

6-Dibutylamino-8-nitroquinoline (32). To a round-bottom flask (10 mL) with 6-bromo-8-nitroquinoline (**18**, 130 mg, 0.5 mmol, 1 equiv), cesium carbonate (230 mg, 0.7 mmol, 1.4 equiv), tris(dibenzylideneacetone)dipalladium(0) (14 mg, 0.015 mmol, 0.03 equiv) and 2,2'-bis(diphenylphosphino)-1,1'-binaphthalene (*rac*-BINAP, 28 mg, 0.045 mmol, 0.09 equiv) under inert atmosphere, degassed anhydrous toluene (5 mL) and dibutylamine (0.10 mL, 0.6 mmol, 1.2 equiv) were added. The reaction mixture was heated to 100 °C for 16 h. Afterwards, the solvents were removed *in vacuo* and the solids were purified by flash column chromatography (silica, dichloromethane). A yellow solid was received as product (yield: 110 mg, 78%)

M($C_{17}H_{23}N_3O_2$) = 301.39 g mol^{-1}. **TLC** (dichloromethane): $R_f = 0.25$ (UV or CAM at rt: pink) **^{1}H NMR** (400 MHz, $CDCl_3$) δ 8.69 (dd, J = 4.2, 1.6 Hz, 1H, H2), 7.94 (dd, J = 8.5, 1.6 Hz, 1H, H4), 7.55 (d, J = 2.8 Hz, 1H, H7), 7.32 (dd, J = 8.4, 4.1 Hz, 1H, H3), 6.84 (d, J = 2.9 Hz, 1H, H5), 3.38 (dd, J = 7.7 Hz, 4H, H9), 1.62 (tt, J = 9.0, 7.0 Hz, 4H, H10), 1.40 (h, J = 7.4 Hz, 4H, H11), 0.98 (t, J = 7.3 Hz, 6H, H12). **^{13}C NMR** (101 MHz, $CDCl_3$) δ 149.0 (C8), 147.9 (C2), 145.0 (C6), 134.0 (C4), 132.8 (C8a), 131.0 (C4a), 122.8 (C3), 113.2 (C7), 107.7 (C5), 51.1 (C9), 29.3 (C10), 20.4 (C11), 14.1 (C12). **IR** (Diamond-ATR, neat) $\tilde{\nu}_{max}$: 3076 (vw), 3042 (vw), 2957 (m), 2927 (m), 2893 (w), 2862 (w), 1974 (vw), 1875 (vw), 1777 (vw), 1624 (s), 1592 (w), 1527 (vs), 1501 (s), 1467 (m), 1440 (m), 1398 (m), 1354 (s), 1315 (w), 1284 (m), 1259 (w), 1228 (m), 1181 (m), 1153 (w), 1136 (m), 1109 (m), 1042 (w), 1018 (w), 988 (w), 948 (w), 895 (m), 873 (m), 840 (vs), 783 (m), 751 (m), 731 (w), 714 (m) cm^{-1}. **MS** (EI) *m/z* (relative intensity): 302 (5%) [$C_{16}{}^{13}CH_{23}N_3O_2^+$], 301 (26%) [$C_{17}H_{23}N_3O_2^+$], 259 (16%) [$C_{13}{}^{13}CH_{16}N_3O_2^+$], 258 (100%) [$C_{14}H_{16}N_3O_2^+$], 217 (5%) [$C_{10}{}^{13}CH_{10}N_3O_2^+$], 216 (39%) [$C_{11}H_{10}N_3O_2^+$], 202 (24%) [$C_{10}H_8N_3O_2^+$], 156 (14%) [$C_{10}H_8N_2^+$], 129 (3%). **HR-MS** (EI): calcd for [$C_{17}H_{23}N_3O_2^+$] 301.1785, found: 301.1784.

N^6,N^6-dibutylquinoline-6,8-diamine (33). In a round-bottom flask (250 mL) the nitroquinoline (**32**) (g, 6.0 mmol, 1.0 equiv) was dissolved in ethanol (75 mL). Then sodium dithionite

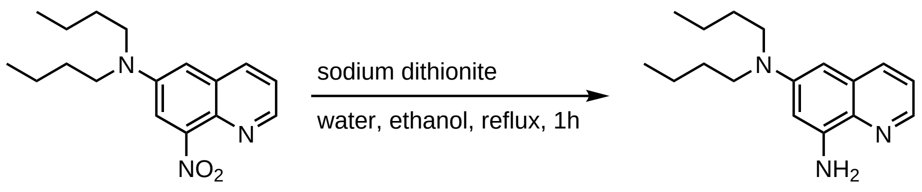

32 **33**

(4.2 g, 24 mmol, 4.0 equiv) was dissolved in water (75 mL) and added to the reaction mixture. The solution was refluxed for one hour, before it was cooled to room temperature. After basifying with aqueous sodium hydroxide solution (1 M, pH 9), the solution was extracted with dichloromethane and the organic phase was dried over sodium sulfate. After removal of the solvents *in vacuo*, a yellow solid was received in a quantitative yield and was used without further purification or analysis. This product is prone to oxidation. Therefore, the workup should be conducted without interruptions. The product should be stored under inert atmosphere at 4 °C or below.

M($C_{17}H_{25}N_3$) = 271.41 g mol^{-1}.

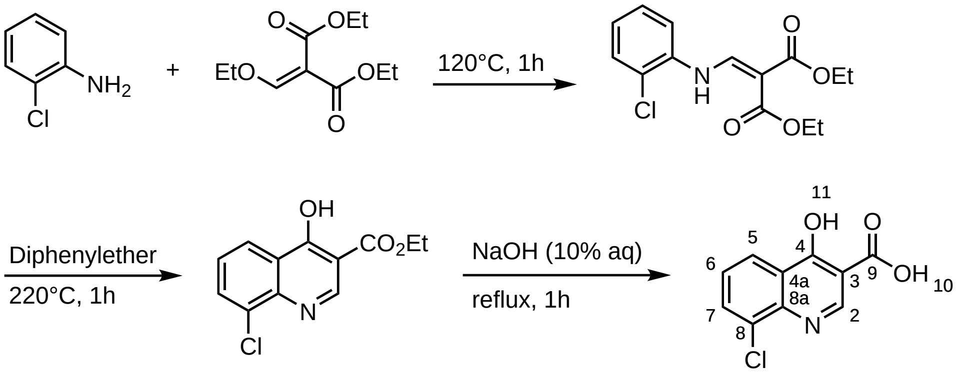

40

8-Chloro-4-hydroxyquinolin-3-carboxylic adic (40) was prepared as described by Price and Roberts[112,113]. 2-Chloroaniline (26.8 g, 22.1 mL, 210 mmol, 1.00 equiv) and diethyl ethoxymethylenemalonate (46.8 g, 43.3 mL, 216 mmol, 1.03 equiv) were combined in a round-bottom flask (500 mL) with a distillation head and cooler and heated to 120 °C until no more evolution of ethanol was observed. Afterward liquid diphenyl ether (140 mL) was added and the reaction was heated to 220 °C until no more evolution of ethanol was observed. Upon cooling, some product precipitated. Precipitation was completed by addition of iso-hexanes (140 mL) and cooling the reaction mixture to 4 °C in a fridge overnight. Afterward the solids were filtered and washed thoroughly with iso-hexanes. Then, the solids were placed in a round-bottom flask with distillation head and cooler and aqueous sodium hydroxide solution (10%, 210 mL, 2.5 equiv) was added. The slurry was heated until all iso-hexanes were removed and then refluxed until all solids were dissolved. The reaction mixture darkened and oily residues were removed by decanting. Then activated charcoal was added to the hot solution. After 15 min, the suspension was filtered hot and the filtrated was cooled to room temperature. Upon cooling, some product precipitated. Precipitation was completed by addition of conc. hydrochloric acid until a pH of 2 was reached. The liquids were removed by decanting and the solids were washed with water (5×150 mL) the same way. Acetonitrile was then added to the wet solids and the solvents were removed as an azeotrope under reduced pressure. If diphenyl ether was present in the final product, the dry solids were mixed with iso-hexanes, heated to reflux and decanted several times. The product was received as a white powder (42.1 g, 90%) with minor impurities.

M($C_{10}H_6NO_3Cl$) = 223.61 g mol^{-1}. **^{1}H NMR** (400 MHz, DMSO-d_6) δ 14.88 (s, 1H, H10), 12.91 (br, 1H, H, H11), 8.64 (s, 1H, C2), 8.24 (dd, J = 8.2, 1.3 Hz, 1H, C5), 8.06 (dd, J = 7.7, 1.4 Hz, 1H, C7), 7.58 (t, J = 7.9 Hz, 1H, C6). **^{13}C NMR** (101 MHz, DMSO-d_6) δ 178.0 (C9), 165.7 (C4), 145.7 (C2), 136.1 (C8a), 133.9 (C7), 126.4 (C4a), 126.1 (C6), 124.5 (C5), 123.1 (C8), 108.3 (C3). **IR** (Diamond-ATR, neat) $\tilde{\nu}_{\text{max}}$: 3444 (vw), 3065 (vw), 2802 (w), 1711 (m), 1670 (w), 1612 (m), 1576 (m), 1559 (m), 1541 (m), 1482 (m), 1439 (m), 1397 (w), 1342 (m), 1299 (w), 1277 (w), 1215 (m), 1168 (vw), 1136 (m), 1069 (w), 1037 (vw), 974 (w), 941 (w), 921 (w), 898 (w), 877 (w), 821 (w), 809 (m), 783 (vs), 750 (m), 690 (m) cm^{-1}. **MS** (EI) m/z (relative intensity): 225 (21%) [$C_{10}H_6NO_3{}^{37}Cl^+$], 223 (9%) [$C_{10}H_6NO_3{}^{35}Cl^+$], 206 (3%) [$C_{10}H_5NO_2{}^{35}Cl^+$], 181 (32%) [$C_9H_6NO^{37}Cl^+$], 179 (100%) [$C_9H_6NO^{35}Cl^+$], 153 (18%) [$C_8H_6N^{37}Cl^+$], 151 (54%) [$C_8H_6N^{35}Cl^+$], 127 (14%), 89 (10%,) 75 (7%), 63 (7%). **HR-MS** (EI): calcd for [$C_{10}H_6NO_3{}^{37}Cl^+$] 225.0006, found: 225.0007. **HR-MS** (EI): calcd for [$C_{10}H_6NO_3{}^{35}Cl^+$] 223.0030, found: 223.0036.

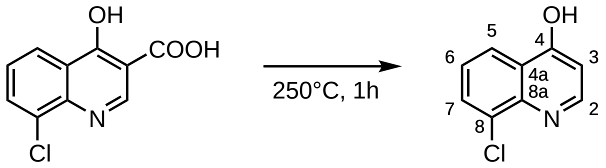

40 **41**

8-Chloroquinolin-4-ol (41) was prepared as described by Price and Roberts[112,113]. The carboxylic acid **40** (1.23 g, 5.5 mmol) was placed inside a sublimation apparatus equipped with a punctured balloon to minimize gas flow. Then the apparatus was slowly heated at atmospheric pressure to 250 °C. The white acid melted and turned black. The heating continued until white needles started to grow on the cooler and only a very small black residue was left at the bottom. The white solids were collected and yielded 0.95 g (96%) of pure product.

M(C_9H_6NOCl) = 179.60 g mol^{-1}. **^{1}H NMR** (400 MHz, DMSO-d_6) δ 11.37 (s, 1H, OH), 8.07 (dd, J = 8.1, 1.4 Hz, 1H, H7), 7.86 (dd, J = 7.4, 6.0 Hz, 1H, H2), 7.83 (dd, J = 7.6, 1.4 Hz, 1H, H5), 7.32 (t, J = 7.9 Hz, 1H, H6), 6.12 (dd, J = 7.5, 0.9 Hz, 1H, H3). **^{13}C NMR** (101 MHz, DMSO-d_6) δ 176.4 (C4), 140.0 (C2), 136.5 (C8a), 131.7 (C5), 127.1

(C4a), 124.4 (C6), 123.3 (C7), 121.5 (C8), 109.5 (C3). **IR** (Diamond-ATR, neat) $\tilde{\nu}_{max}$: 3080 (w), 3038 (w), 2930 (w), 2902 (w), 2817 (w), 1651 (w), 1601 (m), 1582 (m), 1546 (s), 1514 (vs), 1435 (s), 1400 (w), 1336 (s), 1308 (m), 1246 (m), 1217 (m), 1192 (s), 1115 (m), 1078 (m), 1059 (m), 967 (w), 891 (w), 850 (vw), 817 (m), 797 (vs), 790 (vs), 749 (s), 691 (w) cm^{-1}. **MS** (EI) *m/z* (relative intensity): 181 (32%) [$C_9H_6NO^{37}Cl^+$], 179 (100%) [$C_9H_6NO^{35}Cl^+$], 153 (27%) [$C_8H_6N^{37}Cl^+$], 151 (85%) [$C_8H_6N^{35}Cl^+$], 116 (12%), 89 (14%), 75 (12%), 63 (8%). **HR-MS** (EI): calcd for [$C_8{}^{13}CH_6NO^{37}Cl^+$] 182.0142, found: 182.0125. **HR-MS** (EI): calcd for [$C_9H_6NO^{37}Cl^+$] 181.0108, found: 181.0098. **HR-MS** (EI): calcd for [$C_8{}^{13}CH_6NO^{35}Cl^+$] 180.0172, found: 180.0147. **HR-MS** (EI): calcd for [$C_9H_6NO^{35}Cl^+$] 179.0138, found: 179.0132.

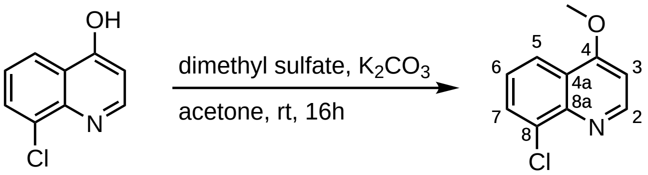

41 **42**

8-Chloro-4-methoxyquinoline (42). In a round-bottom flask (25 mL) 8-Chloroquinolin-4-ol (180 mg, 1 mmol, 1 equiv) and potassium carbonate (207 mg, 1.5 mmol, 1.5 equiv) were dissolved in acetone (10 mL) at room temperature. Then, dimethyl sulfate (0.095 mL, 126 mg, 1.0 mmol, 1 equiv) was added slowly under stirring. The reaction was allowed to stir for 16 h, before it was quenched by addition of conc. aqueous ammonia (1 mL, 25%) and left stirring for another 25 min. Then the reaction was extracted with dichloromethane (25 mL) and washed with water (3×15 mL) and brine (15 mL). The organic phases were combined and dried over sodium sulfate. After removal of the solvents *in vacuo*, the crude product was purified by flash column chromatography (silica, 3% methanol in dichloromethane) and a colorless solid was received (yield: 170 mg, 88%).

M($C_{10}H_8ClNO$) = 193.63 g mol^{-1}. **TLC** (3% methanol in dichloromethane): $R_f = 0.24$ (UV). **^{1}H NMR** (400 MHz, CD_2Cl_2) δ 8.83 (dd, J = 5.2, 0.9 Hz, 1H, H2), 8.14 (dt, J = 8.4, 1.4 Hz, 1H, H5), 7.81 (dt, J = 7.4, 1.0 Hz, 1H, H7), 7.41 (ddd, J = 8.4, 7.4, 0.9 Hz, 1H, H6), 6.83 (dd, J = 5.2, 1.4 Hz, 1H, H3), 4.05 (d, J = 1.1 Hz, 3H, H9). **^{13}C NMR** (101 MHz, CD_2Cl_2) δ 163.0 (C4), 152.5 (C2), 146.0 (C8a), 133.6 (C8), 130.4 (C7), 125.9 (C6), 123.4 (C4a), 121.5 (C5), 101.5 (C3), 56.6 (C9). **IR** (Diamond-ATR, neat) $\tilde{\nu}_{max}$: 3083 (vw), 3047 (vw), 3027 (w), 3002 (w), 2948 (w), 2917 (w), 2856 (vw), 2840 (vw), 2126 (vw), 1905 (vw), 1836 (vw), 1675 (vw), 1614 (w), 1591 (m), 1561 (m), 1500 (m), 1456 (m), 1444 (m), 1406 (m), 1380 (m), 1301 (s), 1273 (m), 1231 (m), 1208 (w), 1191 (w), 1155 (w), 1127 (m), 1085 (m), 1053 (w), 1011 (s), 970 (w), 916 (w), 854 (s), 821 (s), 805 (s), 793 (s), 754 (vs) cm^{-1}. **MS** (EI) *m/z* (relative intensity): 196 (3%) [$C_9{}^{13}CH_8NO^{37}Cl^+$], 195 (33%) [$C_{10}H_8NO^{37}Cl^+$], 194 (13%) [$C_9{}^{13}CH_8NO^{35}Cl^+$], 193 (100%) [$C_{10}H_8NO^{35}Cl^+$], 152 (10%) [$C_8H_5N^{37}Cl^+$], 150 (32%) [$C_8H_5N^{35}Cl^+$], 128 (11%) [$C_9H_6N^+$], 123 (10%) [$C_7H_4{}^{35}Cl^+$], 114 (5%) [$C_8H_4N^+$], 99 (6%) [$C_8H_3^+$], 75 (5%) [$C_6H_3^+$]. **HR-MS** (EI): calcd for [$C_9{}^{13}CH_8NO^{37}Cl^+$] 196.0293, found: 196.0294. **HR-MS** (EI): calcd for [$C_{10}H_8NO^{37}Cl^+$] 195.0260, found: 195.0274. **HR-MS** (EI): calcd for [$C_9{}^{13}CH_8NO^{35}Cl^+$] 194.0323, found: 194.0321. **HR-MS** (EI): calcd for [$C_{10}H_8NO^{35}Cl^+$] 193.0289, found: 193.0289.

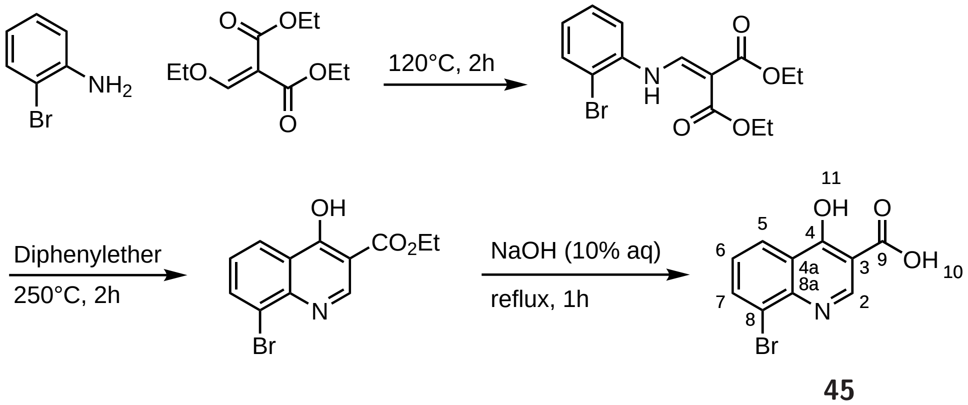

45

8-Bromo-4-hydroxyquinolin-3-carboxylic adic (45) was prepared as described by Price and Roberts[112,113]. 2-Bromoaniline (27.3 g, 18.0 mL, 161 mmol, 1.00 equiv) and diethyl ethoxymethylenemalonate (35.9 g, 33.2 mL, 165.8 mmol, 1.03 equiv) were combined in a round-bottom flask (500 mL) with a distillation head and cooler and heated to 120 °C until no more evolution of ethanol was observed. Afterwards liquid diphenyl ether (80 mL) was added and the reaction was heated to 250 °C until no more evolution of ethanol was observed. Upon cooling, some product precipitated. Precipitation was completed by addition of iso-hexanes (80 mL) and cooling the reaction mixture to 4 °C in a fridge overnight. Afterward the solids were filtered and washed thoroughly with iso-hexanes. Then, the solids were placed in a round-bottom flask with distillation head and cooler and aqueous sodium hydroxide solution (10%, 161 mL, 2.5 equiv) was added. The slurry was heated until all iso-hexanes were removed and then refluxed until all solids were dissolved. The reaction mixture darkened and oily residues were removed by decanting. Then, activated charcoal was added to the hot solution. After 15 min, the suspension was filtered hot and the filtrated was cooled to room temperature. Upon cooling, some product precipitated. Precipitation was completed by addition of conc. hydrochloric acid until a pH of 2 was reached. The liquids were removed by decanting and the solids were washed with water (5×80 mL) the same way. Acetonitrile was then added to the wet solids and the solvents were removed as an azeotrope under reduced pressure. If diphenyl ether was present in the final product, the dry solids were mixed with iso-hexanes, heated to reflux and decanted several times. The product was received as a white powder (34.5 g, 80%) with minor impurities.

M($C_{10}H_6NO_3Br$) = 268.07 g mol^{-1}. **^{1}H NMR** (400 MHz, DMSO-d_6) δ 14.89 (br, 1H, H11), 12.91 (s, 1H, H10), 8.72 (s, 1H, H2), 8.29 (dd, J = 8.1, 1.3 Hz, 1H, H5), 8.22 (dd, J = 7.7, 1.4 Hz, 1H, H7), 7.52 (t, J = 7.9 Hz, 1H, H6). **^{13}C NMR** (101 MHz, DMSO-d_6) δ 178.1 (C4), 165.8 (C9), 146.1 (C2), 137.5 (C7), 137.1 (C8a), 127.0 (C6), 126.2 (C8), 125.1 (C5), 112.8 (C4a), 108.2 (C3). **IR** (Diamond-ATR, neat) $\tilde{\nu}_{\text{max}}$: 3186 (w), 3061 (w), 1720 (m), 1672 (w), 1613 (m), 1549 (s), 1477 (s), 1435 (s), 1423 (m), 1389 (w), 1378 (m), 1337 (m), 1262 (m), 1206 (m), 1176 (m), 1155 (w), 1122 (m), 1063 (w), 1028 (vw), 978 (w), 954 (m), 937 (m), 890 (w), 835 (w), 796 (m), 772 (vs), 746 (m), 695 (w), 689 (vw), 676 (m), 667 (vw), 657 (vw) cm^{-1}. **MS** (HR-ESI) *m/z* (relative intensity): 267.9441 (100%) [$C_{10}H_5NO_3{}^{81}Br^+$], 265.9461 (100%) [$C_{10}H_5NO_3{}^{79}Br^+$], 223.9542 (24%) [$C_9H_5NO^{81}Br^+$], 221.9562 (22%) [$C_9H_5NO^{79}Br^+$].

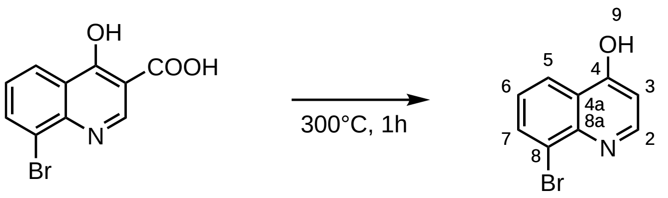

45 **46**

8-Bromoquinolin-4-ol (46) was prepared as described by Price and Roberts[112,113]. The carboxylic acid **45** (2.7 g, 10 mmol) was placed inside a sublimation apparatus equipped with a punctured balloon to minimize gas flow. Then the apparatus was slowly heated at atmospheric pressure to 300 °C. The white acid melted and turned black. The heating continued until white needles started to grow on the cooler and only a very small black residue was left at the bottom. The white solids were collected and yielded 2.0 g (90%) of product.

M(C_9H_6NOBr) = 224.06 g mol^{-1}. **^{1}H NMR** (400 MHz, DMSO-d_6) δ 11.12 (br, 1H, H9), 8.11 (dd, J = 8.1, 1.4 Hz, 1H, H5), 7.98 (dd, J = 7.6, 1.4 Hz, 1H, H7), 7.85 (dd, J = 7.5, 6.1 Hz, 1H, H2), 7.26 (dd, J = 7.8 Hz, 1H, H6), H, 6.12 (dd, J = 7.6, 1.1 Hz, 1H, H3). **^{13}C NMR** (101 MHz, DMSO-d_6) δ 176.4 (C4), 140.3 (C2), 137.6 (C8a), 135.2 (C7), 127.2 (C4a), 125.0 (C5), 123.9 (C6), 111.3 (C8), 109.4 (C3). **IR** (Diamond-ATR, neat) $\tilde{\nu}_{\text{max}}$: 2929 (br, m), 1644 (m), 1618 (m), 1601 (m), 1575 (m), 1543 (s), 1508 (vs), 1429 (s), 1395 (m), 1331 (s), 1304 (m), 1242 (m), 1214 (m), 1187 (s), 1155 (m), 1106 (m), 1072 (m), 1053 (m), 965 (w), 889 (w), 833 (vw), 787 (vs), 753 (s) cm^{-1}. **MS** (EI) *m/z* (relative intensity): 225 (93%) [$C_9H_6NO^{81}Br^+$], 223 (100%) [$C_9H_6NO^{79}Br^+$], 197 (43%) [$C_8H_6N^{81}Br^+$], 195 (44%) [$C_8H_6N^{79}Br^+$], 144 (7%) [$C_9H_6NO^+$], 116 (45%) [$C_8H_6N^+$], 89 (22%) [$C_6H_3N^+$], 63 (18%). **HR-MS** (EI): calcd for [$C_9H_6NO_{81}Br^+$] 224.9607, found: 224.9623. **HR-MS** (EI): calcd for [$C_9H_6NO_{79}Br^+$] 222.9627, found: 222.9631.

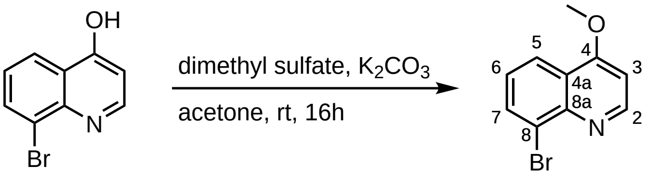

46 **47**

8-Bromo-4-methoxyquinoline (47). In a round-bottom flask (25 mL) 8-Bromoquinolin-4-ol (**46**) (224 mg, 1 mmol, 1 equiv) and potassium carbonate (207 mg, 1.5 mmol, 1.5 equiv) were dissolved in acetone (10 mL) at room temperature. Then, dimethyl sulfate (0.095 mL, 126 mg, 1.0 mmol, 1 equiv) was added slowly under stirring. The reaction was allowed to stir for 16 h, before it was quenched by addition of conc. aqueous ammonia (1 mL, 25%) and left stirring for another 25 min. Then the reaction was extracted with dichloromethane (25 mL) and washed with water (3×15 mL) and brine (15 mL). The organic phases were combined and dried over sodium sulfate. After removal of the solvents *in vacuo*, the crude product was purified by flash column chromatography (silica, 3% methanol in dichloromethane) and a colorless solid was received (yield: 570 mg, 75%).

M($C_{10}H_8NOBr$) = 238.08 g mol^{-1}. **TLC** (3% methanol in dichloromethane): $R_f = 0.64$ (UV). **TLC** (3% methanol in dichloromethane): $R_f = 0.21$ (UV, side product, carbonyl compound). **^{1}H NMR** (400 MHz, CD_2Cl_2) δ 8.80 (d, J = 5.2 Hz, 1H, H2), 8.16 (d, J = 8.3 Hz, 1H, H5), 8.01 (d, J = 7.5 Hz, 1H, H7), 7.33 (dd, J = 8.4, 7.4 Hz, 1H, H6), 6.79 (d, J = 5.3 Hz, 1H, H3), 4.03 (s, 3H, H9). **^{13}C NMR** (101 MHz, CD_2Cl_2) δ 162.9 (C4), 152.6 (C2), 146.6 (C8a), 133.9 (C7), 126.3 (C6), 124.9 (C8), 123.2 (C4a), 122.3 (C5), 101.4 (C3), 56.6 (C9). **IR** (Diamond-ATR, neat) $\tilde{\nu}_{\max}$: 3081 (vw), 3026 (w), 3000 (w), 2971 (vw), 2945 (vw), 2854 (vw), 2838 (vw), 1725 (vw), 1675 (vw), 1608 (w), 1590 (m), 1554 (m), 1520 (w), 1495 (s), 1459 (m), 1444 (m), 1422 (w), 1405 (m), 1381 (s), 1366 (m), 1299 (s), 1273 (m), 1241 (w), 1229 (m), 1191 (w), 1155 (w), 1120 (m), 1083 (m), 1051 (w), 1000 (s), 969 (w), 917 (vw), 902 (vw), 854 (m), 822 (m), 804 (s), 778 (s), 755 (vs), 669 (w), 661 (w) cm^{-1}. **MS** (EI) *m/z* (relative intensity): 240 (11%) $[C_9{}^{13}CH_8NO^{81}Br^+]$, 239 (93%) $[C_{10}H_8NO^{81}Br^+]$, 238 (14%) $[C_9{}^{13}CH_8NO^{79}Br^+]$, 237 (100%) $[C_{10}H_8NO^{79}Br^+]$, 218 (12%) $[C_{15}H_8NO^+]$, 195 (10%) $[C_8H_5N^{81}Br^+]$, 193 (12%) $[C_8H_5N^{79}Br^+]$, 158 (7%) $[C_{10}H_8NO^+]$,128 (15%) $[C_9H_6N^+]$, 115 (17%) $[C_8H_5N^+]$. **HR-MS** (EI): calcd for $[C_{10}H_8NO^{79}Br^+]$ 236.9784, found: 236.9784. **HR-MS** (EI): calcd for $[C_9{}^{13}CH_8NO^{79}Br^+]$ 237.9818, found: 237.9819. **HR-MS** (EI): calcd for $[C_{10}H_8NO^{81}Br^+]$ 238.9764, found: 238.9781. **HR-MS** (EI): calcd for $[C_9{}^{13}CH_8NO^{81}Br^+]$ 239.9797, found: 239.9820.

6.2.2. General synthesis of hybrid quinoline-guanidine ligands

In general, the syntheses of hybrid quinoline-guanidine ligands was based on the synthesis described by Hoffmann *et al.*[140,141] To a 250 ml Schlenk flask with absolute acetonitrile (100 mL) under inert atmosphere degassed, dry triethylamine (2 mL, 14 mmol, 1.4 equiv) and the respective amine (10 mmol, 1.0 equiv) were added. This was followed by slow addition of *N*,*N*,*N'*,*N'*-tetramethylchloroformamidinium chloride (**7**) (2.05 g, 12 mmol, 1.2 equiv) or *N*,*N*,*N'*,*N'*-dimethylethylenechloroformamidinium chloride (**9**) (2.03 g, 12 mmol, 1.2 equiv) in absolute acetonitrile (10 mL, 1.0 equiv) at room temperature. Then, the reaction mixture was refluxed at 83 °C for 6 hours. After completion, sodium hydroxide (4 g, 100 mmol, 10 equiv) in water (10 mL) was added and the reaction was left stirring for 10 min. After separation of the aqueous phase, all solvents were removed *in vacuo*. The residue was dissolved in aqueous acetic acid (5%, 10 mL) and washed with iso-hexanes (3×10 mL) before a 50% aqueous potassium hydroxide solution (5 mL) was added. Afterwards, the crude product was extracted with acetonitrile, dried over sodium sulfate and stirred with activated carbon (500 mg) for 15 min. The suspension was filtered over Celite®, then the solvent was removed. The obtained products were either distilled (oils) or sublimed (solids) at 160 °C under reduced pressure (below 0.5 mbar) by *kugelrohr* distillation apparatus for purification.

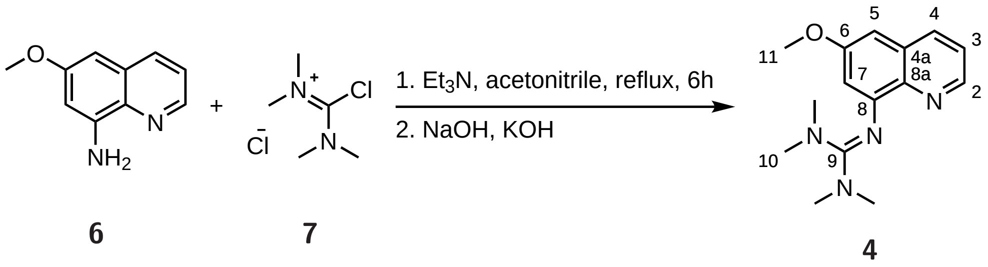

2-(6-Methoxyquinolin-8-yl)-1,1,3,3-tetramethylguanidine (4).
Appearance: yellow oil, 75% yield bp. 140 °C (3×10^{-2} mmHg). **M**($C_{15}H_{20}N_4O$) = 272.35 g mol^{-1}. **^{1}H NMR** (400 MHz, CD_2Cl_2) δ 8.57 (dd, J = 4.1, 1.7 Hz, 1H, H2), 7.95 (dd, J = 8.3, 1.7 Hz, 1H, H4), 7.24 (dd, J = 8.2, 4.1 Hz, 1H, H3), 6.62 (d, J = 2.8 Hz, 1H, H5), 6.57 (d, J = 2.7 Hz, 1H, H7), 3.87 (s, 3H, H11), 2.66 (s, 12H, H10). **^{13}C NMR** (101 MHz, CD_2Cl_2) δ 162.0 (C9), 159.2 (C6), 152.3 (C8), 146.3 (C2), 140.1 (C8a), 135.1 (C4), 130.6 (C4a), 121.5 (C3), 110.7 (C7), 97.7 (C5), 55.7 (C11), 39.8 (C10). **IR** (Diamond-ATR, neat) $\tilde{\nu}_{\text{max}}$: 2997 (w), 2930 (w), 2886 (w), 1581 (s), 1553 (s), 1506 (m), 1486 (s), 1460 (s), 1416 (m), 1374 (vs), 1338 (m), 1319 (m), 1273 (w), 1226 (m), 1198 (m), 1140 (vs), 1096 (m), 1061 (m), 1047 (m), 1029 (m), 1013 (s), 953 (m), 920 (m), 896 (m), 884 (w), 858 (m), 824 (m), 802 (m), 773 (m), 749 (m), 725 (m), 669 (m), 654 (m) cm^{-1}. **MS** (EI) m/z (relative intensity): 272 (100%) [$C_{15}H_{20}N_4O^+$], 228 (64%) [$C_{13}H_{14}NO^+$], 214 (33%) [$C_{12}H_{11}N_4{}^+$], 201 (39%), 187 (30%) [$C_{11}H_{11}N_2O^+$], 185 (34%) [$C_{11}H_{11}N_3{}^+$], 173 (13%) [$C_{10}H_9N_2O^+$], 172 (13%) [$C_{10}H_{10}N_3{}^+$], 170 (13%) [$C_{10}H_8N_3{}^+$], 159 (10%) [$C_{10}H_9NO^+$], 142 (12%) [$C_9H_6N_2{}^+$], 100 (16%). **HR-MS** (EI): calcd for [$C_{15}H_{20}N_4O^+$] 272.1637, found: 272.1633.

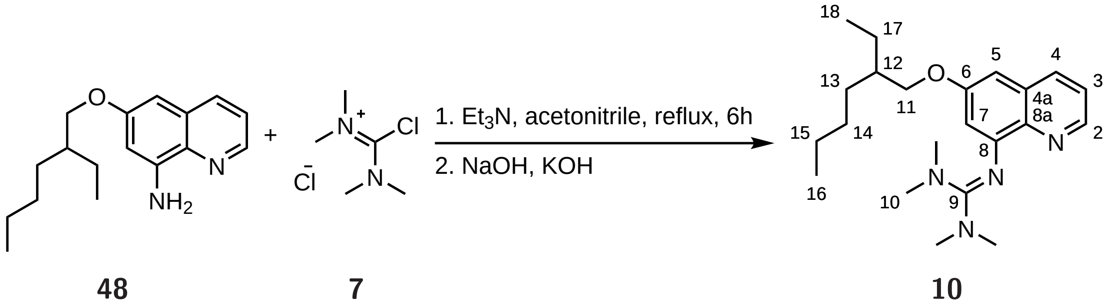

2-(6-((2-Ethylhexyl)oxy)quinolin-8-yl)-1,1,3,3-tetramethylguanidine (10). Appearance: yellow oil, 70% yield. **M**($C_{22}H_{34}N_4O$) = 370.54 g mol^{-1}. **^{1}H NMR** (400 MHz, $CDCl_3$) δ 8.66 (dd, J = 4.2, 1.7 Hz, 1H, H2), 7.90 (dd, J = 8.3, 1.7 Hz, 1H, H4), 7.22 (dd, J = 8.2, 4.2 Hz, 1H, H3), 6.61 (d, J = 2.7 Hz, 1H, H7), 6.54 (d, J = 2.6 Hz, 1H, H5), 3.92 (dd, J = 5.9, 0.8 Hz, 2H, H11), 2.72 (s, 12H, H10), 1.76 (hept, $J = 6.1$ Hz, 1H, H12), 1.63 – 1.35 (m, 4H, H13, H17), 1.39 – 1.27 (m, 4H, H14, H15), 0.98 – 0.85 (m, 6H, H16, H18). **^{13}C NMR** (101 MHz, $CDCl_3$) δ 161.7 (C9), 158.4 (C6), 151.5 (C8), 146.2 (C2), 139.9 (C8a), 134.7 (C4), 130.2 (C4a), 121.0 (C3), 110.8 (C7), 98.5 (C5), 70.8 (C11), 39.7 (C10), 39.5 (C12), 30.8 (C13), 29.2 (C14), 24.1 (C17), 23.2 (C15), 14.2 (C16), 11.3 (C18). **IR** (Diamond-ATR, neat) $\tilde{\nu}_{max}$: 2926 (m), 2866 (m), 2067 (vw), 1810 (vw), 1705 (vw), 1651 (w), 1586 (s), 1557 (s), 1505 (m), 1485 (m), 1455 (m), 1420 (m), 1375 (vs), 1336 (m), 1234 (w), 1197 (w), 1141 (vs), 1044 (m), 1012 (m), 922 (w), 861 (w), 820 (m), 800 (m), 772 (w), 740 (w), 675 (w) cm^{-1}. **MS** (EI) m/z (relative intensity): 370 (100%) $[C_{22}H_{34}N_4O^+]$, 369 (100%) $[C_{22}H_{33}N_4O^+]$, 326 (30%) $[C_{20}H_{28}N_3O^+]$, 299 (100%) $[C_{17}H_{23}N_4O^+]$, 285 (35%) $[C_{16}H_{21}N_4O^+]$, 214 (40%) $[C_{12}H_{12}N_3O^+]$, 200 (20%) $[C_{13}H_{14}NO^+]$, 171 (30%) $[C_{11}H_9NO^+]$, 100 (60%) $[C_5H_{14}N_2^+]$, 85 (10%) $[C_6H_{13}^+]$, 43 (35%) $[C_3H_7^+]$. **HR-MS** (ESI): calcd for $[C_{22}H_{35}N_4O^+]$ 371.2806, found: 371.2806. **HR-MS** (ESI): calcd for $[C_{21}{}^{13}CH_{35}N_4O^+]$ 372.2840, found: 372.2841.

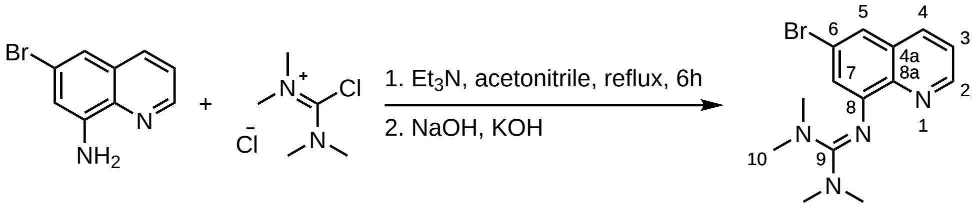

19 **7** **17**

2-(6-Bromoquinolin-8-yl)-1,1,3,3-tetramethylguanidine (17). Appearance: yellow oil, 75% yield. **M**($C_{14}H_{17}N_4Br$) = 321.22 g mol^{-1}. **^{1}H NMR** (400 MHz, CD_2Cl_2) δ 8.72 (dd, $J = 4.1$, 1.8 Hz, 1H, H2), 7.97 (dd, $J = 8.3$, 1.8 Hz, 1H, H4), 7.38 (d, $J = 2.2$ Hz, 1H, H5), 7.31 (dd, $J = 8.3$, 4.1 Hz, 1H, H3), 7.00 (d, $J = 2.2$ Hz, 1H, H7), 2.67 (s, 12H, H11). **^{13}C NMR** (101 MHz, CD_2Cl_2) δ 162.5 (C9), 152.8 (C8), 148.9 (C2), 142.0 (C8a), 135.4 (C4), 130.7 (C4a), 122.1 (C7), 122.0 (C3), 121.6 (C6), 120.2 (C5), 39.8 (C10). **IR** (Diamond-ATR, neat) $\tilde{\nu}_{max}$: 3012 (vw), 2926 (w), 2885 (w), 2792 (vw), 1574 (s), 1547 (vs), 1512 (m), 1477 (s), 1440 (m), 1423 (m), 1381 (s), 1356 (m), 1305 (w), 1234 (w), 1189 (vw), 1146 (m), 1096 (w), 1062 (vw), 1016 (m), 920 (vw), 900 (w), 842 (m), 805 (w), 775 (w), 746 (w), 690 (w), 673 (vw), 668 (vw), 655 (w) cm^{-1}. **MS** (EI) m/z (relative intensity): 322 (88%) $[C_{14}H_{17}N_4{}^{81}Br^+]$, 320 (90%) $[C_{14}H_{17}N_4{}^{79}Br^+]$, 307 (10%) $[C_{13}H_{14}N_4{}^{81}Br^+]$, 305 (10%) $[C_{13}H_{14}N_4{}^{79}Br^+]$, 278 (91%) $[C_{12}H_{11}N_3{}^{81}Br^+]$, 276 (93%) $[C_{12}H_{11}N_3{}^{79}Br^+]$, 264 (42%) $[C_{11}H_9N_3{}^{81}Br^+]$, 262 (59%) $[C_{11}H_9N_3{}^{79}Br^+]$, 251 (60%) $[C_{10}H_9N_3{}^{81}Br^+]$, 249 (62%) $[C_{10}H_9N_3{}^{79}Br^+]$, 237 (41%) $[C_{10}H_8N_2{}^{81}Br^+]$, 235 (100%) $[C_{10}H_8N_2{}^{79}Br^+]$, 233 (65%) $[C_{10}H_6N_2{}^{79}Br^+]$, $[C_{10}H_6N_2{}^{81}Br^+]$, 209 (26%) $[C_9H_6N^{81}Br^+]$, 207 (27%) $[C_9H_6N^{79}Br^+]$, 154 (34%) $[C_{10}H_6N_2^+]$, 127 (31%) $[C_9H_5N^+]$, 100 (93%) $[C_5H_{12}N_2^+]$, 85 (26%) $[C_4H_9N_2^+]$, 44 (32%) $[C_2H_6N^+]$. **HR-MS** (EI): calcd for $[C_{14}H_{17}N_4{}^{79}Br^+]$ 320.0632, found: 320.0630. **HR-MS** (EI): calcd for $[C_{13}{}^{13}CH_{17}N_4{}^{79}Br^+]$ 321.0665, found: 321.0572. **HR-MS** (EI): calcd for $[C_{14}H_{17}N_4{}^{81}Br^+]$ 322.0611, found: 322.0597.

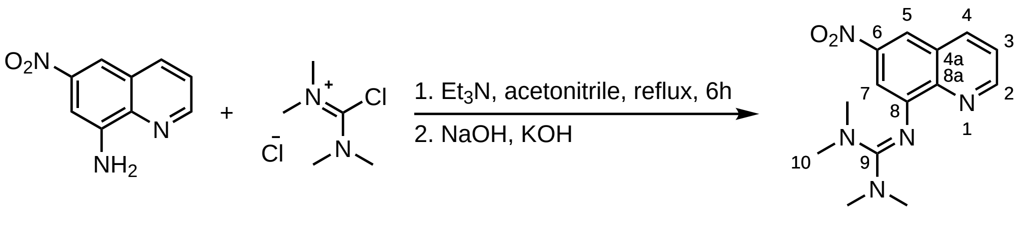

15 **7** **16**

2-(6-Nitroquinolin-8-yl)-1,1,3,3-tetramethylguanidine (16). Appearance: red powder, 65% yield. **M**($C_{14}H_{17}N_5O_2$) = 287.32 g mol^{-1}. **^{1}H NMR** (400 MHz, $CDCl_3$) δ 8.97 (ddd, J = 4.2, 1.8, 0.7 Hz, 1H, H2), 8.23 (dd, J = 8.3, 1.8 Hz, 1H, H4), 8.19 (d, J = 2.5 Hz, 1H, H5), 7.62 (d, J = 2.1 Hz, 1H, H7), 7.45 (dd, J = 8.3, 4.2 Hz, 1H, H3), 2.78 (s, 12H, H10). **^{13}C NMR** (101 MHz, $CDCl_3$) δ 162.7 (C9), 152.3 (C6), 151.6 (C2), 146.6 (C8), 145.1 (C8a), 138.0 (C4), 128.0 (C4a), 122.4 (C3), 113.9 (C5), 110.7 (C7), 39.7 (C10). **IR** (Diamond-ATR, neat) $\tilde{\nu}_{max}$: 2925 (br), 1578 (m), 1551 (s), 1514 (s), 1485 (m), 1468 (s), 1421 (s), 1404 (m), 1380 (s), 1366 (m), 1335 (vs), 1307 (s), 1235 (m), 1191 (w), 1177 (w), 1151 (s), 1076 (m), 1036 (w), 1019 (m), 984 (w), 948 (w), 918 (w), 889 (s), 811 (w), 793 (vs), 774 (m), 747 (s), 689 (s), 655 (m) cm^{-1}. **MS** (EI) m/z (relative intensity): 287 (100%) [$C_{14}H_{17}N_5O_2^+$], 272 (12%) [$C_{13}H_{14}N_5O^+$], 243 (74%) [$C_{12}H_{11}N_4O_2^+$], 229 (31%) [$C_{11}H_9N_4O_2^+$], 216 (43%) [$C_{10}H_8N_4O_2^+$], 202 (27%) [$C_{10}H_8N_3O_2^+$], 201 (30%) [$C_{10}H_7N_3O_2^+$], 197 (83%) [$C_{12}H_{11}N_3^+$], 183 (18%) [$C_{11}H_9N_3^+$], 182 (19) [$C_{11}H_8N_3^+$], 170 (11%) [$C_{10}H_8N_3^+$], 155 (12%) [$C_{10}H_7N_2^+$], 154 (14%) [$C_{10}H_6N_2^+$], 141 (24%) [$C_9H_5N_2^+$], 128 (15%) [$C_9H_6N^+$], 127 (15%) [$C_9H_5N^+$], 114 (9%) [$C_9H_6^+$], 100 (25%), 85 (15%) [$C_4H_9N_2^+$]. **HR-MS** (EI): calcd for [$C_{14}H_{17}N_5O_2^+$] 287.1382, found: 287.1382.

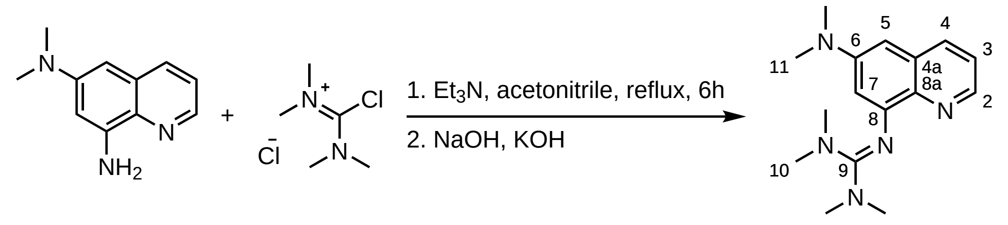

21 **7** **20**

2-(6-(Dimethylamino)quinolin-8-yl)-1,1,3,3-tetramethylguanidine (21). Appearance: red oil, 40% yield. **M**($C_{16}H_{23}N_5$) = 285.40 g mol^{-1}. **^{1}H NMR** (400 MHz, CD_2Cl_2) δ 8.43 (dd, J = 4.1, 1.7 Hz, 1H, H2), 7.85 (ddd, J = 8.2, 1.7, 0.4 Hz, 1H, H4), 7.15 (dd, J = 8.3, 4.1 Hz, 1H, H3), 6.64 (d, J = 2.8 Hz, 1H, H7), 6.39 (d, J = 2.8 Hz, 1H, H5), 3.02 (s, 6H, H11), 2.66 (s, 12H, H10). **^{13}C NMR** (101 MHz, CD_2Cl_2) δ 161.8 (C9), 151.1 (C8), 150.2 (C6), 144.7 (C2), 138.0 (C8a), 134.3 (C4), 131.1 (C4a), 121.4 (C3), 109.4 (C7), 98.3 (C5), 41.1 (C11), 39.7 (C10). **IR** (Diamond-ATR, neat) $\tilde{\nu}_{max}$: 2993 (vw), 2922 (w), 2867 (w), 2795 (w), 1577 (vs), 1552 (s), 1496 (m), 1478 (s), 1445 (m), 1419 (s), 1364 (vs), 1286 (m), 1227 (m), 1202 (m), 1138 (s), 1119 (m), 1059 (m), 1013 (m), 989 (s), 925 (w), 907 (w), 868 (w), 850 (w), 817 (m), 795 (m), 776 (m), 747 (w), 714 (w), 668 (w), 662 (w), 657 (w) cm^{-1}. **MS** (EI) *m/z* (relative intensity): 285 (100%) [$C_{16}H_{23}N_5^+$], 270 (7%) [$C_{15}H_{20}N_5^+$], 241 (62%) [$C_{14}H_{17}N_4^+$], 214 (65%) [$C_{12}H_{14}N_4^+$], 200 (49%) [$C_{12}H_{14}N_3^+$], 198 (24%) [$C_{12}H_{12}N_3^+$], 185 (22%) [$C_{11}H_{11}N_3^+$], 129 (6%) [$C_9H_7N^+$], 120 (31%), 100 (31%) [$C_5H_{12}N_2^+$], 99 (10%) [$C_5H_{11}N_2^+$]. **HR-MS** (EI): calcd for [$C_{15}{}^{13}CH_{23}N_5^+$] 286.1982, found: 286.1964 **HR-MS** (EI): calcd for [$C_{16}H_{23}N_5^+$] 285.1949, found: 285.1949.

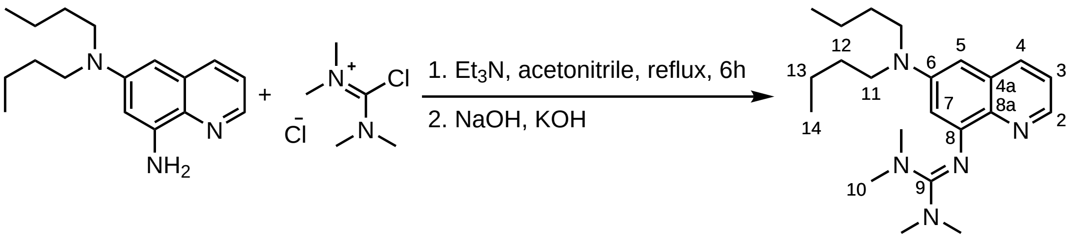

33 **7** **31**

2-(6-(Dibutylamino)quinolin-8-yl)-1,1,3,3-tetramethylguanidine (31). Appearance: yellow oil, 45% yield. **M**($C_{22}H_{35}N_5$) = 369.56 g mol^{-1}. **^{1}H NMR** (400 MHz, CD_2Cl_2) δ 8.37 (dd, J = 4.1, 1.7 Hz, 1H, H2), 7.79 (dd, J = 8.3, 1.7 Hz, 1H, H4), 7.11 (dd, J = 8.3, 4.1 Hz, 1H, H3), 6.58 (d, J = 2.8 Hz, 1H, H7), 6.31 (d, J = 2.8 Hz, 1H, H5), 3.42 – 3.30 (m, 4H, H11), 2.67 (s, 12H, H10), 1.63 (tt, J = 7.7, 6.5 Hz, 4H, H12), 1.39 (h, J = 7.4 Hz, 4H, H13), 0.97 (t, J = 7.3 Hz, 6H, H14). **^{13}C NMR** (101 MHz, CD_2Cl_2) δ 161.6 (C9), 151.0 (C8), 147.8 (C6), 144.1 (C2), 137.5 (C8a), 133.9 (C4), 131.4 (C4a), 121.3 (C3), 109.1 (C7), 97.5 (C5), 51.3 (C11), 39.8 (C10), 30.3 (C12), 21.0 (C13), 14.4 (C14). **IR** (Diamond-ATR, neat) $\tilde{\nu}_{\max}$: 2954 (w), 2926 (m), 2869 (m), 1578 (vs), 1552 (s), 1502 (m), 1478 (s), 1422 (m), 1366 (vs), 1276 (m), 1232 (m), 1214 (m), 1185 (m), 1139 (s), 1109 (m), 1060 (w), 1010 (m), 944 (w), 924 (w), 912 (vw), 851 (w), 815 (m), 795 (m), 777 (w), 750 (w), 719 (w), 674 (w), 667 (w) cm^{-1}. **MS** (EI) *m/z* (relative intensity): 370 (24%) [$^{13}CC_{21}H_{35}N_5^+$], 369 (100%) [$C_{22}H_{35}N_5^+$], 326 (26%) [$C_{19}H_{28}N_5^+$], 325 (26%) [$C_{19}H_{27}N_5^+$], 298 (90%) [$C_{17}H_{23}N_5^+$], 284 (44%) [$C_{16}H_{22}N_5^+$], 270 (26%) [$C_{15}H_{20}N_5^+$], 226 (12%) [$C_{13}H_{14}N_5^+$], 225 (40%) [$C_{13}H_{13}N_5^+$], 182 (21%) [$C_{10}H_6N_4^+$], 100 (44%) [$C_5H_{10}N_2^+$]. **HR-MS** (EI): calcd for [$C_{22}H_{35}N_5^+$] 369.2887, found: 369.2886.

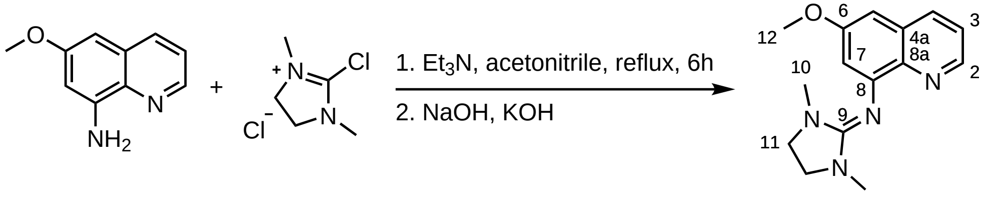

6 **9** **8**

***N*-(6-Methoxyquinolin-8-yl)-1,3-dimethylimidazolidin-2-imine (8).** Appearance: yellow solid, 75% yield. **M**($C_{15}H_{18}N_4O$) = 270.34 g mol^{-1}. **^{1}H NMR** (CD_2Cl_2 MHz, 400) δ 8.63 (dd, J = 4.1, 1.7 Hz, 1H, H2), 7.96 (ddd, J = 8.2, 1.8, 0.4 Hz, 1H, H4), 7.26 (dd, J =

8.2, 4.1 Hz, 1H, H3), 6.71 (d, $J = 2.8$ Hz, 1H, H7), 6.65 (d, $J = 2.8$ Hz, 1H, H5), 3.87 (s, 3H, H12), 3.31 (s, 4H, H11), 2.56 (s, 6H, H10). **^{13}C NMR** (CD_2Cl_2 MHz, 101) δ 158.8 (C6), 156.0 (C9), 150.7 (C8), 146.4 (C2), 140.7 (C8a), 135.1 (C4), 130.6 (C4a), 121.6 (C3), 111.5 (C7), 98.1 (C5), 55.8 (C12), 48.8 (C11), 34.9 (C10). **IR** (Diamond-ATR, neat) $\tilde{\nu}_{\text{max}}$: 3038 (vw), 2998 (w), 2957 (w), 2928 (w), 2871 (w), 1637 (vs), 1589 (vs), 1558 (s), 1505 (m), 1482 (s), 1457 (s), 1436 (s), 1409 (s), 1390 (s), 1368 (vw), 1336 (m), 1287 (s), 1250 (m), 1195 (m), 1157 (m), 1145 (vs), 1102 (m), 1056 (m), 1033 (vs), 973 (m), 952 (m), 897 (w), 862 (m), 836 (vs), 803 (s), 789 (m), 776 (m), 735 (m), 701 (s), 679 (w), 663 (vw) cm^{-1}. **MS** (EI) *m/z* (relative intensity): 270 (100%) [$C_{15}H_{18}N_4O^+$], 255 (8%) [$C_{14}H_{15}N_4O^+$], 213 (9%) [$C_{11}H_9N_4O^+$], 185 (14%) [$C_{11}H_9N_2O^+$], 159 (12%) [$C_{10}H_9NO^+$], 114 (4%) [$C_5H_{12}N_3{}^+$], 98 (37%) [$C_5H_{10}N_2{}^+$], 69 (4%) [$C_3H_5N_2{}^+$], 58 (10%) [$C_3H_8N^+$], 43 (19%) [$C_2H_5N^+$]. **HR-MS** (EI): calcd for [$C_{15}H_{18}N_4O^+$] 270.1476, found: 270.1475

6.2.3. Preparation of copper(I) halide salts

The copper(I) halide salts used in this work were prepared by reduction of $Cu^{II}SO_4 \cdot 5\,H_2O$ in presence of a respective halide salt. After synthesis and drying, the salts were stored in a dry glove box under inert atmosphere (nitrogen or argon gas).

CuBr. To a stirred solution of $CuSO_4 \cdot 5\,H_2O$ (30 g, 120 mmol, 1 equiv) in water (50 mL) sodium bromide (12.3 g, 120 mmol, 1 equiv) in water (40 mL) was added. The green solution was then discolored by addition of sodium metabisulfite (11.5 g, 60 mmol, 0.5 equiv) in water (100 mL). The resulting suspension was poured in a vigorously stirred solution of concentrated hydrobromic acid (4 mL, 48%) and sodium metabisulfite (1.8 g) in water (500 mL). Then the suspension was allowed to settle, before it was decanted. The precipitate was washed into a Schlenk-type glass filter frit and washed with diluted sulfuric acid (5 mL concentrated H_2SO_4 in 500 mL water) under inert atmosphere. Subsequently, the product was washed with absolute alcohol (3×60 mL) and anhydrous diethylether (6×60 mL). Finally, the product was dried under reduced pressure for 2 h. A white powder was received and used without further analysis.

CuCl. In a two-neck round-bottom flask (500 mL), $CuSO_4 \cdot 5\,H_2O$ (15 g, 60 mmol, 1 equiv) and sodium chloride (7.2 g, 123 mmol, 1.03 equiv) was dissolved in water (100 mL) and heated to 70 °C. Then, sulfur dioxide gas was passed through the solution for 30 min. After disappearance of the color, the suspension was cooled to room temperature and the remaining sulfur dioxide was removed with a nitrogen current. The colorless solid was filtered and washed with water (3×50 mL), glacial acetic acid (3×50 mL) and the with anhydrous diethyl ether (6×50 mL). The product was dried in a desiccator over P_4O_{10} under reduced pressure and was used without further purification.[142]

6.2.4. Titration of aqueous titanium(III) chloride solution

The titanium(III) chloride solution (16.3% $TiCl_3$ in hydrochloride acid (11%) according to the manufacturer's certificate of analysis) used for reduction reactions was titrated before first use or longer periods of storage. The solution was stored under inert atmosphere at a temperature of 4 °C. For determination of the accurate Ti^{3+} concentration, a stock solution of $[Fe(SCN)_6]^{3+}$ was prepared. Therefore, two aqueous solutions of $NH_4Fe(SO_4)_2$ (0.100 M, 1.00 mL) and KSCN (0.100 M, 9.0 mL) were combined to form the dark red iron complex. For each titration, an aliquot of the $TiCl_3$ solution (0.10 mL) was diluted with water (to 2 mL). Under vigorous stirring, the stock solution was added until a permanent red color remained.

6.3. Synthesis of Copper Complexes

In general, dried and degassed solvents were used for the syntheses of the complexes. Furthermore, all synthetic procedures were held within a glove box in an inert atmosphere and under exclusion of moisture.

General procedure: a solution of anhydrous copper(I) or copper (II) halide (0.1 mmol, 1.0 equiv) in acetonitrile (1 ml to 4 ml) and a solution of the ligand (0.2 mmol, 2.0 equiv) in acetonitrile (1 ml to 3 ml) were added to a 15 mL test tube. When $CuCl_2$ or DMEG6Methoxyqu was used, the resulting suspension was temporarily heated to complete dissolution. The test tube was placed in a 50 mL Schlenk-tube with antisolvent (toluene or diethylether). Red (Cu^I) or yellow (Cu^{II}) crystals precipitated between two days and six weeks. The crystals were washed with diethylether and dried by evaporation of the solvent. For characterization data, see below.

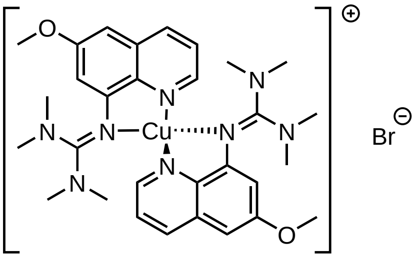

[Cu(TMG6Methoxyqu)$_2$]Br (**C1**). **M**($C_{30}H_{40}N_8O_2BrCu$) = 688.15 g mol^{-1}. **Crystal habit:** red block. **IR** (Diamond-ATR, neat) $\tilde{\nu}_{max}$: 3043 (vw, ν(C−H$_{arom.}$)), 2997 (vw, ν(C−H$_{arom.}$)), 2953 (vw, ν(C−H$_{aliph.}$)), 2930 (w, ν(C−H$_{aliph.}$)), 2900 (vw, ν(C−H$_{aliph.}$)), 2864 (w, ν(C−H$_{aliph.}$)), 2793 (vw, ν(C−H$_{aliph.}$)), 1603 (m, ν(N=C)), 1575 (m, ν(N=C)), 1520 (vs), 1489 (s), 1473 (m), 1463 (s), 1432 (m), 1421 (s), 1407 (s), 1386 (vs), 1338 (m), 1270 (w), 1232 (m), 1220 (m), 1201 (m), 1192 (m), 1156 (vs), 1141 (s), 1057 (w), 1036 (m), 1012 (n), 957 (w), 920 (w), 910 (w), 852 (m), 838 (m), 809 (w), 782 (m), 760 (w), 727 (w), 673 (m), 654 (w) cm^{-1}. **MS** (FAB+) *m/z*: 688 [$C_{30}H_{40}N_8O_2{}^{79}Br^{65}Cu^+$] [$C_{30}H_{40}N_8O_2{}^{81}Br^{63}Cu^+$], 609 [$C_{30}H_{40}N_8O_2{}^{65}Cu^+$], 607 [$C_{30}H_{40}N_8O_2{}^{63}Cu^+$], 416

[$C_{15}H_{20}N_4O^{79}Br^{65}Cu^+$] [$C_{15}H_{20}N_4O^{81}Br^{63}Cu^+$], 414 [$C_{15}H_{20}N_4O^{79}Br^{63}Cu^+$], 337 [$C_{15}H_{20}N_4O^{65}Cu^+$], 335 [$C_{15}H_{20}N_4O^{63}Cu^+$], 292 [$C_{13}H_{15}N_3O^{63}Cu^+$], 276 [$C_{12}H_{11}N_3O^{63}Cu^+$], 272 [$C_{15}H_{20}N_4O^+$], 263 [$C_{11}H_{10}N_3OCu^+$], 247 [$C_{11}H_8N_2OCu^+$], 228 [$C_{13}H_{14}N_3O^+$], 201 [$C_{11}H_{10}N_3O^+$], 185 [$C_{11}H_9N_2O^+$], 85 [$C_4H_9N_2{}^+$].

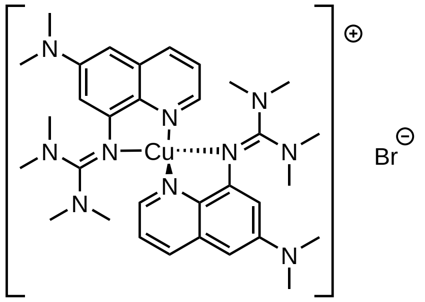

[Cu(TMG6dmaqu)$_2$]Br (**C2**). **M**($C_{32}H_{46}N_{10}BrCu$) = 714.24 g mol^{-1}. **Crystal habit:** red. **IR** (Diamond-ATR, neat) $\tilde{\nu}_{\text{max}}$: 2989 (vw), 2924 (w), 2863 (w), 2794 (w), 1598 (m), 1524 (vs), 1484 (s), 1469 (s), 1419 (s), 1404 (s), 1394 (s), 1372 (vs), 1332 (m), 1293 (m), 1273 (m), 1238 (m), 1209 (m), 1148 (m), 1128 (m), 1064 (m), 1016 (m), 997 (m), 934 (w), 912 (w), 869 (w), 846 (m), 826 (m), 815 (m), 808 (m), 778 (m), 724 (w), 667 (w), 663 (w), 657 (w) cm^{-1}. **MS** (FAB+) *m/z* (relative intensity): 635 (10%) [$C_{32}H_{46}N_{10}{}^{65}Cu^+$], 634 (8%) [$C_{31}{}^{13}CH_{46}N_{10}{}^{63}Cu^+$], 633 (20%) [$C_{32}H_{46}N_{10}{}^{63}Cu^+$], 515 (6%) [$C_{26}H_{28}N_8{}^{63}Cu^+$], 348 (20%) [$C_{16}H_{23}N_5{}^{63}Cu^+$], 286 (80%) [$C_{16}H_{24}N_5{}^+$], 241 (20%) [$C_{14}H_{17}N_4{}^+$]. **HR-MS** (FAB+): calcd for [$C_{32}H_{46}N_{10}{}^{63}Cu^+$] 633.3198, found: 633.3220. **HR-MS** (FAB+): calcd for [$C_{31}{}^{13}CH_{46}N_{10}{}^{63}Cu^+$] 634.3232, found: 634.3229. **HR-MS** (FAB+): calcd for [$C_{32}H_{46}N_{10}{}^{65}Cu^+$] 635.3180, found: 635.3265. **HR-MS** (FAB+): calcd for [$C_{31}{}^{13}CH_{46}N_{10}{}^{65}Cu^+$] 636.3213, found: 636.3281.

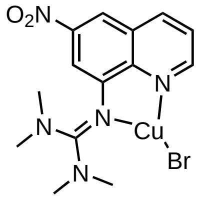

[Cu(TMG6Nitroqu)Br] (**C3**). **M**($C_{14}H_{17}N_5O_2BrCu$) = 430.77 g mol^{-1}. **Crystal habit:** orange platelet. **IR** (Diamond-ATR, neat) $\tilde{\nu}_{\text{max}}$: 2933 (vw, ν(C−H$_{\text{aliph.}}$)), 1604 (w, ν(N=C)), 1551 (m), 1520 (s), 1488 (s), 1462 (s), 1394 (vs), 1376 (s), 1339 (vs), 1264 (m), 1227 (m), 1191 (m), 1160 (m), 1142 (m), 1112 (m), 1079 (m), 1064 (m), 1053 (m), 1016 (m), 955 (w), 911 (w), 902 (w), 863 (m), 818 (w), 795 (s), 787 (s), 735 (m), 708 (m) cm^{-1}. **MS** (FAB+) *m/z* (relative intensity): 350 (50%) [$C_{14}H_{17}N_5O_2{}^{63}Cu^+$], 288 (100%) [$C_{14}H_{18}N_5O_2{}^+$], 243 (40%) [$C_{12}H_{11}N_4O_2{}^+$]. **HR-MS** (FAB+): calcd for [$C_{14}H_{17}N_5O_2{}^{63}Cu^+$] 350.0673, found: 350.0682. **HR-MS** (FAB+): calcd for [$C_{14}H_{17}N_5O_2{}^{65}Cu^+$] 352.0655, found: 352.0604.

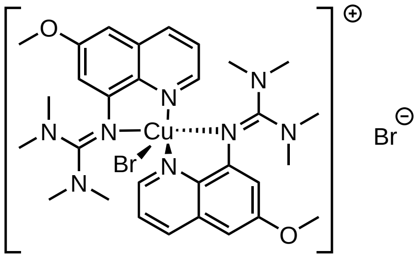

$[Cu(TMG6Methoxyqu)_2Br]Br$ (**C5**). **M**($C_{30}H_{40}N_8O_2Br_2Cu$) = 768.06 g mol^{-1}. **Crystal habit:** brown platelet. **IR** (Diamond-ATR, neat) $\tilde{\nu}_{max}$: 3050 (vw, ν(C−H$_{arom.}$)), 2998 (vw, ν(C−H$_{arom.}$)), 2957 (w, ν(C−H$_{aliph.}$)), 2934 (w, ν(C−H$_{aliph.}$)), 2869 (w, ν(C−H$_{aliph.}$)), 2795 (vw, ν(C−H$_{aliph.}$)), 1602 (m, ν(N=C)), 1574 (m, ν(N=C)), 1519 (s), 1492 (s), 1463 (s), 1420 (m), 1407 (s), 1379 (vs), 1343 (m), 1327 (m), 1309 (m), 1260 (m), 1229 (m), 1200 (m), 1158 (vs), 1144 (m), 1137 (m), 1103 (m), 1059 (m), 1036 (s), 1012 (s), 958 (w), 918 (vw), 906 (w), 842 (m), 824 (m), 799 (m), 784 (s), 732 (vw), 673 (m), 654 (w) cm^{-1}. **MS** (FAB+) *m/z*: 690 [$C_{30}H_{40}N_8O_2{}^{81}Br^{65}Cu^+$], 688 [$C_{30}H_{40}N_8O_2{}^{79}Br^{65}Cu^+$] [$C_{30}H_{40}N_8O_2{}^{81}Br^{63}Cu^+$], 686 [$C_{30}H_{40}N_8O_2{}^{79}Br^{63}Cu^+$], 609 [$C_{30}H_{40}N_8O_2{}^{65}Cu^+$], 607 [$C_{30}H_{40}N_8O_2{}^{63}Cu^+$], 418 [$C_{15}H_{20}N_4O^{81}Br^{65}Cu^+$], 416 [$C_{15}H_{20}N_4O^{79}Br^{65}Cu^+$] [$C_{15}H_{20}N_4O^{81}Br^{63}Cu^+$], 414 [$C_{15}H_{20}N_4O^{79}Br^{63}Cu^+$], 335 [[^{63}Cu(TMG6Methoxyqu)]$^+$], 273 [$C_{15}H_{21}N_4O^+$], 228 [$C_{13}H_{14}N_3O^+$], 201 [$C_{11}H_{10}N_3O^+$], 85 [$C_4H_9N_2^+$]. **HR-MS** (FAB+): calcd for [$C_{30}H_{40}N_8O_2{}^{81}Br^{65}Cu^+$] 690.1715, found: 690.1647. **HR-MS** (FAB+): calcd for [$C_{30}H_{40}N_8O_2{}^{79}Br^{65}Cu^+$] 688.1735, found: 688.1759. **HR-MS** (FAB+): calcd for [$C_{30}H_{40}N_8O_2{}^{81}Br^{63}Cu^+$] 688.1733, found: 688.1759. **HR-MS** (FAB+): calcd for [$C_{30}H_{40}N_8O_2{}^{79}Br^{63}Cu^+$] 686.1754, found: 686.1759.

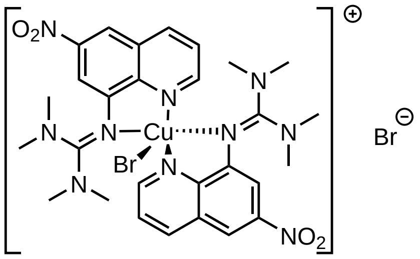

$[Cu(TMG6Nitroqu)_2Br]Br$ (**C7**). **M**($C_{28}H_{34}N_{10}O_4Br_2Cu$) = 798.00 g mol^{-1}. **Crystal habit:** brown block. **IR** (Diamond-ATR, neat) $\tilde{\nu}_{max}$: 3070 (vw, ν(C−H$_{arom.}$)), 2924 (vw, ν(C−H$_{aliph.}$)), 2797 (vw, ν(C−H$_{aliph.}$)), 1605 (w, ν(N=C)), 1574 (m, ν(N=C)), 1537 (m), 1532 (m), 1517 (m), 1493 (vs), 1468 (m), 1454 (m), 1418 (m), 1396 (vs), 1377 (vs), 1346 (vs), 1326 (s), 1268 (m), 1228 (m), 1196 (w), 1166 (m), 1142 (m), 1119 (m), 1086 (m), 1066 (m), 1022 (m), 964 (vw), 911 (w), 867 (m), 833 (m), 809 (w), 797 (m), 790 (m), 764 (w), 738 (m), 720 (m) cm^{-1}. **MS** (FAB+) *m/z* (relative intensity): 718 (2%) [$C_{28}H_{34}N_{10}O_4{}^{79}Br^{65}Cu^+$] [$C_{28}H_{34}N_{10}O_4{}^{81}Br^{63}Cu^+$] , 637 (4%) [$C_{28}H_{34}N_{10}O_4{}^{63}Cu^+$], 431 (4%) [$C_{14}H_{18}N_5O_2{}^{79}Br^{65}Cu^+$] [$C_{14}H_{18}N_5O_2{}^{81}Br^{63}Cu^+$], 350 (14%) [$C_{14}H_{18}N_5O_2{}^{63}Cu^+$], 288 (100%) [$C_{14}H_{18}N_5O_2^+$], 243 (25%) [$C_{12}H_{11}N_4O_2^+$]. **HR-MS** (FAB+): calcd for [$C_{28}H_{34}N_{10}O_4{}^{79}Br^{63}Cu^+$] 716.1239, found: 716.1185. **HR-MS** (FAB+): calcd for

$[C_{27}{}^{13}CH_{34}N_{10}O_4{}^{79}Br^{63}Cu^+]$ 717.1273, found: 717.1306. **HR-MS** (FAB+): calcd for $[C_{28}H_{34}N_{10}O_4{}^{81}Br^{63}Cu^+]$ 718.1219, found: 718.1213. **HR-MS** (FAB+): calcd for $[C_{28}H_{34}N_{10}O_4{}^{79}Br^{65}Cu^+]$ 718.1221, found: 718.1213. **HR-MS** (FAB+): calcd for $[C_{27}{}^{13}CH_{34}N_{10}O_4{}^{81}Br^{63}Cu^+]$ 719.1252, found: 719.1270. **HR-MS** (FAB+): calcd for $[C_{27}{}^{13}CH_{34}N_{10}O_4{}^{79}Br^{65}Cu^+]$ 719.1255, found: 719.1270. **HR-MS** (FAB+): calcd for $[C_{28}H_{34}N_{10}O_4{}^{81}Br^{65}Cu^+]$ 720.1201, found: 720.1118. **HR-MS** (FAB+): calcd for $[C_{27}{}^{13}CH_{34}N_{10}O_4{}^{81}Br^{65}Cu^+]$ 721.1234, found: 721.1476.

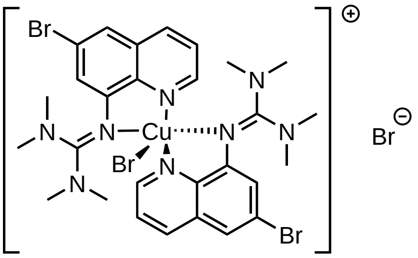

[Cu(TMG6Brqu)$_2$Br]Br (**C8**). **M**($C_{28}H_{34}N_8Br_4Cu$) = 865.80 g mol^{-1}. **Crystal habit:** orange platelet. **IR** (Diamond-ATR, neat) $\tilde{\nu}_{max}$: 3365 (vw), 3058 (vw, ν(C−H$_{arom.}$)), 2923 (w, ν(C−H$_{aliph.}$)), 2869 (w, ν(C−H$_{aliph.}$)), 1567 (m, ν(N=C)), 1514 (m), 1488 (s), 1466 (s), 1450 (m), 1420 (s), 1410 (m), 1393 (vs), 1372 (vs), 1324 (s), 1269 (m), 1219 (m), 1194 (m), 1165 (m), 1137 (m), 1116 (m), 1088 (w), 1066 (m), 1020 (m), 963 (w), 932 (w), 904 (w), 844 (s), 826 (m), 785 (m), 762 (m), 742 (w), 734 (w), 714 (m), 693 (w), 680 (vw), 668 (w), 661 (vw), 653 (vw) cm^{-1}. **MS** (FAB+) *m/z* (relative intensity): 786 (2%) $[C_{28}H_{34}N_8Br_3Cu^+]$, 705 (4%) $[C_{28}H_{34}N_8{}^{79}Br_2{}^{65}Cu^+]$ $[C_{28}H_{34}N_8{}^{79}Br^{81}Br^{63}Cu^+]$, 385 (22%) $[C_{14}H_{17}N_4{}^{79}Br^{65}Cu^+]$ $[C_{14}H_{17}N_4{}^{81}Br^{63}Cu^+]$, 383 (16%) $[C_{14}H_{17}N_4{}^{79}Br^{63}Cu^+]$, 323 (90%) $[C_{11}H_{18}N_4{}^{81}Br^+]$, 321 (100%) $[C_{11}H_{18}N_4{}^{79}Br^+]$, 278 (32%) $[C_{12}H_{11}N_3{}^{81}Br^+]$, 276 (30%) $[C_{12}H_{11}N_3{}^{79}Br^+]$. **HR-MS** (FAB+): calcd for $[C_{28}H_{34}N_8{}^{79}Br_3{}^{63}Cu^+]$ 781.9748, found: 782.0119. **HR-MS** (FAB+): calcd for $[C_{28}H_{34}N_8{}^{79}Br_2{}^{81}Br^{63}Cu^+]$ 783.9727, found: 783.9685. **HR-MS** (FAB+): calcd for $[C_{28}H_{34}N_8{}^{79}Br^{65}Cu^+]$ 783.9729, found: 783.9685. **HR-MS** (FAB+): calcd for $[C_{28}H_{34}N_8{}^{79}Br^{81}Br_2{}^{63}Cu^+]$ 785.9707, found: 785.9719. **HR-MS** (FAB+): calcd for $[C_{28}H_{34}N_8{}^{79}Br_2{}^{81}Br^{65}Cu^+]$ 785.9709, found: 785.9719. **HR-MS** (FAB+): calcd for $[C_{28}H_{34}N_8{}^{81}Br_3{}^{63}Cu^+]$ 787.9686, found: 787.9738. **HR-MS** (FAB+): calcd for $[C_{28}H_{34}N_8{}^{79}Br^{81}Br_2{}^{65}Cu^+]$ 787.9689, found: 787.9738. **HR-MS** (FAB+): calcd for $[C_{28}H_{34}N_8{}^{81}Br^{65}Cu^+]$ 789.9668, found: 789.9732.

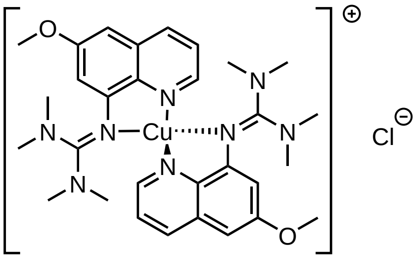

[Cu(TMG6Methoxyqu)$_2$]Cl (**C9**). **M**($C_{30}H_{40}N_8O_2ClCu$) = 643.70 g mol^{-1}. **Crystal habit:**

red block. **IR** (Diamond-ATR, neat) $\tilde{\nu}_{max}$: 3077 (vw, ν(C−H$_{arom.}$)), 3003 (vw, ν(C−H$_{arom.}$)), 2929 (w, ν(C−H$_{aliph.}$)), 2866 (w, ν(C−H$_{aliph.}$)), 2793 (vw, ν(C−H$_{aliph.}$)), 1601 (m, ν(N=C)), 1572 (m, ν(N=C)), 1520 (s), 1489 (m), 1466 (s), 1419 (m), 1405 (s), 1379 (vs), 1339 (m), 1275 (w), 1227 (m), 1210 (m), 1160 (s), 1063 (w), 1052 (m), 1033 (m), 1012 (m), 957 (w), 920 (w), 909 (w), 844 (m), 812 (w), 784 (m), 730 (w), 674 (m), 652 (w) cm^{-1}. **MS** (FAB+) *m/z*: 644 [$C_{30}H_{40}N_8O_2{}^{37}Cl^{63}Cu^+$] [$C_{30}H_{40}N_8O_2{}^{35}Cl^{65}Cu^+$], 642 [$C_{30}H_{40}N_8O_2{}^{35}Cl^{63}Cu^+$], 609 [$C_{30}H_{40}N_8O_2{}^{65}Cu^+$], 607 [$C_{30}H_{40}N_8O_2{}^{63}Cu^+$], 372 [$C_{15}H_{20}N_4O^{37}Cl^{63}Cu^+$] [$C_{15}H_{20}N_4O^{35}Cl^{65}Cu^+$], 370 [$C_{15}H_{20}N_4O^{35}Cl^{63}Cu^+$], 337 [$C_{15}H_{20}N_4O^{65}Cu^+$], 335 [$C_{15}H_{20}N_4O^{63}Cu^+$], 292 [$C_{13}H_{15}N_3O^{63}Cu^+$], 273 [$C_{15}H_{20}N_4O^+$], 247 [$C_{11}H_8N_2OCu^+$], 228 [$C_{13}H_{14}N_3O^+$], 201 [$C_{11}H_{10}N_3O^+$], 185 [$C_{11}H_9N_2O^+$], 100 [$C_5H_{12}N_2{}^+$], 85 [$C_4H_9N_2{}^+$], 73 [$C_3H_9N_2{}^+$], 44 [$C_2H_6N^+$].

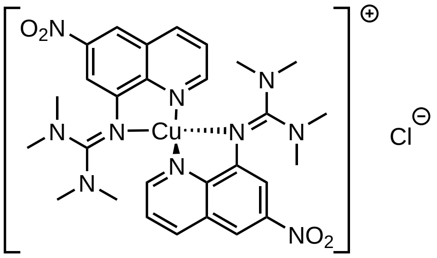

[Cu(TMG6Nitroqu)$_2$]CuCl$_2$ (**C10**). **M**($C_{28}H_{34}N_{10}O_4ClCu$) = 673.64 g mol^{-1}. **Crystal habit:** black block. **IR** (Diamond-ATR, neat) $\tilde{\nu}_{max}$: 3056 (vw, ν(C−H$_{arom.}$)), 2941 (vw, ν(C−H$_{aliph.}$)), 2869 (vw, ν(C−H$_{aliph.}$)), 2794 (vw, ν(C−H$_{aliph.}$)), 1602 (w, ν(N=C)), 1519 (s), 1487 (vs), 1471 (s), 1451 (s), 1395 (vs), 1376 (vs), 1343 (vs), 1270 (m), 1236 (m), 1196 (w), 1158 (m), 1139 (m), 1113 (m), 1084 (m), 1069 (w), 1018 (m), 957 (vw), 917 (w), 904 (w), 884 (m), 863 (w), 820 (w), 797 (s), 786 (s), 740 (m), 712 (w), 668 (w), 652 (w) cm^{-1}. **MS** (FAB+) *m/z* (relative intensity): 638 (33%) [$C_{28}H_{34}N_{10}O_4{}^{63}Cu^+$], 385 (25%) [$C_{14}H_{17}N_5O_2{}^{35}Cl^{63}Cu^+$], 350 (100%) [$C_{14}H_{17}N_5O_2{}^{63}Cu^+$], 243 (40%) [$C_{12}H_{11}N_4O_2{}^+$].
HR-MS (FAB+): calcd for [$C_{28}H_{34}N_{10}O_4{}^{63}Cu^+$] 637.2056, found: 637.2035.
HR-MS (FAB+): calcd for [$C_{27}{}^{13}CH_{34}N_{10}O_4{}^{63}Cu^+$] 638.2089, found: 638.1934.
HR-MS (FAB+): calcd for [$C_{28}H_{34}N_{10}O_4{}^{65}Cu^+$] 639.2038, found: 639.1840.
HR-MS (FAB+): calcd for [$C_{27}{}^{13}CH_{34}N_{10}O_4{}^{65}Cu^+$] 640.2071, found: 640.1882.

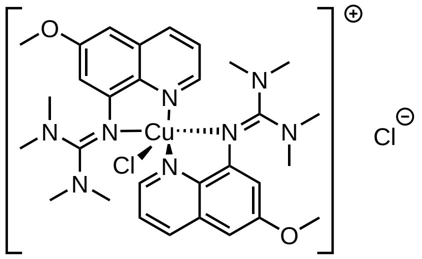

[Cu(TMG6Methoxyqu)$_2$Cl]Cl (**C11**). **M**($C_{30}H_{40}N_8O_2Cl_2Cu$) = 679.15 g mol^{-1}. **Crystal habit:** yellow block. **IR** (Diamond-ATR, neat) $\tilde{\nu}_{max}$: 3072 (vw, ν(C−H$_{arom.}$)), 3003 (vw, ν(C−H$_{arom.}$)), 2961 (w, ν(C−H$_{aliph.}$)), 2872 (vw, ν(C−H$_{aliph.}$)), 1601 (m, ν(N=C)), 1561 (m, ν(N=C)), 1515 (m), 1497 (s), 1466 (m), 1420 (m), 1394 (vs), 1377 (vs), 1340 (m), 1316 (m), 1260 (m), 1228 (m), 1214 (m), 1201 (m), 1159 (s), 1092 (s), 1058 (s), 1035 (vs), 1015 (vs), 927 (vw), 906 (w), 848 (m), 832 (m), 821 (m), 799 (s), 786 (s), 766 (m), 73 (w), 700 (vw), 673 (m) cm^{-1}. **MS** (FAB+) *m/z*: 644 [$C_{30}H_{40}N_8O_2{}^{35}Cl^{65}Cu^+$] [$C_{30}H_{40}N_8O_2{}^{37}Cl^{63}Cu^+$], 642 [$C_{30}H_{40}N_8O_2{}^{35}Cl^{63}Cu^+$], 609 [$C_{30}H_{40}N_8O_2{}^{65}Cu^+$], 607 [$C_{30}H_{40}N_8O_2{}^{63}Cu^+$], 372 [$C_{15}H_{20}N_4O^{35}Cl^{65}Cu^+$] [$C_{15}H_{20}N_4O^{37}Cl^{63}Cu^+$], 370 [$C_{15}H_{20}N_4O^{35}Cl^{63}Cu^+$], 337 [$C_{15}H_{20}N_4O^{65}Cu^+$], 335 [$C_{15}H_{20}N_4O^{63}Cu^+$], 292 [$C_{13}H_{15}N_3O^{63}Cu^+$], 273 [$C_{15}H_{21}N_4O^+$], 247 [$C_{11}H_8N_2OCu^+$], 228 [$C_{13}H_{14}N_3O^+$], 201 [$C_{11}H_{10}N_3O^+$], 185 [$C_{11}H_9N_2O^+$], 85 [$C_4H_9N_2{}^+$], 73 [$C_3H_9N_2{}^+$].

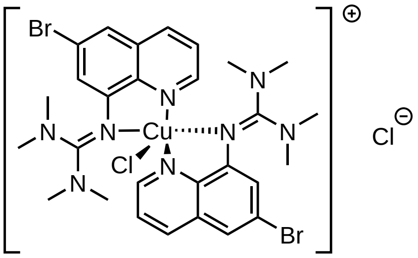

[Cu(TMG6Brqu)$_2$Cl]Cl (**C12**). **M**($C_{28}H_{34}N_8Cl_2Br_2Cu$) = 776.89 g mol^{-1}. **Crystal habit:** bronze platelet. **IR** (Diamond-ATR, neat) $\tilde{\nu}_{\mathrm{max}}$: 3283 (vw, ν(C−H)), 2928 (vw, ν(C−H)), 2868 (vw, ν(C−H)), 1566 (s, ν(N=C)), 1516 (m), 1488 (s), 1468 (s), 1449 (m), 1421 (s), 1409 (m), 1395 (vs), 1371 (vs), 1322 (m), 1269 (w), 1219 (m), 1199 (w), 1165 (m), 1148 (m), 1137 (m), 1119 (w), 1094 (w), 1065 (w), 1021 (m), 930 (w), 906 (w), 842 (vs), 826 (m), 790 (m), 784 (m), 762 (m), 742 (w), 715 (m), 699 (w), 677 (w), 668 (w), 663 (vw) cm^{-1}. **MS** (FAB+) *m/z* (relative intensity): 742 (18%) [$C_{28}H_{34}N_8{}^{37}Cl^{79}Br^{81}Br^{63}Cu^+$] [$C_{28}H_{34}N_8{}^{35}Cl^{81}Br_2{}^{63}Cu^+$] [$C_{28}H_{34}N_8{}^{37}Cl^{79}Br_2{}^{65}Cu^+$] [$C_{28}H_{34}N_8{}^{35}Cl^{79}Br^{81}Br^{65}Cu^+$], 740 (18%) [$C_{28}H_{34}N_8{}^{37}Cl^{79}Br_2{}^{63}Cu^+$] [$C_{28}H_{34}N_8{}^{35}Cl^{79}Br^{81}Br^{63}Cu^+$] [$C_{28}H_{34}N_8{}^{35}Cl^{79}Br_2{}^{65}Cu^+$] 707 (20%) [$C_{28}H_{34}N_8{}^{79}Br^{81}Br^{65}Cu^+$] [$C_{28}H_{34}N_8{}^{81}Br_2{}^{63}Cu^+$], 705 (25%) [$C_{28}H_{34}N_8{}^{79}Br^{81}Br^{63}Cu^+$] [$C_{28}H_{34}N_8{}^{79}Br_2{}^{65}Cu^+$], 703 (10%) [$C_{28}H_{34}N_8{}^{79}Br_2{}^{63}Cu^+$], 385 (50%) [$C_{14}H_{17}N_4{}^{81}BrCu^+$], 383 (38%) [$C_{14}H_{17}N_4{}^{79}BrCu^+$], 323 (91%) [$C_{11}H_{18}N_4{}^{81}Br^+$], 321 (96%) [$C_{11}H_{18}N_4{}^{79}Br^+$], 278 (55%) [$C_{12}H_{11}N_3{}^{81}Br^+$], 276 (55%) [$C_{12}H_{11}N_3{}^{79}Br^+$].
HR-MS (FAB+): calcd for [$C_{28}H_{34}N_8{}^{35}Cl^{79}Br_2{}^{63}Cu^+$] 738.0253, found: 738.0312.
HR-MS (FAB+): calcd for [$C_{28}H_{34}N_8{}^{37}Cl^{79}Br_2{}^{63}Cu^+$] 740.0223, found: 740.0287.
HR-MS (FAB+): calcd for [$C_{28}H_{34}N_8{}^{35}Cl^{79}Br^{81}Br^{63}Cu^+$] 740.0232, found: 740.0287.
HR-MS (FAB+): calcd for [$C_{28}H_{34}N_8{}^{35}Cl^{79}Br_2{}^{65}Cu^+$] 740.0235, found: 740.0287.
HR-MS (FAB+): calcd for [$C_{28}H_{34}N_8{}^{37}Cl^{79}Br^{81}Br^{63}Cu^+$] 742.0203, found: 742.0208.
HR-MS (FAB+): calcd for [$C_{28}H_{34}N_8{}^{35}Cl^{81}Br_2{}^{63}Cu^+$] 742.0205, found: 742.0208.
HR-MS (FAB+): calcd for [$C_{28}H_{34}N_8{}^{37}Cl^{79}Br_2{}^{65}Cu^+$] 742.0212, found: 742.0208.
HR-MS (FAB+): calcd for [$C_{28}H_{34}N_8{}^{35}Cl^{79}Br^{81}Br^{65}Cu^+$] 742.0214, found: 742.0208.
HR-MS (FAB+): calcd for [$C_{28}H_{34}N_8{}^{37}Cl^{81}Br_2{}^{63}Cu^+$] 744.0182, found: 744.0168.
HR-MS (FAB+): calcd for [$C_{28}H_{34}N_8{}^{37}Cl^{79}Br^{81}Br^{65}Cu^+$] 744.0185, found: 744.0168.
HR-MS (FAB+): calcd for [$C_{28}H_{34}N_8{}^{35}Cl^{81}Br_2{}^{65}Cu^+$] 744.0194, found: 744.0168.

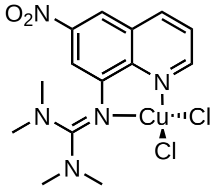

[Cu(TMG6Nitroqu)Cl$_2$] (**C13**). **M**($C_{14}H_{17}N_5O_2Cl_2Cu$) = 421.77 g mol^{-1}. **Crystal habit:** brown platelet. **IR** (Diamond-ATR, neat) $\tilde{\nu}_{\mathrm{max}}$: 3072 (vw, ν(C−H$_{\mathrm{arom.}}$)), 3013 (vw, ν(C−H$_{\mathrm{aliph.}}$)), 2927 (vw, ν(C−H$_{\mathrm{aliph.}}$)), 2799 (vw, ν(C−H$_{\mathrm{aliph.}}$)), 1594 (m, ν(N=C)), 1520 (m), 1497 (vs), 1450 (m), 1399 (vs), 1380 (s), 1342 (vs), 1328 (vs), 1226 (m), 1199 (m), 1172 (m), 1146 (m), 1121 (m), 1083 (m), 1066 (m), 1027 (m), 962 (vw), 908 (m), 866 (m), 846 (m), 807 (w), 797 (s), 786 (vs), 769 (m), 738 (m), 719 (m) cm^{-1}. **MS** (FAB+) *m/z* (relative intensity): 387 (15%) [$C_{14}H_{18}N_5O_2{}^{37}Cl^{63}Cu^+$], 385 (17%) [$C_{14}H_{18}N_5O_2{}^{35}Cl^{63}Cu^+$], 350 (16%) [$C_{14}H_{18}N_5O_2{}^{63}Cu^+$], 288 (100%) [$C_{14}H_{18}N_5O_2{}^+$], 243 (28%) [$C_{12}H_{11}N_4O_2{}^+$]. **HR-MS** (FAB+): calcd for [$C_{14}H_{17}N_5O_2{}^{35}Cl^{63}Cu^+$] 385.0362, found: 385.0377. **HR-MS** (FAB+): calcd for [$C_{1313}CH_{17}N_5O_2{}^{35}Cl^{63}Cu^+$] 386.0395, found: 386.0499. **HR-MS** (FAB+): calcd for [$C_{14}H_{17}N_5O_2{}^{37}Cl^{63}Cu^+$] 387.0333, found: 387.0301. **HR-MS** (FAB+): calcd for [$C_{14}H_{17}N_5O_2{}^{35}Cl^{65}Cu^+$] 387.0349, found: 387.0301. **HR-MS** (FAB+): calcd for [$C_{1313}CH_{17}N_5O_2{}^{37}Cl^{63}Cu^+$] 388.0366, found: 388.0560. **HR-MS** (FAB+): calcd for [$C_{1313}CH_{17}N_5O_2{}^{35}Cl^{65}Cu^+$] 388.0377, found: 388.0560. **HR-MS** (FAB+): calcd for [$C_{14}H_{17}N_5O_2{}^{37}Cl^{65}Cu^+$] 389.0319, found: 389.0424.

[Cu(DMEG6Methoxyqu)$_2$Br]Br (**C14**). **M**($C_{30}H_{36}N_8O_2Br_2Cu$) = 764.03 g mol^{-1}. **IR** (Diamond-ATR, neat) $\tilde{\nu}_{\mathrm{max}}$: 2993 (vw ν(C−H)), 2931 (vw ν(C−H)), 2871 (vw ν(C−H)), 2158 (w), 2029 (w), 1968 (w), 1599 (m ν(N=C)), 1549 (vs), 1495 (s), 1465 (m), 1451 (m), 1414 (m), 1389 (vs), 1337 (m), 1292 (m), 1217 (s), 1198 (m), 1159 (s), 1138 (m), 1118 (m), 1089 (w), 1059 (m), 1041 (m), 1022 (m), 978 (m), 960 (w), 924 (w), 889 (w), 822 (s), 784 (m), 778 (m), 745 (w), 737 (w), 729 (w), 719 (vw), 706 (vw), 689 (vw), 684 (w), 673 (m), 665 (m), 651 (m) cm^{-1}. **MS** (EI) *m/z* (relative intensity): 538 (3%) [$C_{30}H_{34}N_8O_2{}^+$], 350 (5%) [$C_{15}H_{17}N_4O^{81}Br^+$], 348 (5%) [$C_{15}H_{17}N_4O^{79}Br^+$], 270 (100%) [$C_{15}H_{18}N_4O^+$], 213 (8%) [$C_{12}H_{11}N_3O^+$], 185 (12%) [$C_{11}H_9N_2O^+$], 135 (6%), 98 (20%) [$C_5H_{10}N_2{}^+$], 43 (4%) [$C_2H_5N^+$]. **HR-MS** (FAB+): calcd for [$C_{30}H_{36}N_8O_2{}^{79}Br^{63}Cu^+$] 682.1435, found: 682.1378. **HR-MS** (FAB+): calcd for [$C_{23}{}^{13}CH_{36}N_8O_2{}^{79}Br^{63}Cu^+$] 683.1469, found: 683.1384. **HR-MS** (FAB+): calcd for [$C_{30}H_{36}N_8O_2{}^{81}Br^{63}Cu^+$] 684.1415, found: 684.1425. **HR-MS** (FAB+): calcd for [$C_{30}H_{36}N_8O_2{}^{79}Br^{65}Cu^+$] 684.1418, found: 684.1425. **HR-MS** (FAB+): calcd for [$C_{29}{}^{13}CH_{36}N_8O_2{}^{81}Br^{63}Cu^+$] 685.1449, found: 685.1402. **HR-MS** (FAB+): calcd for [$C_{29}{}^{13}CH_{36}N_8O_2{}^{79}Br^{65}Cu^+$] 685.1451, found: 685.1402. **HR-MS** (FAB+): calcd for [$C_{30}H_{36}N_8O_2{}^{81}Br^{65}Cu^+$] 686.1397, found: 686.1379. **HR-MS** (FAB+): calcd for [$C_{29}{}^{13}CH_{36}N_8O_2{}^{81}Br^{65}Cu^+$] 687.1431, found: 687.1469.

[Cu(TMG6EHoxyqu)$_2$Br]Br solution in acetonitrile. **M**($C_{44}H_{68}N_8O_2Br_2Cu$) = 964.44 g mol^{-1}. **MS** (FAB+) *m/z* (relative intensity): 884 (<1%) [$C_{44}H_{68}N_8O_2BrCu^+$], 803

(14%) [$C_{44}H_{68}N_8O_2{}^{63}Cu^+$], 600 (11%), 585 (3%), 433 (32%) [$C_{22}H_{34}N_4O^{63}Cu^+$], 371 (100%) [$C_{22}H_{35}N_4O^+$].

[Cu(TMG6EHoxyqu)$_2$Cl]Cl solution in acetonitrile. **M**($C_{44}H_{68}N_8O_2Cl_2Cu$) = 875.53 g mol^{-1}. **MS** (FAB+) *m/z* (relative intensity): 838 (3%) [$C_{44}H_{68}N_8O_2{}^{35}Cl^{63}Cu^+$], 803 (4%) [$C_{44}H_{68}N_8O_2{}^{63}Cu^+$], 654 (10%), 587 (6%), 505 (4%), 468 (90%) [$C_{22}H_{34}N_4O^{35}Cl^{63}Cu^+$], 433 (45%) [$C_{22}H_{34}N_4O^{63}Cu^+$], 371 (100%) [$C_{22}H_{35}N_4O^+$].
HR-MS (FAB+): calcd for [$C_{44}H_{68}N_8O_2{}^{35}Cl^{63}Cu^+$] 838.4450, found: 838.4485.
HR-MS (FAB+): calcd for [$C_{43}{}^{13}CH_{68}N_8O_2{}^{35}Cl^{63}Cu^+$] 839.4483, found: 839.4476.
HR-MS (FAB+): calcd for [$C_{44}H_{68}N_8O_2{}^{37}Cl^{63}Cu^+$] 840.4420, found: 840.4463.
HR-MS (FAB+): calcd for [$C_{44}H_{68}N_8O_2{}^{35}Cl^{65}Cu^+$] 840.4432, found: 840.4463.

6.4. Polymerization of Styrene

The polymerization of styrene was performed under an inert atmosphere. A 10 mL Schlenk-tube, was loaded with the respective ligand (0.46 mmol, 2 equiv) and copper salt (0.23 mmol, 1 equiv) in a glove box. Afterward, the closed tube was removed from the glove box, attached to a Schlenk-line and the monomer stock solution was added. The two stock solutions used were composed of degassed, dry and destabilized styrene (2.60 mL, 2.40 g, 23.0 mmol, 100 equiv) with distilled and degassed benzonitrile (1.13 mL) or without benzonitrile. Before initiation, the polymerization essay was preheated in a aluminum heating block. For reactions containing CuCl, the polymerization was conducted at 130 °C, for CuBr a temperature of 110 °C was applied. The polymerization was initiated by rapid injection of degassed initiator (0.230 mmol) into the thoroughly stirred solution. The choice of initiator was adapted to the choice of copper salt. Polymerization reaction containing CuCl as copper source were initiated with 1-phenylethyl chloride, for CuBr 1-phenylethyl bromide was used respectively.

Samples were taken every ten to fifteen minutes. Therefore, an aliquot (0.2 mL) of the reaction solution was transferred into a NMR tube and filled with $CDCl_3$. After analysis by ^1H NMR, the samples were precipitated in ethanol (5 mL) at room temperature. The the samples were separated in a centrifuge and decanted. The solids were dissolved in dichloromethane (1 mL) and re-precipitated in ethanol (5 mL). After separation in a centrifuge and decanting, the white polymer powders were dried in an oven at 50 °C for 12 h. For final analysis, samples of the dry powders were dissolved in tetrahydrofuran (5 mg in 1 mL) and separated with a GPC.

6.5. Analytical Methods

6.5.1. Determination of K_{ATRP} and k_{act} constants

Experimental setup. UV/Vis absorption spectra were recorded in a screw cap cuvette with a silicon septum (section 6.1.1). The light source was connected to fiber optics which was connected to a cuvette holder. The cuvette holder was placed over a magnetic stirrer to minimize gradients within the solution. The cuvette holder was manufactured in such a fashion that the magnetic stir bar did not interfere with the optic pathway. The cuvette holder was then connected to the spectrometer by fiber optics. The cuvette was filled with solvent in a glove box and the screw cap was closed. All reagents were then filled into Hamilton Gastight syringes under inert atmosphere and the needles were capped with rubber stoppers. Just before starting the measurement, the rubber stoppers were removed and the needles were pushed through the cell's septum. Therefore, the impact of oxygen contamination was reduced to a minimum.

Determination of K_{ATRP} values. The background of the UV/Vis absorption spectra for K_{ATRP} determination was measured with acetonitrile only. Afterward, the Cu^{I} catalyst solution was added and the spectrometer was started to collect data (Figure 6.1). After ten seconds, the initiator solution was added and the increase of the Cu^{II} concentration was detected at a wavelength (λ) of 940 nm. The reaction was conducted for 20 min and data read outs were saved every two seconds. After collection, the data was processed. The analysis contained Fisher–Fukuda and Matyjaszewski plots and the K_{ATRP} values were calculated by applying the methods of Fisher and Fukuda as well as of Matyaszewski.[17,126] The stock solutions of complexes and initiator were prepared under inert atmosphere. Cu^{I} complex and EBriB solutions in acetonitrile were introduced to yield initial concentrations of 5 mM in the cuvette (2 mL).

$$\mathrm{CuX(L)_2} + \mathrm{R{-}X} \overset{K_{ATRP}}{\rightleftharpoons} \mathrm{CuX_2(L)_2} + \mathrm{R^{\bullet}} \overset{k_t}{\dashrightarrow}$$

Figure 6.1: Equilibrium reaction during K_{ATRP} determination.

Determination of k_{act} values. The background of the UV/Vis absorption spectra for k_{act} value determination experiments was recorded with acetonitrile, TEMPO and EBriB. The spectrometer was allowed to record data and after ten seconds, the Cu^{I} catalyst solution was added (Figure 6.2). The increase of the Cu^{II} concentration was detected at a wavelength (λ) of 940 nm. The reaction was conducted for 5 min and data read outs were saved every 500 ms. After collection, the data was processed and analyzed. The initial concentration of the Cu^{I} complex was determined to 3 mM, whereas the initiator and TEMPO solutions were each introduced yielding a tenfold concentration of 30 mM in the cuvette (2 mL).

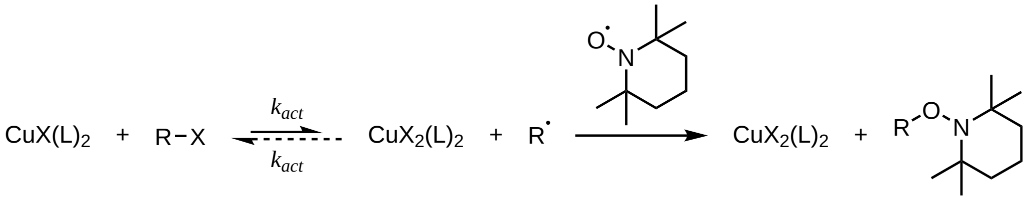

Figure 6.2: Suppressed reverse reaction of the ATRP equilibrium during k_{act} determination.

Table 6.2: Extinction coefficients ε_λ of the Cu^{II} complexes, which were received during determination of k_{act}.

Ligands of Cu^{II} complexes	$\varepsilon_{940\,nm}$ [$L\,mol^{-1}\,cm^{-1}$]
TMG6Brqu	500
DMEG6Methoxyqu	410
TMG6Methoxyqu	500
TMG6EHoxyqu	540
TMG6dbaqu	470
TMG6dmaqu	490

References

[1] Matyjaszewski, K.; Tsarevsky, N. V. *J. Am. Chem. Soc.* **2014**, *136*, 6513–6533.

[2] Boyer, C.; Corrigan, N. A.; Jung, K.; Nguyen, D.; Nguyen, T.-K.; Adnan, N. N. M.; Oliver, S.; Shanmugam, S.; Yeow, J. *Chem. Rev.* **2016**, *116*, 1803–1949.

[3] Dervaux, B.; Junkers, T.; Barner-Kowollik, C.; Du Prez, F. E. *Macromol. React. Eng.* **2009**, *3*, 529–538.

[4] Statistisches Bundesamt, *Fachserie 4* **2013**, *Reihe 3.1*, 1–305.

[5] Odian, G. *Principles of Polymerization*, 4th ed.; Wiley Interscience: New York, NY, USA, 2004; p 832.

[6] Berkenwald, E.; Spies, C.; Morales, G.; Estenoz, D. *Polym. Eng. Sci.* **2015**, *55*, 145–155.

[7] Zavitsas, A. A. *J. Phys. Chem. A* **2003**, *107*, 897–898.

[8] Goto, A.; Fukuda, T. *Prog. Polym. Sci.* **2004**, *29*, 329–385.

[9] Wang, J.-S.; Matyjaszewski, K. *J. Am. Chem. Soc.* **1995**, *117*, 5614–5615.

[10] Matyjaszewski, K.; Spanswick, J. *Mater. Today* **2005**, *8*, 26–33.

[11] Zhong, M.; Matyjaszewski, K. *Macromolecules* **2011**, *44*, 2668–2677.

[12] Matyjaszewski, K. *Macromolecules* **2012**, *45*, 4015–4039.

[13] Zipse, H. In *Radicals Synth. I*; Gansäuer, A., Ed.; Topics in Current Chemistry; Springer-Verlag: Berlin/Heidelberg, Germany, 2006; Vol. 263; pp 163–189.

[14] Griller, D.; Ingold, K. U. *Acc. Chem. Res.* **1976**, *9*, 13–19.

[15] Boyer, C.; Soeriyadi, A. H.; Zetterlund, P. B.; Whittaker, M. R. *Macromolecules* **2011**, *44*, 8028–8033.

[16] Hoffmann, A.; Börner, J.; Flörke, U.; Herres-Pawlis, S. *Inorganica Chim. Acta* **2009**, *362*, 1185–1193.

[17] Rösener, T.; Bienemann, O.; Sigl, K.; Schopp, N.; Schnitter, F.; Flörke, U.; Hoffmann, A.; Döring, A.; Kuckling, D.; Herres-Pawlis, S. *Chem. Eur. J.* **2016**, *22*, 13550–13562.

[18] Kato, M.; Kamigaito, M.; Sawamoto, M.; Higashimura, T. *Macromolecules* **1995**, *28*, 1721–1723.

[19] Zhong, M.; Natesakhawat, S.; Baltrus, J. P.; Luebke, D.; Nulwala, H.; Matyjaszewski, K.; Kowalewski, T. *Chem. Commun.* **2012**, *48*, 11516–11518.

[20] Nalawade, P. P.; Soucek, M. D. *Macromol. Chem. Phys.* **2017**, 1700234.

[21] Kaner, P.; Hu, X.; Thomas, S. W.; Asatekin, A. *ACS Appl. Mater. Interfaces* **2017**, *9*, 13619–13631.

[22] Hui, C. M.; Pietrasik, J.; Schmitt, M.; Mahoney, C.; Choi, J.; Bockstaller, M. R.; Matyjaszewski, K. *Chem. Mater.* **2014**, *26*, 745–762.

[23] Dehghani, E. S.; Spencer, N. D.; Ramakrishna, S. N.; Benetti, E. M. *Langmuir* **2016**, *32*, 10317–10327.

[24] Xu, L. Q.; Li, N. N.; Chen, J. C.; Fu, G. D.; Kang, E.-T. *RSC Adv.* **2015**, *5*, 61742–61751.

[25] Li, Y.; Bai, X.; Xu, M.; Xu, S.; Hu, G.; Wang, L. *Sci. China Mater.* **2016**, *59*, 254–264.

[26] Kim, J. Y.; Lee, B. S.; Choi, J.; Kim, B. J.; Choi, J. Y.; Kang, S. M.; Yang, S. H.; Choi, I. S. *Angew. Chemie Int. Ed.* **2016**, *55*, 15306–15309.

[27] Çayli, G.; Meier, M. A. R. *Eur. J. Lipid Sci. Technol.* **2008**, *110*, 853–859.

[28] Wilbon, P. A.; Zheng, Y.; Yao, K.; Tang, C. *Macromolecules* **2010**, *43*, 8747–8754.

[29] Wang, J.; Yao, K.; Korich, A. L.; Li, S.; Ma, S.; Ploehn, H. J.; Iovine, P. M.; Wang, C.; Chu, F.; Tang, C. *J. Polym. Sci. Part A Polym. Chem.* **2011**, *49*, 3728–3738.

[30] Liu, Y.; Yao, K.; Chen, X.; Wang, J.; Wang, Z.; Ploehn, H. J.; Wang, C.; Chu, F.; Tang, C. *Polym. Chem.* **2014**, *5*, 3170.

[31] Suresh, K. I.; Jaikrishna, M. *J. Polym. Sci. Part A Polym. Chem.* **2005**, *43*, 5953–5961.

[32] Reza Fareghi, A.; Najafi Moghaddam, P.; Akbar Entezami, A.; Ensafi Avval, M. *Iran. Polym. J.* **2013**, *22*, 361–367.

[33] Li, D. J.; Fu, Y. J.; Qin, M. H. *Adv. Mater. Res.* **2013**, *734-737*, 2108–2112.

[34] Yu, J.; Lu, C.; Wang, C.; Wang, J.; Fan, Y.; Chu, F. *Carbohydr. Polym.* **2017**, *176*, 83–90.

[35] Mosnáček, J.; Matyjaszewski, K. *Macromolecules* **2008**, *41*, 5509–5511.

[36] Cabane, E.; Keplinger, T.; Künniger, T.; Merk, V.; Burgert, I. *Sci. Rep.* **2016**, *6*, 31287.

[37] Schröder, K.; Mathers, R. T.; Buback, J.; Konkolewicz, D.; Magenau, A. J. D.; Matyjaszewski, K. *ACS Macro Lett.* **2012**, *1*, 1037–1040.

[38] Magenau, A. J. D.; Kwak, Y.; Schröder, K.; Matyjaszewski, K. *ACS Macro Lett.* **2012**, *1*, 508–512.

[39] Hoffmann, A.; Bienemann, O.; Vieira, I.; Herres-Pawlis, S. *Polymers (Basel).* **2014**, *6*, 995–1007.

[40] Kaur, A.; Ribelli, T. G.; Schröder, K.; Matyjaszewski, K.; Pintauer, T. *Inorg. Chem.* **2015**, *54*, 1474–1486.

[41] Bortolamei, N.; Isse, A. A.; Di Marco, V. B.; Gennaro, A.; Matyjaszewski, K. *Macromolecules* **2010**, *43*, 9257–9267.

[42] Percec, V.; Guliashvili, T.; Ladislaw, J. S.; Wistrand, A.; Stjerndahl, A.; Sienkowska, M. J.; Monteiro, M. J.; Sahoo, S. *J. Am. Chem. Soc.* **2006**, *128*, 14156–14165.

[43] Konkolewicz, D.; Wang, Y.; Zhong, M.; Krys, P.; Isse, A. a.; Gennaro, A.; Matyjaszewski, K. *Macromolecules* **2013**, *46*, 8749–8772.

[44] Lin, C. Y.; Coote, M. L.; Gennaro, A.; Matyjaszewski, K. *J. Am. Chem. Soc.* **2008**, *130*, 12762–12774.

[45] Guliashvili, T.; Mendonça, P. V.; Serra, A. C.; Popov, A. V.; Coelho, J. F. J. *Chem. Eur. J.* **2012**, *18*, 4607–4612.

[46] Harrisson, S.; Couvreur, P.; Nicolas, J. *Macromolecules* **2012**, *45*, 7388–7396.

[47] Wang, Y.; Zhong, M.; Zhu, W.; Peng, C.-H.; Zhang, Y.; Konkolewicz, D.; Bortolamei, N.; Isse, A. A.; Gennaro, A.; Matyjaszewski, K. *Macromolecules* **2013**, *46*, 3793–3802.

[48] Peng, C.-H.; Zhong, M.; Wang, Y.; Kwak, Y.; Zhang, Y.; Zhu, W.; Tonge, M.; Buback, J.; Park, S.; Krys, P.; Konkolewicz, D.; Gennaro, A.; Matyjaszewski, K. *Macromolecules* **2013**, *46*, 3803–3815.

[49] Zhong, M.; Wang, Y.; Krys, P.; Konkolewicz, D.; Matyjaszewski, K. *Macromolecules* **2013**, *46*, 3816–3827.

[50] Isse, A. A.; Gennaro, A.; Lin, C. Y.; Hodgson, J. L.; Coote, M. L.; Guliashvili, T. *J. Am. Chem. Soc.* **2011**, *133*, 6254–6264.

[51] Tsarevsky, N. V.; Braunecker, W. A.; Matyjaszewski, K. *J. Organomet. Chem.* **2007**, *692*, 3212–3222.

[52] Foll, A.; Le Démezet, M.; Courtot-Coupez, J. *J. Electroanal. Chem. Interfacial Electrochem.* **1972**, *35*, 41–54.

[53] Levere, M. E.; Nguyen, N. H.; Leng, X.; Percec, V. *Polym. Chem.* **2013**, *4*, 1635–1647.

[54] Isse, A. A.; Lin, C. Y.; Coote, M. L.; Gennaro, A. *J. Phys. Chem. B* **2011**, *115*, 678–684.

[55] Isse, A. A.; Bortolamei, N.; De Paoli, P.; Gennaro, A. *Electrochim. Acta* **2013**, *110*, 655–662.

[56] Konkolewicz, D.; Krys, P.; Góis, J. R.; Mendonça, P. V.; Zhong, M.; Wang, Y.; Gennaro, A.; Isse, A. A.; Fantin, M.; Matyjaszewski, K. *Macromolecules* **2014**, *47*, 560–570.

[57] Konkolewicz, D.; Wang, Y.; Krys, P.; Zhong, M.; Isse, A. A.; Gennaro, A.; Matyjaszewski, K. *Polym. Chem.* **2014**, *5*, 4409.

[58] Lin, C. Y.; Marque, S. R. A.; Matyjaszewski, K.; Coote, M. L. *Macromolecules* **2011**, *44*, 7568–7583.

[59] Tang, W.; Kwak, Y.; Braunecker, W.; Tsarevsky, N. V.; Coote, M. L.; Matyjaszewski, K. *J. Am. Chem. Soc.* **2008**, *130*, 10702–10713.

[60] Tang, W.; Matyjaszewski, K. *Macromolecules* **2007**, *40*, 1858–1863.

[61] Iovu, M. C.; Matyjaszewski, K. *Macromolecules* **2003**, *36*, 9346–9354.

[62] Tsarevsky, N. V.; Pintauer, T.; Matyjaszewski, K. *Macromolecules* **2004**, *37*, 9768–9778.

[63] Schröder, K.; Konkolewicz, D.; Poli, R.; Matyjaszewski, K. *Organometallics* **2012**, *31*, 7994–7999.

[64] Tsarevsky, N. V.; Braunecker, W. A.; Tang, W.; Brooks, S. J.; Matyjaszewski, K.; Weisman, G. R.; Wong, E. H. *J. Mol. Catal. A Chem.* **2006**, *257*, 132–140.

[65] Exner, O. *Dipole moments in organic chemistry*; Thieme: Stuttgart, Germany, 1975; p 156.

[66] Braunecker, W. A.; Tsarevsky, N. V.; Gennaro, A.; Matyjaszewski, K. *Macromolecules* **2009**, *42*, 6348–6360.

[67] Patai, S.; Rappoport, Z. *Nitro and Nitroso Groups: Vol. 2 (1970)*; John Wiley & Sons Ltd: Chichester, UK, 1970; Vol. 2; p 918.

[68] Sundermeyer, J.; Raab, V.; Gaoutchenova, E.; Garrelts, U.; Abacilar, N.; Harms, K. In *Act. Unreactive Substrates Role Second. Interact.*; Bolm, C., Hahn, F. E., Eds.; Wiley-VCH Verlag GmbH & Co. KGaA: Weinheim, Germany, 2009; pp 17–37.

[69] Raab, V.; Harms, K.; Sundermeyer, J.; Kovacević, B.; Maksić, Z. B. *J. Org. Chem.* **2003**, *68*, 8790–8797.

[70] Bordwell, F. G.; Ji, G. Z. *J. Am. Chem. Soc.* **1991**, *113*, 8398–8401.

[71] Ishikawa, T. *Chem. Pharm. Bull. (Tokyo).* **2010**, *58*, 1555–1564.

[72] Kantlehner, W.; Edelmann, K.; Gissel, A.; Scherr, O.; Vetter, J.; Wezstein, M.; Ziegler, G.; Mezger, J.; Iliev, B. *Acta Chim. Solvenica* **2009**, *53*, 612–621.

[73] Kantlehner, W.; Haug, E.; Mergen, W. W.; Speh, P.; Maier, T.; Kapassakalidis, J. J.; Bräuner, H.-J.; Hagen, H. *Liebigs Ann. der Chemie* **1984**, *1984*, 108–126.

[74] Peters, A.; Kaifer, E.; Himmel, H.-J. *European J. Org. Chem.* **2008**, *2008*, 5907–5914.

[75] Evindar, G.; Batey, R. A. *Org. Lett.* **2003**, *5*, 133–136.

[76] Limatibul, S.; Watson, J. *J. Org. Chem.* **1971**, *36*, 3805–3807.

[77] Gund, P. *J. Chem. Educ.* **1972**, *49*, 100.

[78] Longhi, R.; Drago, R. S. *Inorg. Chem.* **1965**, *4*, 11–14.

[79] Stanek, J.; Rösener, T.; Metz, A.; Mannsperger, J.; Hoffmann, A.; Herres-Pawlis, S. In *Guanidines as Reagents Catalysts II*, 1st ed.; Selig, P., Ed.; Topics in Heterocyclic Chemistry; Springer International Publishing: Cham, Switzerland, 2017; Vol. 51; Chapter 4, pp 95–164.

[80] Oakley, S. H.; Coles, M. P.; Hitchcock, P. B. *Inorg. Chem.* **2003**, *42*, 3154–3156.

[81] Bailey, P. J.; Pace, S. *Coord. Chem. Rev.* **2001**, *214*, 91–141.

[82] Bienemann, O.; Haase, R.; Jesser, A.; Beschnitt, T.; Döring, A.; Kuckling, D.; dos Santos Vieira, I.; Flörke, U.; Herres-Pawlis, S. *Eur. J. Inorg. Chem.* **2011**, *2011*, 2367–2379.

[83] Bienemann, O.; Hoffmann, A.; Herres-Pawlis, S. *Rev. Inorg. Chem.* **2011**, *31*, 83–108.

[84] Petrovic, D.; Hill, L. M. R.; Jones, P. G.; Tolman, W. B.; Tamm, M. *Dalton Trans.* **2008**, 887–894.

[85] Schäfer, P. M.; Fuchs, M.; Ohligschläger, A.; Rittinghaus, R.; McKeown, P.; Akin, E.; Schmidt, M.; Hoffmann, A.; Liauw, M. A.; Jones, M. D.; Herres-Pawlis, S. *ChemSusChem* **2017**, *10*, 3547–3556.

[86] Metz, A.; Hoffmann, A.; Hock, K.; Herres-Pawlis, S. *Chem. Unserer Zeit* **2016**, *50*, 316–325.

[87] Metz, A.; Plothe, R.; Glowacki, B.; Koszalkowski, A.; Scheckenbach, M.; Beringer, A.; Rösener, T.; Michaelis de Vasconcellos, J.; Haase, R.; Flörke, U.; Hoffmann, A.; Herres-Pawlis, S. *Eur. J. Inorg. Chem.* **2016**, *2016*, 4974–4987.

[88] Hoffmann, A.; Wern, M.; Hoppe, T.; Witte, M.; Haase, R.; Liebhäuser, P.; Glatthaar, J.; Herres-Pawlis, S.; Schindler, S. *Eur. J. Inorg. Chem.* **2016**, *2016*, 4744–4751.

[89] Strassl, F.; Grimm-Lebsanft, B.; Rukser, D.; Biebl, F.; Biednov, M.; Brett, C.; Timmermann, R.; Metz, F.; Hoffmann, A.; Rübhausen, M.; Herres-Pawlis, S. *Eur. J. Inorg. Chem.* **2017**, *2017*, 3350–3359.

[90] Hoffmann, A.; Bienemann, O.; Vieira, I. D. S.; Herres-Pawlis, S. *Zeitschrift für Naturforsch. B* **2014**, *69b*, 589–595.

[91] Herres-Pawlis, S.; Bienemann, O.; Haase, R.; Flörke, U.; Döring, A.; Kuckling, D. *Zeitschrift für Naturforsch. B* **2010**, *65*, 798–806.

[92] Hammond, G. S. *J. Am. Chem. Soc.* **1955**, *77*, 334–338.

[93] Hoffmann, A.; Binder, S.; Jesser, A.; Haase, R.; Flörke, U.; Gnida, M.; Salomone Stagni, M.; Meyer-Klaucke, W.; Lebsanft, B.; Grünig, L. E.; Schneider, S.; Hashemi, M.; Goos, A.; Wetzel, A.; Rübhausen, M.; Herres-Pawlis, S. *Angew. Chemie Int. Ed.* **2014**, *53*, 299–304.

[94] Hoffmann, A.; Stanek, J.; Dicke, B.; Peters, L.; Grimm-Lebsanft, B.; Wetzel, A.; Jesser, A.; Bauer, M.; Gnida, M.; Meyer-Klaucke, W.; Rübhausen, M.; Herres-Pawlis, S. *Eur. J. Inorg. Chem.* **2016**, *2016*, 4731–4743.

[95] Stanek, J.; Sackers, N.; Fink, F.; Paul, M.; Peters, L.; Grunzke, R.; Hoffmann, A.; Herres-Pawlis, S. *Chem. Eur. J.* **2017**, *23*, 15738–15745.

[96] Mewshaw, R. E.; Zhou, P.; Zhou, D.; Meagher, K. L.; Asselin, M.; Evrard, D. A.; Gilbert, A. M. (American Home Products Corp). Preparation of arylpiperazinyl-cyclohexyl indole derivatives for the treatment of depression. US 6,313,126 B1. 2001.

[97] Smil, D.; Leit, S.; Ajamian, A.; Allan, M.; Chantigny, Y. A.; Deziel, R.; Therrien, E.; Wahhab, A.; Manku, S. (MethylGene Inc.). Sulfamide and sulfamate derivatives as histone deacetylase inhibitors. US 2007/0293530 A1. 2007.

[98] Skraup, Z. H. *Berichte der Dtsch. Chem. Gesellschaft* **1880**, *13*, 2086.

[99] Rieche, A.; Schmitz, E.; Dietrich, P. *Chem. Ber.* **1959**, *92*, 2239–2252.

[100] Schofield, J.; Smalley, R. K.; Scopes, D. I. C. *Chem. Ind.* **1986**, 587.

[101] Wielgosz-Collin, G.; Duflos, M.; Pinson, P.; Le Baut, G.; Renard, P.; Bennejean, C.; Boutin, J.; Boulanger, M. *J. Enzyme Inhib. Med. Chem.* **2002**, *17*, 449–453.

[102] Lee, B. K.; Biscoe, M. R.; Buchwald, S. L. *Tetrahedron Lett.* **2009**, *50*, 3672–3674.

[103] Bhattacharyya, S.; Chatterjee, A.; Duttachowdhury, S. K. *J. Chem. Soc. Perkin Trans. 1* **1994**, *36*, 1.

[104] Rosenau, T.; Potthast, A.; Röhrling, J.; Hofinger, A.; Sixta, H.; Kosma, P. *Synth. Commun.* **2002**, *32*, 457.

[105] Baxter, E. W.; Reitz, A. B. *Organic Reactions Vol. 59*; John Wiley & Sons, Inc.: Hoboken, NJ, USA, 2002; pp 1–714.

[106] Palmer, A. M.; Webel, M.; Scheufler, C.; Haag, D.; Müller, B. *Org. Process Res. Dev.* **2008**, *12*, 1170–1182.

[107] Denmark, S. E.; Cresswell, A. J. *J. Org. Chem.* **2013**, *78*, 12593–12628.

[108] Ochiai, E. *J. Org. Chem.* **1953**, *18*, 534–551.

[109] Limpach, L. *Berichte der Dtsch. Chem. Gesellschaft (A B Ser.* **1931**, *64*, 969–970.

[110] Gould, R. G.; Jacobs, W. A. *J. Am. Chem. Soc.* **1939**, *61*, 2890–2895.

[111] Baker, R. H.; Lappin, G. R.; Albisetti, C. J.; Riegel, B. *J. Am. Chem. Soc.* **1946**, *68*, 1267–1267.

[112] Price, C. C.; Roberts, R. M. *J. Am. Chem. Soc.* **1946**, *68*, 1204–1208.

[113] Price, C. C.; Roberts, R. M.; Roland, C. J. R.; Schreiber, R. S. *Org. Synth.* **1948**, *28*, 38.

[114] Riegel, B.; Lappin, G. R.; Adelson, B. H.; Jackson, R. I.; Albisetti, C. J.; Dodson, R. M.; Baker, R. H. *J. Am. Chem. Soc.* **1946**, *68*, 1264–1266.

[115] Lee, S.; Jørgensen, M.; Hartwig, J. F. *Org. Lett.* **2001**, *3*, 2729–2732.

[116] Huang, X.; Buchwald, S. L. *Org. Lett.* **2001**, *3*, 3417–3419.

[117] Surry, D. S.; Buchwald, S. L. *J. Am. Chem. Soc.* **2007**, *129*, 10354–10355.

[118] Bhagwanth, S.; Adjabeng, G. M.; Hornberger, K. R. *Tetrahedron Lett.* **2009**, *50*, 1582–1585.

[119] Vo, G. D.; Hartwig, J. F. *J. Am. Chem. Soc.* **2009**, *131*, 11049–11061.

[120] Yang, L.; Powell, D. R.; Houser, R. P. *Dalton Trans.* **2007**, 955–964.

[121] Addison, A. W.; Rao, T. N.; Reedijk, J.; van Rijn, J.; Verschoor, G. C. *J. Chem. Soc. Dalton Trans.* **1984**, 1349–1356.

[122] Herres-Pawlis, S.; Haase, R.; Verma, P.; Hoffmann, A.; Kang, P.; Stack, T. D. P. *Eur. J. Inorg. Chem.* **2015**, *2015*, 5426–5436.

[123] Spingler, B.; Schnidrig, S.; Todorova, T.; Wild, F. *CrystEngComm* **2012**, *14*, 751–757.

[124] Bhatt, S.; Nayak, S. K. *Synth. Commun.* **2007**, *37*, 1381–1388.

[125] Cheng, Z.; Zhu, X.; Zhou, N.; Lu, J. *J. Appl. Polym. Sci.* **2003**, *90*, 1532–1538.

[126] Tang, W.; Tsarevsky, N. V.; Matyjaszewski, K. *J. Am. Chem. Soc.* **2006**, *128*, 1598–1604.

[127] Fischer, H. *Chem. Rev.* **2001**, *101*, 3581–3610.

[128] Zhang, H.; Klumperman, B.; Ming, W.; Fischer, H.; van der Linde, R. *Macromolecules* **2001**, *34*, 6169–6173.

[129] Xu, H.; Wolf, C. *Chem. Commun.* **2009**, 3035.

[130] Hwang, H.; Kim, J.; Jeong, J.; Chang, S. *J. Am. Chem. Soc.* **2014**, *136*, 10770–10776.

[131] Marco-Contelles, J.; Pérez-Mayoral, E.; Samadi, A.; Carreiras, M. d. C.; Soriano, E. *Chem. Rev.* **2009**, *109*, 2652–2671.

[132] Leonard, J.; Lygo, B.; Procter, G. *Advanced Practical Organic Chemistry*, 3rd ed.; CRC Press: Boca Raton, 2013; p 356.

[133] Still, W. C.; Kahn, M.; Mitra, A. *J. Org. Chem.* **1978**, *43*, 2923–2925.

[134] Fulmer, G. R.; Miller, A. J. M.; Sherden, N. H.; Gottlieb, H. E.; Nudelman, A.; Stoltz, B. M.; Bercaw, J. E.; Goldberg, K. I. *Organometallics* **2010**, *29*, 2176–2179.

[135] Bruker, SMART (Version 5.62), SAINT (Version 8.18C, 2011), SHELXTL (Version 6.10), SADABS (Version V2012/1), AXS Inc., Madison, Wisconsin, USA, **2002**.

[136] Bruker, XPREP, Bruker AXS Inc., Madison, Wisconsin, USA, **2007**.

[137] Sheldrick, G. M. *Acta Crystallogr. Sect. A* **1990**, *46*, 467–473.

[138] Hübschle, C. B.; Sheldrick, G. M.; Dittrich, B. *J. Appl. Cryst.* **2011**, *44*, 1281–1284.

[139] Basel, Y.; Hassner, A. *Synthesis* **2001**, *4*, 550–552.

[140] Herres-Pawlis, S.; Flörke, U.; Henkel, G. *Eur. J. Inorg. Chem.* **2005**, *2005*, 3815–3824.

[141] Herres-Pawlis, S.; Neuba, A.; Seewald, O.; Seshadri, T.; Egold, H.; Flörke, U.; Henkel, G. *European J. Org. Chem.* **2005**, *2005*, 4879–4890.

[142] Brauer, G. *Handbuch der präparativen anorganischen Chemie. Bd. III*, 3rd ed.; Ferdinand Enke Verlag: Stuttgart, 1981; p 2113.

A. NMR Data

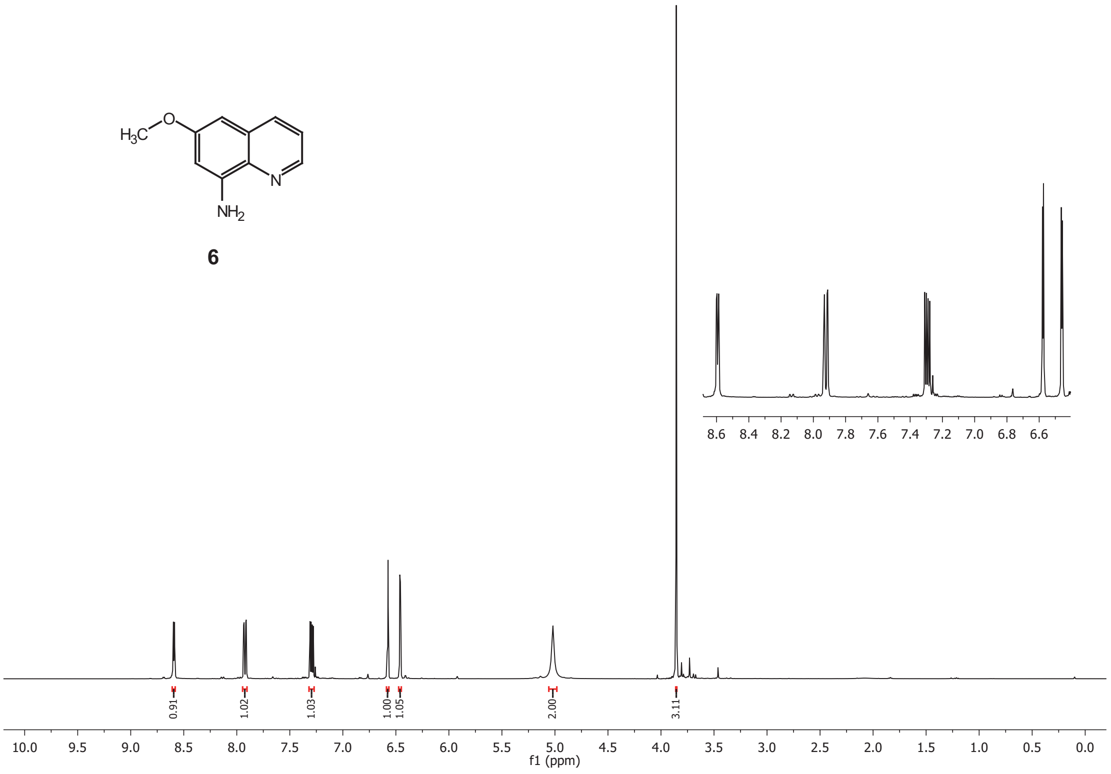
H3C
O
N
NH2
6
8.6 8.4 8.2 8.0 7.8 7.6 7.4 7.2 7.0 6.8 6.6
0.91
1.02
1.03
1.00
1.05
2.00
3.11
10.0 9.5 9.0 8.5 8.0 7.5 7.0 6.5 6.0 5.5 5.0 4.5 4.0 3.5 3.0 2.5 2.0 1.5 1.0 0.5 0.0
f1 (ppm)

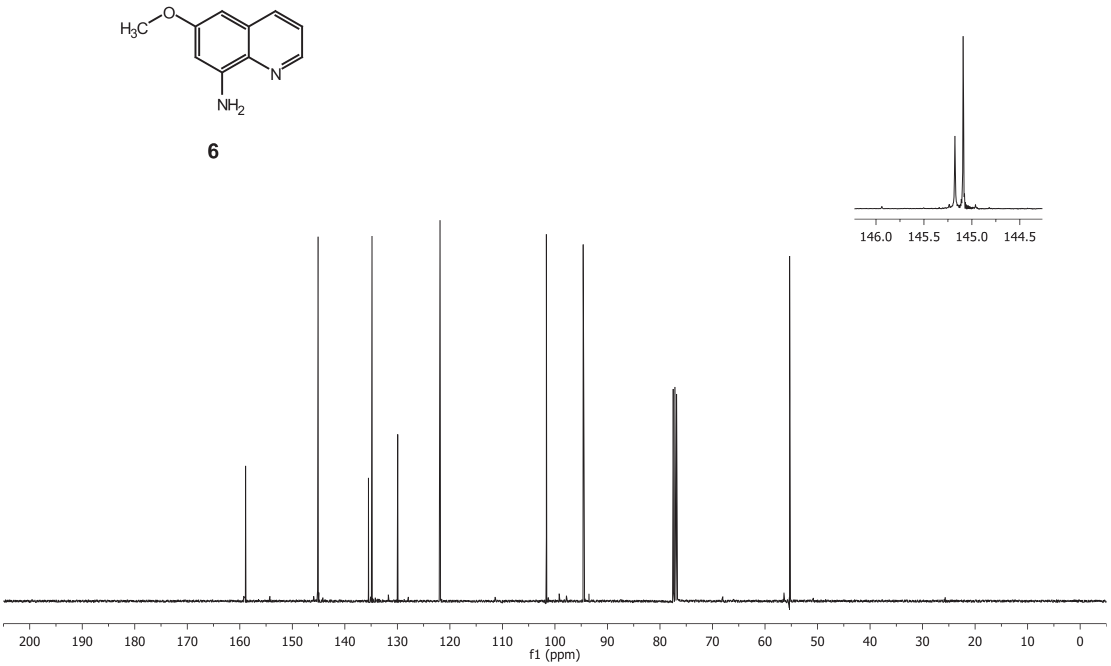
H3C
O
N
NH2
6
146.0 145.5 145.0 144.5
200 190 180 170 160 150 140 130 120 110 100 90 80 70 60 50 40 30 20 10 0
f1 (ppm)

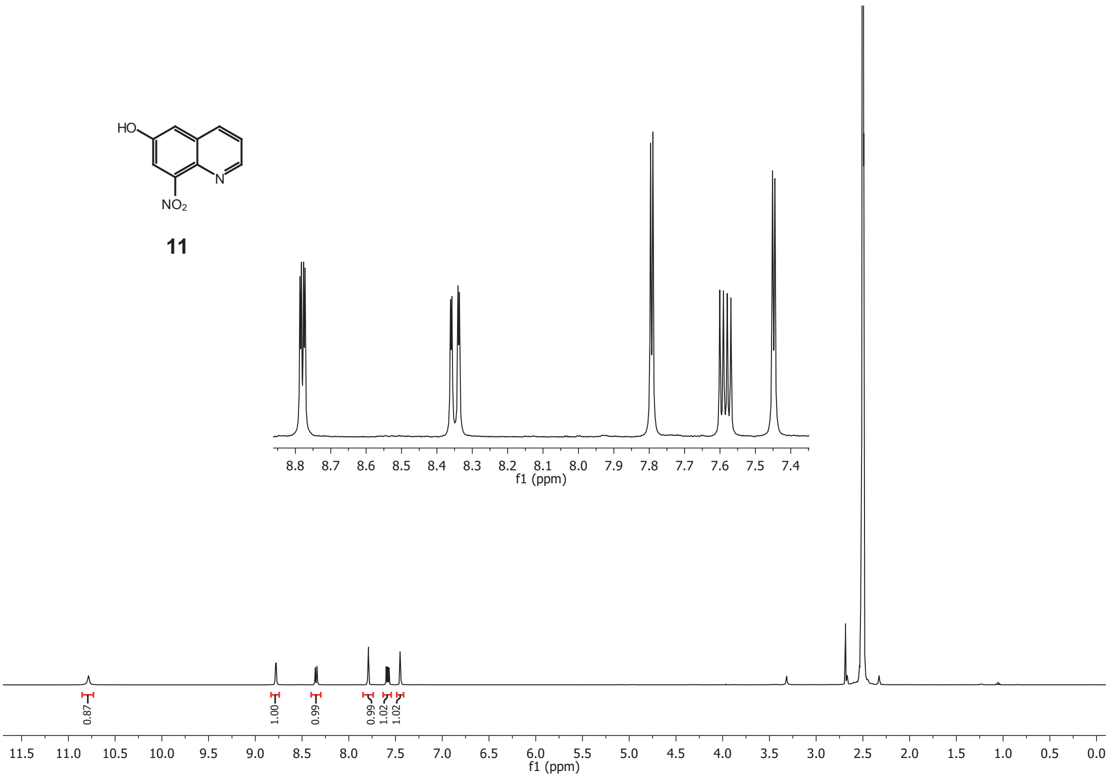
HO
N
NO2
8.8
8.7
8.6
8.5
8.4
8.3
8.2
8.1
8.0
7.9
7.8
7.7
7.6
7.5
7.4
f1 (ppm)
0.87
1.00
0.99
0.99
1.02
1.02
11.5
11.0
10.5
10.0
9.5
9.0
8.5
8.0
7.5
7.0
6.5
6.0
5.5
5.0
4.5
4.0
3.5
3.0
2.5
2.0
1.5
1.0
0.5
0.0
f1 (ppm)

11

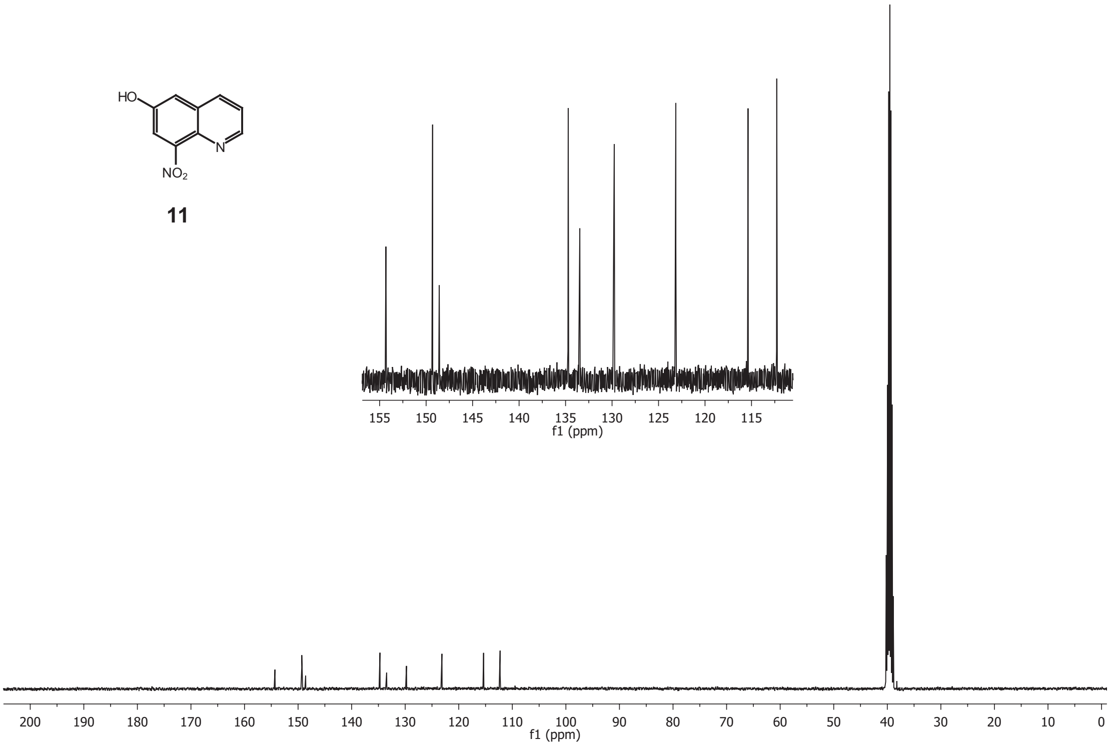
HO
N
NO2
155
150
145
140
135
130
125
120
115
f1 (ppm)
200
190
180
170
160
150
140
130
120
110
100
90
80
70
60
50
40
30
20
10
0
f1 (ppm)

11

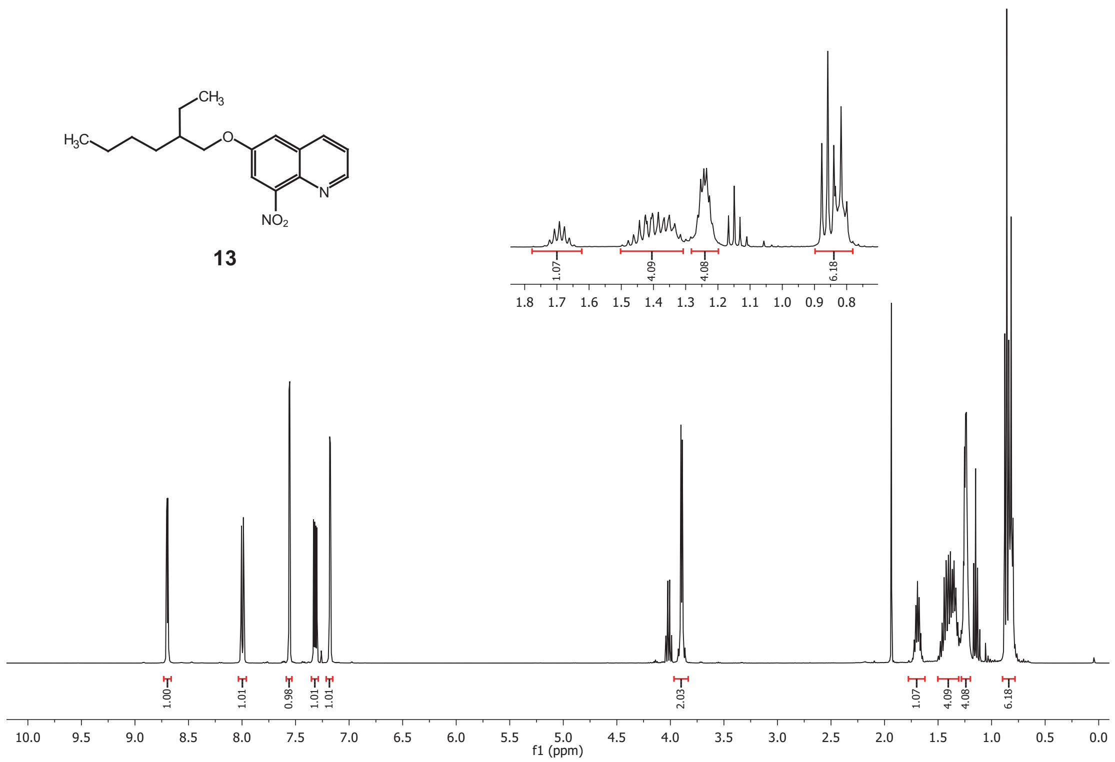
13
CH3
H3C
O
N
NO2
1.07
4.09
4.08
6.18
1.8 1.7 1.6 1.5 1.4 1.3 1.2 1.1 1.0 0.9 0.8
1.00
1.01
0.98
1.01
1.01
2.03
1.07
4.09
4.08
6.18
10.0 9.5 9.0 8.5 8.0 7.5 7.0 6.5 6.0 5.5 5.0 4.5 4.0 3.5 3.0 2.5 2.0 1.5 1.0 0.5 0.0
f1 (ppm)

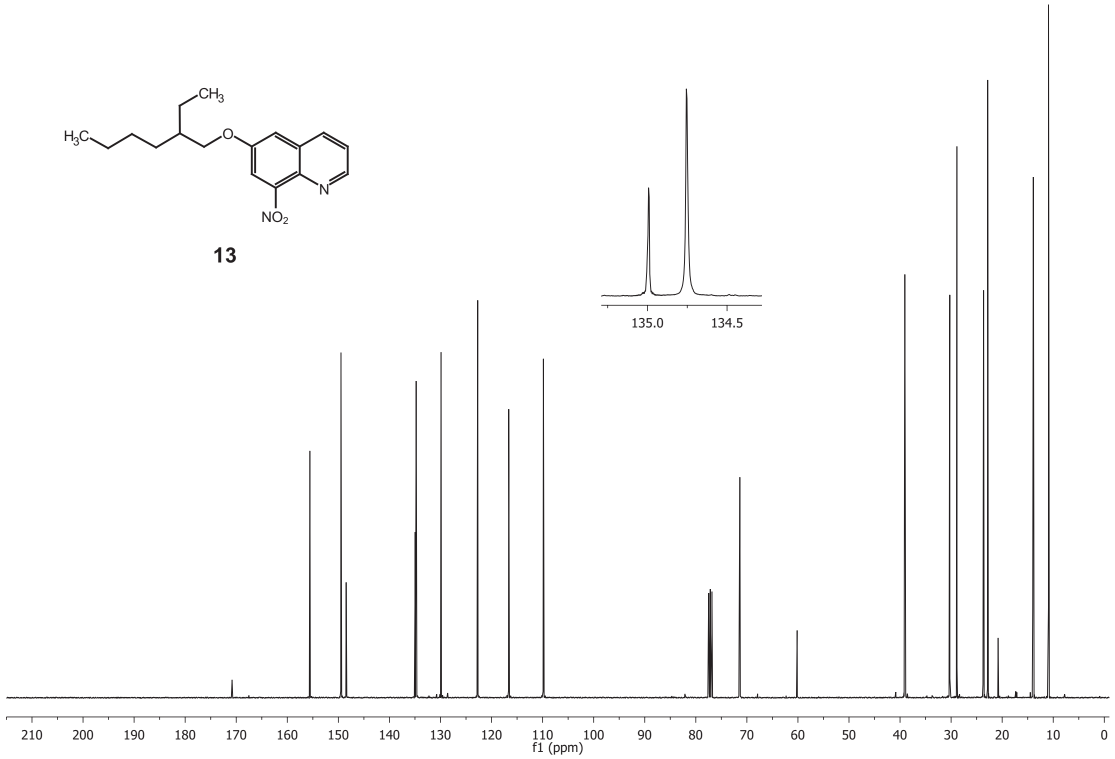
13
CH3
H3C
O
N
NO2
135.0
134.5
210 200 190 180 170 160 150 140 130 120 110 100 90 80 70 60 50 40 30 20 10 0
f1 (ppm)

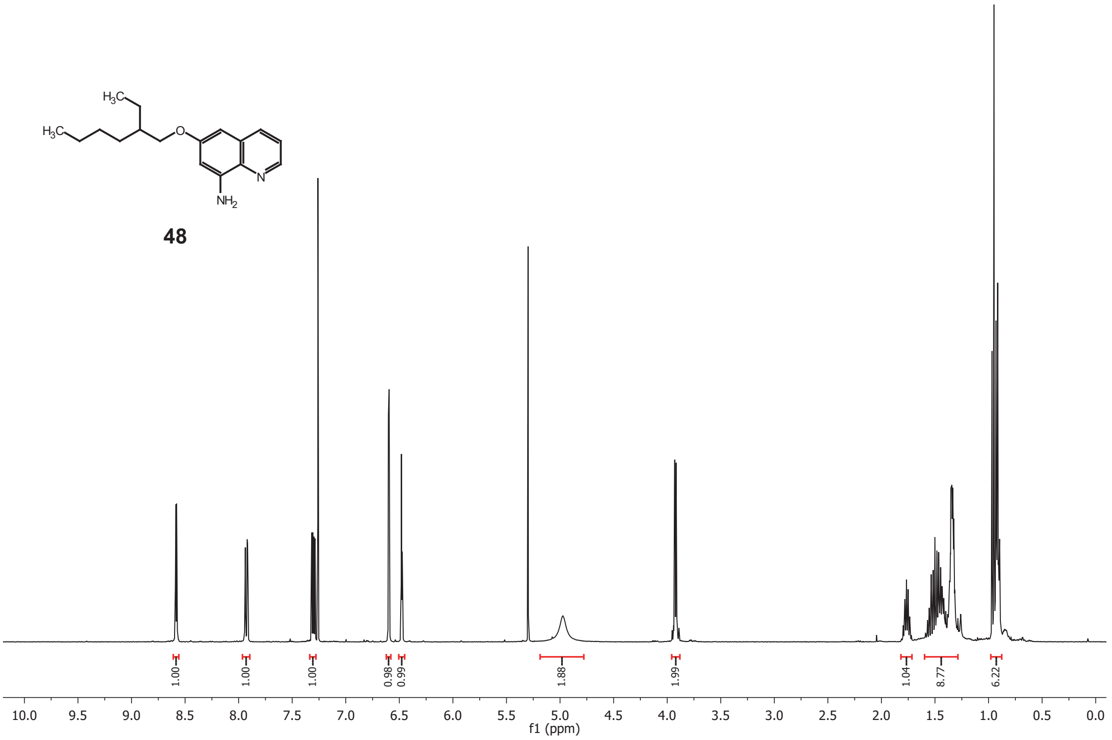

48

H$_3$C
H$_3$C
O
N
NH$_2$
1.00
1.00
1.00
0.98
0.99
1.88
1.99
1.04
8.77
6.22
10.0
9.5
9.0
8.5
8.0
7.5
7.0
6.5
6.0
5.5
5.0
4.5
4.0
3.5
3.0
2.5
2.0
1.5
1.0
0.5
0.0
f1 (ppm)

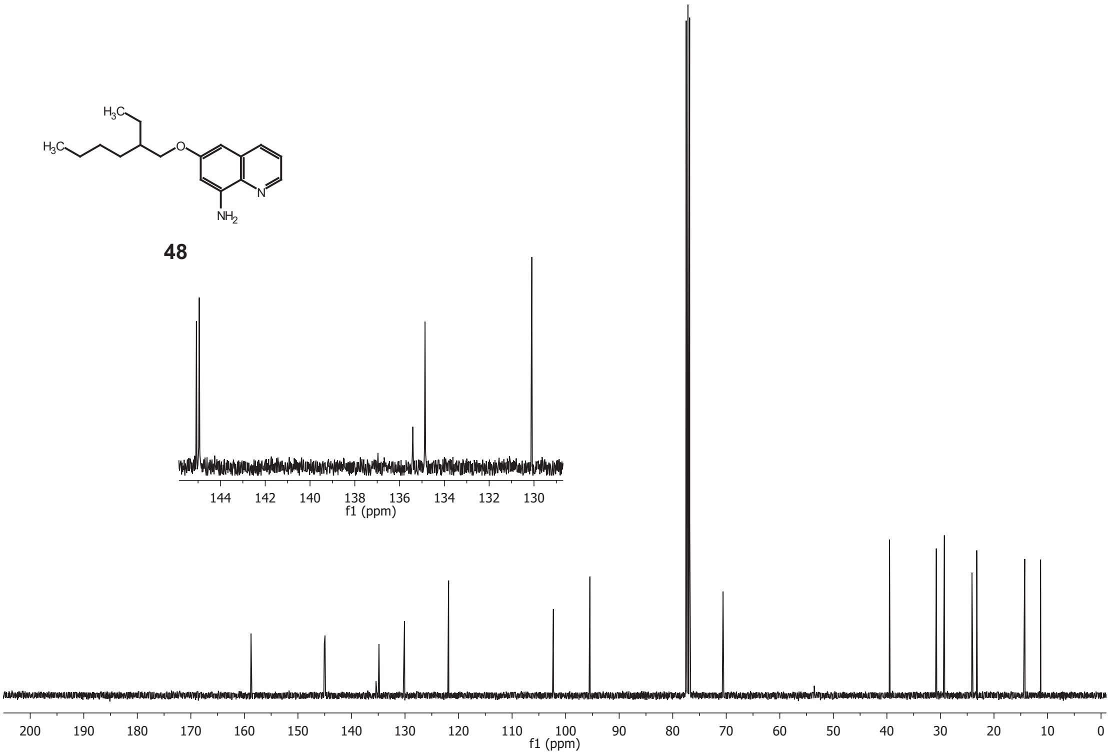

48

H$_3$C
H$_3$C
O
N
NH$_2$
144
142
140
138
136
134
132
130
f1 (ppm)
200
190
180
170
160
150
140
130
120
110
100
90
80
70
60
50
40
30
20
10
0
f1 (ppm)

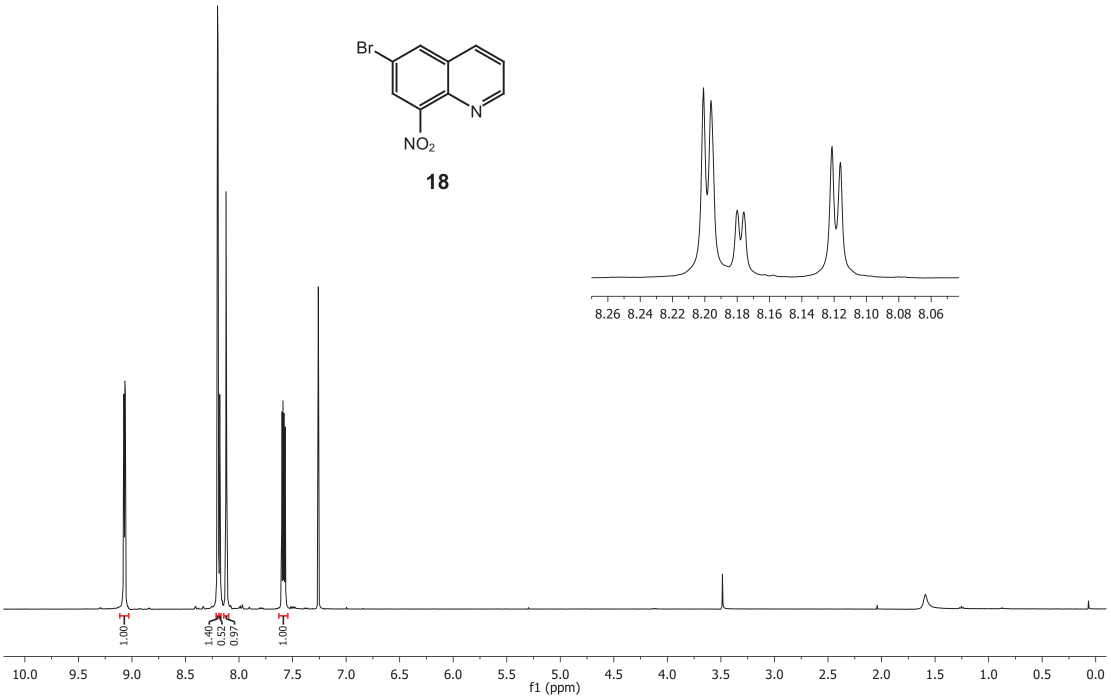
Br
N
NO2
8.26 8.24 8.22 8.20 8.18 8.16 8.14 8.12 8.10 8.08 8.06
1.00
1.40
0.52
0.97
1.00
10.0 9.5 9.0 8.5 8.0 7.5 7.0 6.5 6.0 5.5 5.0 4.5 4.0 3.5 3.0 2.5 2.0 1.5 1.0 0.5 0.0
f1 (ppm)

18

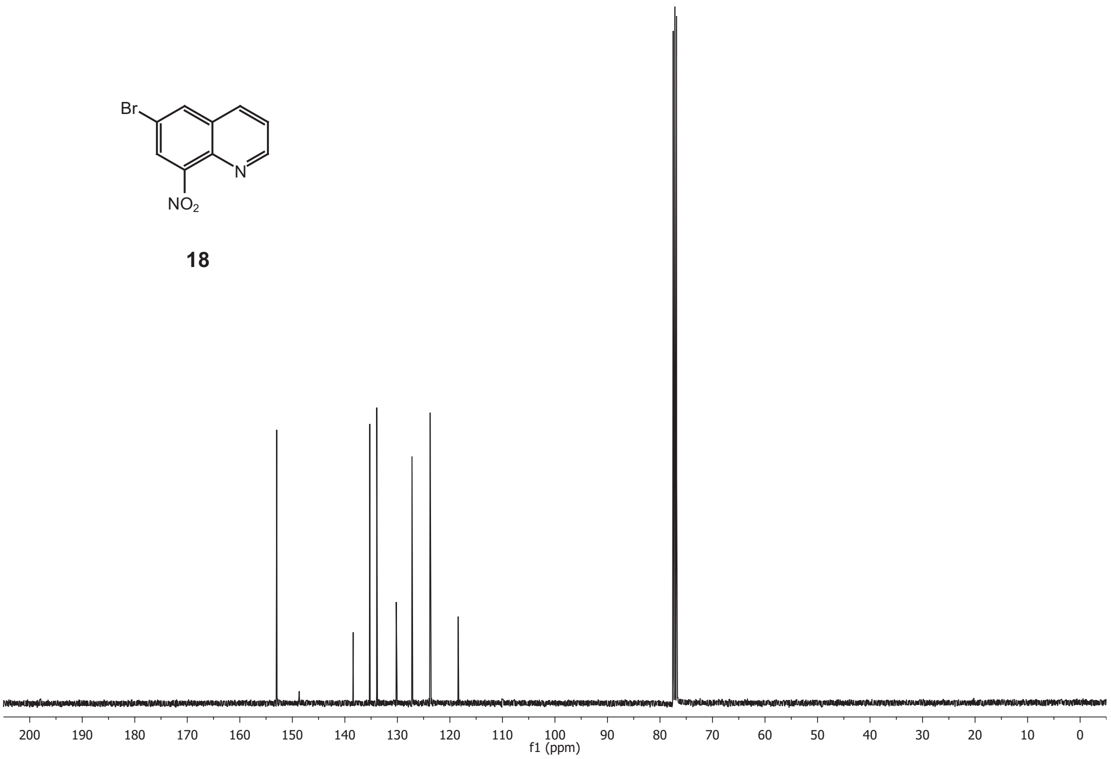
Br
N
NO2
200 190 180 170 160 150 140 130 120 110 100 90 80 70 60 50 40 30 20 10 0
f1 (ppm)

18

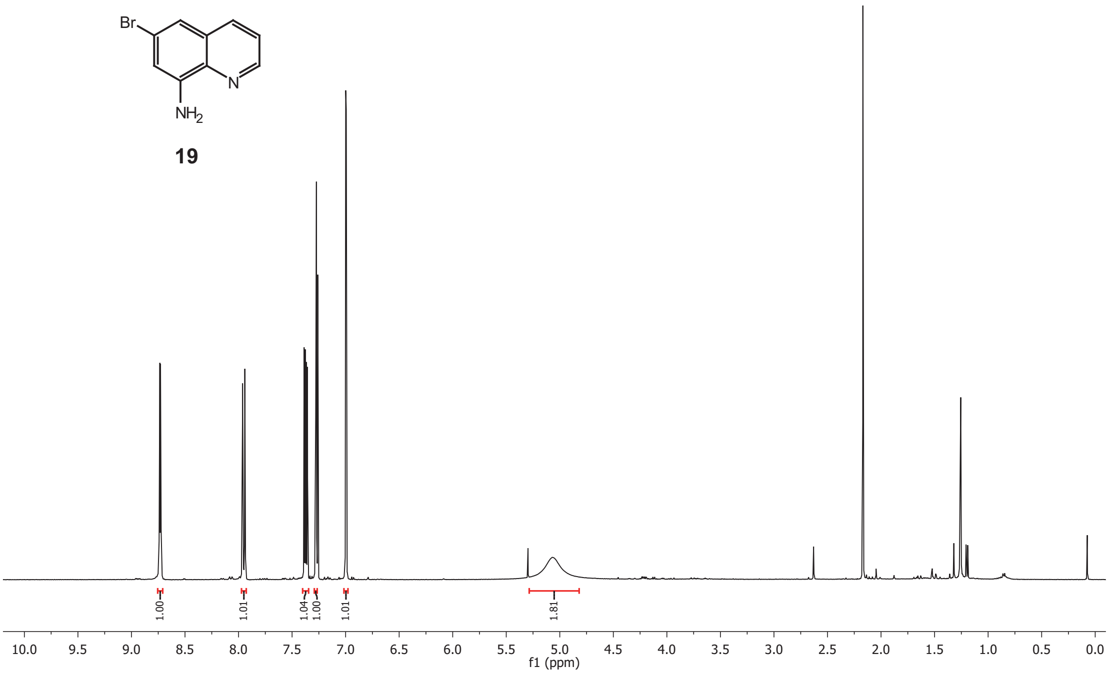
Br
N
NH2
1.00
1.01
1.04
1.00
1.01
1.81
10.0 9.5 9.0 8.5 8.0 7.5 7.0 6.5 6.0 5.5 5.0 4.5 4.0 3.5 3.0 2.5 2.0 1.5 1.0 0.5 0.0
f1 (ppm)

19

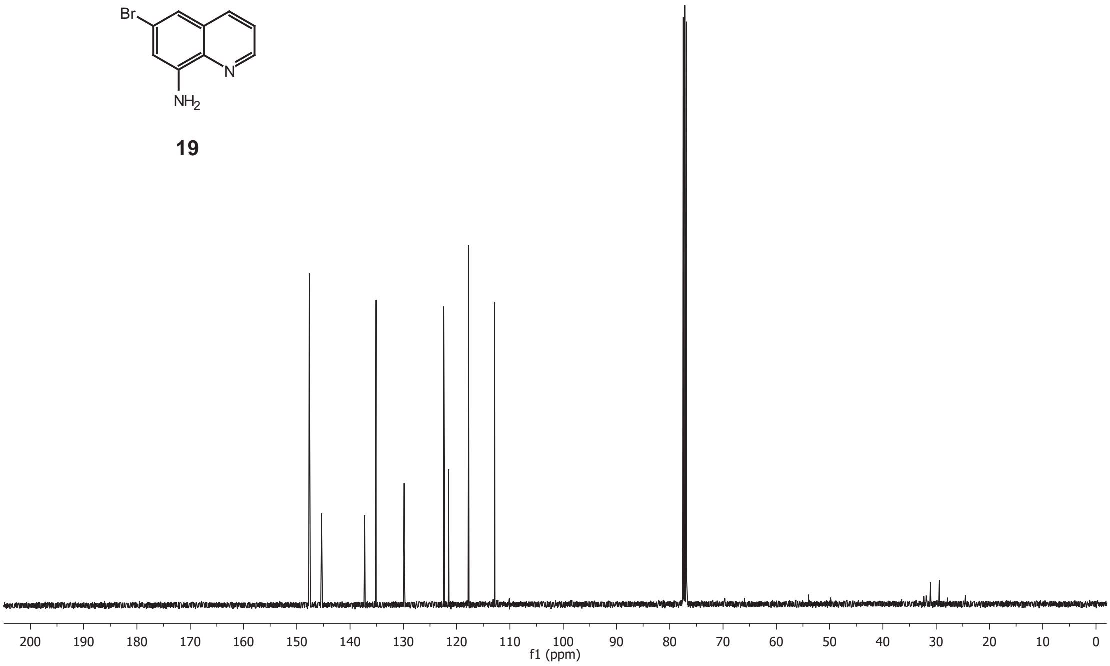
Br
N
NH2
200 190 180 170 160 150 140 130 120 110 100 90 80 70 60 50 40 30 20 10 0
f1 (ppm)

19

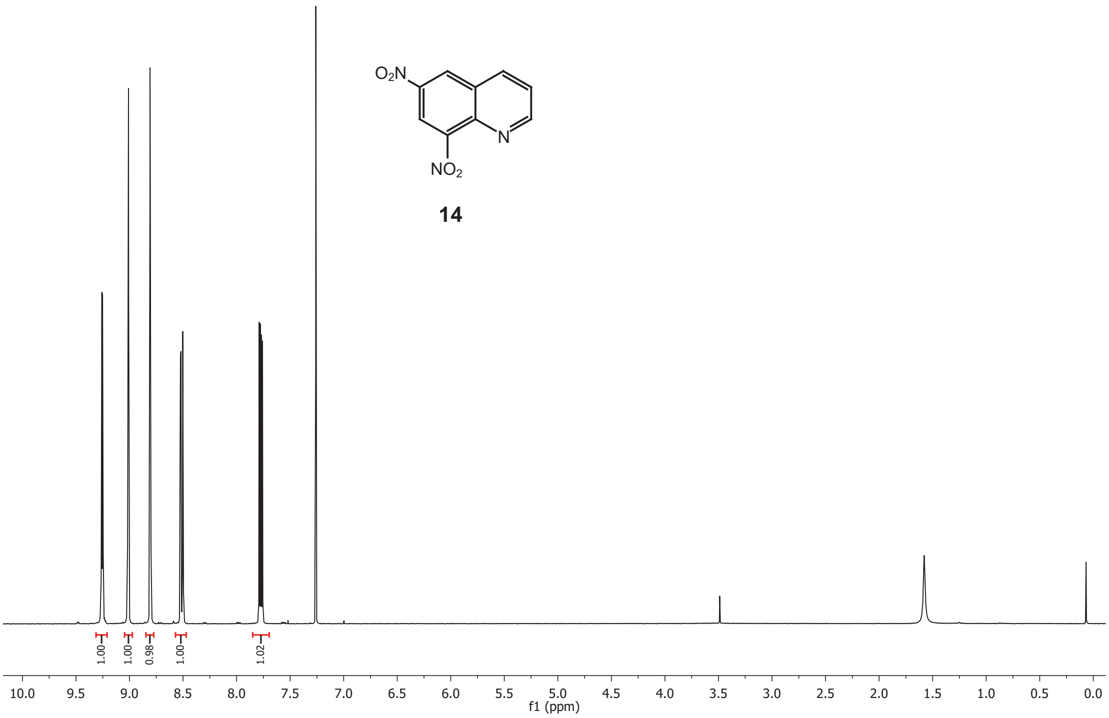
O$_2$N
N
NO$_2$
14
1.00
1.00
0.98
1.00
1.02
10.0 9.5 9.0 8.5 8.0 7.5 7.0 6.5 6.0 5.5 5.0 4.5 4.0 3.5 3.0 2.5 2.0 1.5 1.0 0.5 0.0
f1 (ppm)

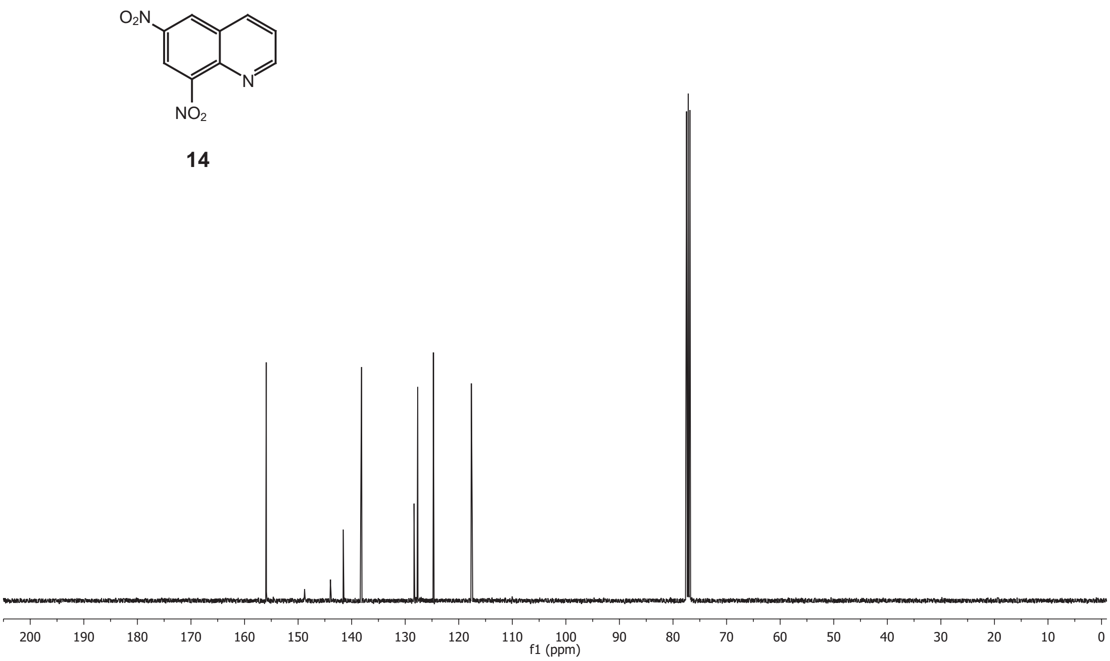
O$_2$N
N
NO$_2$
14
200 190 180 170 160 150 140 130 120 110 100 90 80 70 60 50 40 30 20 10 0
f1 (ppm)

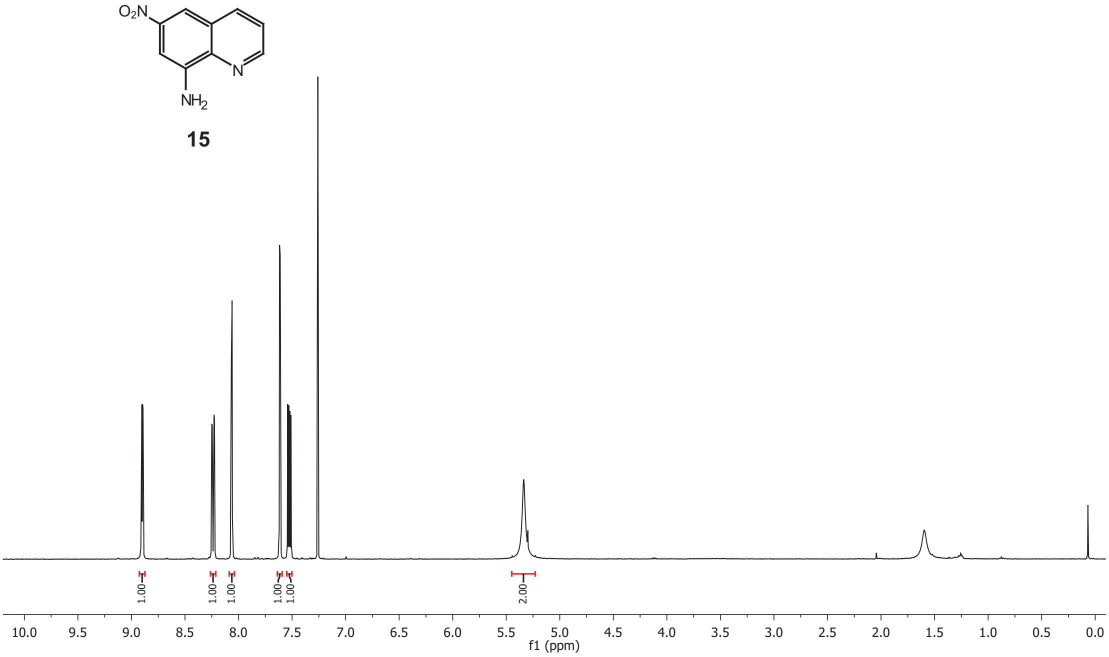
O2N
N
NH2
1.00
1.00
1.00
1.00
1.00
2.00
10.0 9.5 9.0 8.5 8.0 7.5 7.0 6.5 6.0 5.5 5.0 4.5 4.0 3.5 3.0 2.5 2.0 1.5 1.0 0.5 0.0
f1 (ppm)

15

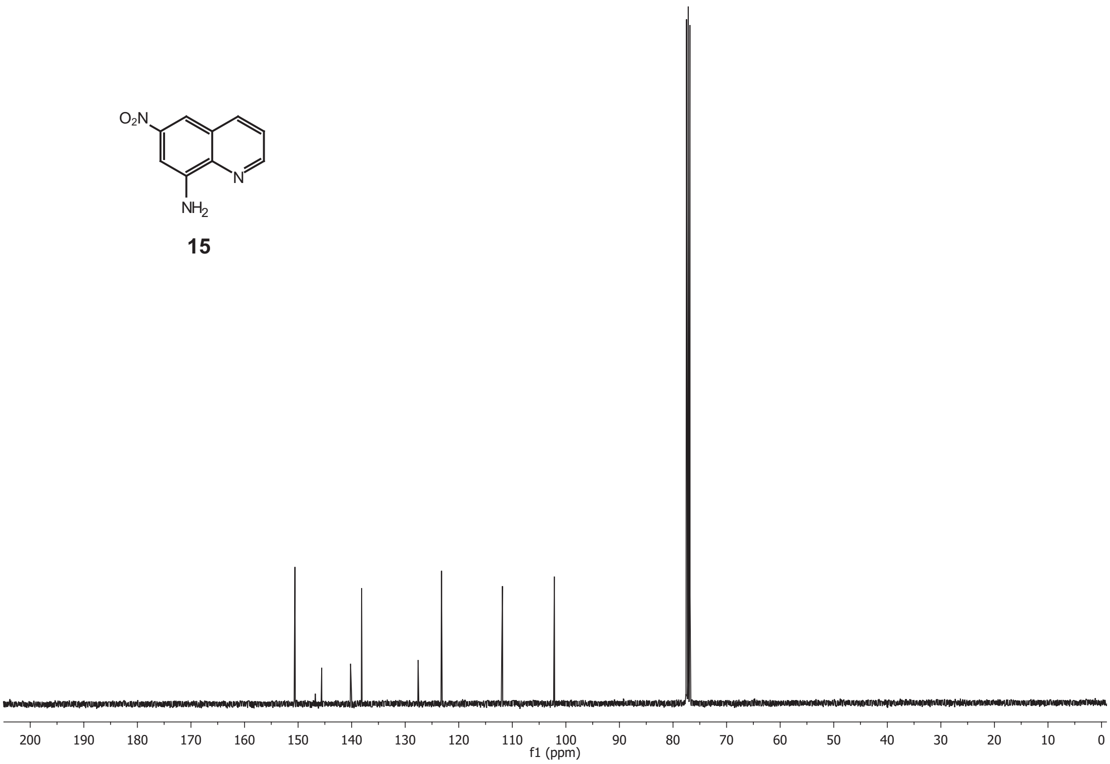
O2N
N
NH2
200 190 180 170 160 150 140 130 120 110 100 90 80 70 60 50 40 30 20 10 0
f1 (ppm)

15

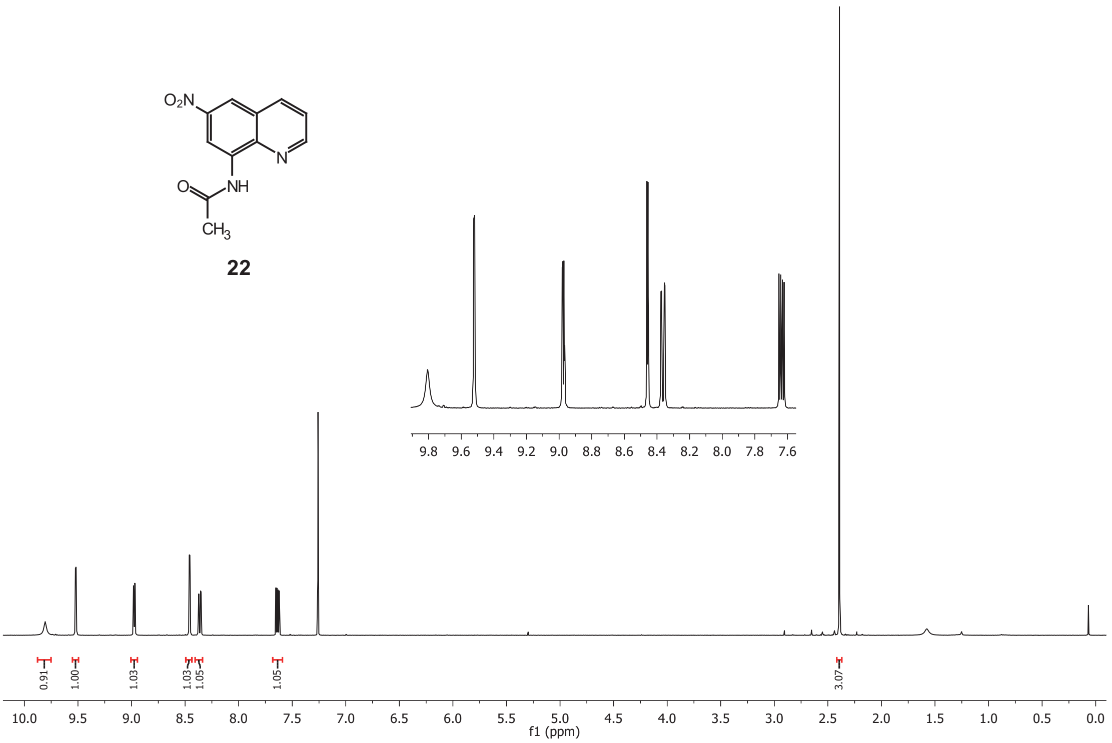
O₂N
NH
N
O
CH₃
9.8 9.6 9.4 9.2 9.0 8.8 8.6 8.4 8.2 8.0 7.8 7.6
0.91
1.00
1.03
1.03
1.05
1.05
3.07
10.0 9.5 9.0 8.5 8.0 7.5 7.0 6.5 6.0 5.5 5.0 4.5 4.0 3.5 3.0 2.5 2.0 1.5 1.0 0.5 0.0
f1 (ppm)

22

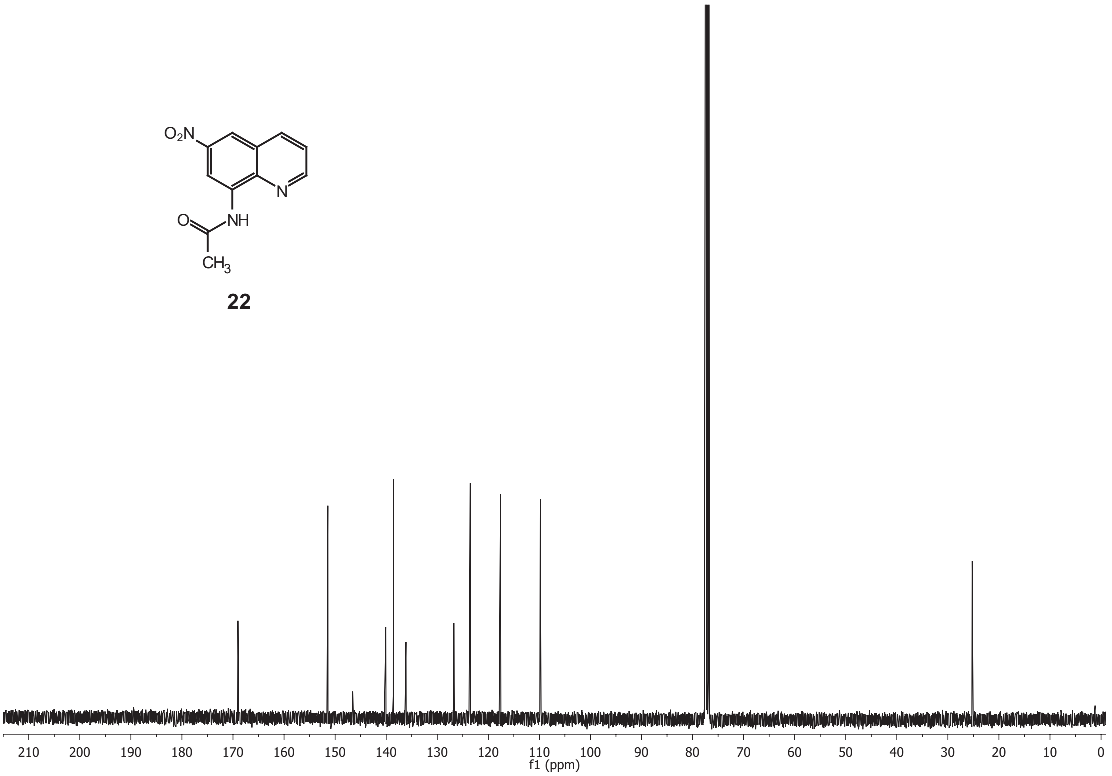
O₂N
NH
N
O
CH₃
210 200 190 180 170 160 150 140 130 120 110 100 90 80 70 60 50 40 30 20 10 0
f1 (ppm)

22

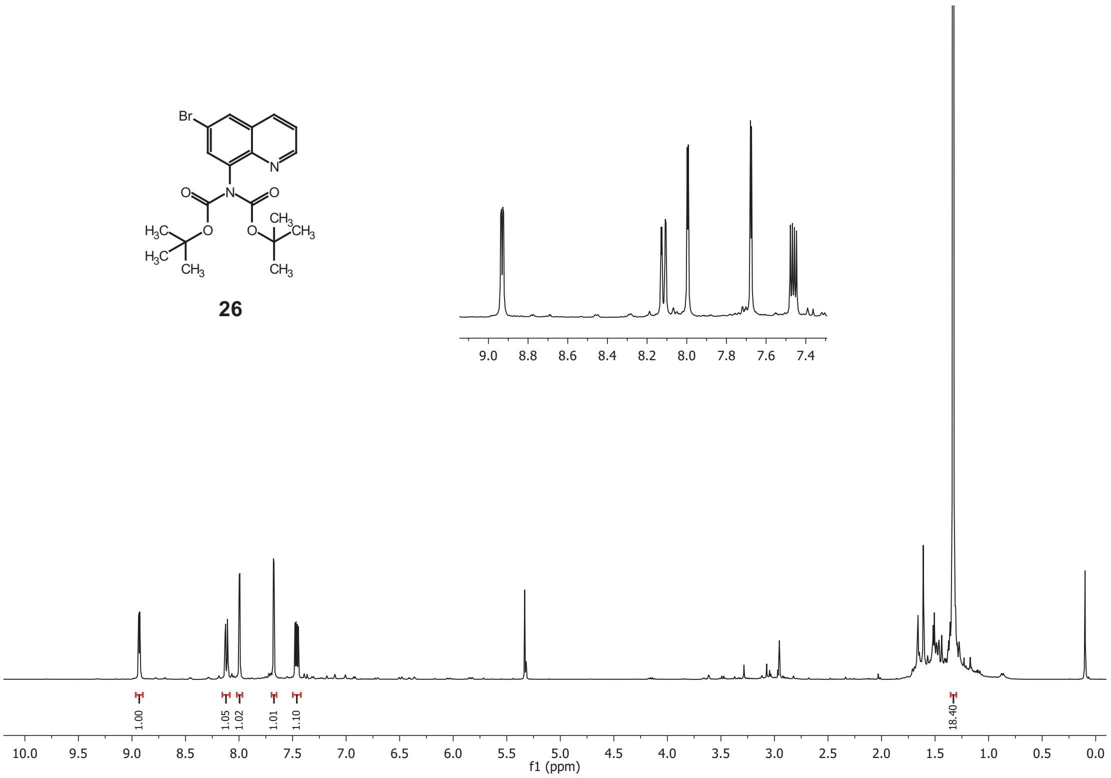
Br
N
O
O
O
O
H3C
H3C
CH3
CH3
CH3
CH3
26
9.0 8.8 8.6 8.4 8.2 8.0 7.8 7.6 7.4
1.00
1.05
1.02
1.01
1.10
18.40
10.0 9.5 9.0 8.5 8.0 7.5 7.0 6.5 6.0 5.5 5.0 4.5 4.0 3.5 3.0 2.5 2.0 1.5 1.0 0.5 0.0
f1 (ppm)

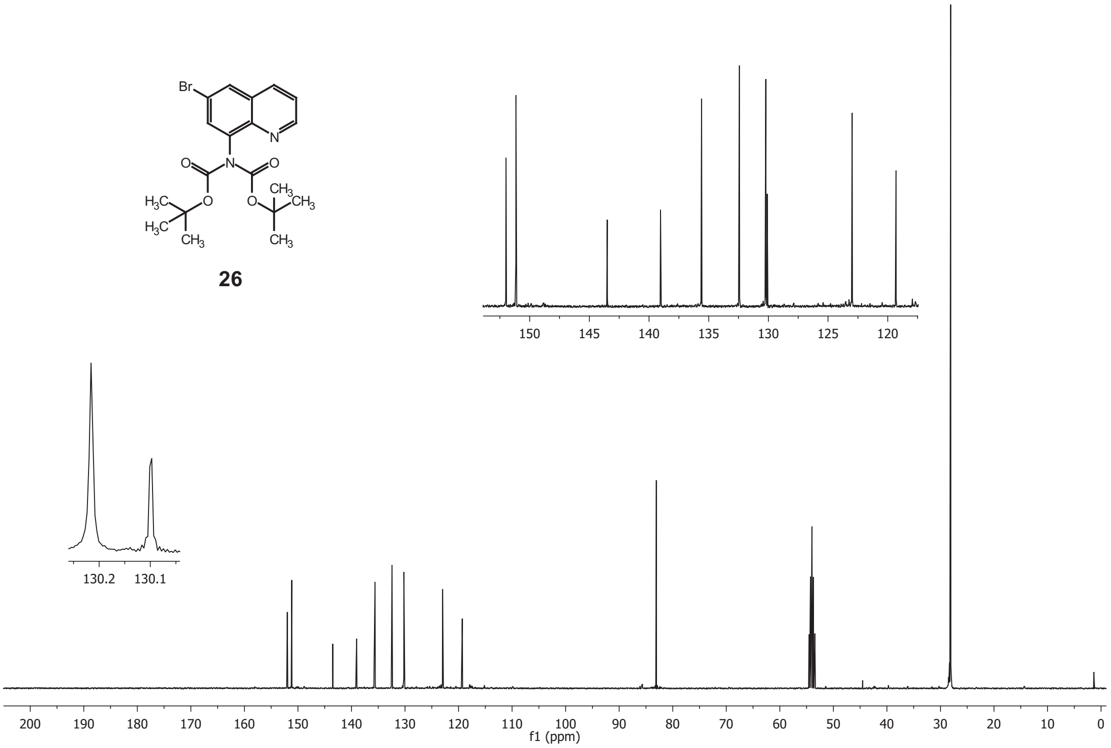
Br
N
O
O
O
O
H3C
H3C
CH3
CH3
CH3
CH3
26
150 145 140 135 130 125 120
130.2 130.1
200 190 180 170 160 150 140 130 120 110 100 90 80 70 60 50 40 30 20 10 0
f1 (ppm)

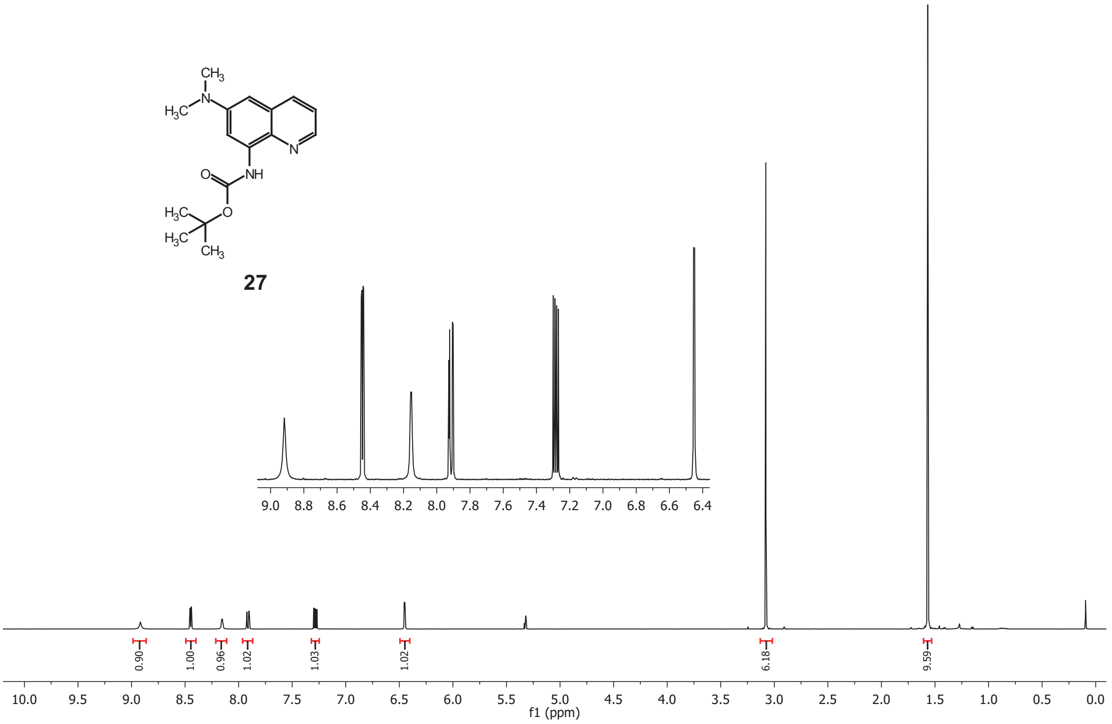
CH3
N
H3C
N
NH
O
O
H3C
H3C
CH3
9.0 8.8 8.6 8.4 8.2 8.0 7.8 7.6 7.4 7.2 7.0 6.8 6.6 6.4
0.90
1.00
0.96
1.02
1.03
1.02
6.18
9.59
10.0 9.5 9.0 8.5 8.0 7.5 7.0 6.5 6.0 5.5 5.0 4.5 4.0 3.5 3.0 2.5 2.0 1.5 1.0 0.5 0.0
f1 (ppm)

27

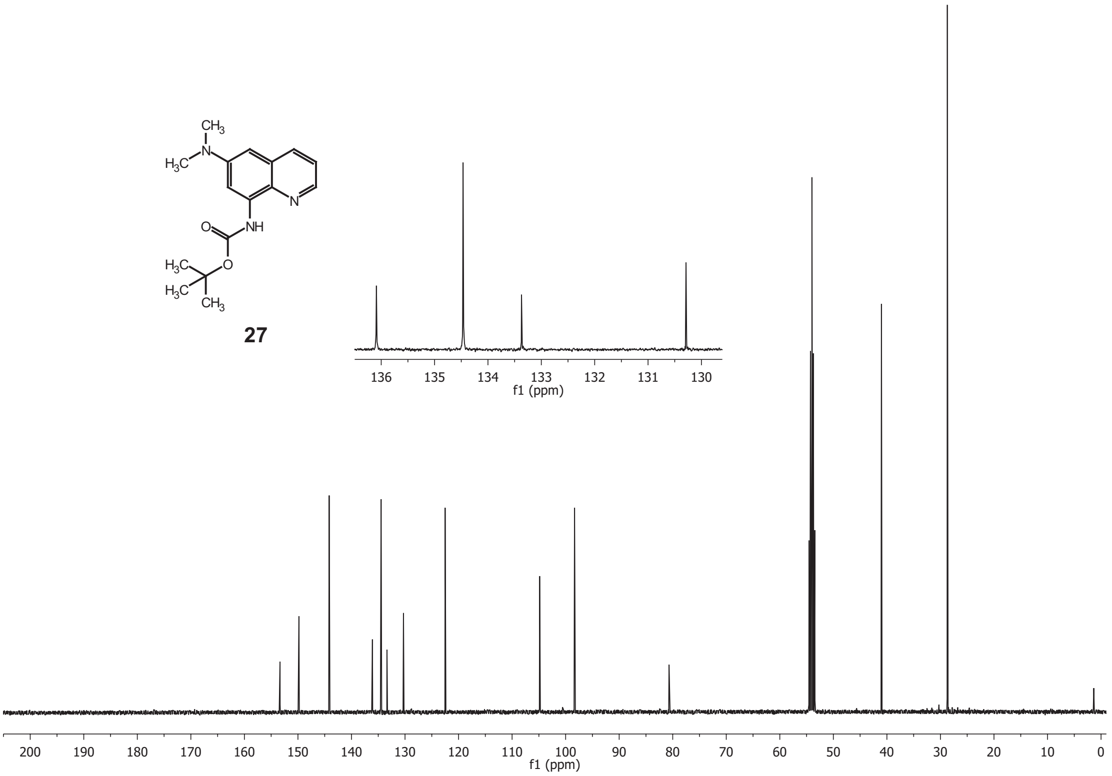
CH3
N
H3C
N
NH
O
O
H3C
H3C
CH3
136 135 134 133 132 131 130
f1 (ppm)
200 190 180 170 160 150 140 130 120 110 100 90 80 70 60 50 40 30 20 10 0
f1 (ppm)

27

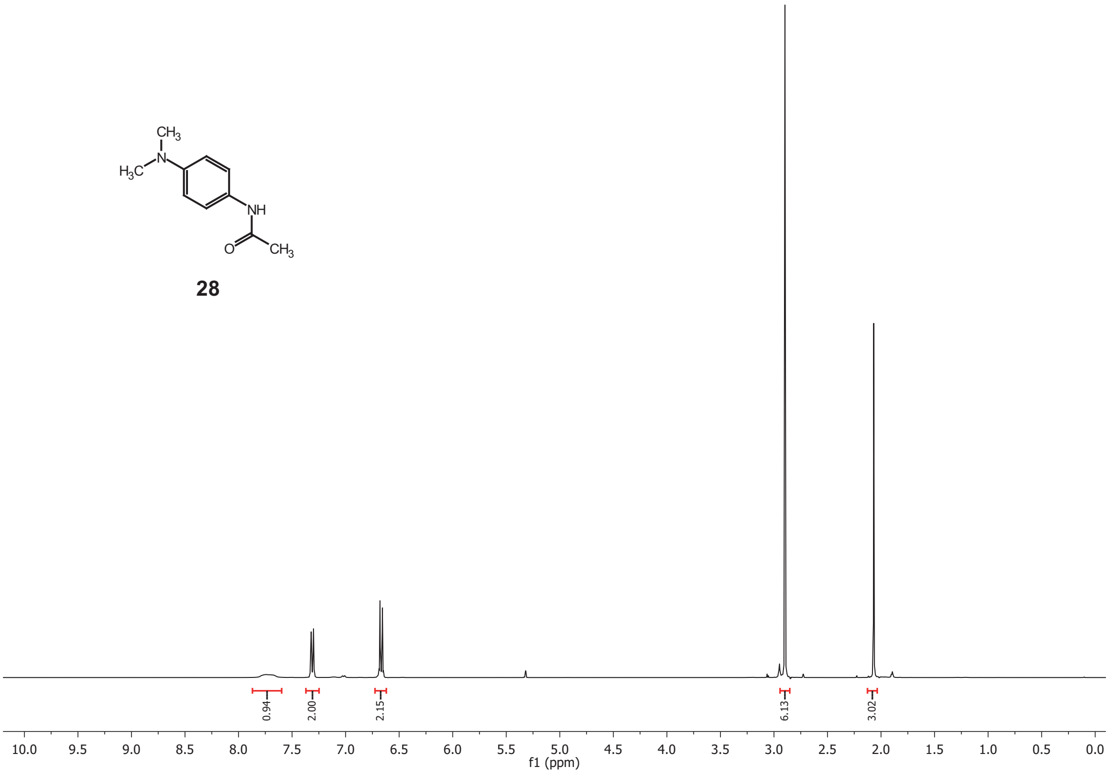

28

CH3
H3C
N
NH
O
CH3
0.94
2.00
2.15
6.13
3.02
10.0
9.5
9.0
8.5
8.0
7.5
7.0
6.5
6.0
5.5
5.0
4.5
4.0
3.5
3.0
2.5
2.0
1.5
1.0
0.5
0.0
f1 (ppm)

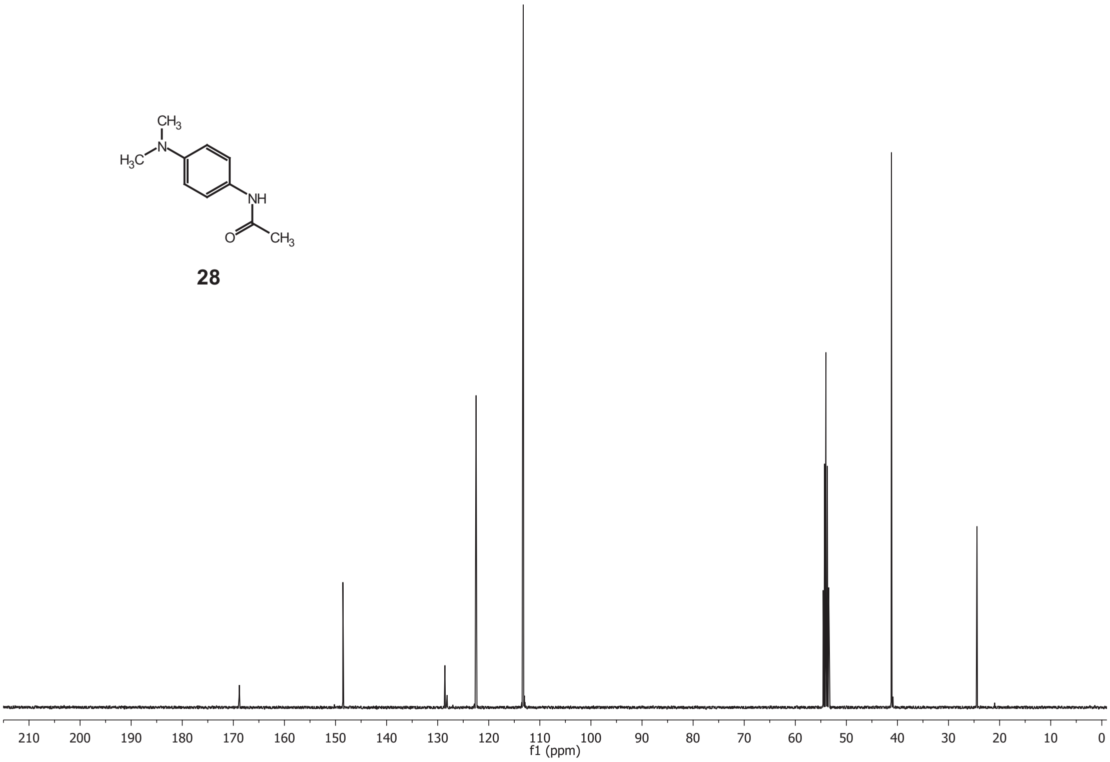

28

CH3
H3C
N
NH
O
CH3
210
200
190
180
170
160
150
140
130
120
110
100
90
80
70
60
50
40
30
20
10
0
f1 (ppm)

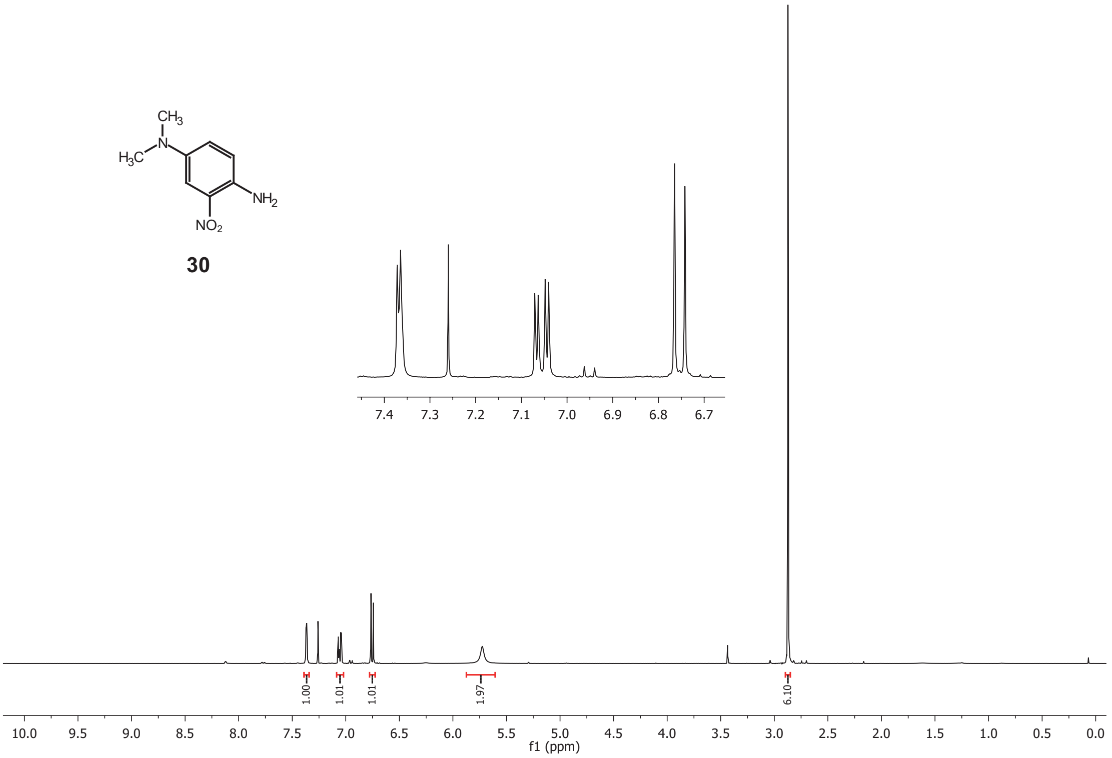

30

CH3
H3C
N
NH2
NO2
7.4 7.3 7.2 7.1 7.0 6.9 6.8 6.7
1.00
1.01
1.01
1.97
6.10
10.0 9.5 9.0 8.5 8.0 7.5 7.0 6.5 6.0 5.5 5.0 4.5 4.0 3.5 3.0 2.5 2.0 1.5 1.0 0.5 0.0
f1 (ppm)

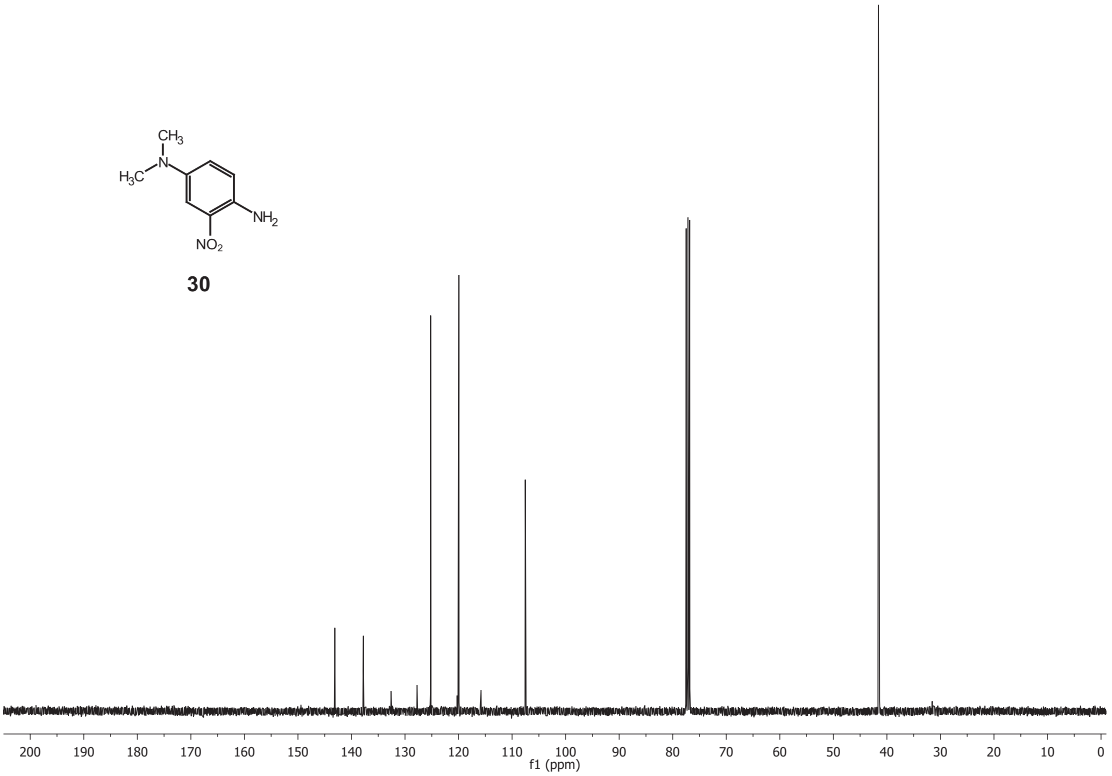

30

CH3
H3C
N
NH2
NO2
200 190 180 170 160 150 140 130 120 110 100 90 80 70 60 50 40 30 20 10 0
f1 (ppm)

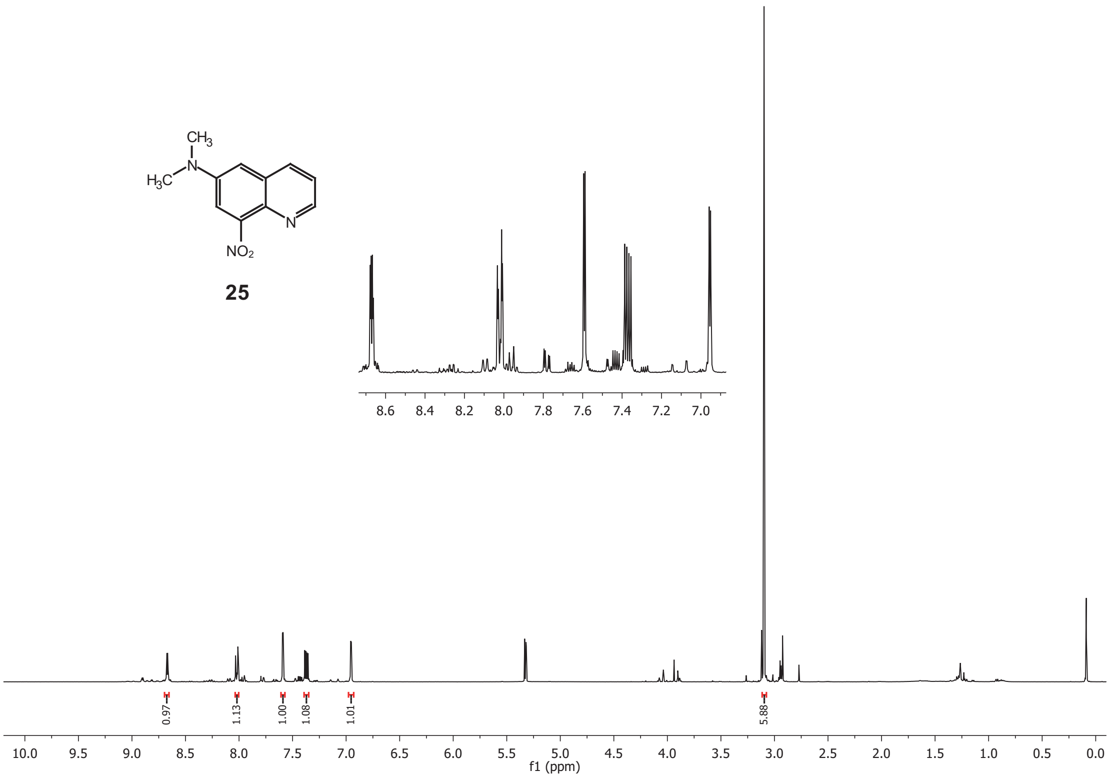
CH3
H3C
N
N
NO2
25
8.6
8.4
8.2
8.0
7.8
7.6
7.4
7.2
7.0
0.97
1.13
1.00
1.08
1.01
5.88
10.0
9.5
9.0
8.5
8.0
7.5
7.0
6.5
6.0
5.5
5.0
4.5
4.0
3.5
3.0
2.5
2.0
1.5
1.0
0.5
0.0
f1 (ppm)

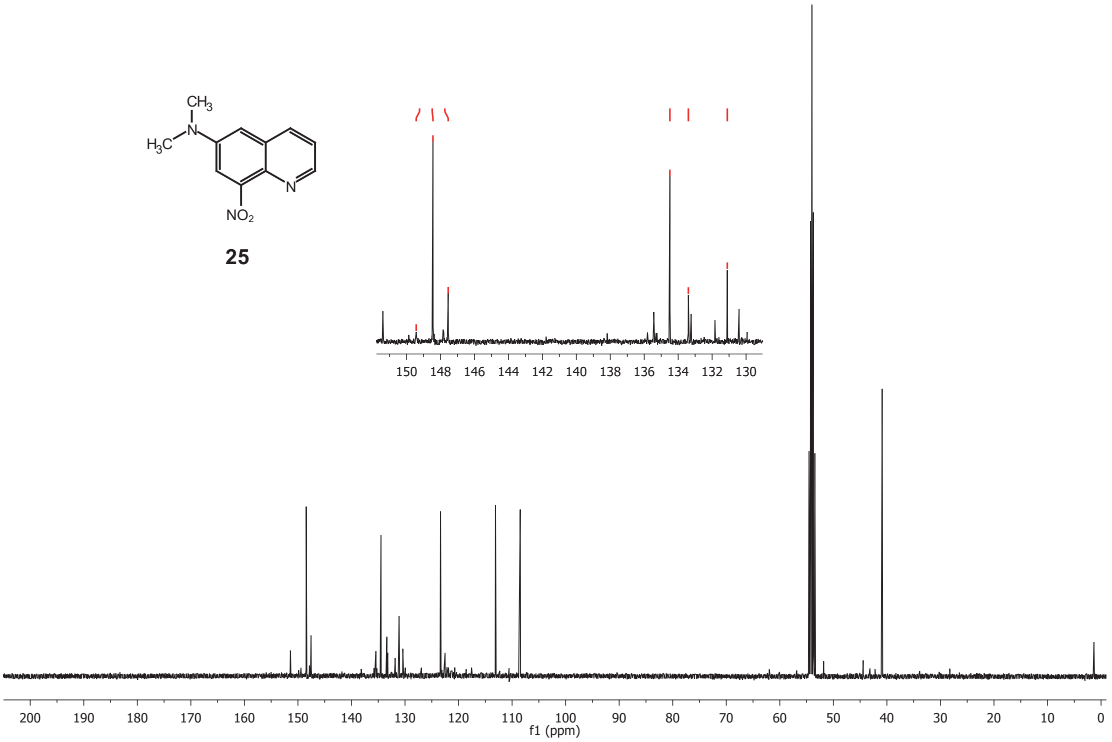
CH3
H3C
N
N
NO2
25
150
148
146
144
142
140
138
136
134
132
130
200
190
180
170
160
150
140
130
120
110
100
90
80
70
60
50
40
30
20
10
0
f1 (ppm)

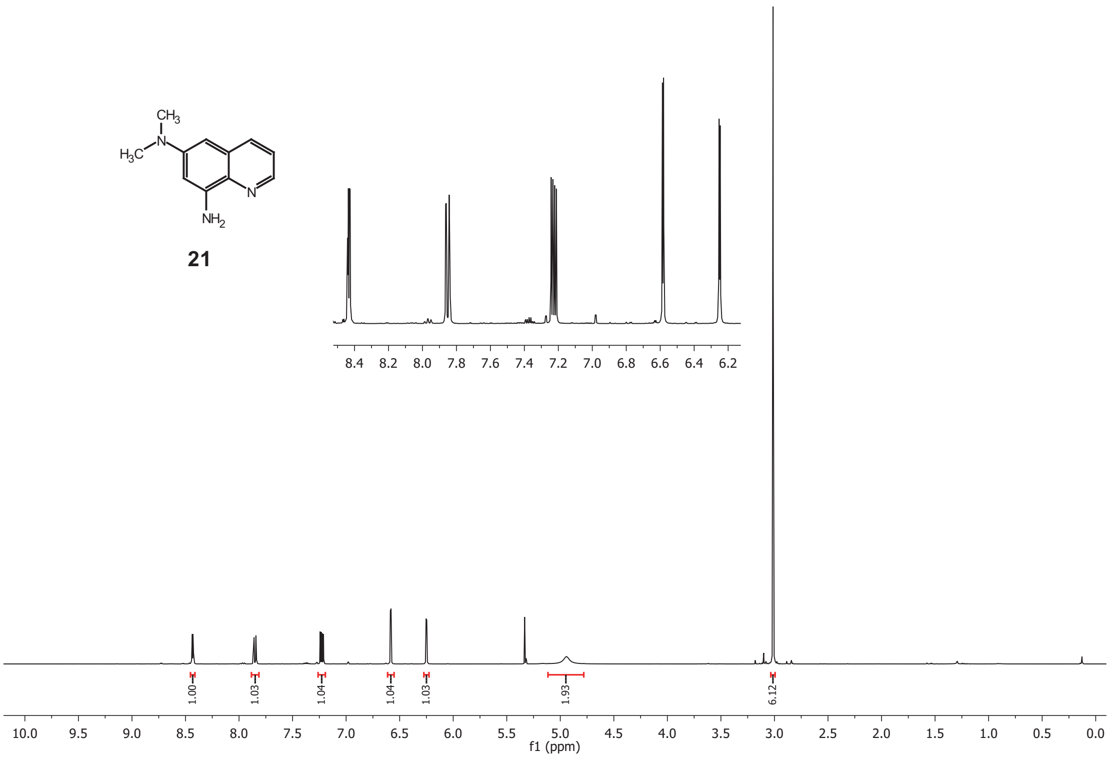

21

CH3
H3C
N
N
NH2
8.4 8.2 8.0 7.8 7.6 7.4 7.2 7.0 6.8 6.6 6.4 6.2
1.00
1.03
1.04
1.04
1.03
1.93
6.12
10.0 9.5 9.0 8.5 8.0 7.5 7.0 6.5 6.0 5.5 5.0 4.5 4.0 3.5 3.0 2.5 2.0 1.5 1.0 0.5 0.0
f1 (ppm)

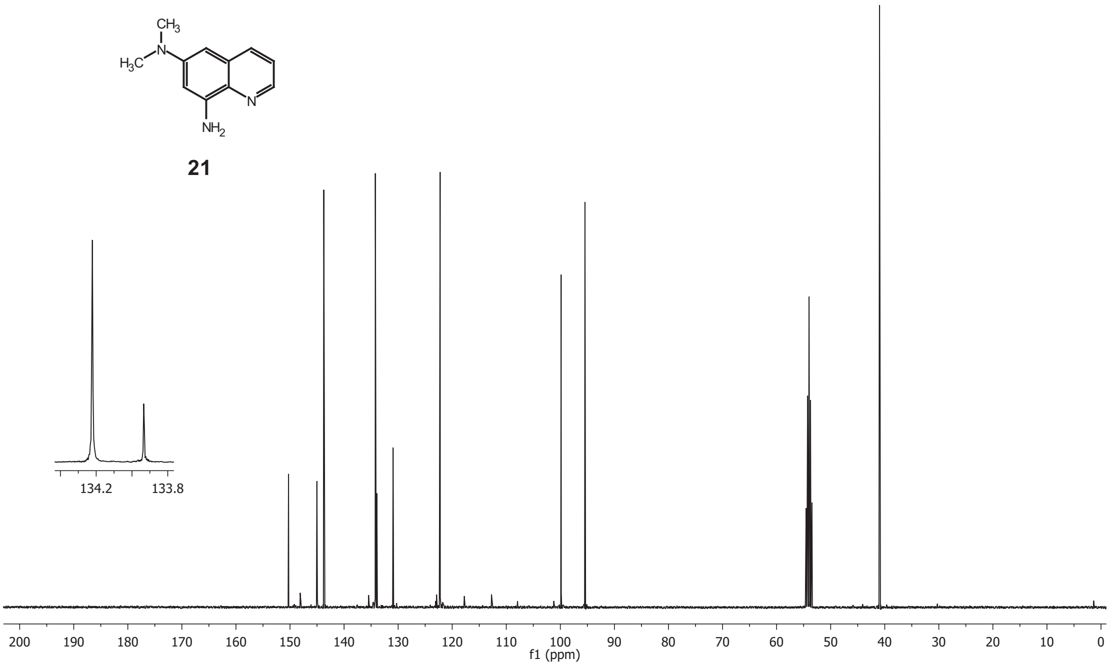

21

CH3
H3C
N
N
NH2
134.2 133.8
200 190 180 170 160 150 140 130 120 110 100 90 80 70 60 50 40 30 20 10 0
f1 (ppm)

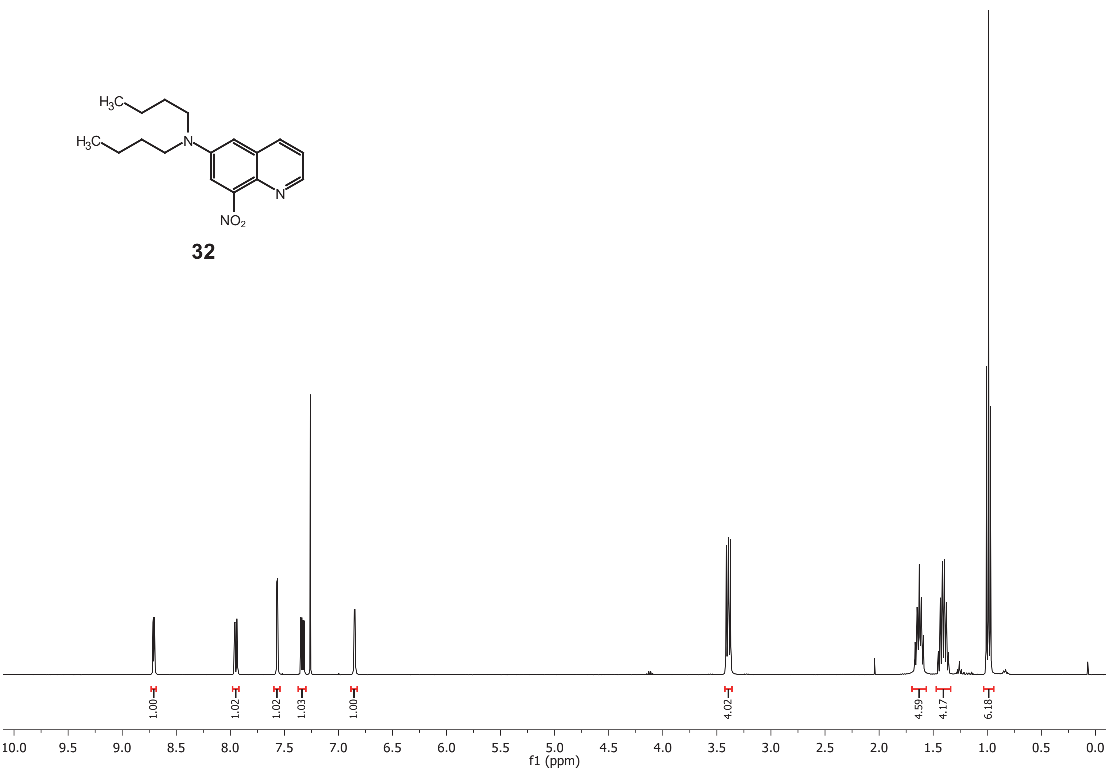
H$_3$C
H$_3$C
N
N
NO$_2$
1.00
1.02
1.02
1.03
1.00
4.02
4.59
4.17
6.18
10.0 9.5 9.0 8.5 8.0 7.5 7.0 6.5 6.0 5.5 5.0 4.5 4.0 3.5 3.0 2.5 2.0 1.5 1.0 0.5 0.0
f1 (ppm)

32

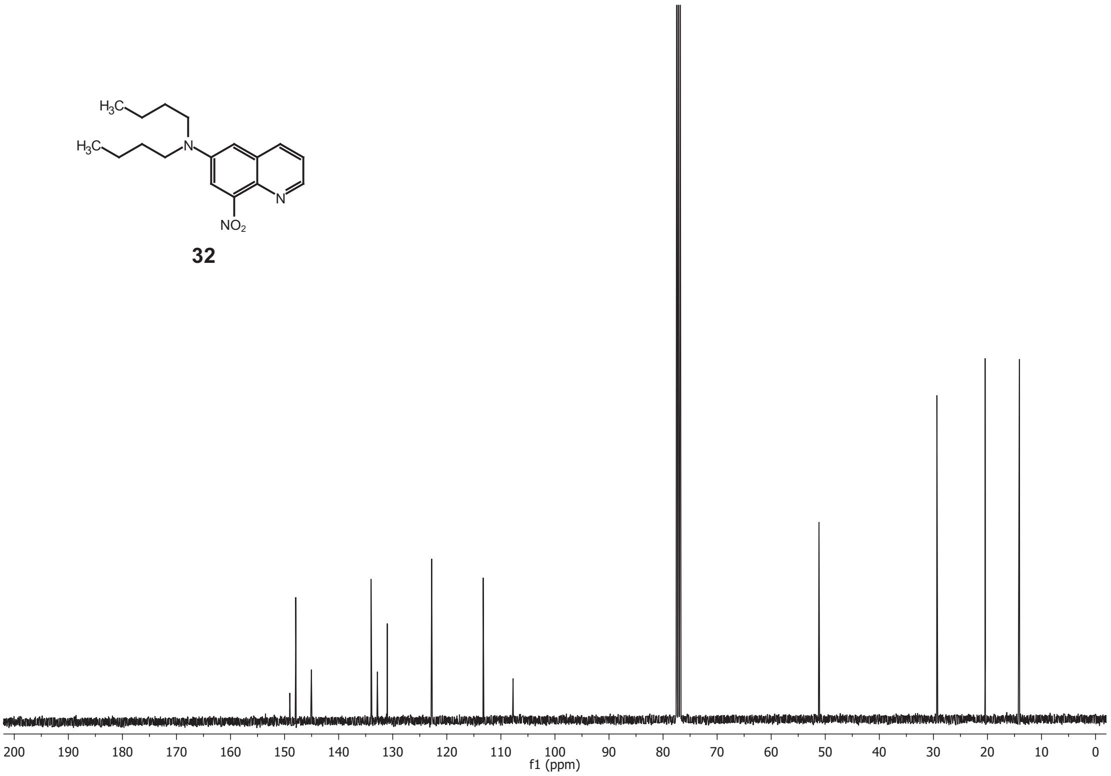
H$_3$C
H$_3$C
N
N
NO$_2$
200 190 180 170 160 150 140 130 120 110 100 90 80 70 60 50 40 30 20 10 0
f1 (ppm)

32

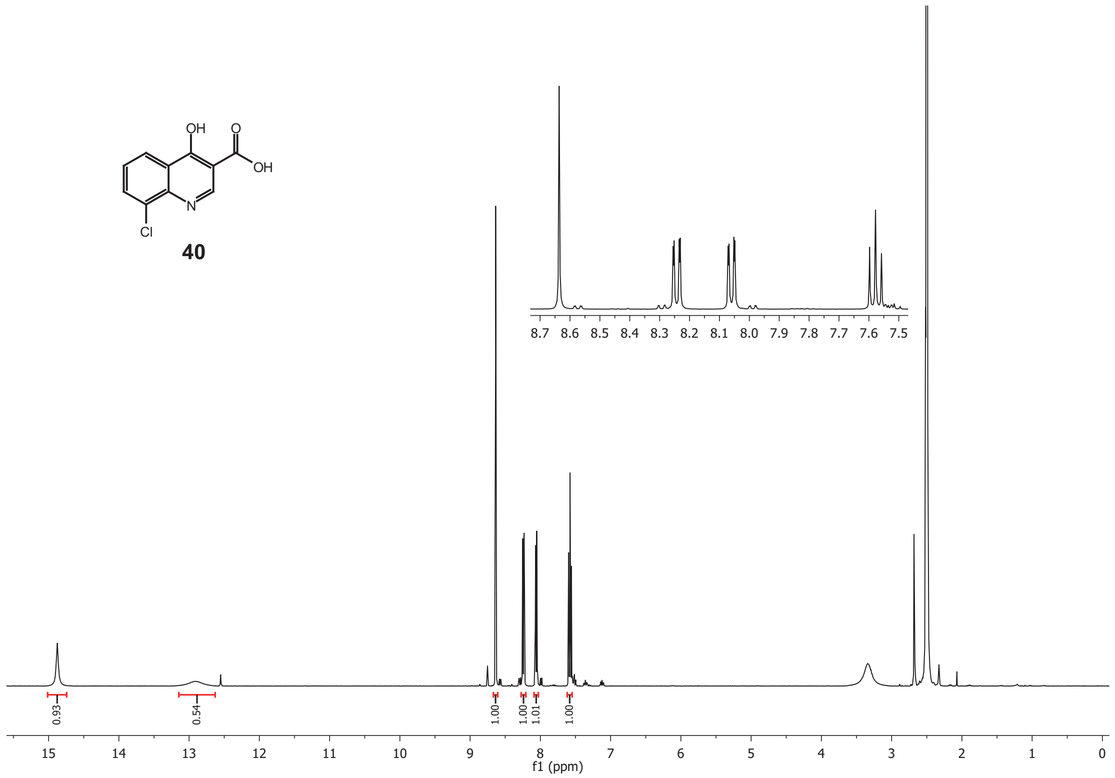
OH
O
OH
N
Cl
40
8.7 8.6 8.5 8.4 8.3 8.2 8.1 8.0 7.9 7.8 7.7 7.6 7.5
0.93
0.54
1.00
1.00
1.01
1.00
15 14 13 12 11 10 9 8 7 6 5 4 3 2 1 0
f1 (ppm)

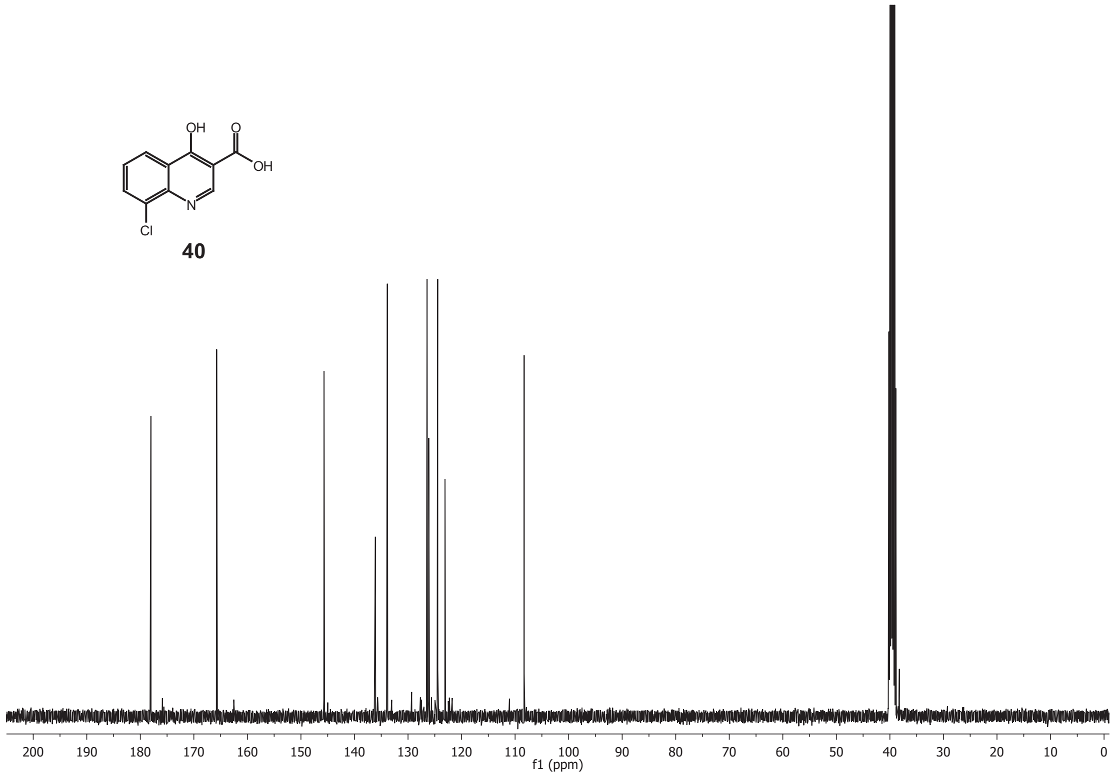
OH
O
OH
N
Cl
40
200 190 180 170 160 150 140 130 120 110 100 90 80 70 60 50 40 30 20 10 0
f1 (ppm)

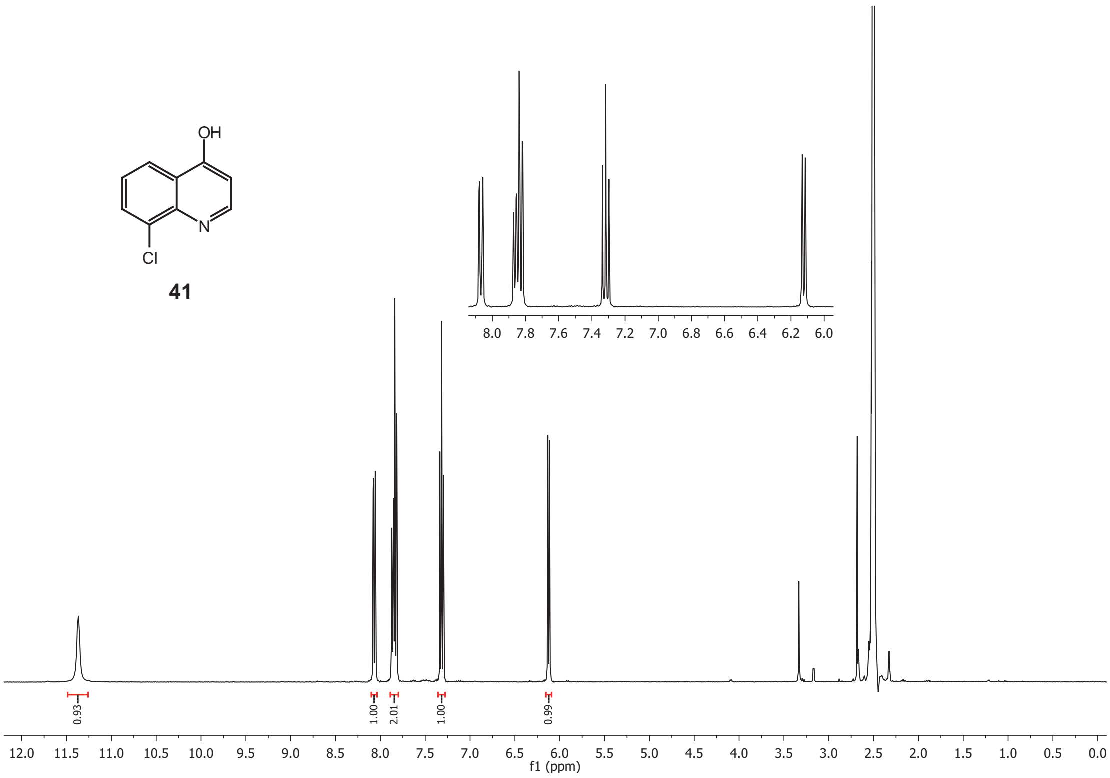
OH
N
Cl
41
8.0
7.8
7.6
7.4
7.2
7.0
6.8
6.6
6.4
6.2
6.0
0.93
1.00
2.01
1.00
0.99
12.0
11.5
11.0
10.5
10.0
9.5
9.0
8.5
8.0
7.5
7.0
6.5
6.0
5.5
5.0
4.5
4.0
3.5
3.0
2.5
2.0
1.5
1.0
0.5
0.0
f1 (ppm)

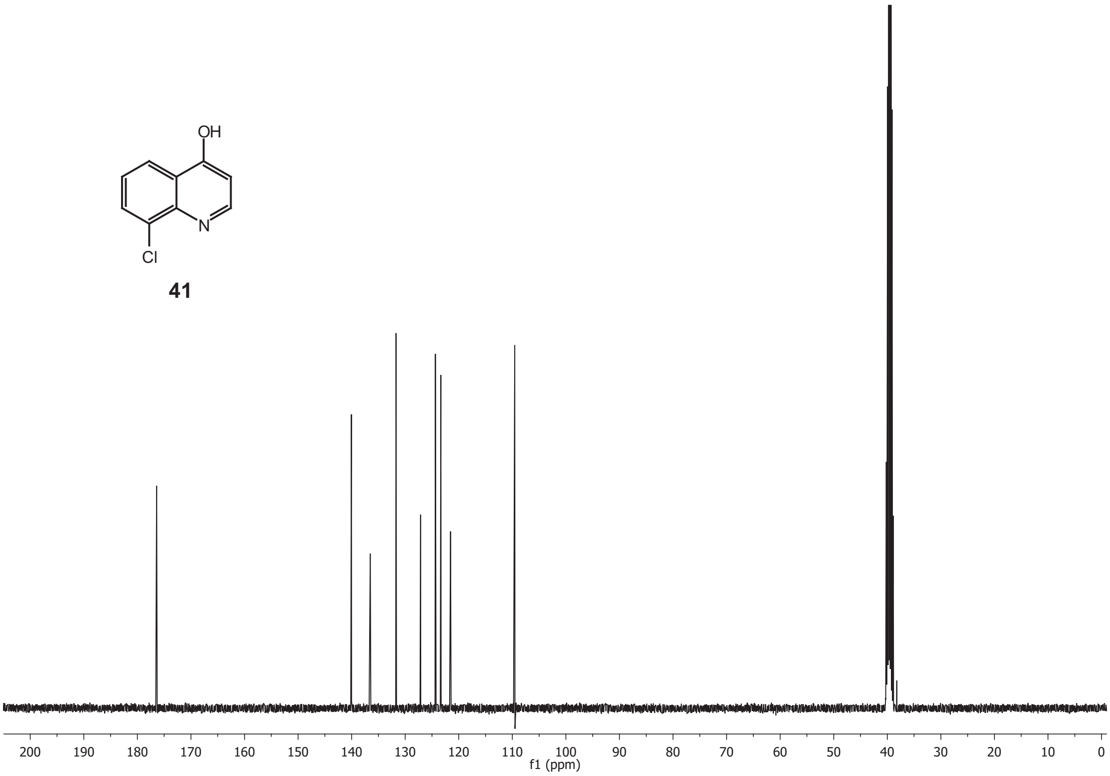
OH
N
Cl
41
200
190
180
170
160
150
140
130
120
110
100
90
80
70
60
50
40
30
20
10
0
f1 (ppm)

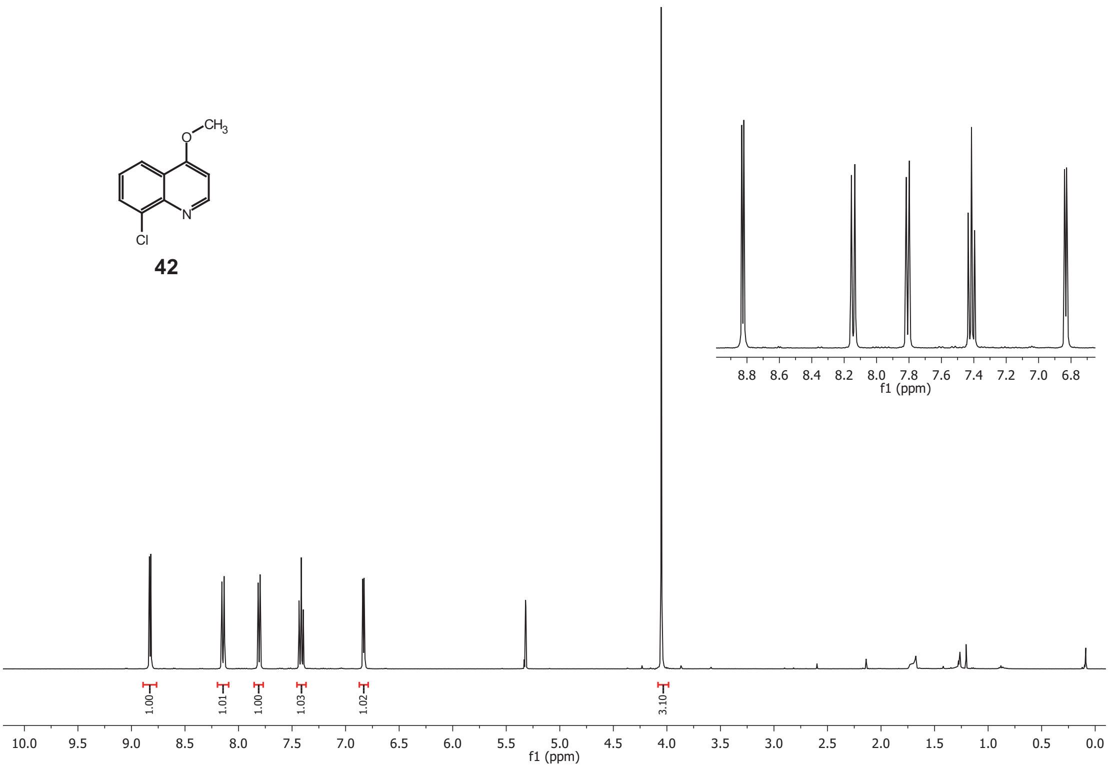
O
CH3
N
Cl
42
1.00
1.01
1.00
1.03
1.02
3.10
10.0 9.5 9.0 8.5 8.0 7.5 7.0 6.5 6.0 5.5 5.0 4.5 4.0 3.5 3.0 2.5 2.0 1.5 1.0 0.5 0.0
f1 (ppm)
8.8 8.6 8.4 8.2 8.0 7.8 7.6 7.4 7.2 7.0 6.8
f1 (ppm)

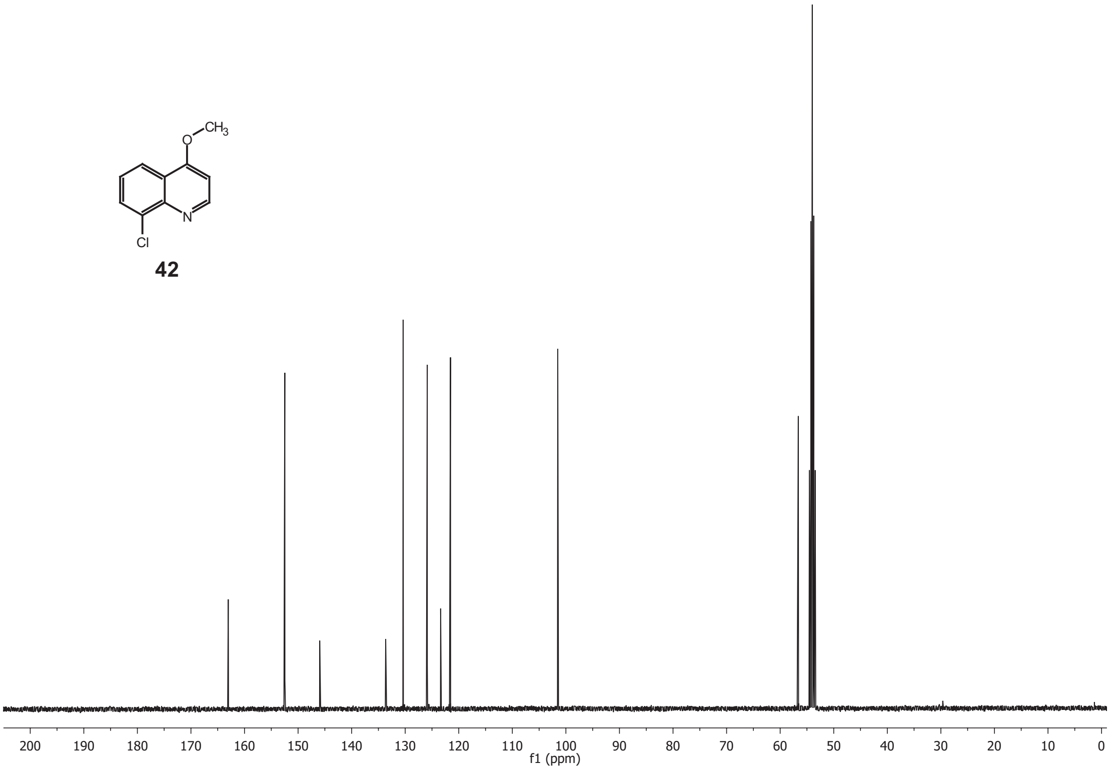
O
CH3
N
Cl
42
200 190 180 170 160 150 140 130 120 110 100 90 80 70 60 50 40 30 20 10 0
f1 (ppm)

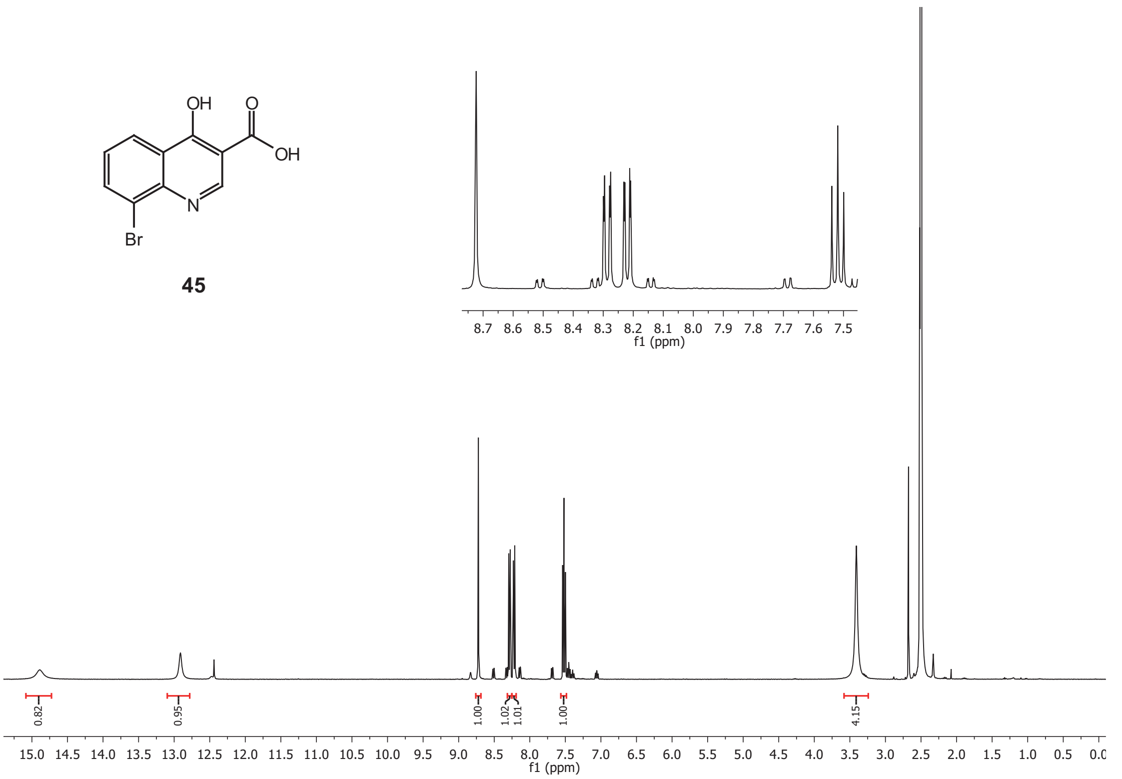

OH
O
OH
N
Br
45
8.7 8.6 8.5 8.4 8.3 8.2 8.1 8.0 7.9 7.8 7.7 7.6 7.5
f1 (ppm)
0.82
0.95
1.00
1.02
1.01
1.00
4.15
15.0 14.5 14.0 13.5 13.0 12.5 12.0 11.5 11.0 10.5 10.0 9.5 9.0 8.5 8.0 7.5 7.0 6.5 6.0 5.5 5.0 4.5 4.0 3.5 3.0 2.5 2.0 1.5 1.0 0.5 0.0
f1 (ppm)

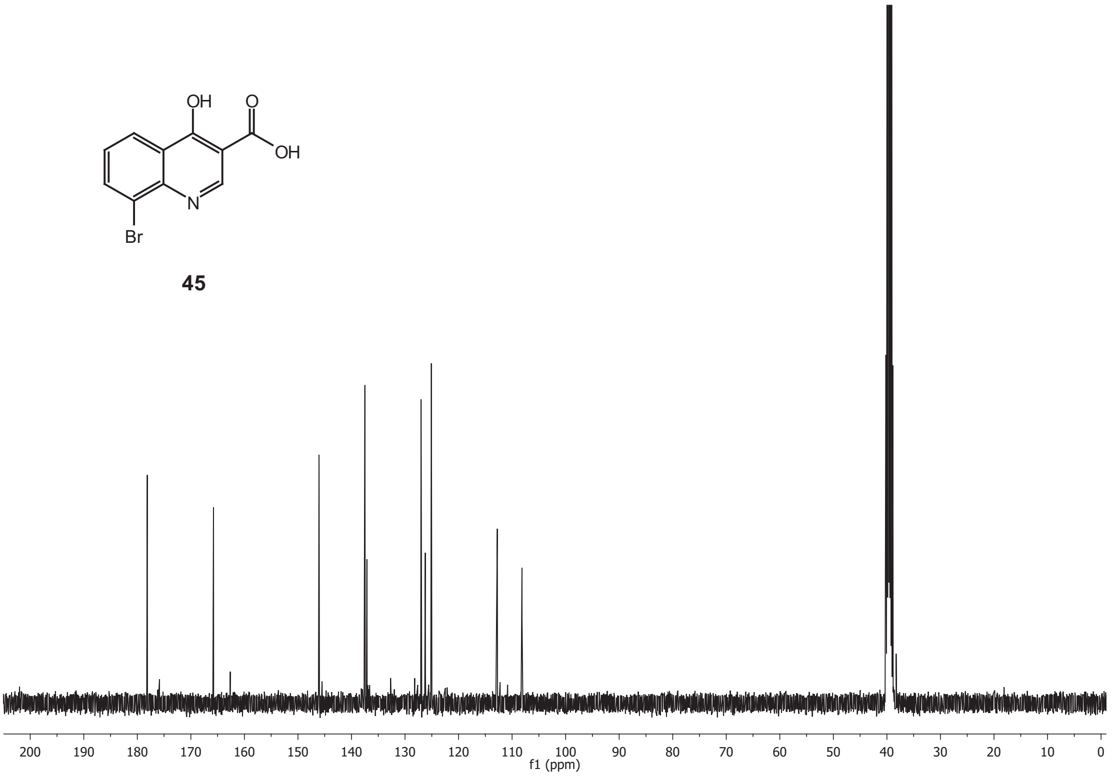

OH
O
OH
N
Br
45
200 190 180 170 160 150 140 130 120 110 100 90 80 70 60 50 40 30 20 10 0
f1 (ppm)

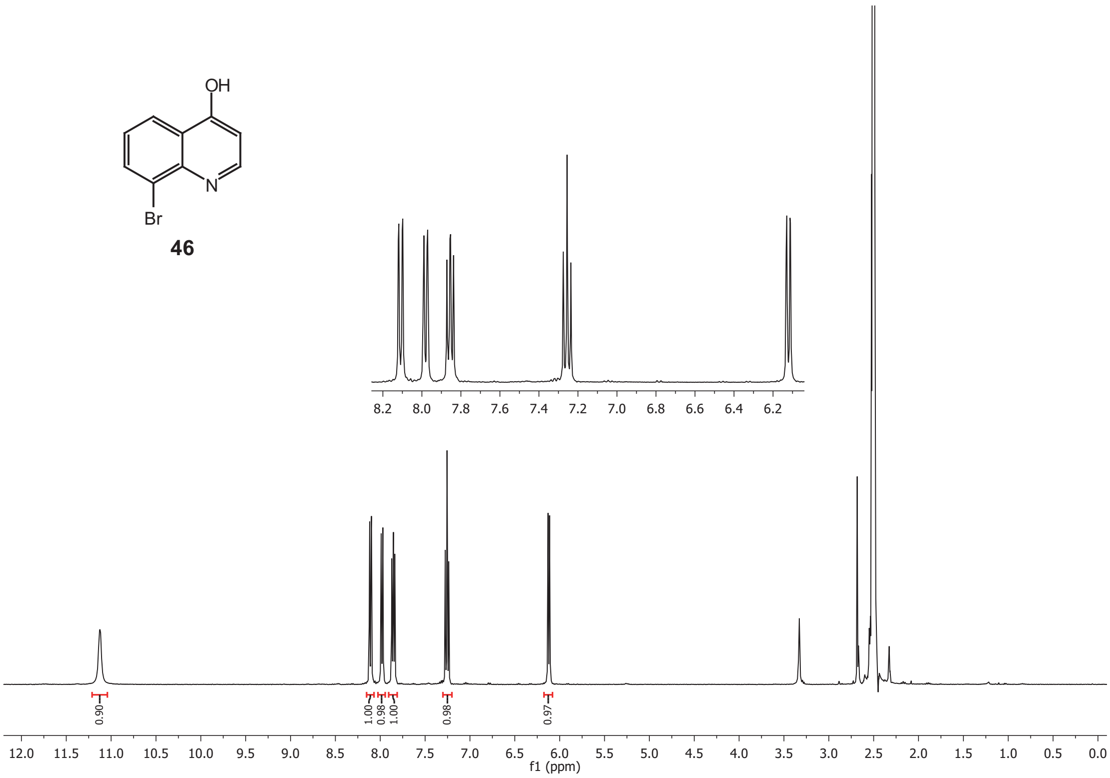
46
OH
N
Br
8.2
8.0
7.8
7.6
7.4
7.2
7.0
6.8
6.6
6.4
6.2
0.90
1.00
0.98
1.00
0.98
0.97
12.0
11.5
11.0
10.5
10.0
9.5
9.0
8.5
8.0
7.5
7.0
6.5
6.0
5.5
5.0
4.5
4.0
3.5
3.0
2.5
2.0
1.5
1.0
0.5
0.0
f1 (ppm)

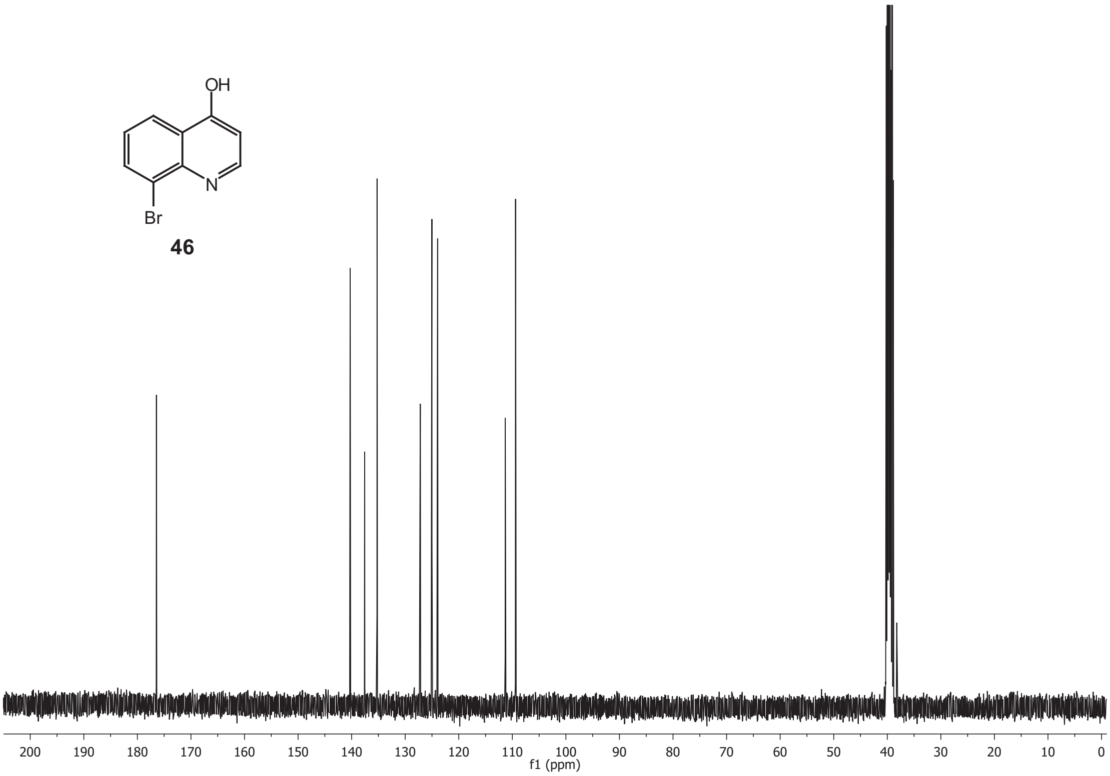
46
OH
N
Br
200
190
180
170
160
150
140
130
120
110
100
90
80
70
60
50
40
30
20
10
0
f1 (ppm)

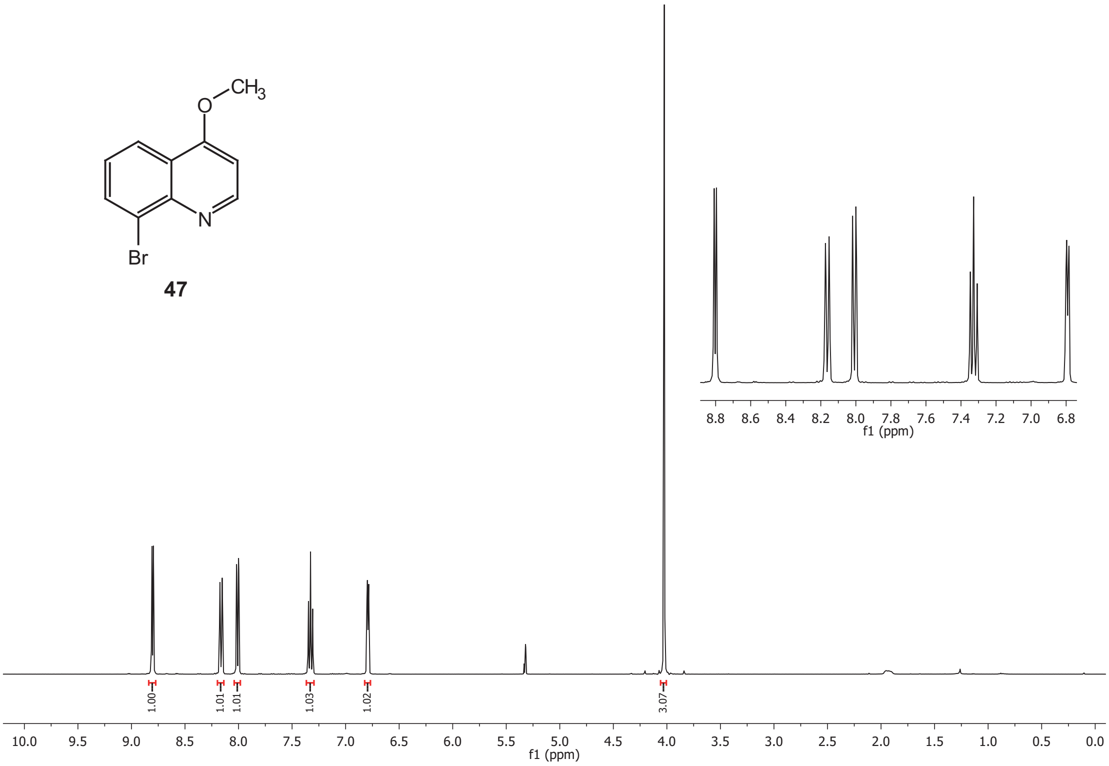
O
CH3
N
Br
47
1.00
1.01
1.01
1.03
1.02
3.07
10.0 9.5 9.0 8.5 8.0 7.5 7.0 6.5 6.0 5.5 5.0 4.5 4.0 3.5 3.0 2.5 2.0 1.5 1.0 0.5 0.0
f1 (ppm)
8.8 8.6 8.4 8.2 8.0 7.8 7.6 7.4 7.2 7.0 6.8
f1 (ppm)

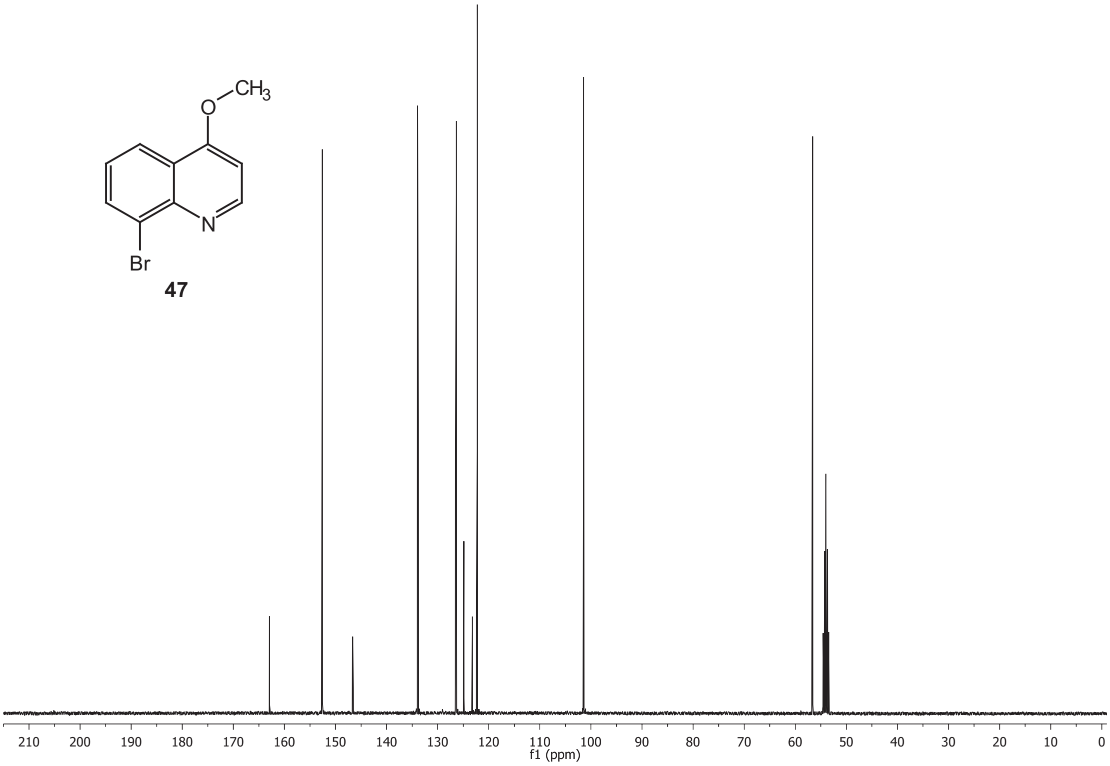
O
CH3
N
Br
47
210 200 190 180 170 160 150 140 130 120 110 100 90 80 70 60 50 40 30 20 10 0
f1 (ppm)

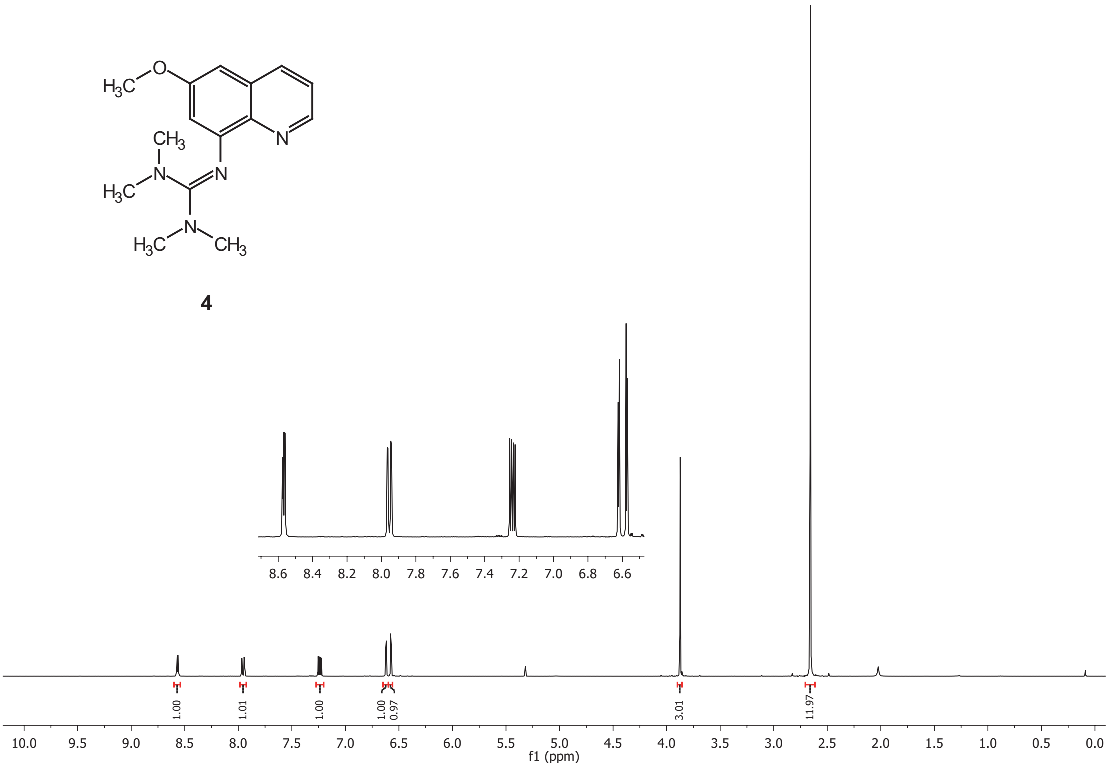

4

H_3C
O
N
CH_3
N
H_3C
N
N
H_3C
CH_3
8.6 8.4 8.2 8.0 7.8 7.6 7.4 7.2 7.0 6.8 6.6
1.00
1.01
1.00
1.00
0.97
3.01
11.97
10.0 9.5 9.0 8.5 8.0 7.5 7.0 6.5 6.0 5.5 5.0 4.5 4.0 3.5 3.0 2.5 2.0 1.5 1.0 0.5 0.0
f1 (ppm)

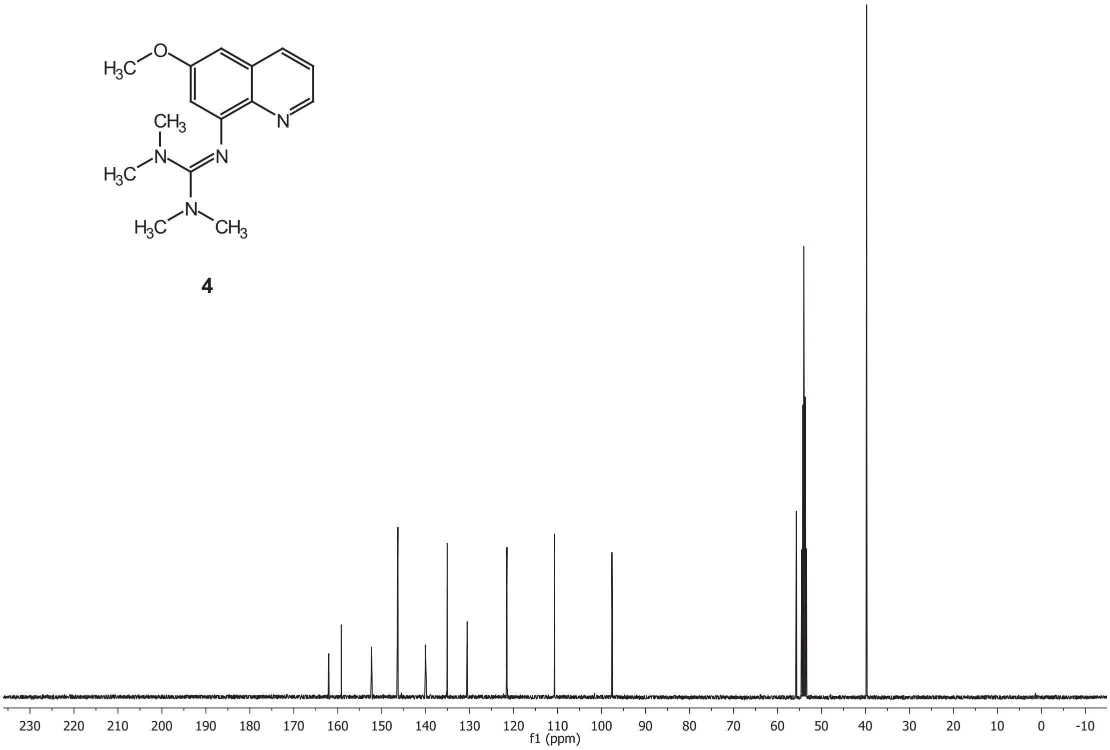

4

H_3C
O
N
CH_3
N
H_3C
N
N
H_3C
CH_3
230 220 210 200 190 180 170 160 150 140 130 120 110 100 90 80 70 60 50 40 30 20 10 0 -10
f1 (ppm)

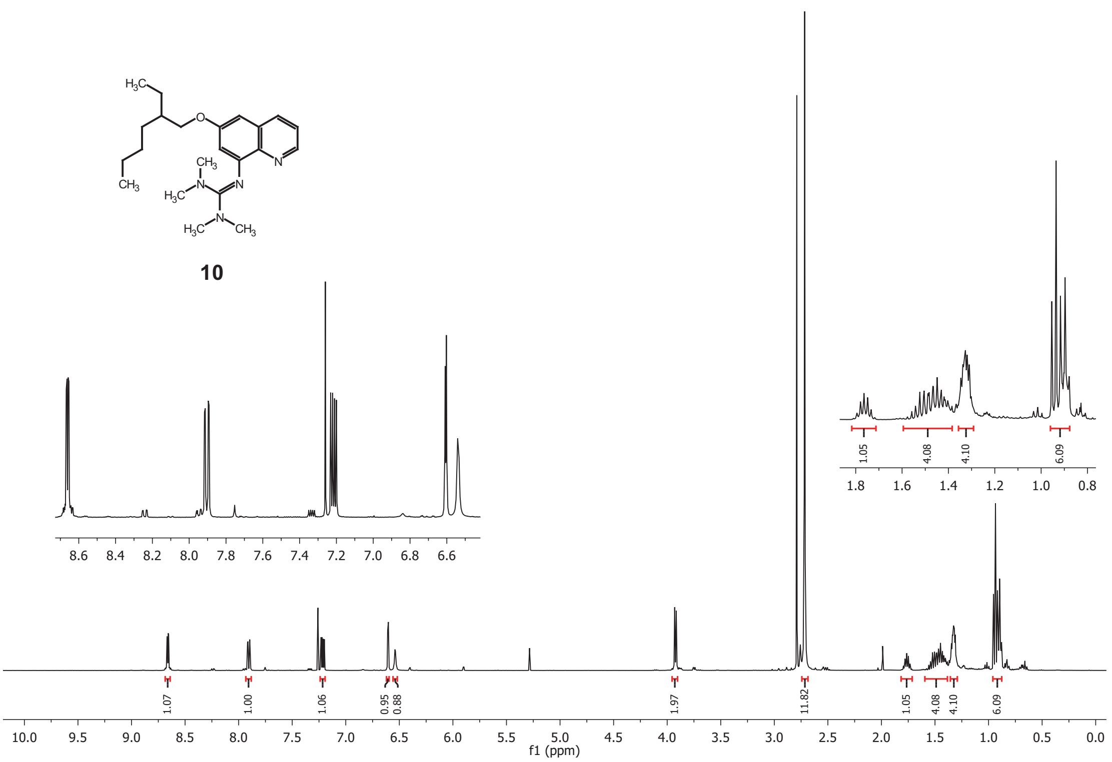
10

H3C
O
N
CH3
CH3
H3C
N
N
H3C
CH3
1.07
1.00
1.06
0.95
0.88
1.97
11.82
1.05
4.08
4.10
6.09
10.0 9.5 9.0 8.5 8.0 7.5 7.0 6.5 6.0 5.5 5.0 4.5 4.0 3.5 3.0 2.5 2.0 1.5 1.0 0.5 0.0
f1 (ppm)
8.6 8.4 8.2 8.0 7.8 7.6 7.4 7.2 7.0 6.8 6.6
1.8 1.6 1.4 1.2 1.0 0.8

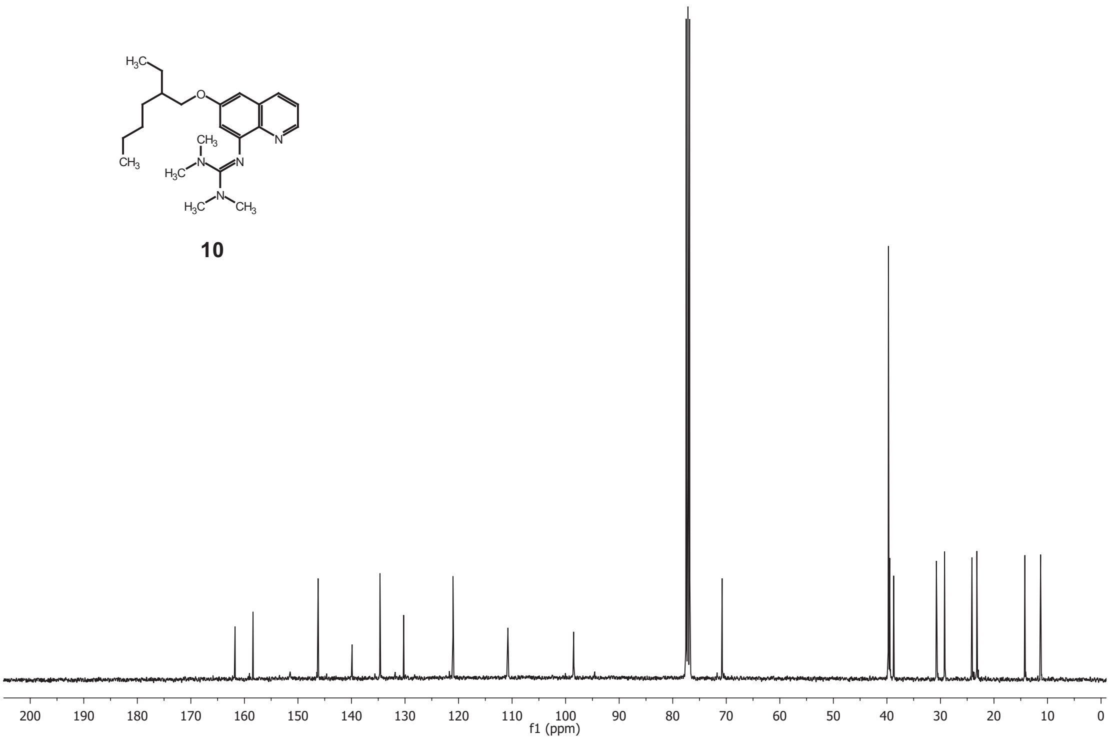
10

H3C
O
N
CH3
CH3
H3C
N
N
H3C
CH3
200 190 180 170 160 150 140 130 120 110 100 90 80 70 60 50 40 30 20 10 0
f1 (ppm)

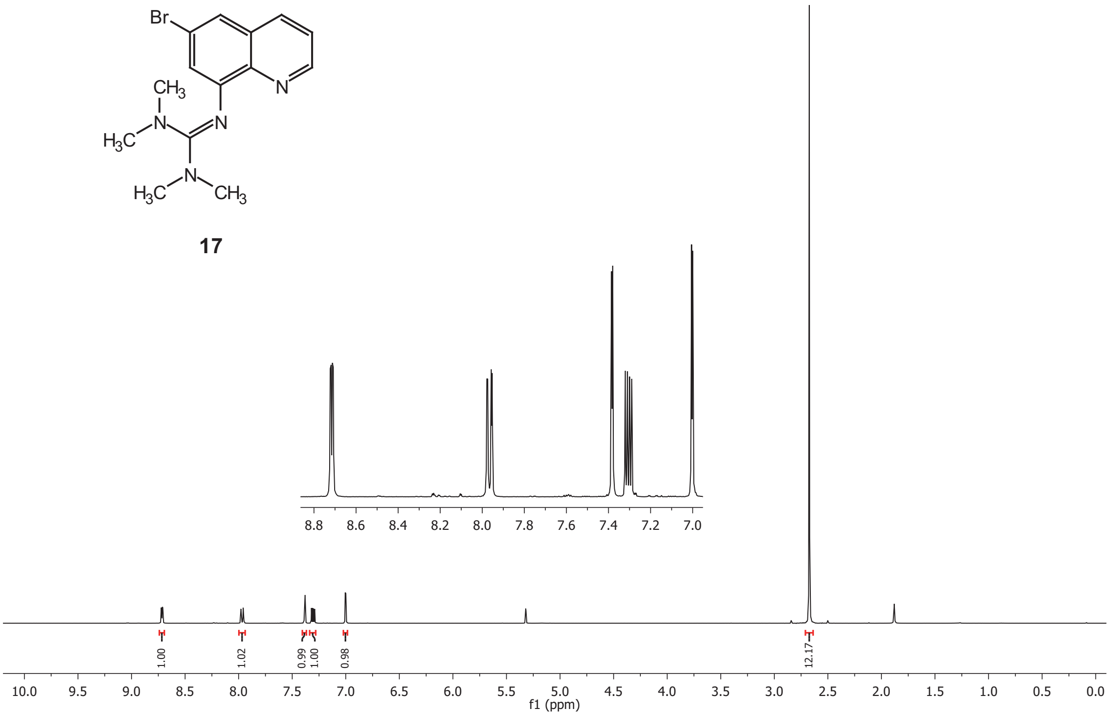

17

Br
N
CH3
N
H3C
N
H3C
CH3
N
8.8
8.6
8.4
8.2
8.0
7.8
7.6
7.4
7.2
7.0
1.00
1.02
0.99
1.00
0.98
12.17
10.0
9.5
9.0
8.5
8.0
7.5
7.0
6.5
6.0
5.5
5.0
4.5
4.0
3.5
3.0
2.5
2.0
1.5
1.0
0.5
0.0
f1 (ppm)

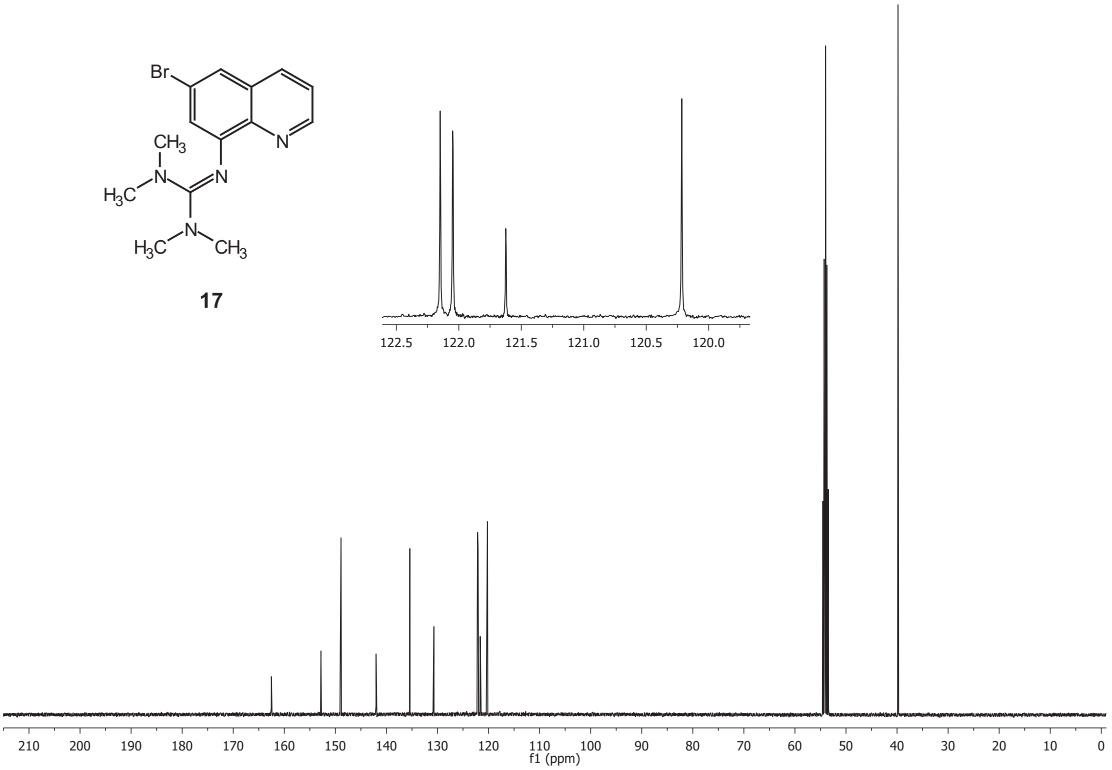

17

Br
N
CH3
N
H3C
N
H3C
CH3
N
122.5
122.0
121.5
121.0
120.5
120.0
210
200
190
180
170
160
150
140
130
120
110
100
90
80
70
60
50
40
30
20
10
0
f1 (ppm)

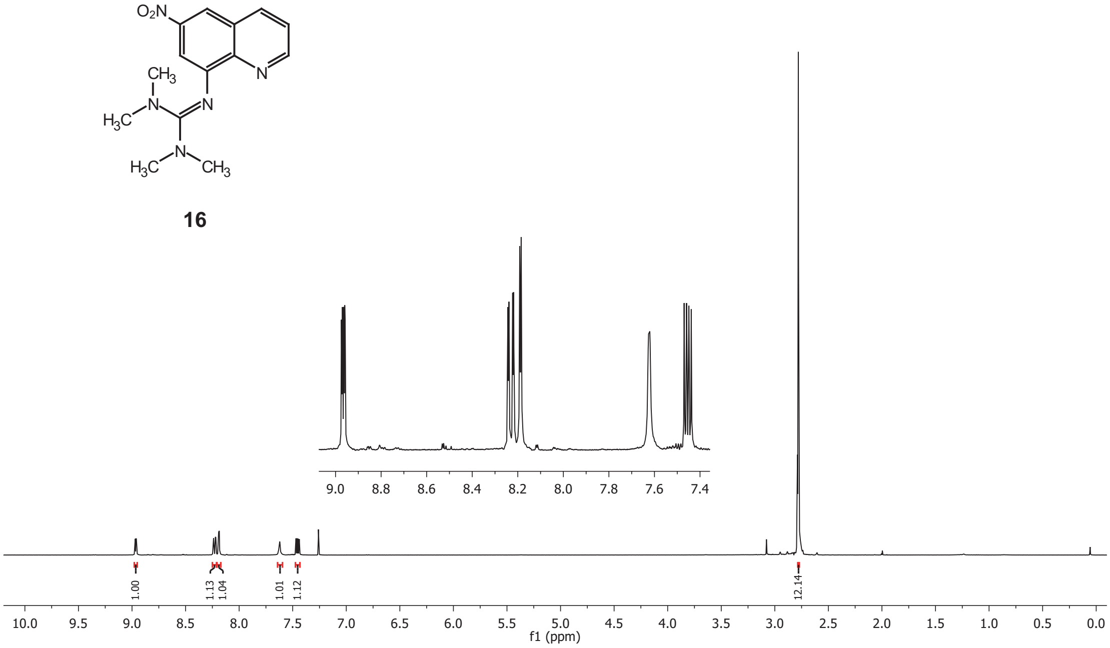
O_2N
N
CH_3
N
H_3C
N
N
H_3C
CH_3
9.0 8.8 8.6 8.4 8.2 8.0 7.8 7.6 7.4
1.00
1.13
1.04
1.01
1.12
12.14
10.0 9.5 9.0 8.5 8.0 7.5 7.0 6.5 6.0 5.5 5.0 4.5 4.0 3.5 3.0 2.5 2.0 1.5 1.0 0.5 0.0
f1 (ppm)

16

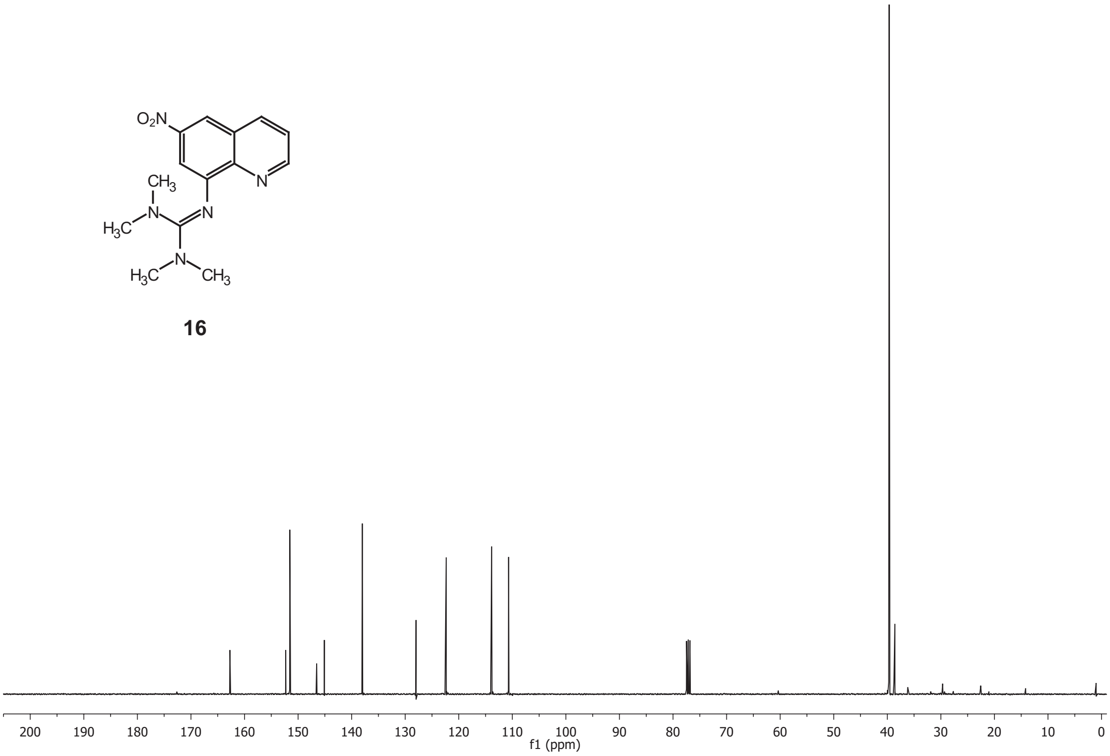
O_2N
N
CH_3
N
H_3C
N
N
H_3C
CH_3
200 190 180 170 160 150 140 130 120 110 100 90 80 70 60 50 40 30 20 10 0
f1 (ppm)

16

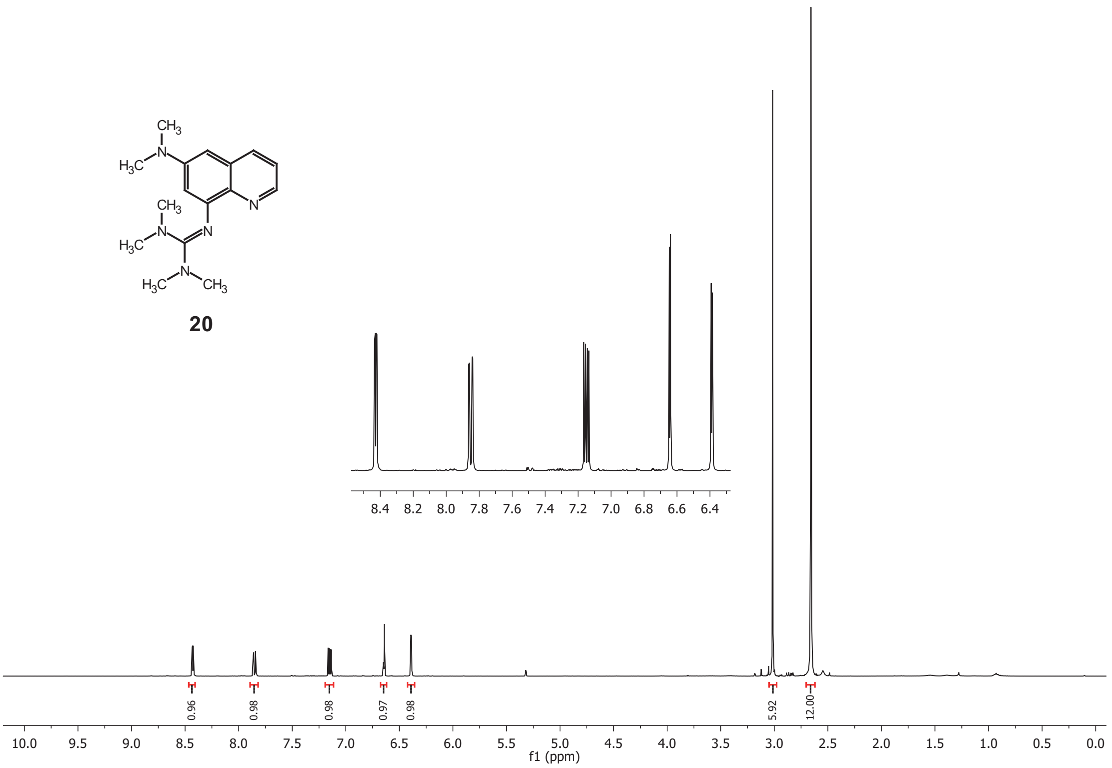
CH3
H3C
N
N
CH3
H3C
N
N
H3C
N
CH3
8.4 8.2 8.0 7.8 7.6 7.4 7.2 7.0 6.8 6.6 6.4
0.96
0.98
0.98
0.97
0.98
5.92
12.00
10.0 9.5 9.0 8.5 8.0 7.5 7.0 6.5 6.0 5.5 5.0 4.5 4.0 3.5 3.0 2.5 2.0 1.5 1.0 0.5 0.0
f1 (ppm)

20

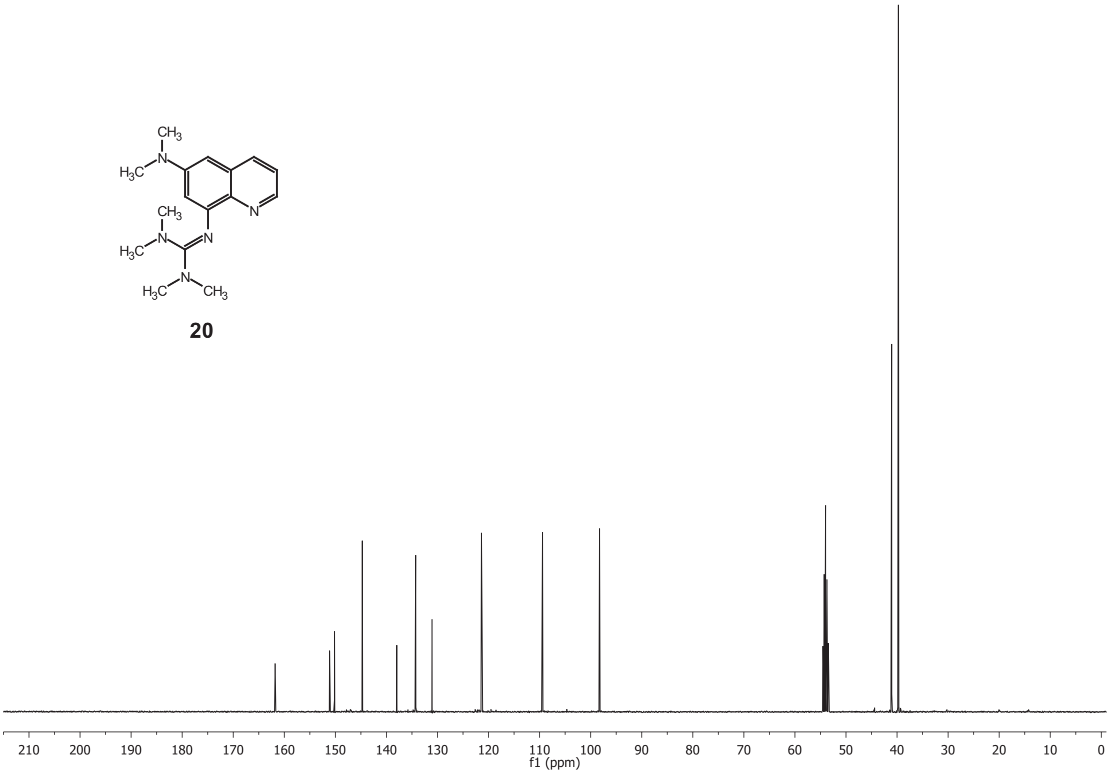
CH3
H3C
N
N
CH3
H3C
N
N
H3C
N
CH3
210 200 190 180 170 160 150 140 130 120 110 100 90 80 70 60 50 40 30 20 10 0
f1 (ppm)

20

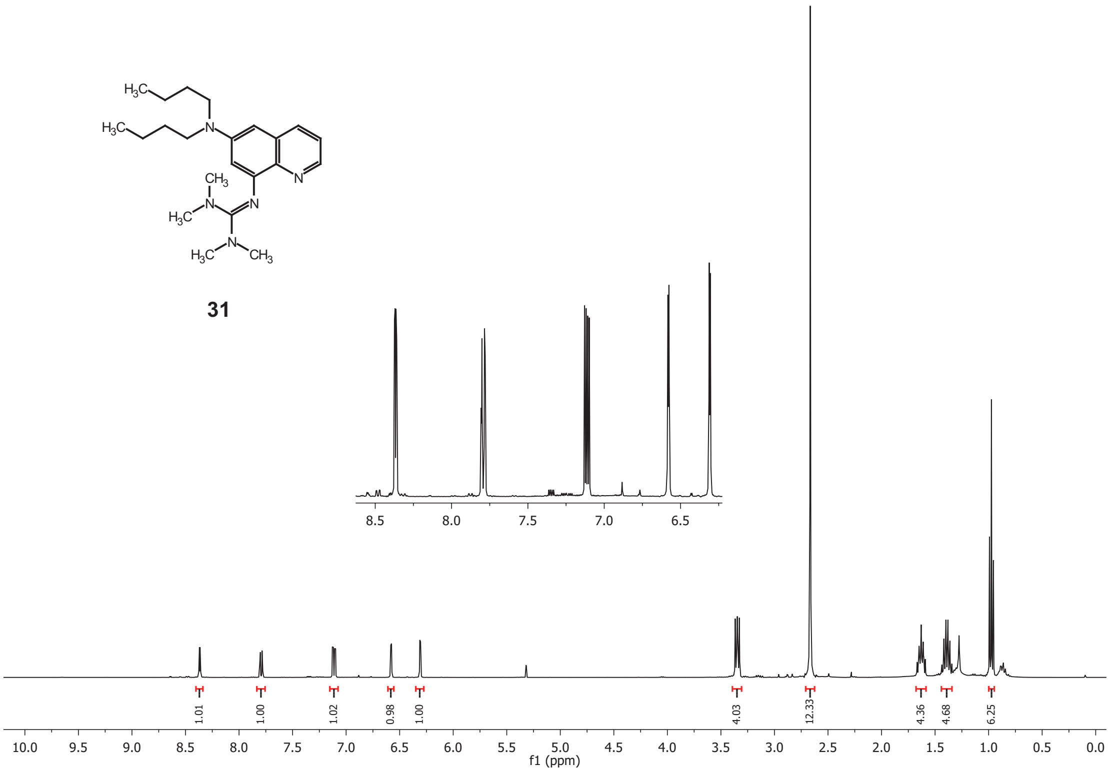

31

8.5
8.0
7.5
7.0
6.5
1.01
1.00
1.02
0.98
1.00
4.03
12.33
4.36
4.68
6.25
10.0 9.5 9.0 8.5 8.0 7.5 7.0 6.5 6.0 5.5 5.0 4.5 4.0 3.5 3.0 2.5 2.0 1.5 1.0 0.5 0.0
f1 (ppm)

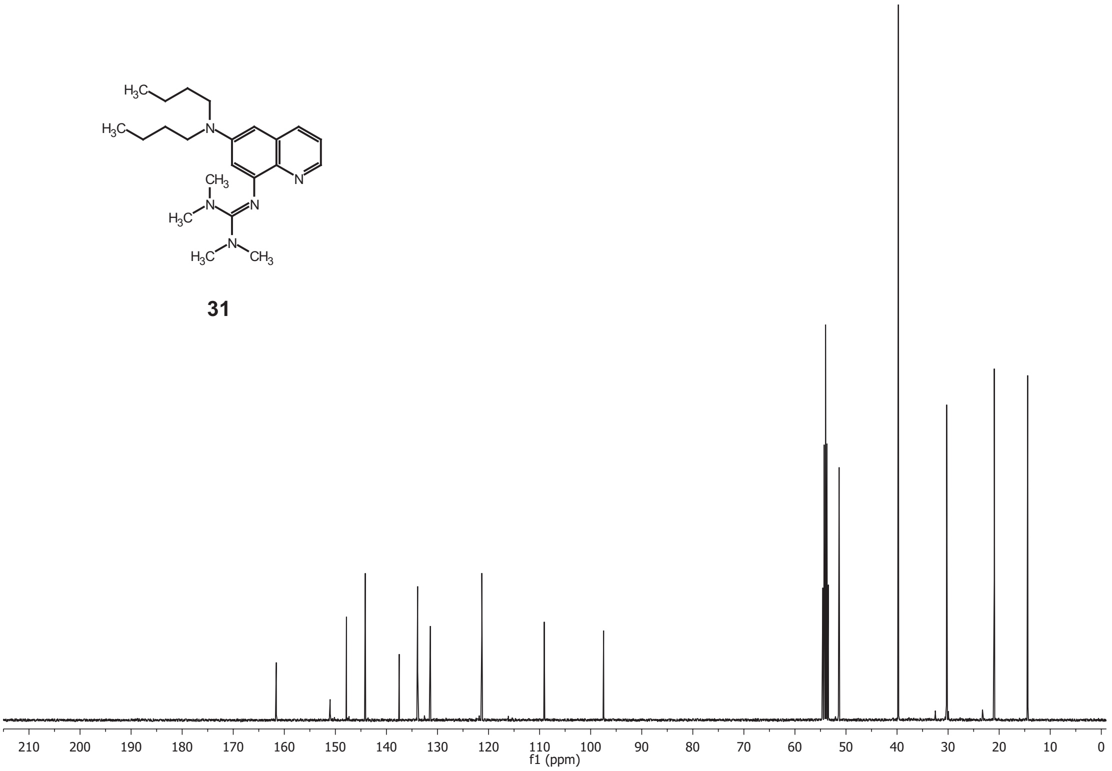

31

210 200 190 180 170 160 150 140 130 120 110 100 90 80 70 60 50 40 30 20 10 0
f1 (ppm)

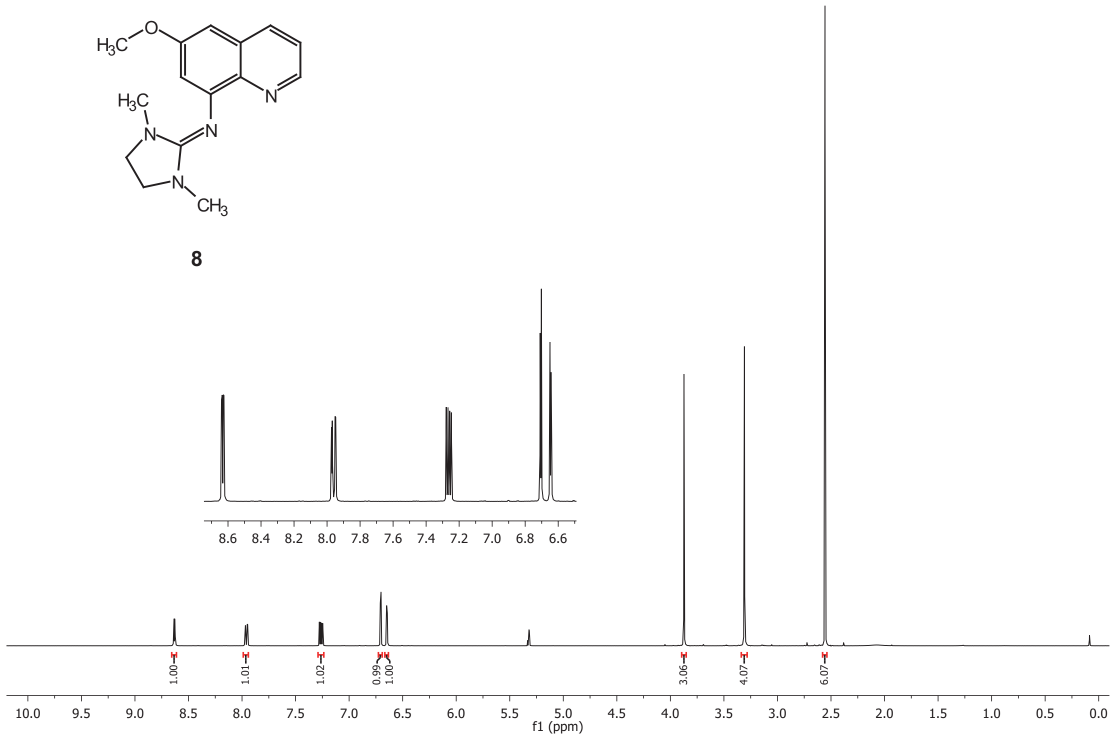
8
H3C
O
N
H3C
N
N
N
CH3
8.6
8.4
8.2
8.0
7.8
7.6
7.4
7.2
7.0
6.8
6.6
1.00
1.01
1.02
0.99
1.00
3.06
4.07
6.07
10.0
9.5
9.0
8.5
8.0
7.5
7.0
6.5
6.0
5.5
5.0
4.5
4.0
3.5
3.0
2.5
2.0
1.5
1.0
0.5
0.0
f1 (ppm)

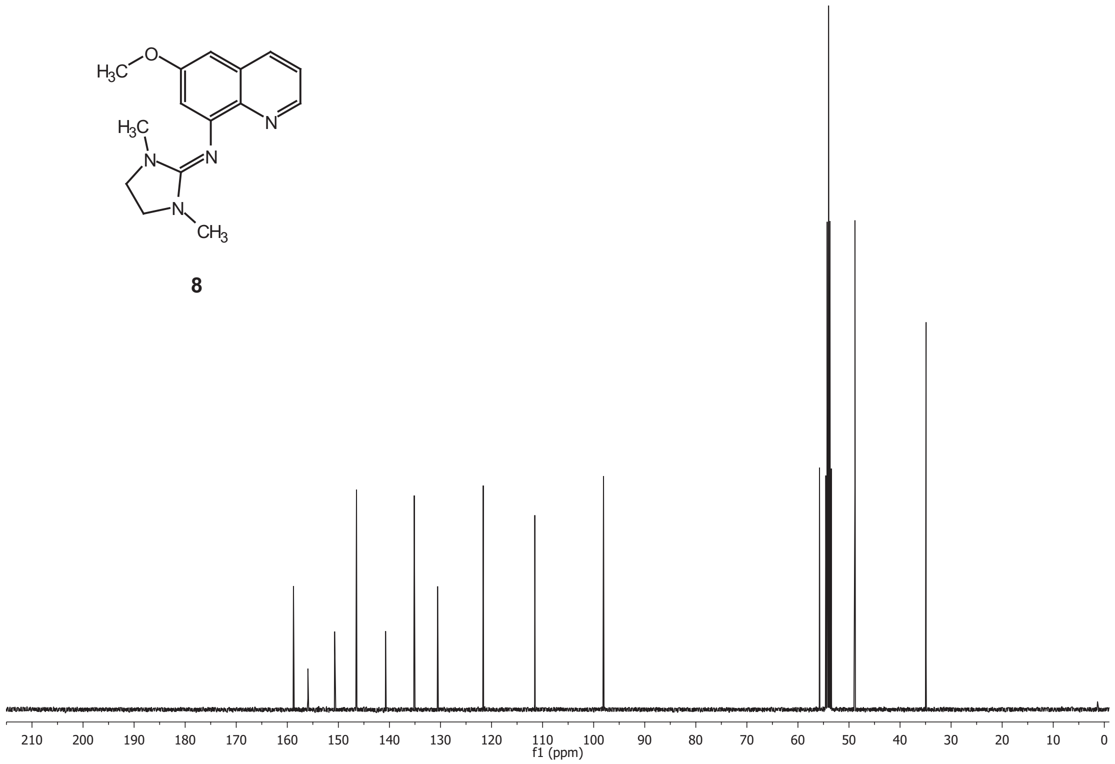
8
H3C
O
N
H3C
N
N
N
CH3
210
200
190
180
170
160
150
140
130
120
110
100
90
80
70
60
50
40
30
20
10
0
f1 (ppm)

B. Cyclic voltammetry spectra

All cyclic voltammograms are recorded in acetonitrile with (TBA)PF_6 (0.1 M) at ambient temperature.

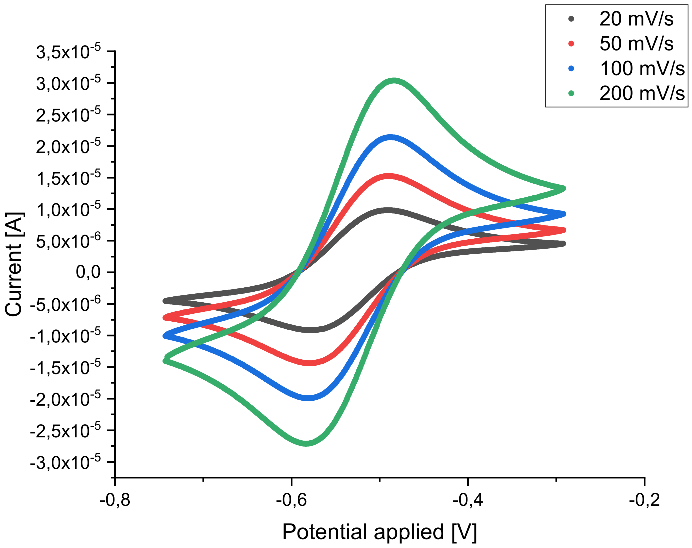

Figure B1: Cyclic voltammogram of two equivalents TMG6EHoxyqu ligand with $CuBr_2$.

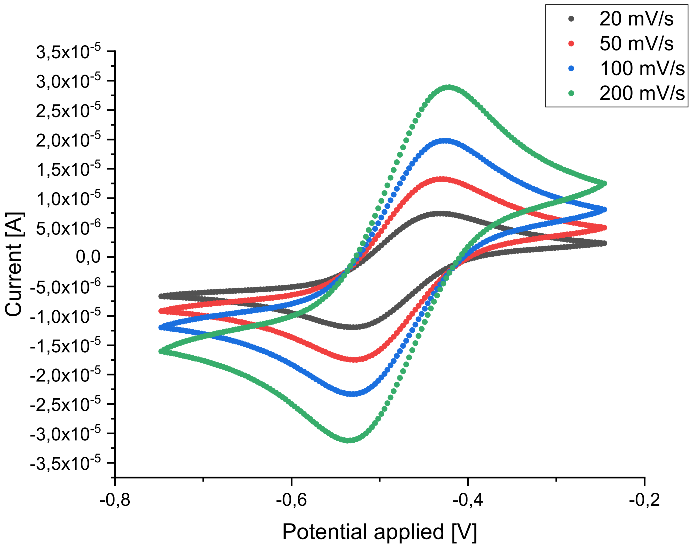

Figure B2: Cyclic voltammogram of the complex $[Cu(TMG6Brqu)_2Br]Br$.

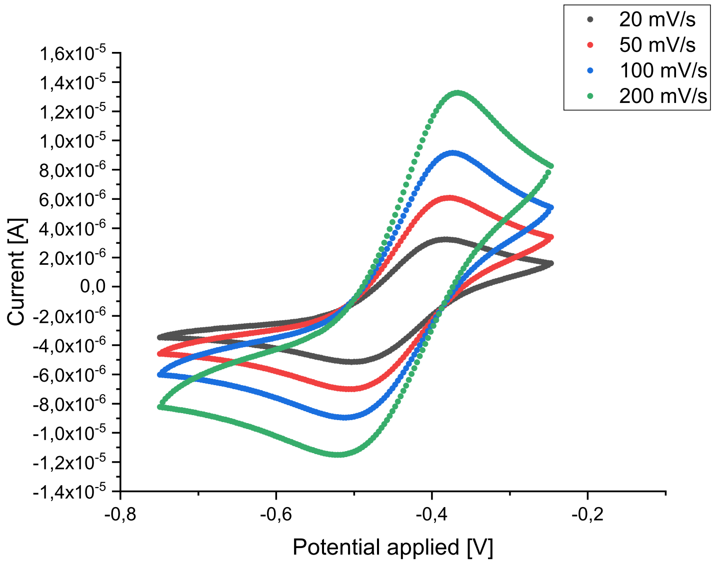

Figure B3: Cyclic voltammogram of the complex [Cu(TMG6Nitroqu)$_2$Br]Br.

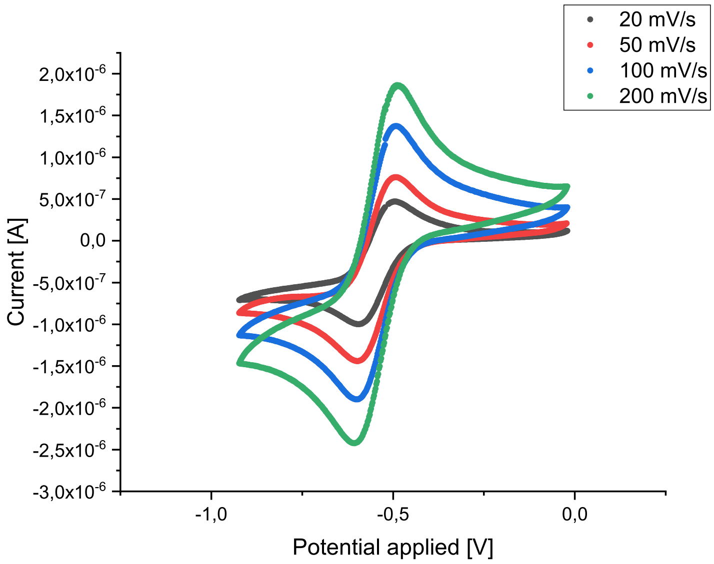

Figure B4: Cyclic voltammogram of two equivalents TMG6dmaqu ligand and CuBr$_2$.

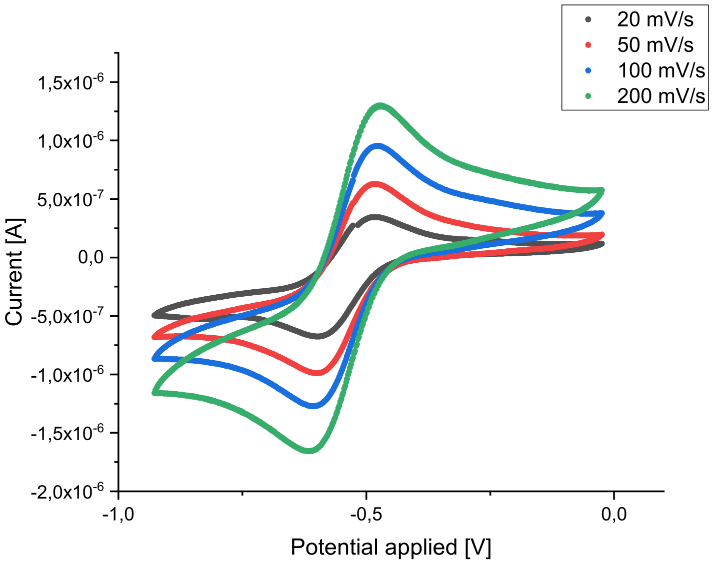

Figure B5: Cyclic voltammogram of two equivalents TMG6dbaqu ligand with $CuBr_2$.

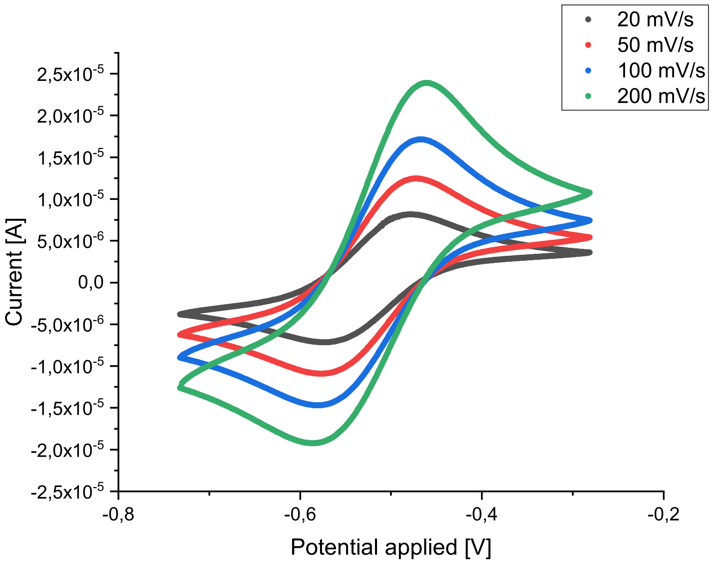

Figure B6: Cyclic voltammogram of the complex $[Cu(DMEG6Methoxyqu)_2Br]Br$.

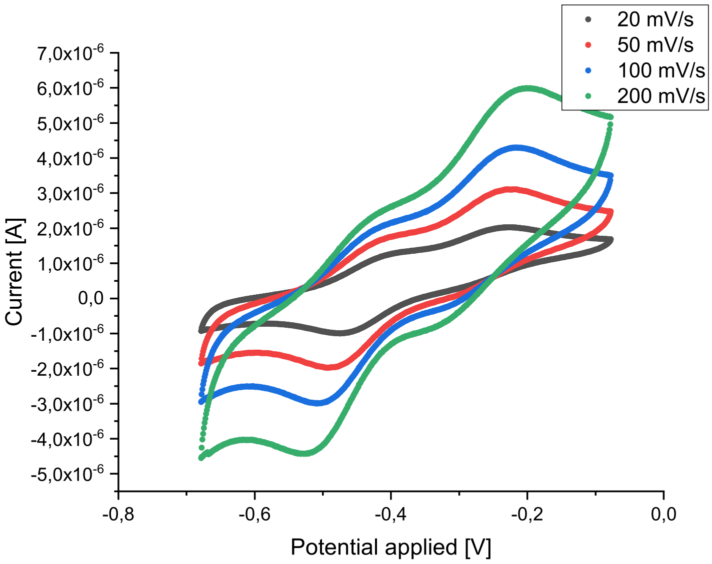

Figure B7: Cyclic voltammogram of 0,5 eq of the ligand TMG6EHoxyqu with CuBr.

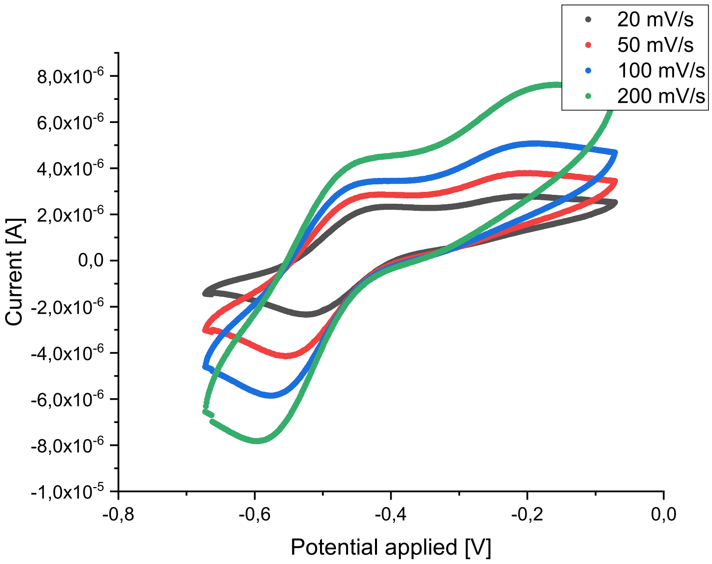

Figure B8: Cyclic voltammogram of 1,0 eq of the ligand TMG6EHoxyqu with CuBr.

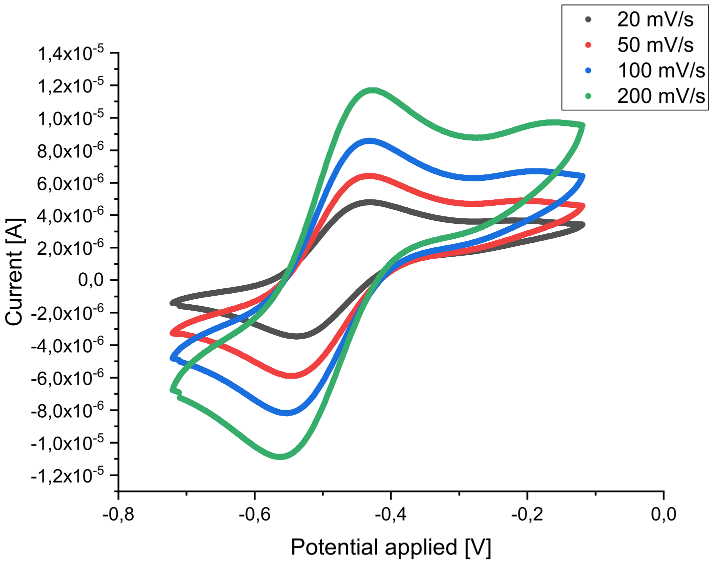

Figure B9: Cyclic voltammogram of 1,95 eq of the ligand TMG6EHoxyqu with CuBr.

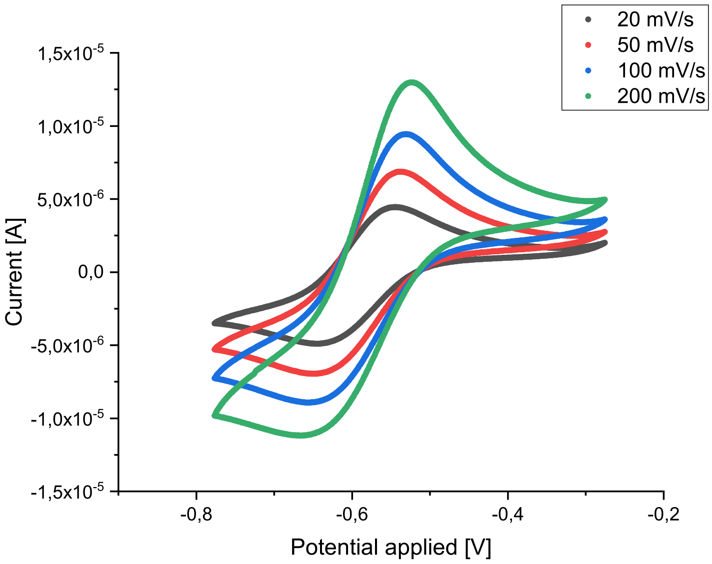

Figure B10: Cyclic voltammogram of two equivalents TMG6EHoxyqu ligand with $CuCl_2$.

C. Crystallographic Data

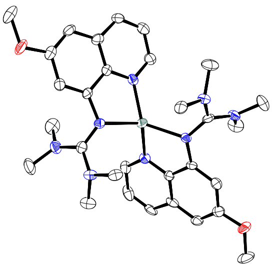

Table C1: Crystal data and structure refinement of [Cu(TMG6Methoxyqu)$_2$]Br, **C1**. One of two complexes of the asymmetric unit shown. Hydrogen atoms and non-coordinating bromide anions omitted for clarity.

X-ray Code	rv474ap	
Empirical formula	$C_{30}H_{40}BrCuN_8O_2$	
Formula weight	688.15	
Temperature	100(2) K	
Wavelength	0.710 69 Å	
Crystal system, space group	$Pna2_1$	
Unit cell dimensions	a = 26.886(3) Å	$\alpha = 90°$
	b = 11.7494(10) Å	$\beta = 90°$
	c = 20.5926(17) Å	$\gamma = 90°$
Volume	6505.2(10) Å^3	
Z, Calculated density	8, 1.405 Mg/m^3	
Absorption coefficient	1.94 mm^{-1}	
F(000)	2848	
Crystal size	0.16 x 0.15 x 0.10 mm	
Theta range for data collection	2.30 to 25.37°	
Limiting indices	$-32 \leq h \leq 27$	
	$-14 \leq k \leq 13$	
	$-20 \leq l \leq 24$	
Reflections collected / unique	77266 / 11514 [R(int) = 0.0699]	
Completeness to θ = 25.37	99.3%	
Absorption correction	Semi-empirical from equivalents	
Max. and min. transmission	0.8297 and 0.7466	
Refinement method	Full-matrix least-squares on F^2	
Data / restraints / parameters	11514 / 1 / 777	
Goodness-of-fit on F^2	1.033	
Final R indices [I>2σ(I)]	$R_1 = 0.0410$, $wR_2 = 0.0769$	
R indices (all data)	$R_1 = 0.0692$, $wR_2 = 0.0856$	
Largest diff. peak and hole	0.014(7) e.Å^{-3}	

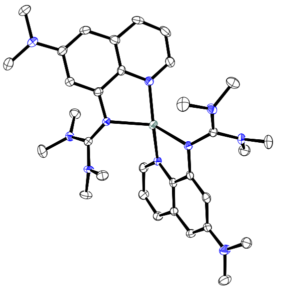

Table C2: Crystal data and structure refinement [Cu(TMG6dmaqu)$_2$]Br, **C2**. Hydrogen atoms and non-coordinating bromide anions omitted for clarity.

X-ray Code	vo008	
Empirical formula	$C_{32}H_{46}BrCuN_{10}$	
Formula weight	714.24	
Temperature	153(2) K	
Wavelength	0.710 73 Å	
Crystal system, space group	Triclinic, $P\bar{1}$	
Unit cell dimensions	a = 11.5357(8) Å	α = 105.212(5)°
	b = 11.7485(7) Å	β = 92.990(5)°
	c = 13.8297(9) Å	γ = 110.187(6)°
Volume	1676.32(19) $Å^3$	
Z, Calculated density	2, 1.415 Mg/m^3	
Absorption coefficient	1.882 mm^{-1}	
F(000)	744	
Crystal size	0.35 x 0.22 x 0.19 mm	
Theta range for data collection	4.17 to 27.48°	
Limiting indices	$-14 \le h \le 14$	
	$-14 \le k \le 15$	
	$-17 \le l \le 17$	
Reflections collected / unique	11361 / 7575 [R(int) = 0.0324]	
Completeness to θ = 27.48	98.6%	
Absorption correction	Semi-empirical from equivalents	
Max. and min. transmission	1 and 0.84482	
Refinement method	Full-matrix least-squares on F^2	
Data / restraints / parameters	7575 / 0 / 409	
Goodness-of-fit on F^2	1.021	
Final R indices [I>2σ(I)]	R_1 = 0.0401, wR_2 = 0.0785	
R indices (all data)	R_1 = 0.0583, wR_2 = 0.0889	
Largest diff. peak and hole	0.606 and -0.495 e.$Å^{-3}$	

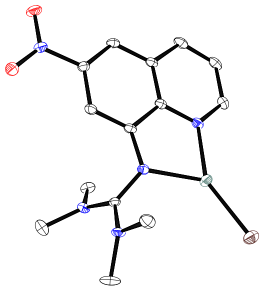

Table C3: Crystal data and structure refinement [Cu(TMG6Nitroqu)Br], **C3**. Hydrogen atoms omitted for clarity.

X-ray Code	uv082	
Empirical formula	$C_{14}H_{17}BrCuN_5O_2$	
Formula weight	430.78	
Temperature	100(2) K	
Wavelength	0.710 73 Å	
Crystal system, space group	Triclinic, $P\bar{1}$	
Unit cell dimensions	a = 8.0090(4) Å	$\alpha = 95.195(2)°$
	b = 10.3265(6) Å	$\beta = 109.858(2)°$
	c = 10.3366(5) Å	$\gamma = 95.495(2)°$
Volume	793.41(7) Å^3	
Z, Calculated density	2, 1.803 Mg/m^3	
Absorption coefficient	3.911 mm^{-1}	
F(000)	432	
Crystal size	0.07 x 0.05 x 0.04 mm	
Theta range for data collection	3.09 to 33.16°	
Limiting indices	$-12 \leq h \leq 10$	
	$-15 \leq k \leq 15$	
	$-15 \leq l \leq 15$	
Reflections collected / unique	11842 / 6024 [R(int) = 0.0443]	
Completeness to $\theta = 33.16$	99.5%	
Absorption correction	Semi-empirical from equivalents	
Max. and min. transmission	0.8593 and 0.7714	
Refinement method	Full-matrix least-squares on F^2	
Data / restraints / parameters	6024 / 0 / 212	
Goodness-of-fit on F^2	1.041	
Final R indices [$I>2\sigma(I)$]	$R_1 = 0.0442$, $wR_2 = 0.1155$	
R indices (all data)	$R_1 = 0.0610$, $wR_2 = 0.1241$	
Largest diff. peak and hole	0.927 and -1.229 e.Å^{-3}	

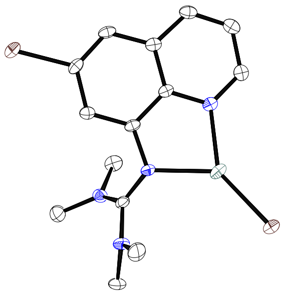

Table C4: Crystal data and structure refinement [Cu(TMG6Brqu)Br], **C4**. Hydrogen atoms omitted for clarity.

X-ray Code	uv576	
Empirical formula	$C_{14}H_{17}Br_2CuN_4$	
Formula weight	464.68	
Temperature	100(2) K	
Wavelength	0.710 73 Å	
Crystal system, space group	Triclinic, $P\bar{1}$	
Unit cell dimensions	a = 8.8114(2) Å	$\alpha = 95.9170(10)°$
	b = 10.0367(3) Å	$\beta = 107.1930(10)°$
	c = 10.1104(3) Å	$\gamma = 104.0370(10)°$
Volume	813.81(4) $Å^3$	
Z, Calculated density	2, 1.896 Mg/m^3	
Absorption coefficient	6.25 mm^{-1}	
F(000)	456	
Crystal size	0.10 x 0.08 x 0.02 mm	
Theta range for data collection	2.13 to 27.51°	
Limiting indices	$-11 \leq h \leq 11$	
	$-13 \leq k \leq 13$	
	$-13 \leq l \leq 13$	
Reflections collected / unique	13979 / 3739 [R(int) = 0.0352]	
Completeness to $\theta = 27.51$	99.8%	
Absorption correction	Semi-empirical from equivalents	
Max. and min. transmission	0.8852 and 0.5738	
Refinement method	Full-matrix least-squares on F^2	
Data / restraints / parameters	3739 / 0 / 194	
Goodness-of-fit on F^2	1.172	
Final R indices [I>2σ(I)]	$R_1 = 0.0270$, $wR_2 = 0.0707$	
R indices (all data)	$R_1 = 0.0393$, $wR_2 = 0.1013$	
Largest diff. peak and hole	0.805 and -0.543 e.$Å^{-3}$	

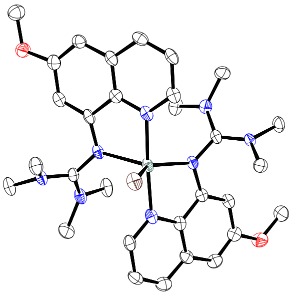

Table C5: Crystal data and structure refinement $[Cu(TMG6Methoxyqu)_2Br]Br$, **C5**. Hydrogen atoms and non-coordinating bromide anions omitted for clarity.

X-ray Code	tv370
Empirical formula	$C_{30}H_{40}Br_2CuN_8O_2$
Formula weight	768.06
Temperature	100(2) K
Wavelength	0.710 73 Å
Crystal system, space group	Orthorhombic, *Pbca*
Unit cell dimensions	a = 12.9486(5) Å $\alpha = 90°$
	b = 16.4932(7) Å $\beta = 90°$
	c = 30.6297(12) Å $\gamma = 90°$
Volume	6541.4(5) $Å^3$
Z, Calculated density	8, 1.56 Mg/m^3
Absorption coefficient	3.152 mm^{-1}
F(000)	3128
Crystal size	0.05 x 0.04 x 0.01 mm
Theta range for data collection	2.81 to 25.11°
Limiting indices	$-13 \leq h \leq 15$
	$-19 \leq k \leq 19$
	$-36 \leq l \leq 34$
Reflections collected / unique	51230 / 5811 [R(int) = 0.0664]
Completeness to $\theta = 25.11$	99.7%
Absorption correction	Semi-empirical from equivalents
Max. and min. transmission	0.9692 and 0.8583
Refinement method	Full-matrix least-squares on F^2
Data / restraints / parameters	5811 / 0 / 398
Goodness-of-fit on F^2	1.063
Final R indices [$I>2\sigma(I)$]	$R_1 = 0.0466$, $wR_2 = 0.0968$
R indices (all data)	$R_1 = 0.0753$, $wR_2 = 0.1067$
Largest diff. peak and hole	1.433 and -0.577 e.$Å^{-3}$

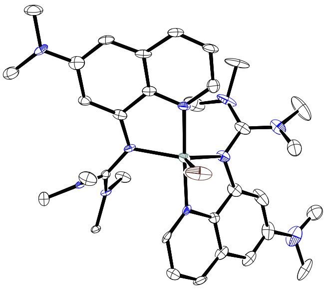

Table C6: Crystal data and structure refinement [Cu(TMG6dmaqu)$_2$Br]Br, **C6**. Hydrogen atoms and non-coordinating bromide anions omitted for clarity.

X-ray Code	vv633	
Empirical formula	$C_{32}H_{46}Br_2CuN_{10} \cdot 2\,C_2H_3N$	
Formula weight	876.26	
Temperature	103(2) K	
Wavelength	0.710 73 Å	
Crystal system, space group	Monoclinic, $P2_1/c$	
Unit cell dimensions	a = 22.9735(7) Å	$\alpha = 90°$
	b = 11.9690(3) Å	$\beta = 109.7932(10)°$
	c = 15.6218(5) Å	$\gamma = 90°$
Volume	4041.7(2) $Å^3$	
Z, Calculated density	4, 1.44 Mg/m^3	
Absorption coefficient	2.559 mm^{-1}	
F(000)	1804	
Crystal size	0.09 x 0.08 x 0.03 mm	
Theta range for data collection	3.18 to 25.68°	
Limiting indices	$-28 \leq h \leq 28$	
	$-14 \leq k \leq 13$	
	$-19 \leq l \leq 19$	
Reflections collected / unique	62289 / 7655 [R(int) = 0.0489]	
Completeness to $\theta = 25.68$	99.8%	
Absorption correction	Semi-empirical from equivalents	
Max. and min. transmission	0.7453 and 0.6891	
Refinement method	Full-matrix least-squares on F^2	
Data / restraints / parameters	7655 / 18 / 515	
Goodness-of-fit on F^2	1.317	
Final R indices [$I>2\sigma(I)$]	$R_1 = 0.0768$, $wR_2 = 0.1679$	
R indices (all data)	$R_1 = 0.0823$, $wR_2 = 0.1700$	
Largest diff. peak and hole	0.919 and -1.545 e.$Å^{-3}$	

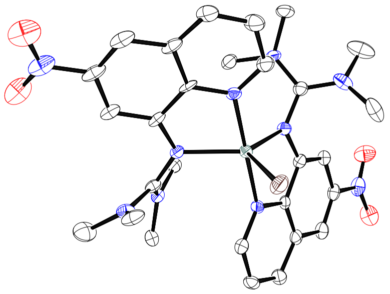

Table C7: Crystal data and structure refinement [Cu(TMG6Nitroqu)$_2$Br]Br, **C7**. Hydrogen atoms, solvents and non-coordinating bromide anions omitted for clarity.

X-ray Code	tv397	
Empirical formula	$C_{28}H_{34}Br_2CuN_{10}O_4 \cdot C_2H_3N$	
Formula weight	839.07	
Temperature	100(2) K	
Wavelength	0.710 73 Å	
Crystal system, space group	Monoclinic, $P2_1/n$	
Unit cell dimensions	a = 11.9778(7) Å	α = 90°
	b = 19.5037(10) Å	β = 110.080(2)°
	c = 16.0479(9) Å	γ = 90°
Volume	3521.1(3) $Å^3$	
Z, Calculated density	4, 1.583 Mg/m^3	
Absorption coefficient	2.942 mm^{-1}	
F(000)	1700	
Crystal size	0.05 x 0.03 x 0.02 mm	
Theta range for data collection	2.79 to 25.40°	
Limiting indices	$-14 \leq h \leq 14$	
	$-23 \leq k \leq 23$	
	$-19 \leq l \leq 19$	
Reflections collected / unique	57172 / 6425 [R(int) = 0.0974]	
Completeness to θ = 25.40	98.9%	
Absorption correction	Semi-empirical from equivalents	
Max. and min. transmission	0.9435 and 0.8669	
Refinement method	Full-matrix least-squares on F^2	
Data / restraints / parameters	6425 / 0 / 442	
Goodness-of-fit on F^2	1.036	
Final R indices [$I>2\sigma(I)$]	R_1 = 0.0503, wR_2 = 0.1082	
R indices (all data)	R_1 = 0.0788, wR_2 = 0.1208	
Largest diff. peak and hole	2.401 and -1.238 e.$Å^{-3}$	

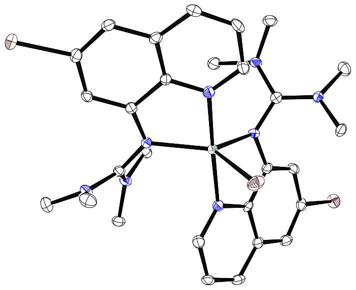

Table C8: Crystal data and structure refinement [Cu(TMG6Brqu)$_2$Br]Br $\cdot$ 2 C_2H_3N $\cdot$ 0.5 C_7H_8, **C8**. Hydrogen atoms, solvents and non-coordinating bromide anions omitted for clarity.

X-ray Code	uv106
Empirical formula	$C_{28}H_{34}Br_4CuN_8 \cdot 2\,C_2H_3N \cdot 0.5\,C_7H_8$
Formula weight	1986.97
Temperature	100(2) K
Wavelength	0.710 73 Å
Crystal system, space group	Monoclinic, $P2_1/n$
Unit cell dimensions	a = 11.8111(6) Å $\alpha = 90°$
	b = 23.2927(15) Å $\beta = 92.473(2)°$
	c = 14.6529(10) Å $\gamma = 90°$
Volume	4027.4(4) Å^3
Z, Calculated density	4, 1.638 Mg/m^3
Absorption coefficient	4.55 mm^{-1}
F(000)	1982
Crystal size	0.25 x 0.20 x 0.10 mm
Theta range for data collection	2.97 to 25.03°
Limiting indices	$-14 \leq h \leq 13$
	$-27 \leq k \leq 27$
	$-17 \leq l \leq 17$
Reflections collected / unique	74547 / 7089 [R(int) = 0.0836]
Completeness to θ = 25.03	99.7%
Absorption correction	Semi-empirical from equivalents
Max. and min. transmission	0.6590 and 0.3959
Refinement method	Full-matrix least-squares on F^2
Data / restraints / parameters	7089 / 0 / 471
Goodness-of-fit on F^2	1.047
Final R indices [I>2σ(I)]	$R_1 = 0.0309$, $wR_2 = 0.0660$
R indices (all data)	$R_1 = 0.0427$, $wR_2 = 0.0703$
Largest diff. peak and hole	1.106 and -0.527 e.Å^{-3}

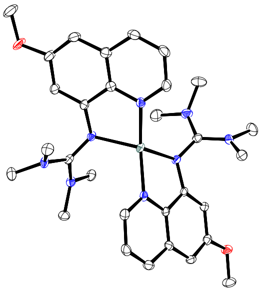

Table C9: Crystal data and structure refinement for [Cu(TMG6Methoxyqu)$_2$][CuCl$_2$], **C9**. Hydrogen atoms and non-coordinating anions omitted for clarity.

X-ray Code	rv481	
Empirical formula	$C_{30}H_{40}CuN_8O_2{}^+$ $CuCl_2{}^-$	
Formula weight	742.68	
Temperature	100(2) K	
Wavelength	0.710 73 Å	
Crystal system, space group	Triclinic, $P\bar{1}$	
Unit cell dimensions	a = 12.1323(9) Å	α = 99.261(2)°
	b = 12.1550(10) Å	β = 111.969(2)°
	c = 14.0323(12) Å	γ = 109.118(2)°
Volume	1715.7(2) $Å^3$	
Z, Calculated density	2, 1.438 Mg/m^3	
Absorption coefficient	1.435 mm^{-1}	
F(000)	768	
Crystal size	0.13 x 0.12 x 0.08 mm	
Theta range for data collection	3.12 to 26.40°	
Limiting indices	$-15 \leq h \leq 14$	
	$-15 \leq k \leq 15$	
	$-17 \leq l \leq 17$	
Reflections collected / unique	29939 / 6955 [R(int) = 0.0548]	
Completeness to θ = 26.40	98.6%	
Absorption correction	Semi-empirical from equivalents	
Max. and min. transmission	0.8939 and 0.8388	
Refinement method	Full-matrix least-squares on F^2	
Data / restraints / parameters	6955 / 0 / 407	
Goodness-of-fit on F^2	1.046	
Final R indices [$I>2\sigma(I)$]	R_1 = 0.0437, wR_2 = 0.0933	
R indices (all data)	R_1 = 0.0746, wR_2 = 0.1056	
Largest diff. peak and hole	0.489 and -0.703 e.Å^{-3}	

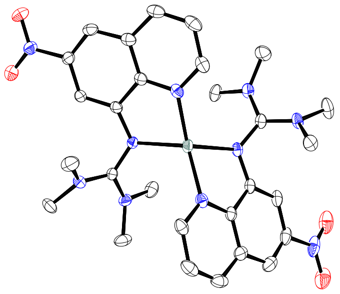

Table C10: Crystal data and structure refinement $[Cu(TMG6Nitroqu)_2][CuCl_2]$, **C10**. Hydrogen atoms and non-coordinating anions omitted for clarity.

X-ray Code	tv434	
Empirical formula	$C_{28}H_{34}CuN_{10}O_4^+$ $CuCl_2^-$	
Formula weight	772.63	
Temperature	100(2) K	
Wavelength	0.710 73 Å	
Crystal system, space group	Monoclinic, $P2_1/n$	
Unit cell dimensions	a = 13.0981(3) Å	$\alpha = 90°$
	b = 14.9536(4) Å	$\beta = 106.7300(10)°$
	c = 17.6099(4) Å	$\gamma = 90°$
Volume	3303.15(14) $Å^3$	
Z, Calculated density	4, 1.554 Mg/m^3	
Absorption coefficient	1.5 mm^{-1}	
F(000)	1584	
Crystal size	0.10 x 0.09 x 0.08 mm	
Theta range for data collection	1.82 to 26.39°	
Limiting indices	$-16 \leq h \leq 16$	
	$-18 \leq k \leq 18$	
	$-22 \leq l \leq 22$	
Reflections collected / unique	63544 / 6754 [R(int) = 0.0486]	
Completeness to $\theta = 26.39$	99.9%	
Absorption correction	Semi-empirical from equivalents	
Max. and min. transmission	0.8894 and 0.8645	
Refinement method	Full-matrix least-squares on F^2	
Data / restraints / parameters	6754 / 0 / 423	
Goodness-of-fit on F^2	1.066	
Final R indices [$I>2\sigma(I)$]	$R_1 = 0.0336$, $wR_2 = 0.0915$	
R indices (all data)	$R_1 = 0.0422$, $wR_2 = 0.1002$	
Largest diff. peak and hole	1.231 and -0.597 e.$Å^{-3}$	

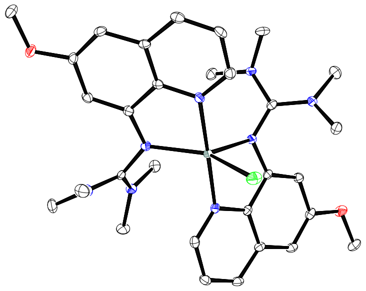

Table C11: Crystal data and structure refinement for [Cu(TMG6Methoxyqu)$_2$Cl]Cl, **C11**. Hydrogen atoms and non-coordinating chloride anions omitted for clarity.

X-ray Code	rv482	
Empirical formula	$C_{34}H_{46}Cl_2CuN_{10}O_2$	
Formula weight	761.25	
Temperature	100(2) K	
Wavelength	0.710 73 Å	
Crystal system, space group	Monoclinic, $P2_1/c$	
Unit cell dimensions	a = 12.8366(10) Å	$\alpha = 90°$
	b = 18.0471(14) Å	$\beta = 122.875(4)°$
	c = 18.4555(10) Å	$\gamma = 90°$
Volume	3590.8(4) $Å^3$	
Z, Calculated density	4, 1.408 Mg/m^3	
Absorption coefficient	0.804 mm^{-1}	
F(000)	1596	
Crystal size	0.18 x 0.09 x 0.06 mm	
Theta range for data collection	2.77 to 26.42°	
Limiting indices	$-16 \leq h \leq 16$	
	$-22 \leq k \leq 22$	
	$-22 \leq l \leq 23$	
Reflections collected / unique	62551 / 7348 [R(int) = 0.0782]	
Completeness to $\theta = 26.42$	99.5%	
Absorption correction	Semi-empirical from equivalents	
Max. and min. transmission	0.9503 and 0.8715	
Refinement method	Full-matrix least-squares on F^2	
Data / restraints / parameters	7348 / 0 / 454	
Goodness-of-fit on F^2	1.044	
Final R indices [$I>2\sigma(I)$]	$R_1 = 0.0410$, $wR_2 = 0.0838$	
R indices (all data)	$R_1 = 0.0712$, $wR_2 = 0.0946$	
Largest diff. peak and hole	0.930 and -0.366 e.$Å^{-3}$	

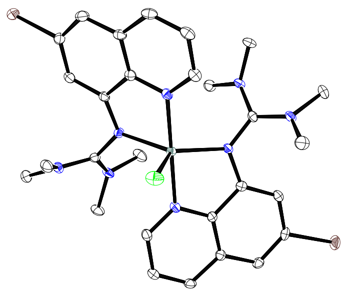

Table C12: Crystal data and structure refinement [Cu(TMG6Brqu)$_2$Cl]Cl $\cdot$ 2 C_2H_3N $\cdot$ 0.5 C_7H_8, **C12**. Hydrogen atoms and solvent molecules omitted for clarity.

X-ray Code	uv239
Empirical formula	$C_{28}H_{34}Br_2Cl_2CuN_8 \cdot 2\,C_2H_3N \cdot 0.5\,C_7H_8$
Formula weight	1809.13
Temperature	100(2) K
Wavelength	0.710 73 Å
Crystal system, space group	Monoclinic, $P2_1/n$
Unit cell dimensions	a = 11.7100(4) Å $\alpha = 90°$
	b = 23.2750(8) Å $\beta = 92.5750(10)°$
	c = 14.4175(4) Å $\gamma = 90°$
Volume	3925.5(2) Å^3
Z, Calculated density	2, 1.531 Mg/m^3
Absorption coefficient	2.768 mm^{-1}
F(000)	1838
Crystal size	0.08 x 0.06 x 0.01 mm
Theta range for data collection	2.19 to 26.39°
Limiting indices	$-14 \leq h \leq 14$
	$-29 \leq k \leq 29$
	$-18 \leq l \leq 18$
Reflections collected / unique	74962 / 8027 [R(int) = 0.0552]
Completeness to $\theta = 26.39$	99.7%
Absorption correction	Semi-empirical from equivalents
Max. and min. transmission	0.9728 and 0.8089
Refinement method	Full-matrix least-squares on F^2
Data / restraints / parameters	8027 / 0 / 474
Goodness-of-fit on F^2	1.07
Final R indices [I>2σ(I)]	$R_1 = 0.0207$, $wR_2 = 0.0595$
R indices (all data)	$R_1 = 0.0330$, $wR_2 = 0.0619$
Largest diff. peak and hole	0.648 and -0.581 e.Å^{-3}

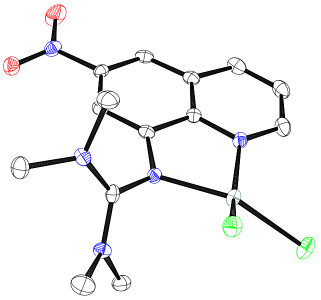

Table C13: Crystal data and structure refinement 2 [Cu(TMG6Nitroqu)Cl_2] · $C_{6.92}H_{7.91}$, **C13**. Hydrogen atoms and solvent molecules omitted for clarity.

X-ray Code	tv402
Empirical formula	$2\,C_{14}H_{17}Cl_2CuN_5O_2 \cdot C_{6.92}H_{7.91}$
Formula weight	933.62
Temperature	100(2) K
Wavelength	0.710 73 Å
Crystal system, space group	Triclinic, $P\bar{1}$
Unit cell dimensions	a = 6.7404(4) Å $\alpha = 109.859(2)°$
	b = 11.6726(7) Å $\beta = 98.057(2)°$
	c = 13.9762(8) Å $\gamma = 94.477(2)°$
Volume	1014.65(10) $Å^3$
Z, Calculated density	2, 1.528 Mg/m^3
Absorption coefficient	1.363 mm^{-1}
F(000)	478
Crystal size	0.10 x 0.06 x 0.01 mm
Theta range for data collection	3.08 to 26.38°
Limiting indices	$-7 \leq h \leq 8$
	$-14 \leq k \leq 14$
	$-14 \leq l \leq 17$
Reflections collected / unique	11476 / 4097 [R(int) = 0.0440]
Completeness to $\theta = 26.38$	98.1%
Absorption correction	Semi-empirical from equivalents
Max. and min. transmission	0.9865 and 0.8758
Refinement method	Full-matrix least-squares on F^2
Data / restraints / parameters	4097 / 0 / 259
Goodness-of-fit on F^2	1.039
Final R indices [$I>2\sigma(I)$]	$R_1 = 0.0403$, $wR_2 = 0.0774$
R indices (all data)	$R_1 = 0.0653$, $wR_2 = 0.0852$
Largest diff. peak and hole	0.511 and -0.537 e.$Å^{-3}$